**US Army Corps
of Engineers**
Waterways Experiment
Station

AD-A273 022

Monitoring Completed Coastal Projects Program

Barbers Point Harbor, Oahu, Hawaii Monitoring Study

by   Linda S. Lillycrop, Michael J. Briggs, Gordon S. Harkins
Coastal Engineering Research Center

Stanley J. Boc
U.S. Army Engineer Division, Pacific Ocean

Michele S. Okihiro
Scripps Institution of Oceanography

DTIC
ELECTE
NOV 22 1993
A

93-28454

93 11 19 095

Barbers Point Harbor, Oahu, Hawaii Monitoring Study

by   Linda S. Lillycrop, Michael J. Briggs, Gordon S. Harkins

Coastal Engineering Research Center

U.S. Army Corps of Engineers
Waterways Experiment Station
3909 Halls Ferry Road
Vicksburg, MS   39180-6199

Stanley J. Boc

U.S. Army Engineer Division, Pacific Ocean
Fort Shafter, HI   96858-5440

Michele S. Okihiro

Scripps Institution of Oceanography
University of California, San Diego
La Jolla, CA   92093

Final report

Approved for public release; distribution is unlimited

DTIC QUALITY INSPECTED 1

**US Army Corps
of Engineers**
Waterways Experiment
Station

INFORMATION
TECHNOLOGY
LABORATORY

N

GEOTECHNICAL
LABORATORY

HEADQUARTERS
BUILDING

COASTAL ENGINEERING
RESEARCH CENTER

MAIN
ENTRANCE

HYDRAULICS
LABORATORY

ENVIRONMENTAL
LABORATORY

STRUCTURES
LABORATORY

SCALE
500   0   500 m

AREA OF RESERVATION = 2.7 sq km

Contents

List of Figures

v

vi

x

List of Tables

Preface

This report was authorized by the Operations and Maintenance Division, Headquarters, U.S. Army Corps of Engineers (HQUSACE). It is a product of the U.S. Army Engineer Waterways Experiment Station (WES) Coastal Engineering Research Center (CERC) Monitoring Completed Coastal Projects (MCCP) Program under the "Barbers Point Harbor, Oahu, HI, Monitoring Study," Work Unit 22119. Messrs. John H. Lockhart, Jr., John G. Housley, and Barry W. Holliday were HQUSACE Technical Monitors. The objectives of the research effort were to evaluate and validate results of model studies conducted for initial harbor design, to perform wave gaging to measure the wave climate in deep water and nearshore areas and long-period oscillations within the harbor, to relate conditions outside the harbor to surge found inside the harbor, to evaluate the effectiveness of the wave absorber, and to compare measured data to the predictions of state-of-the-art numerical and physical model studies.

The research was conducted at CERC under the general direction of Dr. James R. Houston and Mr. Charles C. Calhoun, Jr., Director and Assistant Director, CERC, respectively; and under the direct supervision of Messrs. Thomas W. Richardson, Chief, Engineering Development Division (EDD), and H. Lee Butler, Chief, Research Division (RD). Mr. William L. Preslan was Chief, Prototype Measurement and Analysis Branch, EDD, and Dr. Martin C. Miller was Chief, Coastal Oceanography Branch, RD. Mr. Michael J. Hemsley was initial MCCP Program Manager of the study, and Ms. Carolyn M. Holmes was the MCCP Program Manager through the completion of the study. Research and report preparation were conducted by Ms. Linda S. Lillycrop with the assistance of Ms. Michele Okihiro, Scripps Institution of Oceanography, Messrs. Michael J. Briggs and Gordon S. Harkins, Wave Dynamics Division, and Mr. Stanley J. Boc, Pacific Ocean Division (POD).

Technical review of this report was provided by Drs. Edward F. Thompson, RD, and Andrew W. Garcia, EDD. Technical support throughout the study was provided by Mr. Stanley J. Boc, POD.

Director of WES at the time of publication of this report was Dr. Robert W. Whalin. COL Bruce K. Howard, EN, was Commander.

Conversion Factors, Non-SI to SI Units of Measurement

Non-SI units of measurement used in this report can be converted to SI units as follows:

Multiply	By	To Obtain
acres	4,046.873	square meters
cubic yards	0.7646	cubic meters
degrees (angle)	0.01745329	radians
feet	0.3048	meters
horsepower (550 foot-pounds (force) per second)	745.6999	watts
inches	2.54	centimeters
knots (international)	0.5144444	meters per second
miles (U.S. stat)	1.609	kilometers
square feet	0.09290304	square meters
square miles	2.589998	square kilometers
tons (2,000 pounds, mass)	907.1847	kilograms

1 Introduction

Project Location and General Description

The island of Oahu is the third largest island in the state of Hawaii (Figure 1) and is the center of social, cultural, economic, governmental, and military activities. Although the island comprises only 9.4 percent of the total land area in the state, about 81 percent of the state's population reside on this island. Oahu's economy is integrated with the other islands of Hawaii as well as the national economy of the continental United States. Local and state economies are dependent on waterborne commerce as the primary source of transport, which is centered around Honolulu Harbor (U.S. Army Engineer Division (USAED), Honolulu 1976). In 1963, the U.S. Army Corps of Engineers (USACE), Pacific Ocean Division (POD) completed a detailed study of the deep-draft harbor requirements for the Island of Oahu. The projected volume of waterborne commerce revealed the need to provide a second deep-draft harbor to serve the shipping requirements of the rapidly expanding economy of Oahu and the state. Since a major expansion of Honolulu Harbor could not economically or efficiently satisfy the projected needs, it was recommended that a supplementary deep-draft harbor be constructed at Barbers Point, Oahu (Palmer 1970). Construction of the Barbers Point Deep-Draft Harbor was completed in 1985, and an additional private-resort, small boat harbor was completed in 1989.

The Barbers Point Harbor project is located on the southwest coast of the island of Oahu (Figure 2). The harbor is approximately 2 miles[1] upcoast of the southwestern corner of the island and 15 miles west of Honolulu Harbor. The project area is about 20 road miles from downtown Honolulu, and is within the 1,300-acre Barbers Point Industrial Park. Except for the entrance channel, the harbor complex is situated completely inland from the shoreline, which minimized the impact on coastal resources during construction and eliminated the need for protective offshore structures. The harbor complex consists of an entrance channel, barge harbor, deep-draft basin, and a small boa. ʳbᵒ (Figure 2). An

---

[1] A table of factors for converting non-SI units of measurement to SI units is presented on page xv.
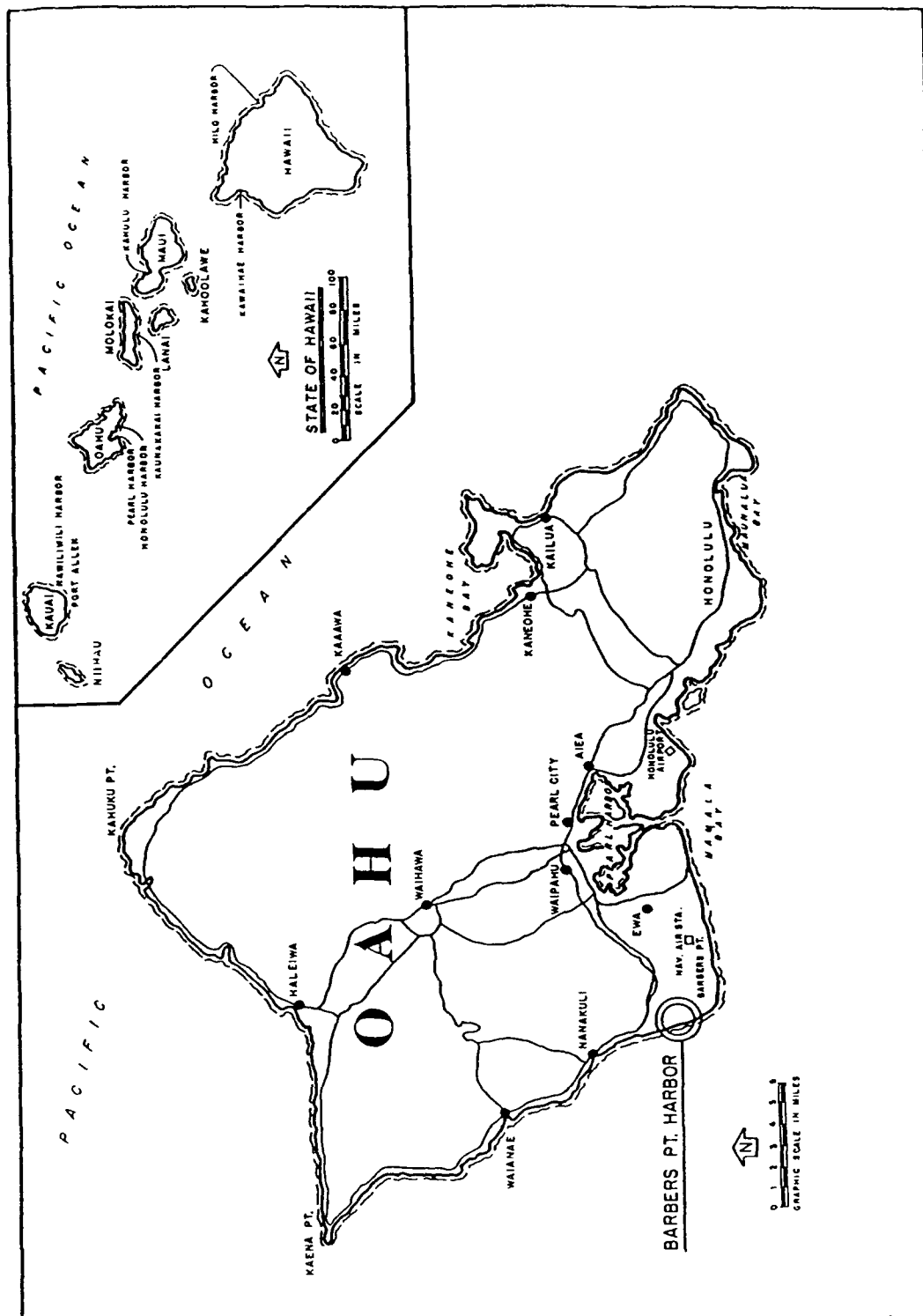
Figure 1. Location map, Island of Oahu
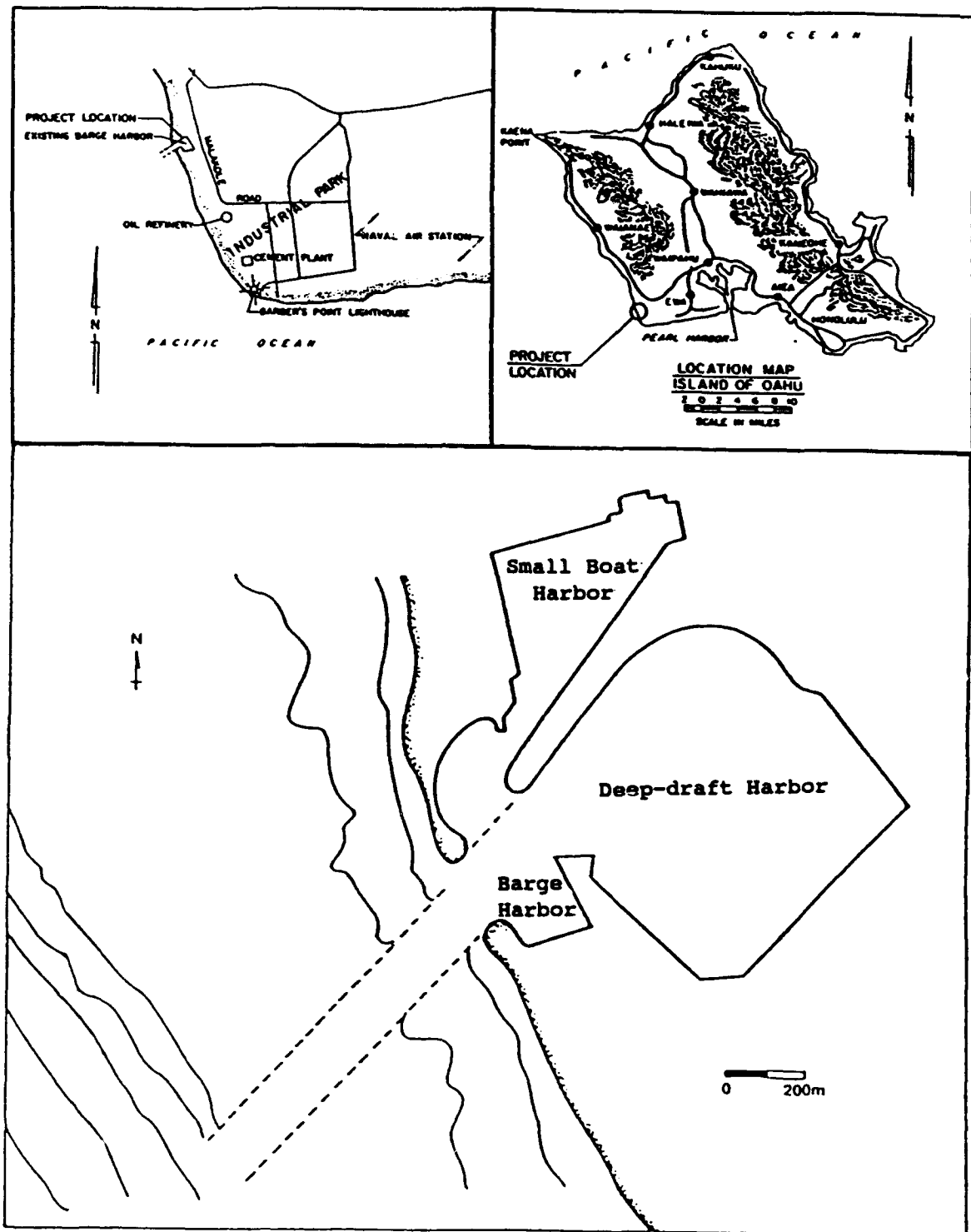
Figure 2.   Location map, Barbers Point Harbor Complex

aerial photograph of the harbor complex is provided in Figure 3. In an effort to reduce the wave energy entering and becoming trapped in the harbor, a stone wave absorber was constructed inland of the shoreline along the northern side of the entrance channel, along the northern corner of the deep-draft basin, and along the east and south sides of the barge harbor. The deep-draft harbor accommodates containerships, tankers, bulk carriers, and assorted barges. The small boat harbor is located northwest of the deep-draft basin and was designed to accommodate 350 to 500 small craft. The components of the harbor are described in detail below.

The 4,280-ft-long, 450-ft-wide, and 38- to 42-ft-deep entrance channel was constructed to provide safe access from the 60-ft-deep offshore waters into the landlocked deep-draft harbor basin. The channel alignment is approximately 16 deg south of an imaginary line perpendicular to the shoreline at a bearing of N45°E. The seaward 3,100-ft-long channel section is 42 ft deep, 450 ft wide, and transitions to a 38-ft-deep, 450-ft-wide channel along a 20-ft-long section. The channel continues as a 38-ft-deep, 450-ft-wide, landlocked channel for another 960 ft, then flares towards the south from the 450-ft width to a 650-ft width along a 200-ft-long sector. The channel terminates at the intersection of the 650-ft-wide flare and the deep-draft harbor basin. The channel sides are dredged at a 1:1 slope from the seaward end to the shoreline and a 1:1.5
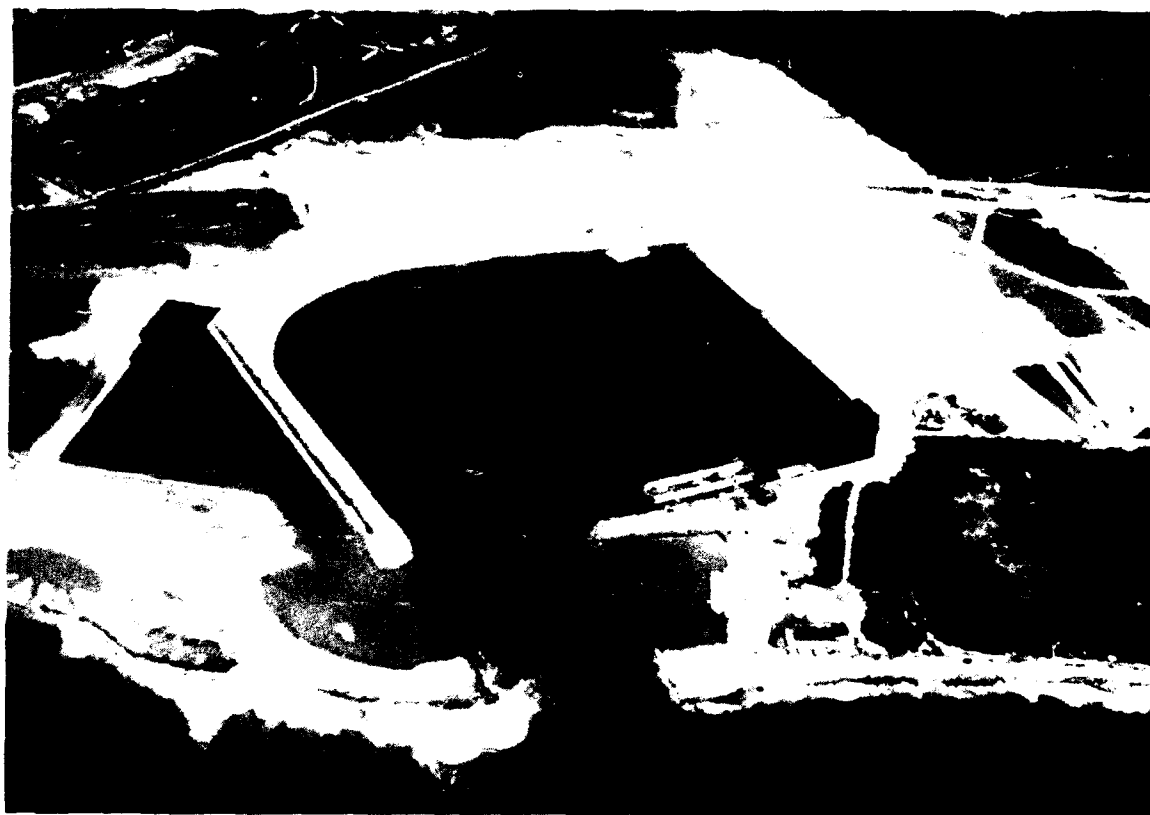
Figure 3.   Aerial photograph, Barbers Point Harbor Complex

slope from the shoreline to the entrance channel terminus (USAED, Honolulu 1977; Palmer 1970).

The 92-acre deep-draft harb⌐ basin was excavated and dredged to create a landlocked, 2,300-ft-wide, 2,100-ft-long, and 38-ft-deep basin. The basin provides for a turning radius in excess of 1,800 ft. Side slopes vary from a 1:1 to 1:2.5 slope based on foundation conditions. Three berthing areas are located adjacent to the harbor basin and are dredged on a reimbursible basis as part of the state's harbor development work. A total of 4,600 ft of angular stone wave absorber was constructed along the side slopes of the northern side of the basin, entrance channel, and near the mouth of the harbor. The three-stone-thick wave absorber is placed on a 1:3 slope from a toe elevation of -11 ft mean lower low water (mllw), to a crest elevation of +5 ft mllw. The stones vary from a 0.5- to 1-ton size at the innermost section of the harbor basin and increase to a 2- to 4-ton size towards the seaward sector of the harbor. Two-dimensional flume tests were used to maximize the design efficiency of the wave absorber (USAED, Honolulu 1977).

The small L-shaped barge harbor is approximately 520 ft wide, 700 ft long, and 21 ft deep, and covers approximately 9 acres. The characteristics of the wave absorber in the deep-draft harbor, as described in the previous paragraph, also apply to the wave absorber constructed along the east wall and southeast corner of the barge harbor. A 250-ft-long concrete wharf is located along the south side of the barge harbor (USAED, Honolulu 1976). A launching ramp previously located in the southeast corner of the barge harbor was eliminated in 1990 upon construction of the wave absorber. Due to hazardous surge under certain conditions and the limited size of the facility, the use of the barge harbor is restricted. The barge harbor is also referred to as the barge basin.

The small boat harbor located adjacent to the deep-draft harbor is 15 ft deep and covers approximately 20 acres. The small boat harbor entrance channel opens into the north side of the deep-draft harbor entrance approximately 200 ft from the shoreline. The basin walls are stone on a near vertical slope with the exception of the deep-draft harbor wave absorber continuing inside the small boat harbor along the south wall. A launching ramp is located along the north side of the entrance channel. In various publications, the small boat harbor is referenced as: shallow-draft harbor, small boat marina, small craft marina, West Beach Marina, and marina.

Site Characteristics

Barbers Point is in the leeward coastal lowlands of Oahu. This area is characterized by abundant sunshine, persistent trade winds, equable temperatures, and moderate humidities. The climate is generally warmer and drier than Honolulu and the rest of the island. The harbor is subject

to waves which approach the Hawaiian Islands from northwest and southwest directions. Wave approach from the west is rare, but does occur during local (Kona) storm conditions. Waves from an easterly direction do not impact the harbor since the Island of Oahu acts as a barrier to the east. During the summer months, waves occur from the southwest; however, the largest waves occur during winter months and are caused by northern swells generated in the Northwest Pacific Ocean.

In most nearshore locations in Hawaii the tidal flow is the primary current component, and past studies (Sea Engineering, Inc. 1980 and 1983; Noda and Associates 1988; and Wyrtki, Graefe, and Patzert 1969) have shown this to be the case in the vicinity of Barbers Point Harbor. Hawaii has predominantly semidiurnal tidal variations with a pronounced diurnal inequality. Tidal flows are typically oriented parallel to the nearshore bottom contours, and since the entrance channel runs perpendicular to the contours, the tidal flows result in cross-channel currents. During flood tide, the offshore current moves from northwest to southeast. During ebb tide, the current reverses and moves from southeast to northwest. Ebb tide conditions and westward oceanic drift predominate. Maximum velocities range from 1 to 2 knots and localized littoral currents vary in velocity and direction. The mean tidal range between mllw and mean higher high water (mhhw) is 1.9 ft, and mean sea level (msl) is 0.8 ft. The estimated maximum extreme range is 4.0 ft (USAED, Honolulu 1976).

There are no fringing offshore coral reefs in the vicinity of Barbers Point; consequently, incoming waves break directly on the coral rock beach. The coral rock beach slopes rather steeply from the shoreline to the 10-ft contour, the bottom then slopes gradually to the 30-ft contour, which occurs approximately 1/2 mile seaward of the surf zone. Beyond the 30-ft contour, the bottom slopes rapidly to a 60-ft depth, then drops off steeply to a 600-ft depth within another half mile. Westerly and southwesterly storm waves are the most critical deepwater waves and cause heavy surge in the harbor. Light surge also occurs during periods of southerly and southeasterly wave approaches (USAED, Honolulu 1976).

Project History

Initial planning for the original navigation project began in 1958 when Congress recommended by resolution that a feasibility study be conducted to determine the need and viability for a second port on the Island of Oahu. In 1961, developers of the industrial park constructed the small L-shaped barge harbor to enable industries to ship products directly to other islands, thereby reducing costs of trucking and trans-shipment to and from Honolulu Harbor. The navigation project consisted of a small L-shaped barge harbor with a 520-ft-wide, 700-ft-long, and 21-ft-deep basin and a 220-ft-wide, 1,100-ft-long, and 22-ft-deep entrance channel. A 250-ft-long concrete wharf was situated on the south side of the basin. The entrance channel and barge harbor were dredged in the coral formation of

the flat coastal plain. Due to hazardous surge conditions resulting from
nearly vertical basin walls and the limited size of the facility, the barge
harbor was used infrequently (USAED, Honolulu 1976).

The Barbers Point deep-draft harbor was authorized by Section 301 of
the River and Harbor Act of 1965, in accordance with the recommenda-
tions contained in the Chief of Engineers' report dated 5 October 1964.
The authorized plan of improvement (Figure 4) was designed to meet the
needs and desires of the local interests in providing a modern deep-draft
harbor to serve shipping requirements of the Barbers Point Industrial Park
and of the general economy of West Oahu. The proposed harbor included
a 42-ft-deep, 450-ft-wide, and 3,100-ft-long entrance channel, a land-
locked 38-ft-deep, 46-acre harbor basin, a protective rubble-mound break-
water on the north side of the harbor entrance, two separate segments of
rubble-mound wave absorbers, totalling 1,320 ft in length, along portions
of the inner shoreline of the harbor basin, and a separate small boat harbor
constructed adjacent to the deep-draft harbor. The deep-draft harbor was
designed to accommodate a 633-ft-long vessel.

Advanced Engineering and Design Studies were initiated in 1967 but
were terminated in 1969 due to the state's inability to complete prelimi-
nary agreements with land acquisition. These studies included a hydraulic
model study, detailed surveys, foundation boring investigations, cost esti-
mates, and coordination with local interests and governmental agencies.
A hydraulic model study was conducted from 1967-1968 by POD, under
contract with the University of Hawaii (USAED, Honolulu 1976). A num-
ber of harbor design plans and modifications to these plans were tested in
the model, including entrance-channel current tests, harbor-dilution tests,
and wave absorber design tests. All design plans incorporated a small
boat harbor extending off the deep-draft harbor basin. Of the various
configurations tested, the most economical and effective in meeting de-
sired wave height criteria (Figure 5) was a near trapezoidal shaped, 38-ft-
deep, 77-acre basin with a 450-ft-wide, 42-ft-deep entrance channel and a
12-ft-deep small boat harbor located to the south of the deep-draft harbor
basin. This plan would adequately serve the 1968 shipping requirements
of Oahu and the state (Palmer 1970). A detailed description of the hydrau-
lic model study is given in Chapter 2 of this report.

Because of the long time interval between authorization of the project
in 1965 and changes in the economic and environmental conditions of the
project area as well as in USACE water resource planning policies, a post-
authorization study was conducted in 1975 by POD. The study was to as-
sess if past planning decisions would provide for a harbor that would meet
the present an! near future navigation requirements for the island of
Oahu, and to provide a harbor project that could respond to these require-
ments. The post-authorization study indicated the need for a basin that
was larger than the design developed through the hydraulic model study.
The harbor must also be capable of accommodating 720-ft-long container
ships and provide sufficient turning area for the 900-ft-long vessels
expected to service the harbor in the future. Using concepts of the 1968

Figure 4. Authorized plan of improvement, 1963
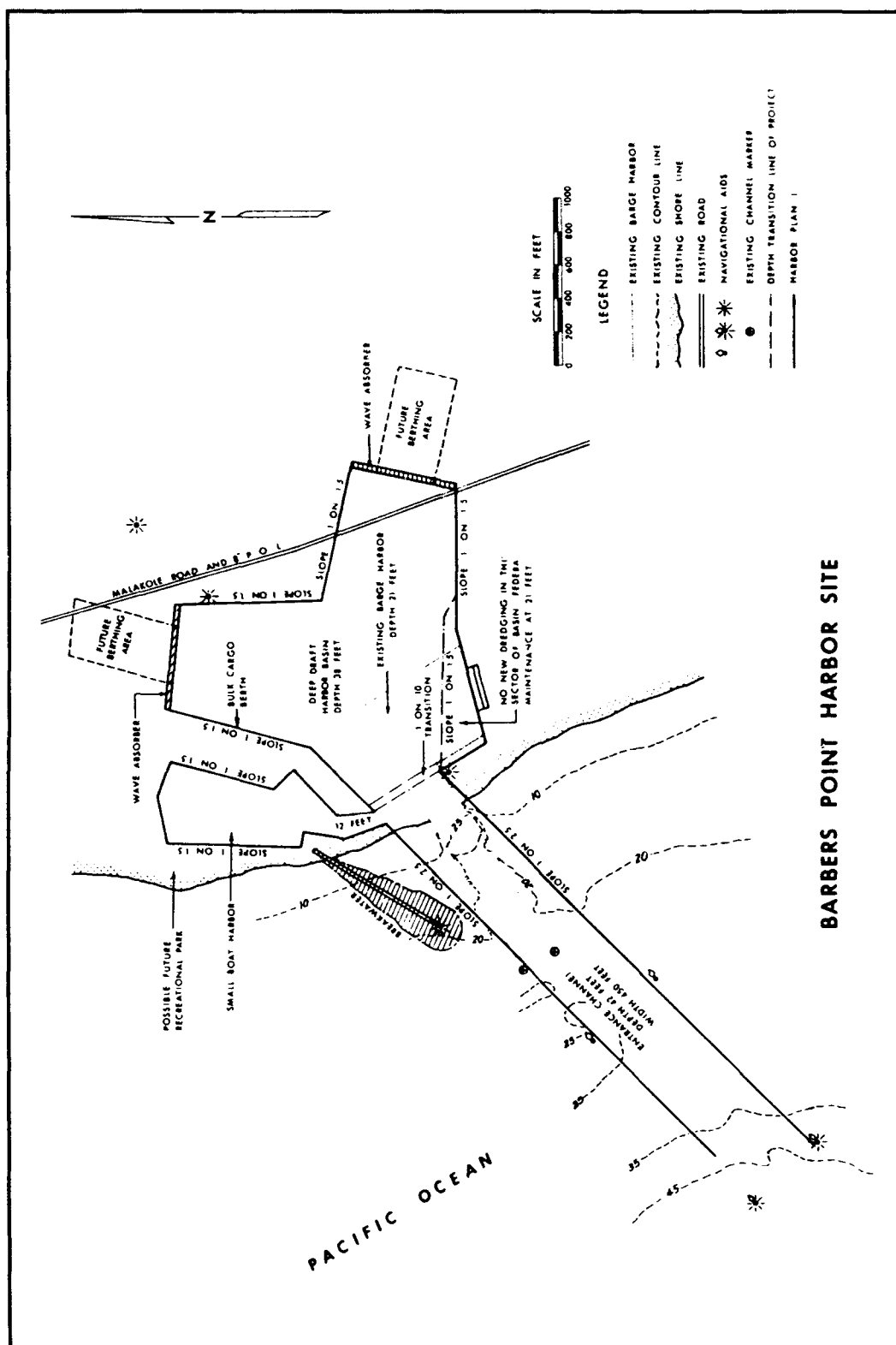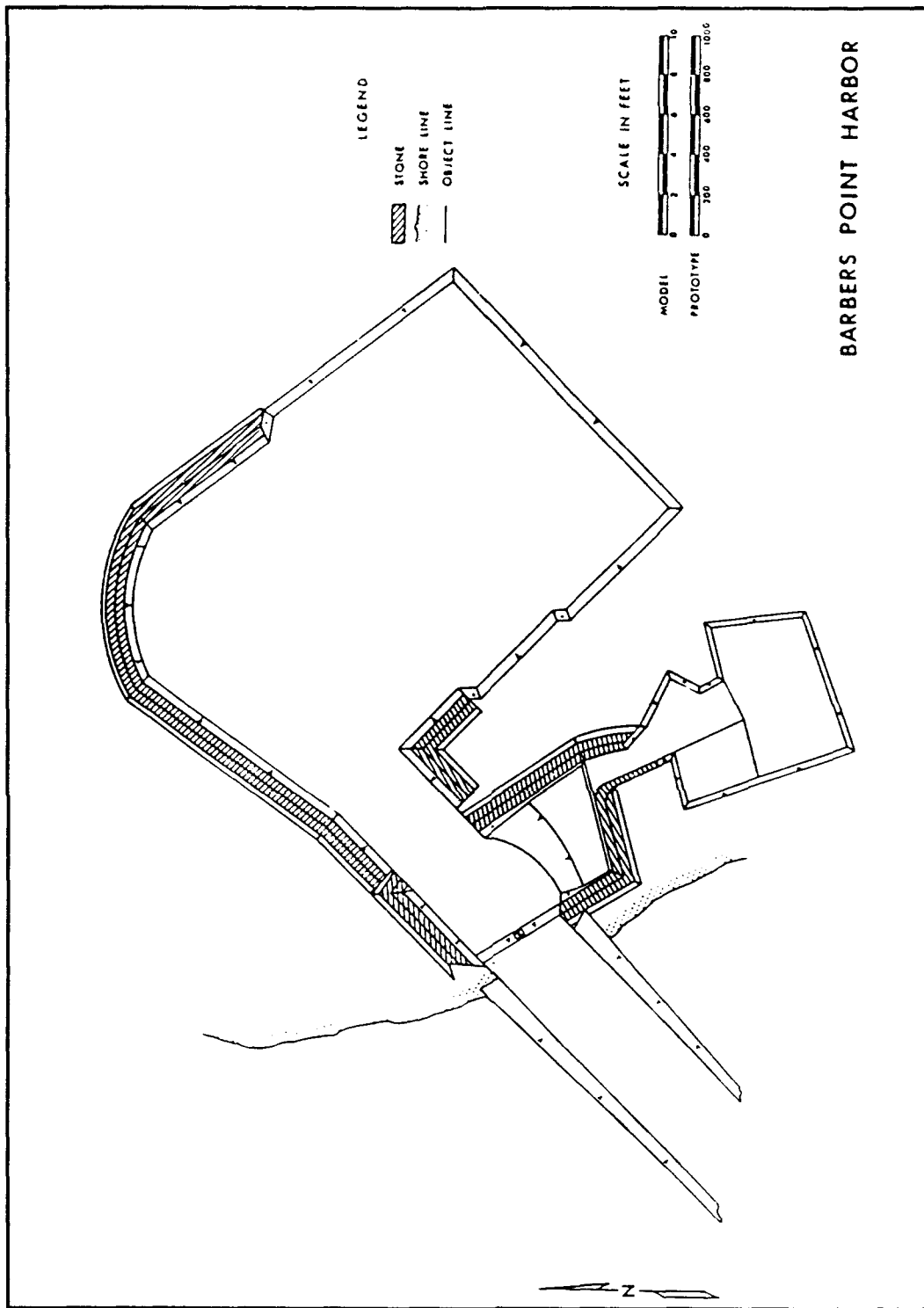
Figure 5. Most effective configuration (University of Hawaii)

hydraulic model study, POD developed a final harbor design plan (Figure 6) that consists of a 4,200-ft-long, 450-ft wide, and 38- to 42-ft-deep entrance channel leading to a 94-acre, 38-ft-deep harbor basin. The alignment of the entrance channel allows the incorporation of a major portion of the existing barge harbor. The proposed harbor configuration can provide approximately 4,400 ft of docks and 4,600 ft of wave absorber along the channel and basin slopes (Durham 1978). A small boat harbor was not included in this plan to accommodate the state of Hawaii's 1972 request that construction of the small boat harbor be deferred indefinitely.

Since the post-authorization study indicated a need for a larger harbor basin than previously analyzed and tested in the hydraulic model study, and the small boat harbor was eliminated from the proposed plan, POD requested that the U.S. Army Engineer Waterways Experiment Station (WES) evaluate the effects of basin enlargement on surging in the proposed deep-draft harbor. The natural periods of oscillation, in particular,
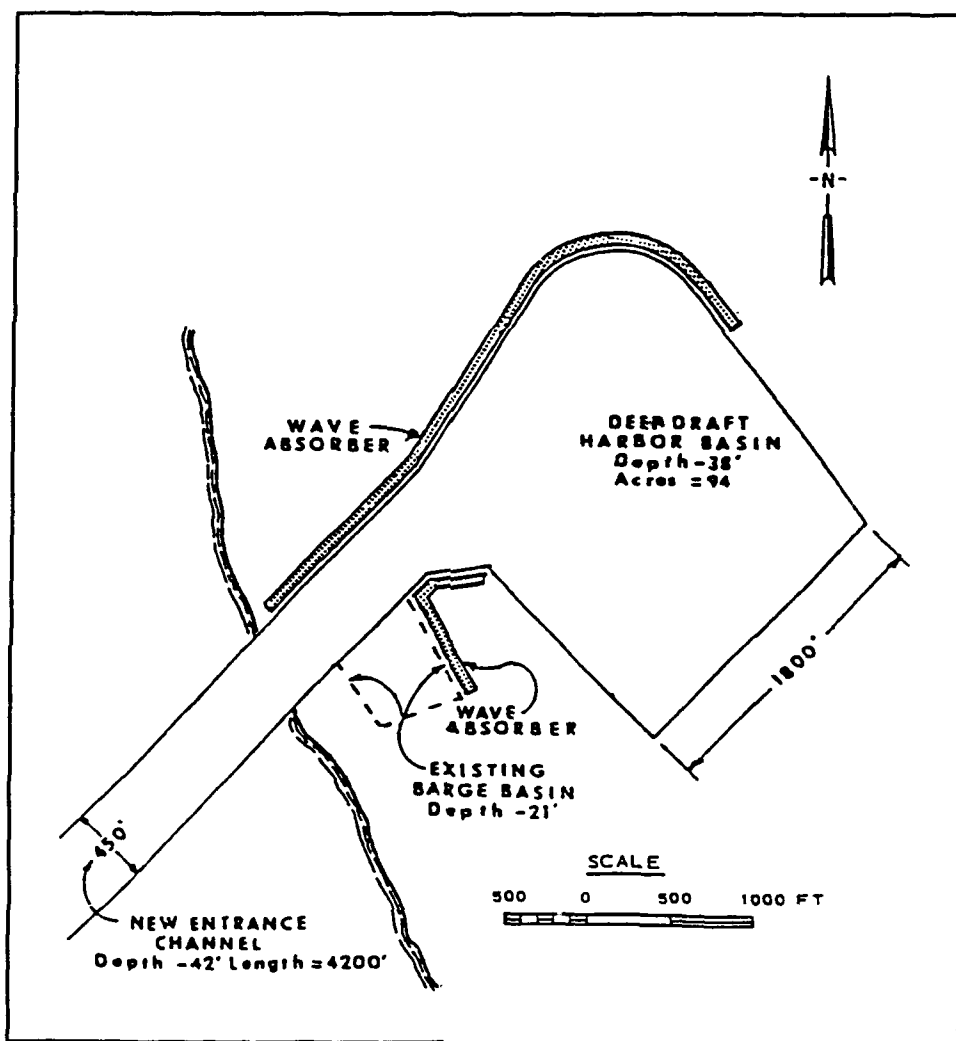
Figure 6.   Final deep-draft harbor design plan, 1975

the fundamental periods of oscillation of the deep-draft harbor, were necessary to determine potential modes of harbor resonance (Durham 1978).

After the many years of planning and engineering, a construction contract was awarded in March 1982 for $47 million. The majority of the basin excavation was completed with a backhoe with a 15-cu-yd bucket. Excavating the entrance channel was accomplished by blasting and using an auger with a 10-ft-diam bit to break up the coral. To minimize the effects of turbidity, the entire inner-harbor area was dredged before access to the ocean was permitted. Approximately 11 million cu yd of coralline material was removed and stockpiled for future use (Hemsley, Boc, and Okihiro 1988).

While the deep-draft harbor was under construction, a second hydraulic model study was conducted in 1984-1985 by West Beach Estates, Honolulu, HI, under contract with the University of Hawaii to verify and refine design concepts of the proposed small boat harbor north of the deep-draft harbor. Three proposed entrance channel designs were evaluated. Results of this study determined that the optimal design would be an entrance channel perpendicular to the deep-draft harbor.

Construction of the deep-draft harbor was completed in 1985. The as-built dimensions of the harbor were a 4,280-ft-long, 450-ft-wide, and 38- to 42-ft-deep entrance channel leading to a 92-acre, 2,100-ft-wide, 2,300-ft-long, and 38-ft-deep harbor basin. Construction of the private resort small boat harbor, located north of the deep-draft harbor, was completed in 1989.

In 1989, the state of Hawaii and POD requested that WES perform further numerical and physical model studies to evaluate harbor modifications that would allow the harbor to accommodate larger vessels and increase the number of available berths. These proposed modifications included widening and deepening the entrance channel, deepening and expanding the harbor basin, and constructing a seaward jetty. A total of eight harbor configurations, including the existing configuration, were evaluated. These studies were conducted from September 1990 to June 1992. The detailed report of this study is provided in Briggs, Lillycrop, and McGehee (1992).

Monitoring Completed Coastal Projects Program

An evaluation of the Barbers Point Harbor project funded through the Monitoring Completed Coastal Projects (MCCP) Program, an Operations and Maintenance Division supported effort, was initiated in 1981 and efforts continue to date. This is a national program that provides for systematic monitoring of coastal projects. The objective of the program is as follows (Hemsley 1985):

Simply stated, the aim of the program is the advancement of coastal engineering technology. It is designed to determine how well projects are accomplishing their purposes and are resisting the attacks of the physical environment. These determinations, combined with the concepts and understanding already available, will lead to upgrading the credibility of predictions of cost-effectiveness of engineering solutions to coastal problems; to strengthening and improving design criteria and methodology; to improving construction practices; and to improving operation and maintenance techniques. Additionally, the monitoring program will identify concerns that laboratories should address more intently. Stated in another way, the objective is the advancement of the engineering science derived from insights into the physics that laboratory studies have developed.

A prioritized listing of the problem areas of interest to the MCCP program is given in Table 1.

Table 1	
MCCP Program Areas of Interest	
	Program Areas of Interest
1	Shoreline and nearshore current response to coastal structures.
2	Wave transmission by overtopping.
3	Prediction of controlling cross section at inlet navigation channels.
4	Wave attenuation by breakwaters (submerged and floating).
5	Bypassing at jettied and unjettied inlets.
6	Wave refraction and steepening by currents.
7	Stability of rubble structures - investigations to determine causes of failure.
8	Comparison of pre- and postconstruction sediment budgets.
9	Wave and current effects on navigation.
10	Dynamics of floating structures.
11	Wave reflection.
12	Effects of construction techniques on scour and deposition near coastal structures.
13	Diffraction around prototype structures.
14	Wave runup on structures.
15	Onshore/offshore sediment movement near coastal structures.
16	Harbor oscillations.
17	Wave transmission through structures.
18	Material life cycle.
19	Ice effects on structures and beaches.
20	Model study verification.
21	Wave translation.
22	Construction techniques.

The opportunity to monitor a new harbor occurs infrequently; therefore, when the Barbers Point Harbor project was nominated for the MCCP during the program's fourth year, FY 84, it was quickly selected. Before construction of the harbor was completed, planning began for the collection of wave data under the MCCP program. Funding for the Barbers Point Harbor monitoring effort began in FY 85. From Table 1, the MCCP areas of interest addressed by this project are: (7) Stability of rubble structures; (9) Wave and current effects on navigation; (16) Harbor oscillations; and (20) Model study verification.

The Barbers Point Harbor monitoring plan was developed with the following objectives: (1) evaluate and validate results of model studies conducted for harbor design; (2) perform wave gaging to measure wave climates in deep water and nearshore areas, and long-period oscillations of the harbor; (3) relate conditions outside the harbor to surge found inside the harbor; (4) evaluate the effectiveness of the wave absorber; and (5) compare the measured data to the predictions of state-of-the-art physical and numerical model studies.

To accomplish the objectives of the monitoring plan, the collection of wave and surge data both outside and within the harbor was required. A total of ten instruments were deployed and data collected at various intervals between July 1986 and March 1990. Figure 7 shows the locations of the instruments. A Datawell Waverider buoy, approximately 1 mile offshore, provided the incident wave conditions for the monitoring effort. A bottom-mounted slope array S_{xy} was located just north of the entrance channel to determine nearshore wave conditions. A total of five non-directional pressure-based wave gages were located offshore and within the harbor. Two gages were placed adjacent to the entrance channel to measure the change in wave energy between the slope array and the harbor entrance. A single gage was placed inside the harbor entrance to measure wave energy entering the harbor and to assist in evaluating the effectiveness of the wave absorber. To measure both waves and long-period surge occurring inside the harbor, the remaining four gages were located at the midpoint of the interior channel and in the three corners of the deep-draft basin. These measurements were used to define wave phase and amplitude inside the harbor, which made it possible to describe individual modal structures, predict problem areas, and identify the existence and locations of nodes and anti-nodes within the basin. Because of the site's remoteness, an instrument building was constructed for a shore station to house the power source and receive the signals from the instruments. Data collection began in 1986 and continued through 1990. Details of the monitoring effort are provided in Chapter 4 of this report, "Monitoring Program."
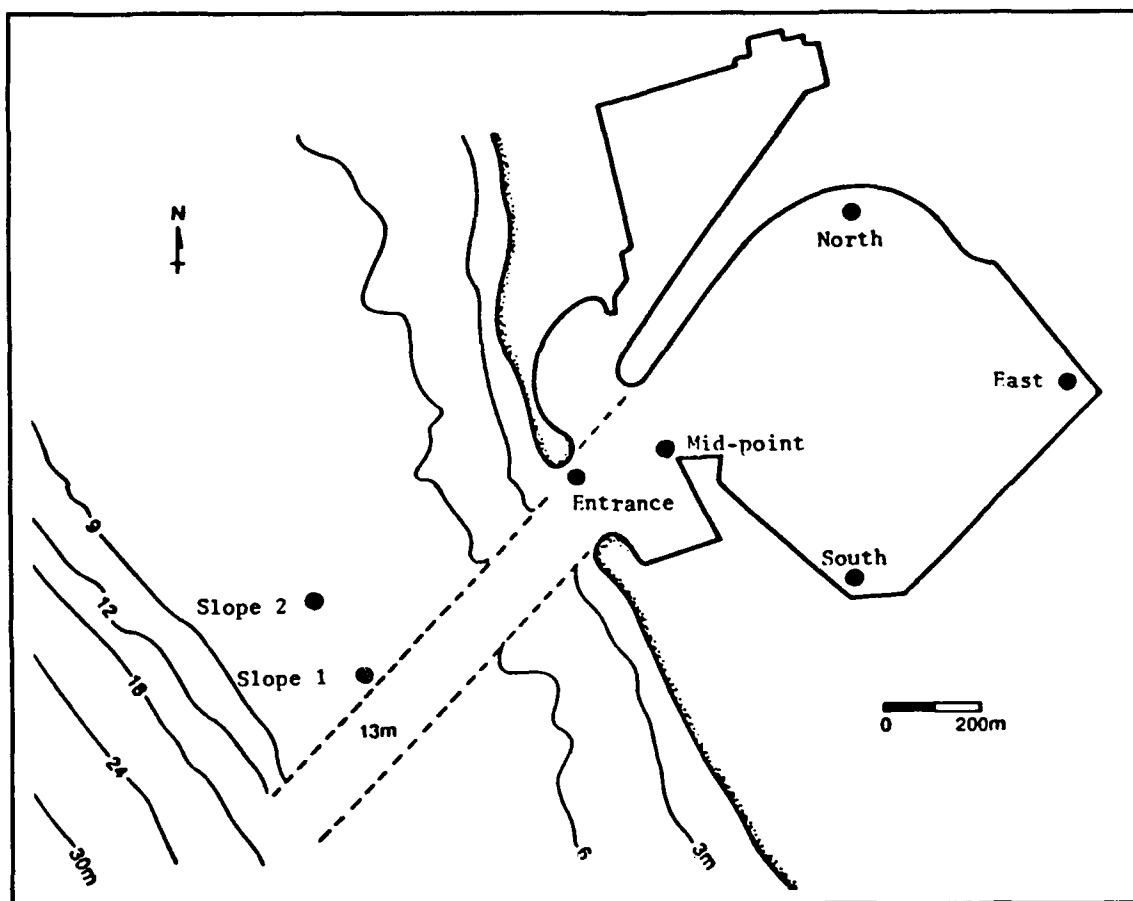
Figure 7.   Location of prototype wave gages

2 Project Design

In the planning stages of the harbor, a number of model studies were conducted to aid in the design and to evaluate proposed modifications to the preliminary designs. A hydraulic model study conducted in 1967 (Palmer 1970) determined the plan on which the actual harbor design was based. A numerical model study conducted in 1977 (Durham 1978) determined the effects of enlarging the deep-draft basin on surging in the harbor. A second hydraulic model study (Lee 1985) was conducted in 1984 and 1985 to investigate the feasibility of a small boat harbor located north of the deep-draft harbor. The description of the model studies and results provided in this chapter are summarized from the final reports of the above-mentioned studies.

Hydraulic Model Study 1967

In April of 1967, POD requested that the University of Hawaii conduct a hydraulic model investigation of the Barbers Point Harbor Project. The problems with which the model study was concerned were of interest to both POD and the State of Hawaii, Department of Transportation Harbors Division (DOT). The purposes of the study were to: (a) study the wave action in the proposed deep-draft and small boat harbors, (b) develop an optimum design for wave absorbers to be used in the harbor entrance and on the perimeter of the harbor basin where necessary, (c) study the circulation and potential of local pollution within the harbor, and (d) develop plans to provide suitable navigation conditions in the entrance channel and satisfactory mooring conditions in the proposed harbors. Base tests and four proposed harbor plans, with modifications to each plan, were tested in the model.

Hydraulic model appurtenances

A geometrically undistorted hydraulic model was constructed to a linear scale of 1:100, model to prototype, to ensure accurate reproduction of wave systems. The deep-draft harbor, small boat harbor, and sufficient coastline and offshore areas were included in the model to permit

generation of test waves from all directions between south and northwest. The offshore area extended to the 60-ft contour with a sloping transition between the 60- and 100-ft contours (Figure 8). The total area of the model was approximately 4,600 ft^2, which reproduced approximately 1.7 square miles of prototype area. The model bathymetry was referenced to mllw, and the local prototype grid system was used for horizontal control.

The model waves were generated to scale using appropriate sections and orientations of the 60-ft-long wave generator. This machine had a vertical-motion type plunger which was adjustable to reproduce the prototype waves to scale. The wave generator incorporated speed and displacement controls that were infinitely variable and therefore was capable of producing the required range of wave heights and periods. The wave generator was mounted on retractable casters, which facilitated changing position and direction. Wave heights were measured at selected locations in the model and were recorded in analog form.

Description of test plans

A number of harbor plans and modifications of these plans were tested in the model, including base tests and four design plans of improvement to the base tests. Entrance-channel current tests and harbor-dilution tests, as well as wave absorber design tests, were also conducted in the model at appropriate stages of the study. The reader is referred to Palmer (1970) for details of the entrance-channel current tests, harbor-dilution tests, and *wave absorber design tests.* Base tests refer to those tests made with the originally proposed design plan of improvement installed in the model and were designated Plan I. The proposed design plans were improvements on the base test plan and are referred to as Plans I, II, III, III-A, V, and V-A. Up to 16 modifications to each proposed design plan were tested. The harbor modifications included:

   a. Harbor configuration.

   b. Location, orientation, and length of breakwaters.

   c. Configuration, length, and location of wave absorbers.

   d. Piers supported on pilings over sloping banks as well as piers with vertical bulkheads.

The base test plan, Figure 9, consisted of a deep-draft harbor with an approximate 46-acre, 38-ft-deep basin, a 3,100-ft-long, 450-ft-wide, and 42-ft-deep entrance channel, and a 12-ft-deep small boat harbor located north of the deep-draft harbor. Wave gage locations for the base test plans are also shown in Figure 9. Design improvements to the base test plan, Plan I and Plans II through V, and the number of modifications to each plan were:
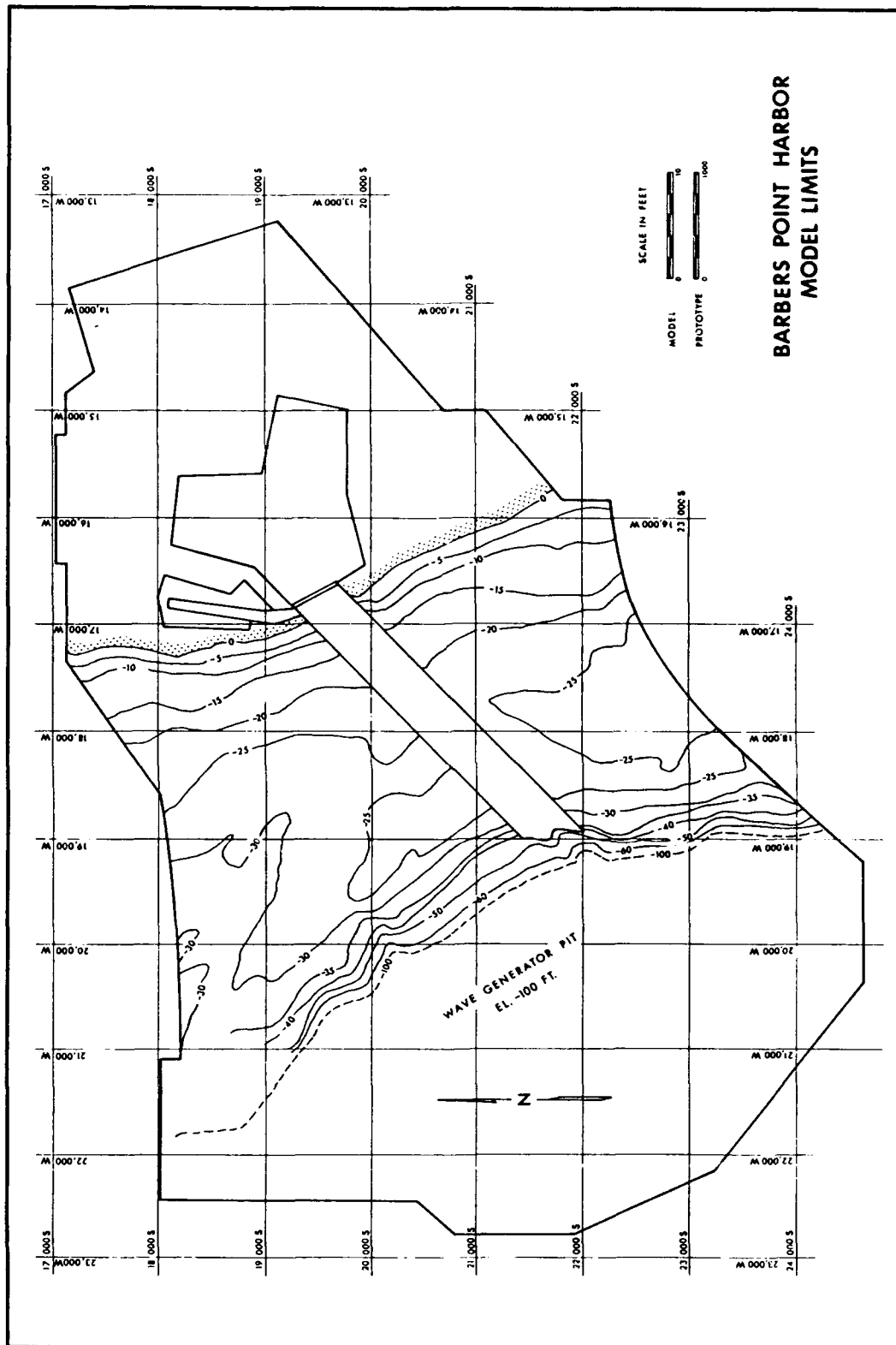
Figure 8. Hydraulic model limits, 1967

a. Plan I, seventeeen modifications (Figures 9 and 10). Involved variations of breakwaters and wave absorbers, and the small boat harbor.

b. Plan II, thirteen modifications (Figures 11 through 13). Involved extension of the entrance channel inland, various wave absorbers in the channel and the perimeter of the harbor basin, and modifications including breakwaters on either side of the entrance channel.

c. Plan III, eleven modifications (Figures 14 through 16). Involved shifting the harbor basin to locate piers in sheltered positions and various wave absorbers and breakwaters.

d. Plan III-A, two modifications (Figure 17). Further refinement of Plan III.

e. Plan V, eight modifications (Figure 18). Involved offsetting the harbor basin to the south to place piers in a sheltered area. Modifications included extensive wave absorbers and wave traps along the entrance channel and breakwaters and vertical sloping bulkheads.

f. Plan V-A, one modification (Figure 19). Eliminated breakwaters and north wave trap of Plan V.

Test conditions

A still-water level (swl) of 3 ft was selected for the model tests to reproduce wave refraction, shoaling, diffraction, reflection, and wave overtopping. These factors were dependent upon water depth, incident wave height, and period. A comparatively high water level was selected to avoid bottom-friction effects, which are common to small-scale models. A high swl also tends to produce conservative results. The tide level, however, was fluctuated to simulate typical tide levels for the tidal dilution tests.

Since tide level records were unavailable for the proposed Barbers Point Harbor, tide elevations and ranges available for Honolulu were used. Wave measurements were also unavailable; therefore, wave hindcast statistics were furnished by POD and WES for testing. The wave characteristics were based on hindcasts by Marine Advisers (1964) supplemented by *wave observations and measurements.* Wave refraction diagrams were constructed graphically by POD, and refraction coefficients were computed for representative waves from critical directions of approach. Shoaling coefficients were obtained from methods presented in the *Shore Protection Planning and Design Manual* (1966).
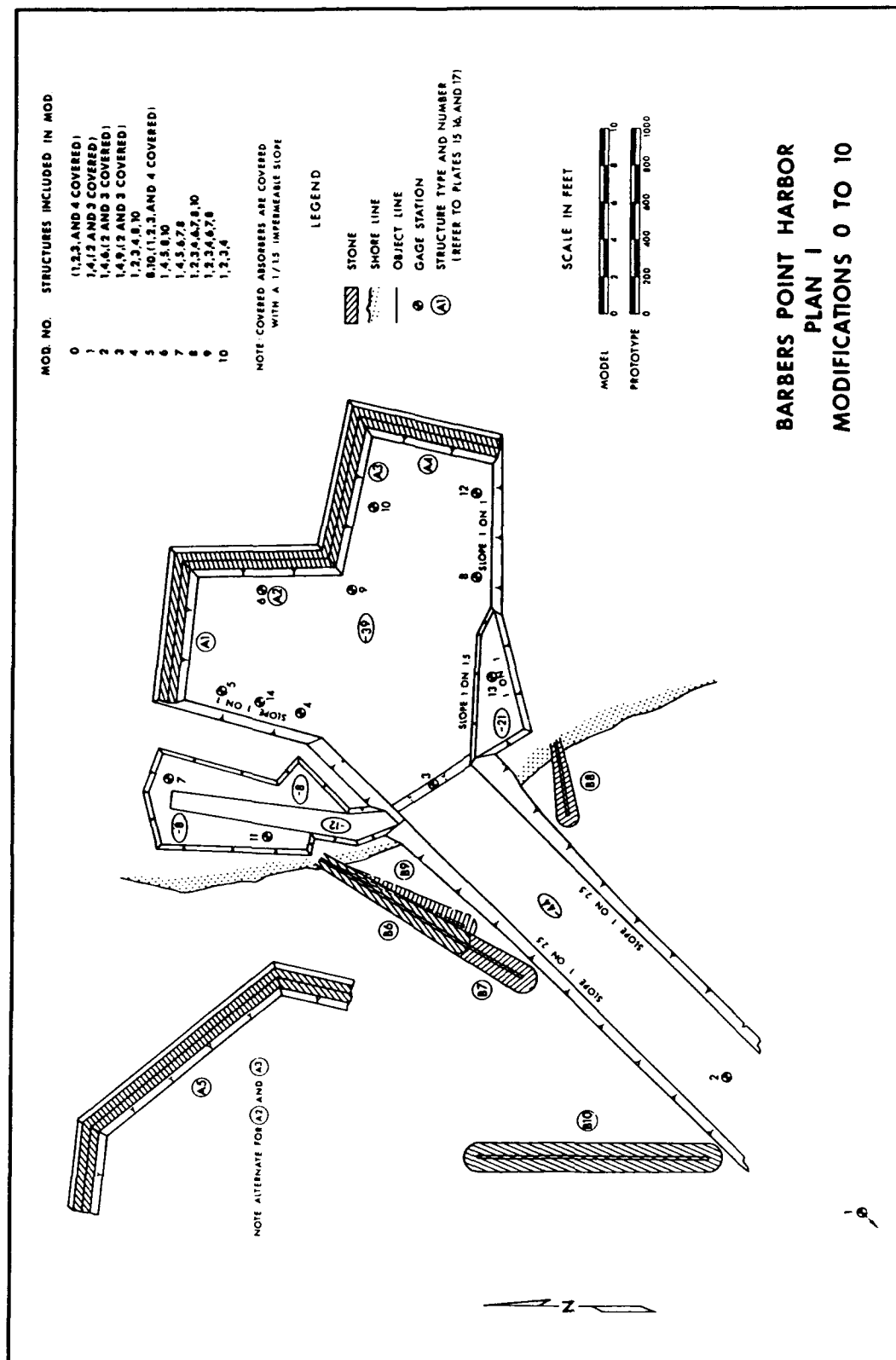
Figure 9. Plan I, Modifications 0 - 10
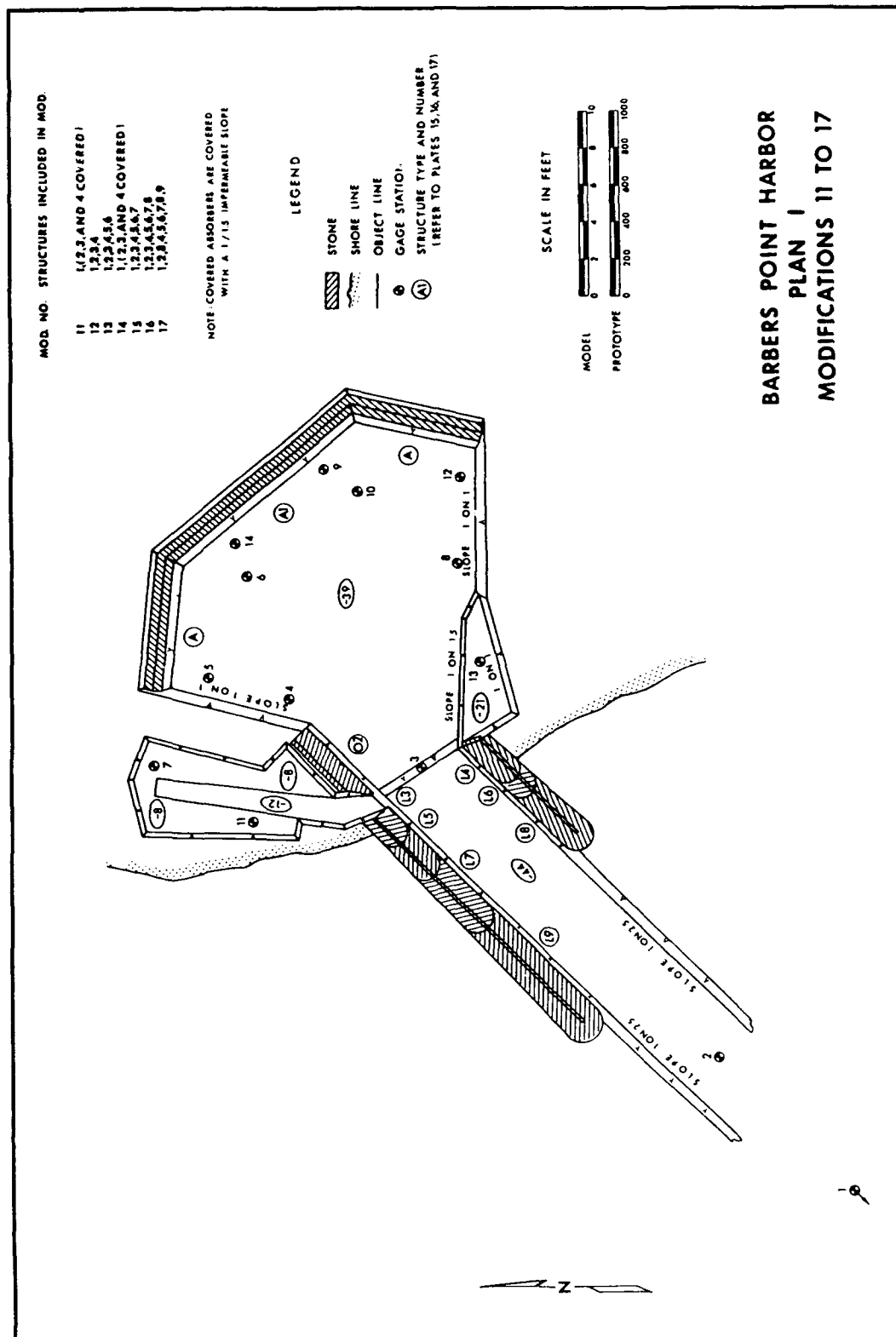
Figure 10. Plan I, Modifications 11 - 17
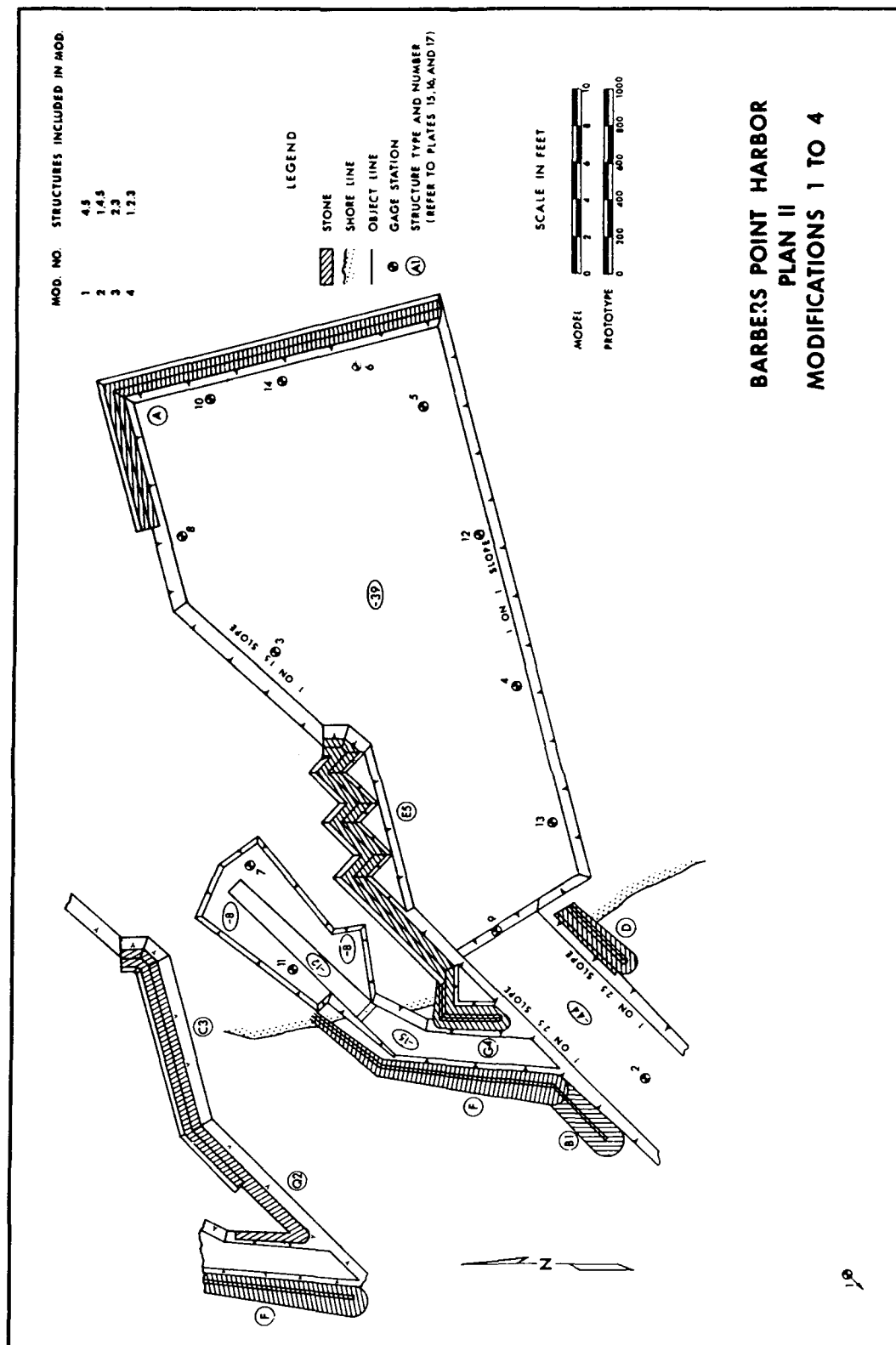
Figure 11.   Plan II, Modifications 1 - 4
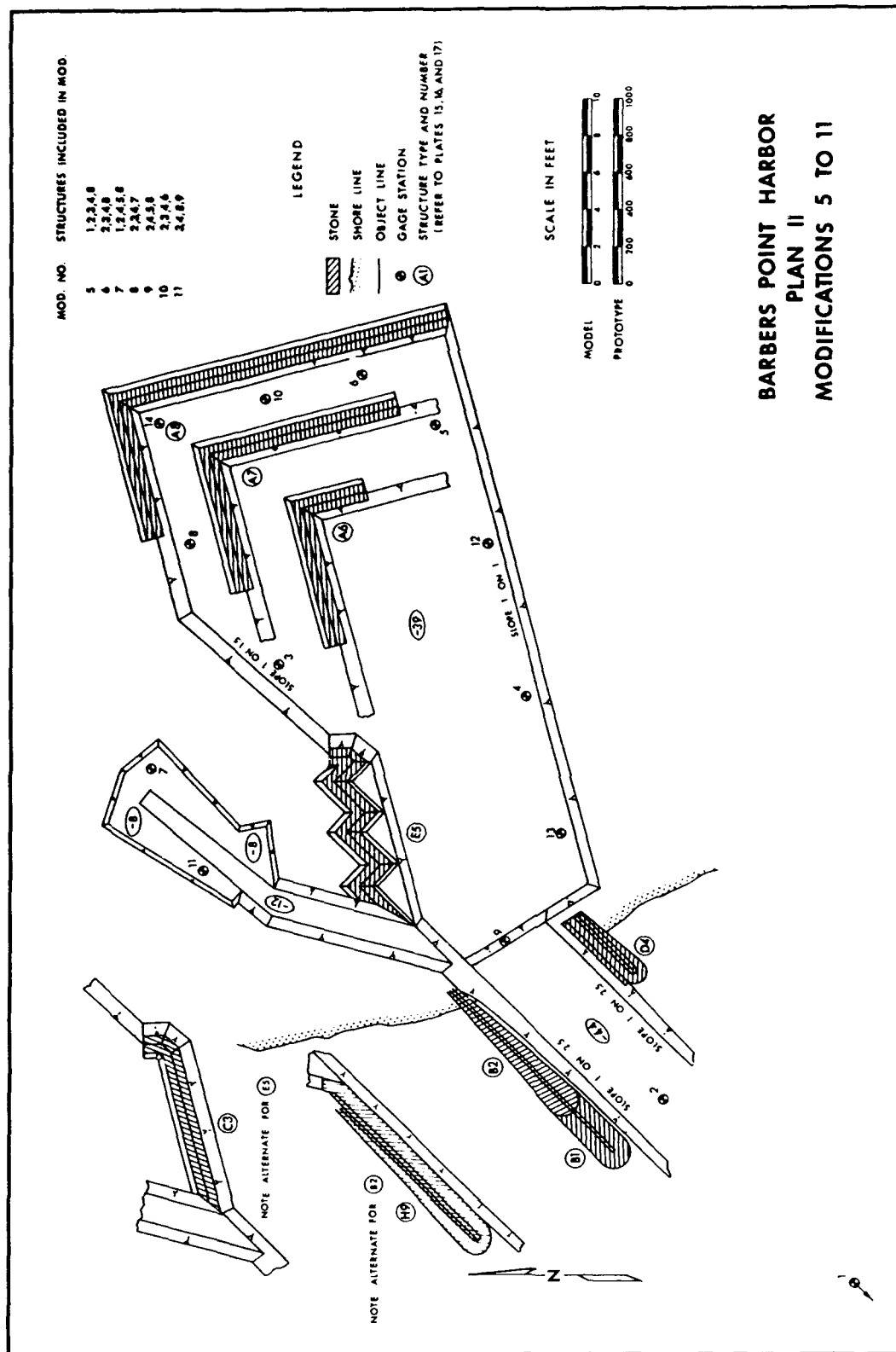
Figure 12. Plan II, Modifications 5 - 11
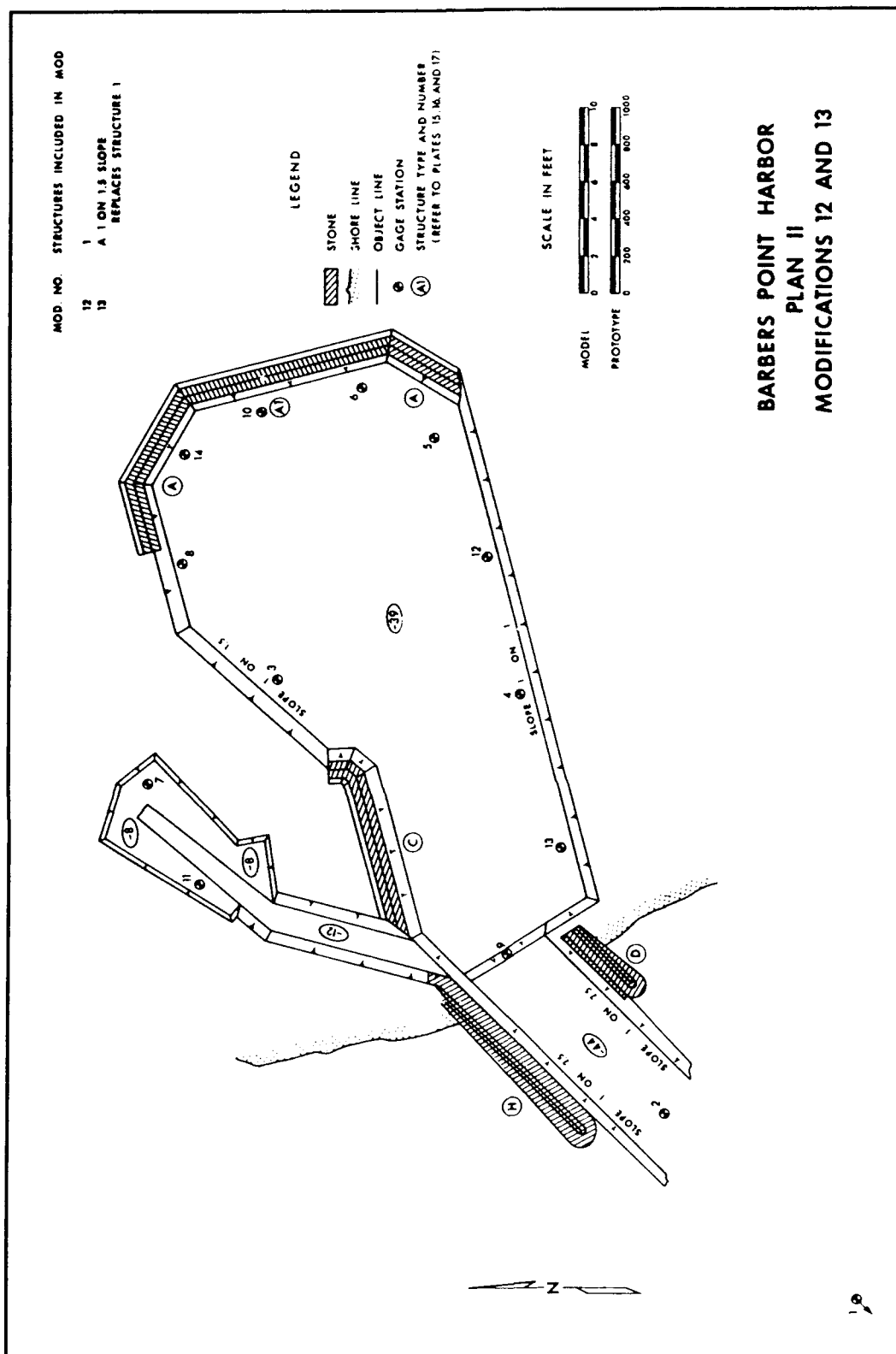
Figure 13. Plan II, Modifications 12 and 13
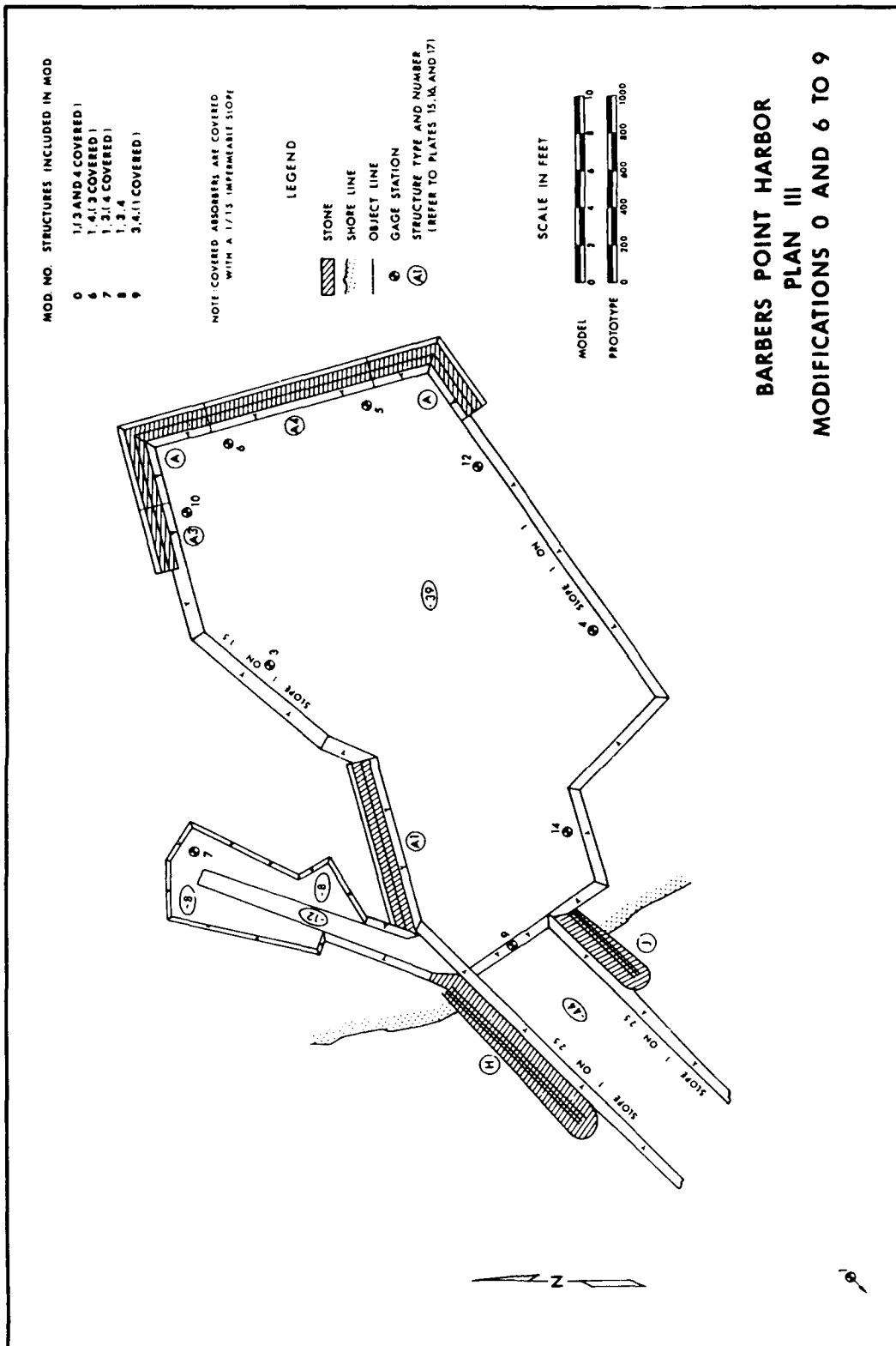
Figure 14. Plan III, Modifications 0, 6 - 9
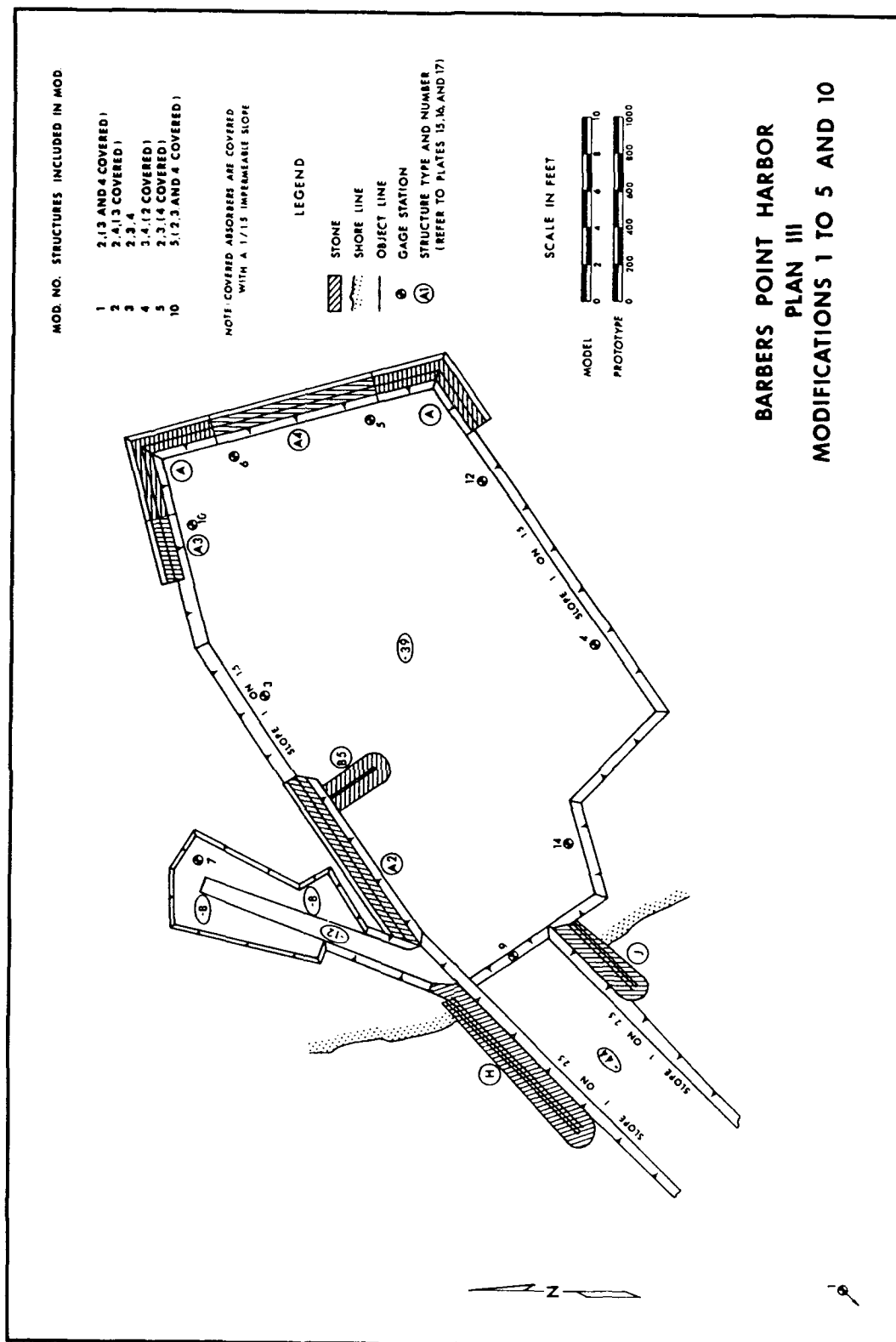
Figure 15. Plan III, Modifications 1 - 5 and 10
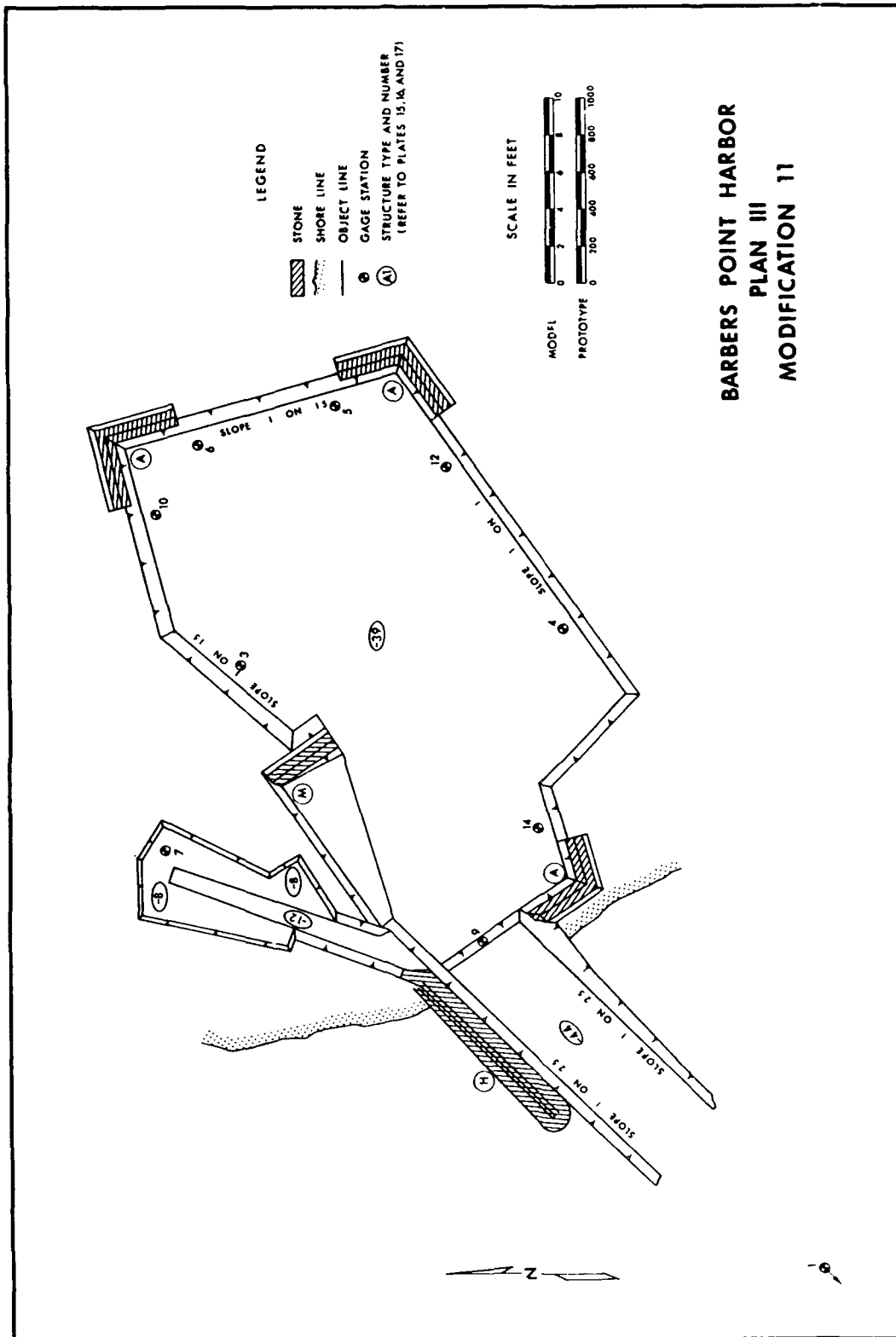
Figure 16. Plan III, Modification 11
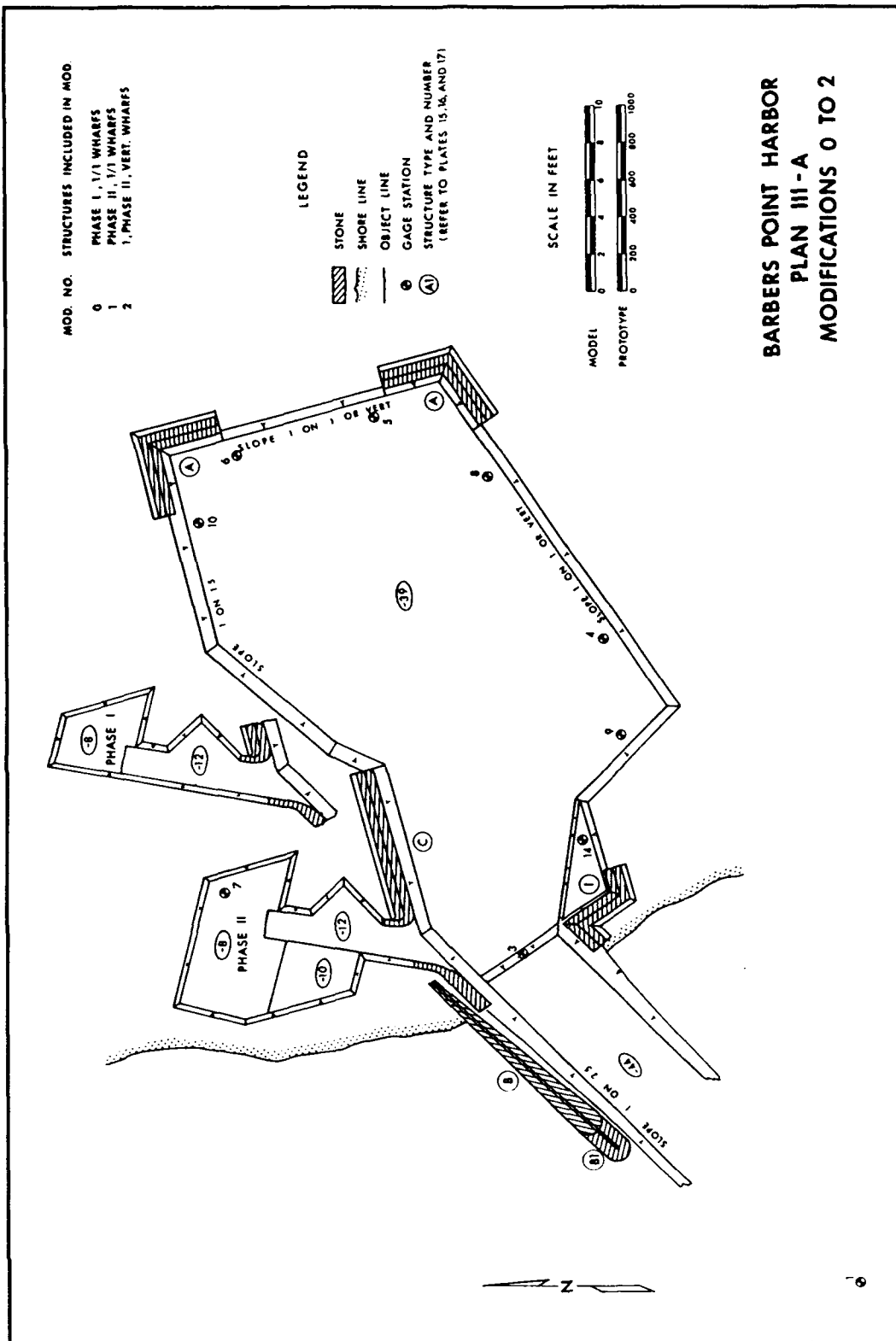
Figure 17. Plan III-A, Modifications 0 - 2
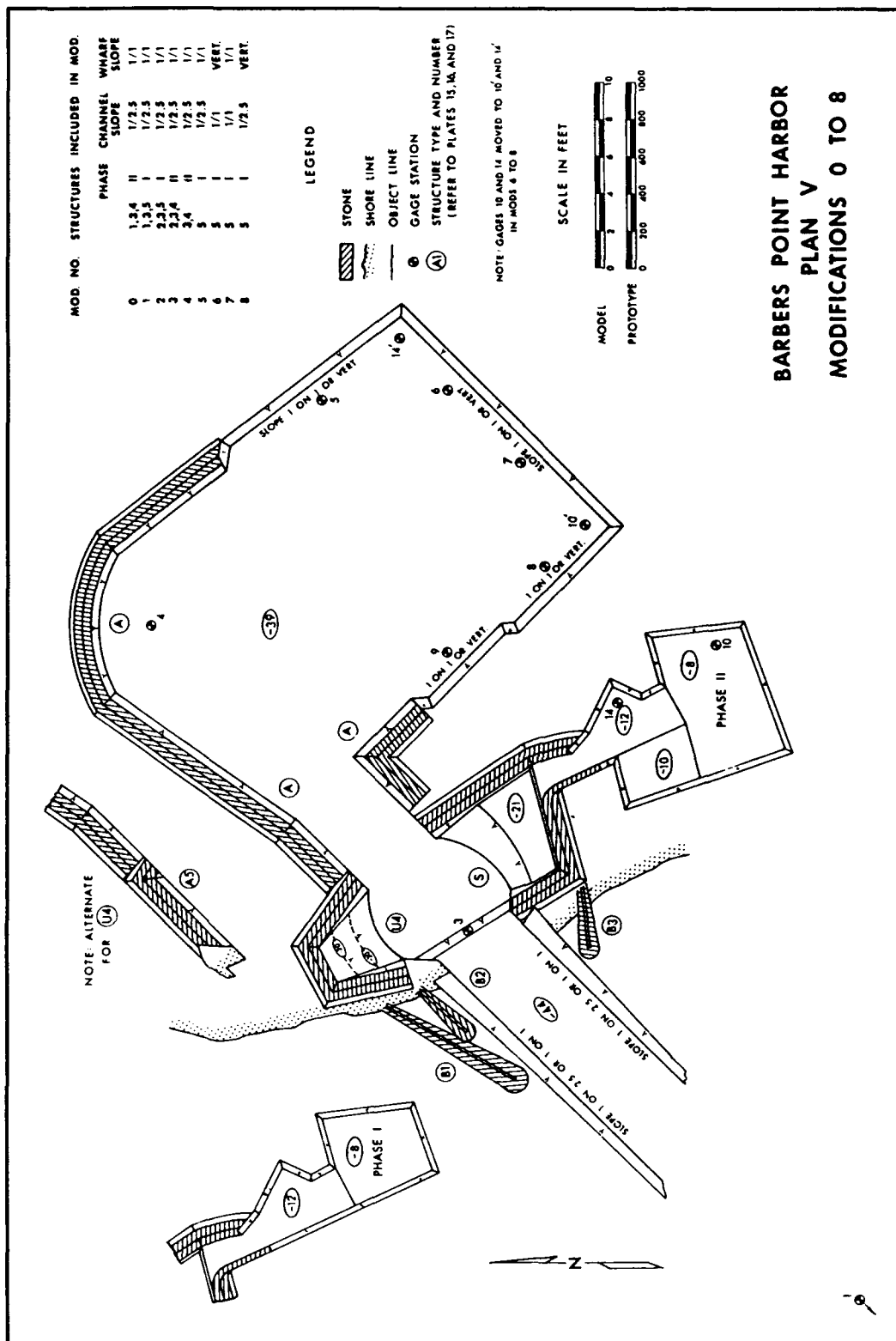
Figure 18. Plan V, Modifications 0 - 8
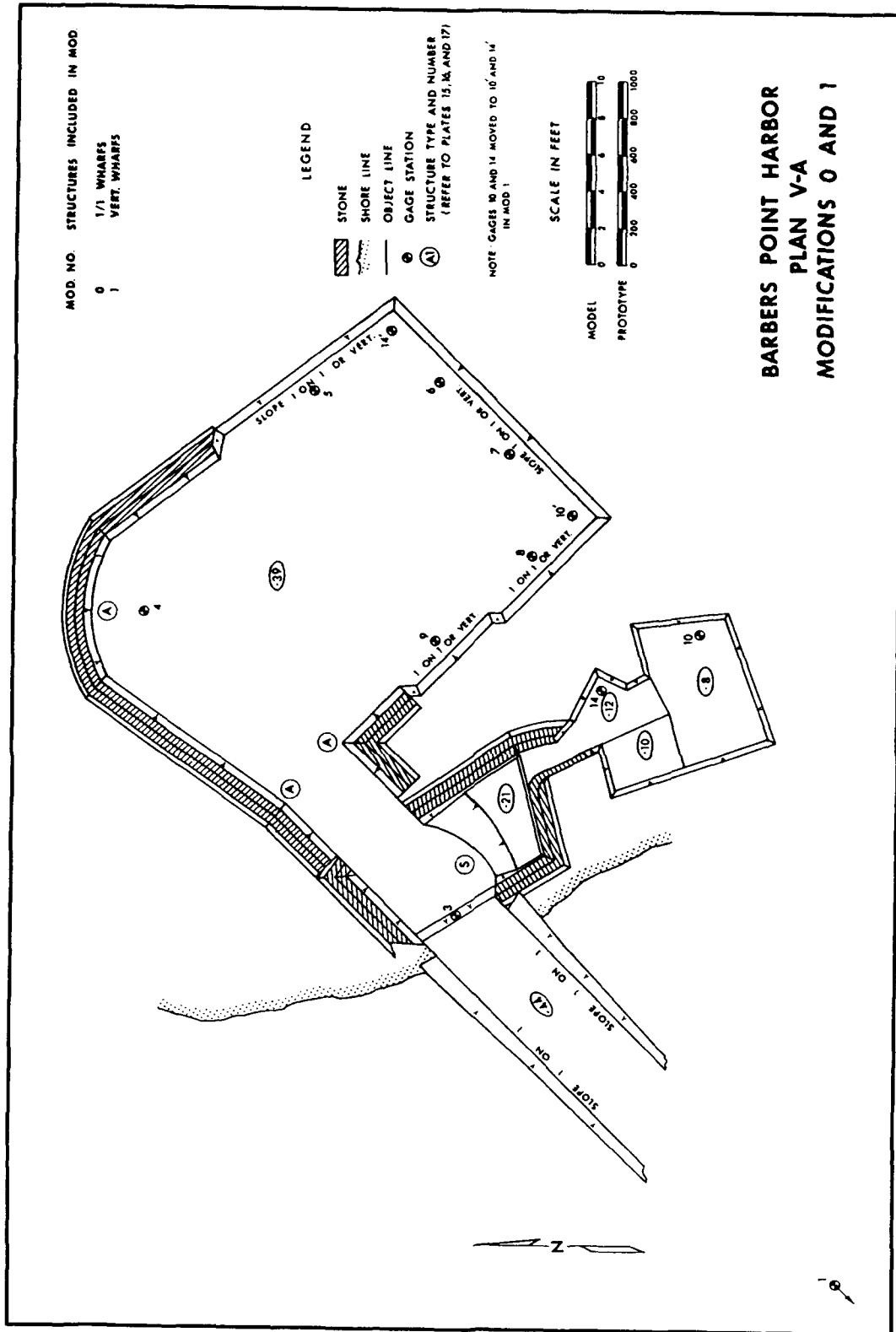
Figure 19. Plan V-A, Modifications 0 and 1

direction. To compensate for the change in wave directions in the model, POD projected the orthogonal rays seaward from the 60-ft contour line considering the modified model bathymetry. The resulting refraction diagrams were analyzed to select groups of waves that could be reasonably combined for one generator position. After revisions by WES, the wave groupings, seven wave generator positions, and an estimation of duration and magnitude of deepwater wave conditions were established. It should be noted that some waves from the same deepwater direction, but with different wave period, were grouped with waves from another direction.

The base tests were run using the prototype estimates of deepwater wave conditions. Results of these tests were used to determine five critical wave conditions selected to facilitate testing of proposed design Plans I, II, and III and modifications to each plan. Selected test wave conditions are tabulated in Table 2. In testing Plan V, wave condition B was modified to an 18-sec wave approaching from the 270-deg azimuth, with deepwater and shallow-water wave heights of 15 and 13.8 ft, respectively. The test wave conditions used for Plan V-A are tabulated in Table 3. Documentation explaining why a separate set of test wave conditions was used and the procedure used to estimate prototype wave conditions is unavailable.

Table 2 Hydraulic Model Selected Test Wave Conditions, Plans I, II, and III				
Wave	Wave Period (sec)	Deepwater Wave Height (ft)	Shallow-Water Wave Height (ft)	Deepwater Wave Direction
A	8	15	13.8	270.0
B	20	10	6.4	315.0
C	14	15	9.4	315.0
D	12	20	17.9	225.0
E	12	18	15.4	202.5

Table 3
Statistical Prototype Wave Conditions for Shallow Water

Wave Height (ft)	Duration (hr/yr) at Indicated Wave Period (sec)									
	4	6	8	10	12	14	16	18	20	Total
Generator Positions 1, 2, and 3 Combined at Generator Position 2 (240 deg)										
1-2	132	0	0	0	885	412	0	0	0	1429
2-4	0	149	0	0	1209	1559	70	0	0	2987
4-6	0	0	70	0	0	0	0	0	0	70
6-8	0	0	18	0	0	0	0	0	0	18
8-10	0	0	0	0	0	0	0	0	0	0
10-12	0	0	0	11	0	0	0	0	0	11
12-14	0	0	0	0	2	0	0	0	0	2
14-16	0	0	0	0	2	0	0	0	0	2
20	0	0	0	0	0	3	0	0	0	3
Total	132	149	88	11	2098	1974	70	0	0	4522
Generator Position 4 (220 deg)										
1-2	35	0	0	0	0	0	0	0	0	35
2-4	0	35	0	0	0	96	140	0	0	271
4-6	0	0	26	0	0	0	0	0	0	26
6-8	0	0	9	0	0	0	0	0	0	9
8-10	0	0	0	0	0	0	0	0	0	0
10-12	0	0	0	9	0	0	0	0	0	9
12-14	0	0	0	0	0	0	0	0	0	0
14-16	0	0	0	0	2	0	0	0	0	2
24	0	0	0	0	1	0	0	0	0	1
Total	35	35	35	9	3	96	140	0	0	353
Generator Position 5 (200 deg)										
1-2	26	0	0	0	0	0	0	0	0	26
2-4	0	26	0	0	0	0	0	0	0	26
4-6	0	0	26	0	0	0	0	35	9	70
6-8	0	0	9	0	0	0	0	44	0	53
8-10	0	0	0	0	0	0	0	61	0	61
10-12	0	0	0	0	0	0	0	26	0	26
12-14	0	0	0	9	0	0	0	0	0	9
14-16	0	0	0	0	2	0	0	0	0	2
20	0	0	0	0	0	0	0	0	1	1
Total	26	26	35	9	2	0	0	166	10	274

(Continued)

Table 3 (Concluded)

Wave Height (ft)	Duration (hr/yr) at Indicated Wave Period (sec)									
	4	6	8	10	12	14	16	18	20	Total
Generator Position 6 (184 deg)										
1-2	0	0	0	0	0	9	184	0	0	193
2-4	9	26	0	0	0	9	192	9	0	245
4-6	0	0	0	0	0	140	126	35	0	301
6-8	0	0	17	0	0	9	56	149	61	292
8-10	0	0	0	0	0	0	0	9	0	9
10-12	0	0	0	3	0	0	0	0	0	3
12-14	0	0	1	0	0	0	0	6	0	7
14-16	0	0	0	0	0	0	0	0	0	0
16-18	0	0	0	0	0	0	9	0	0	9
18-20	0	0	0	0	0	0	0	0	10	10
Total	9	26	18	3	0	167	567	208	71	1069
Generator Position 7 (348 deg)										
1-2	0	0	52	315	254	9	0	0	0	630
2-4	0	0	0	79	358	613	0	0	0	1050
4-6	0	0	0	26	114	78	0	0	0	218
6-8	0	0	0	26	9	9	0	0	0	44
8-10	0	0	9	0	6	8	0	0	0	23
Total	0	0	61	446	741	717	0	0	0	1965

Summary of test results

Results of the study concluded that wave action within the project should be experienced for the tested plans as summarized below:

Plan I - intolerable conditions during most storm periods.

Plans II and III - intolerable conditions but of less duration than Plan I.

Plan III-A - tolerable conditions, generally exceeding maximum desired criteria less than 1 percent of the time.

Plan V - within the maximum desired criteria, except on rare occasions.

Plan V-A - within the maximum desired criteria, except less than 1 percent of the time, in the small boat harbor.

Based on the results of the study, the harbor was designed using the concepts of Plan V-A which consisted of a near trapezoidal shaped, 38-ft-deep, 77-acre basin with a 450-ft-wide, 42-ft-deep entrance channel and a 12-ft-deep small boat harbor located to the south of the deep-draft harbor basin. Results of Plan V-A are provided in Table 4, which lists 34 critical

wave conditions for this plan. The incident wave period and height with resulting wave height at each gage location in the harbor are categorized by the incident wave direction, or wave generator position.

Table 4
Test Results for Plan V-A, Modification 0

Period (sec)	Height (ft)	Resulting Wave Height (ft) by Gage Number								
		3	4	5	6	7	8	9	10	14
Generator Position 2										
6	4	2.2	1.0	0.2	0.1	0.1	0.1	0.1	0.1	0.1
8	8	2.0	0.6	0.1	0.1	0.0	0.0	0.0	0.0	0.3
10	12	2.6	0.6	0.1	0.1	0.1	0.1	0.1	0.1	0.6
12	16	4.2	1.2	0.2	0.2	0.1	0.2	0.1	0.2	0.4
14	14	3.6	0.8	0.2	0.1	0.2	0.1	0.1	0.1	0.4
14	20	5.6	1.4	0.4	0.2	0.4	0.3	0.2	0.4	0.6
16	4	0.8	0.0	0.0	0.0	0.0	0.0	0.0	0.0	0.0
Generator Position 4										
8	8	2.5	0.8	0.2	0.1	0.0	0.1	0.0	0.0	0.3
10	12	4.0	0.7	0.3	0.1	0.2	0.2	0.1	0.3	0.4
12	16	4.2	1.0	0.2	0.2	0.3	0.4	0.3	0.1	0.6
12	24	4.7	1.8	0.4	0.2	0.1	0.4	0.2	0.1	0.6
Generator Position 5										
10	14	4.1	0.9	0.4	0.3	0.3	0.2	0.2	0.3	1.0
12	12	4.2	1.0	0.4	0.6	0.3	0.8	0.3	0.1	0.4
12	16	5.2	1.1	0.3	0.6	0.3	0.9	0.3	0.1	0.6
18	8	5.2	0.7	0.3	0.3	0.2	0.4	0.2	0.1	0.4
18	12	4.5	0.8	0.4	0.3	0.2	0.3	0.2	0.3	0.4
20	6	3.6	0.6	0.2	0.3	0.2	0.2	0.1	0.1	0.1
20	20	6.4	1.4	0.4	0.4	0.4	0.6	0.3	0.3	0.7
Generator Position 6										
4	4	3.1	0.2	0.0	0.0	0.0	0.0	0.0	0.0	0.3
8	14	9.0	2.2	0.9	0.2	0.1	0.1	0.1	0.6	1.1
10	12	6.6	1.9	0.6	0.2	0.3	0.2	0.2	0.6	1.1
14	8	4.1	0.7	0.7	0.2	0.6	0.3	0.3	0.4	0.8
16	8	4.5	1.0	0.4	0.3	0.2	0.2	0.6	0.1	0.7
16	14	6.7	0.8	0.8	0.6	0.4	0.3	1.0	0.3	0.6
16	18	6.0	0.8	0.4	0.7	0.6	0.6	0.6	0.3	1.0
18	10	5.7	1.0	0.3	0.3	0.3	0.4	0.3	0.1	0.4
18	14	6.3	1.1	0.4	0.4	0.6	0.4	0.6	0.3	0.6
20	8	5.6	0.8	0.3	0.6	0.3	0.4	0.4	0.3	0.6
20	10	6.6	1.5	0.8	0.7	0.4	0.4	0.6	0.4	0.7
20	10	5.9	1.9	0.8	0.7	0.4	0.4	0.6	0.4	0.7
										(Continued)

Table 4 (Concluded)										
Period (sec)	Height (ft)	Resulting Wave Height (ft) by Gage Number								
		3	4	5	6	7	8	9	10	14
Generator Position 7										
8	10	7.4	2.4	0.6	0.3	0.1	0.1	0.1	0.1	0.8
10	8	3.4	2.4	0.7	0.3	0.3	0.2	0.4	0.3	1.1
12	10	6.0	1.2	0.4	0.6	0.4	0.9	0.7	0.3	0.7
14	10	6.5	1.4	1.0	0.4	0.9	0.6	0.8	0.4	1.3

Numerical Model Study 1978

A post-authorization study to assess the basic planning decisions for Barbers Point deep-draft harbor indicated a need for a basin larger than the original design. The harbor needed to be capable of accommodating 720-ft-long container vessels as well as 900-ft-long vessels projected to use the facility in the future. Based on concepts resulting from the hydraulic model study, a new plan consisting of a 94-acre, 38-ft-deep basin, with a 4,280-ft-wide and 38 to 42-ft-deep entrance channel was developed (Figure 20). The small boat harbor was eliminated. At the request of POD, WES conducted a numerical harbor oscillation study of the final deep-draft harbor design during the period 1 January 1977 to 1 April 1977. The purpose of the study was to investigate the harbor oscillations excited by waves with periods from 20 sec to 15 min. The investigation was conducted to ensure that the deep-draft basin expansion would not introduce undesirable oscillations in the barge harbor or characteristic oscillations of its own.

Numerical model

The response of the proposed deep-draft harbor to long period waves was determined through application of a hybrid finite element model developed by Chen and Mei (1974). The linear, long wave model allows arbitrary configurations and variable bathymetry. The harbor response is calculated for each incident wave condition with results available for wave height amplification factors at each nodal point and current velocities at each element centroid. This report will concentrate on the results involving the wave height amplification factors. For details involving the investigation of current velocities, the reader is referenced to Durham (1978). At the time of the study, the hybrid element model was the only numerical harbor oscillation model available with the capability to economically calculate resonance effec. .n large complex harbors. The amplification peaks predicted by the numerical model may be much larger than the peaks which actually occur in nature since the model neglects all dissipative processes except radiation of energy from the harbor. The
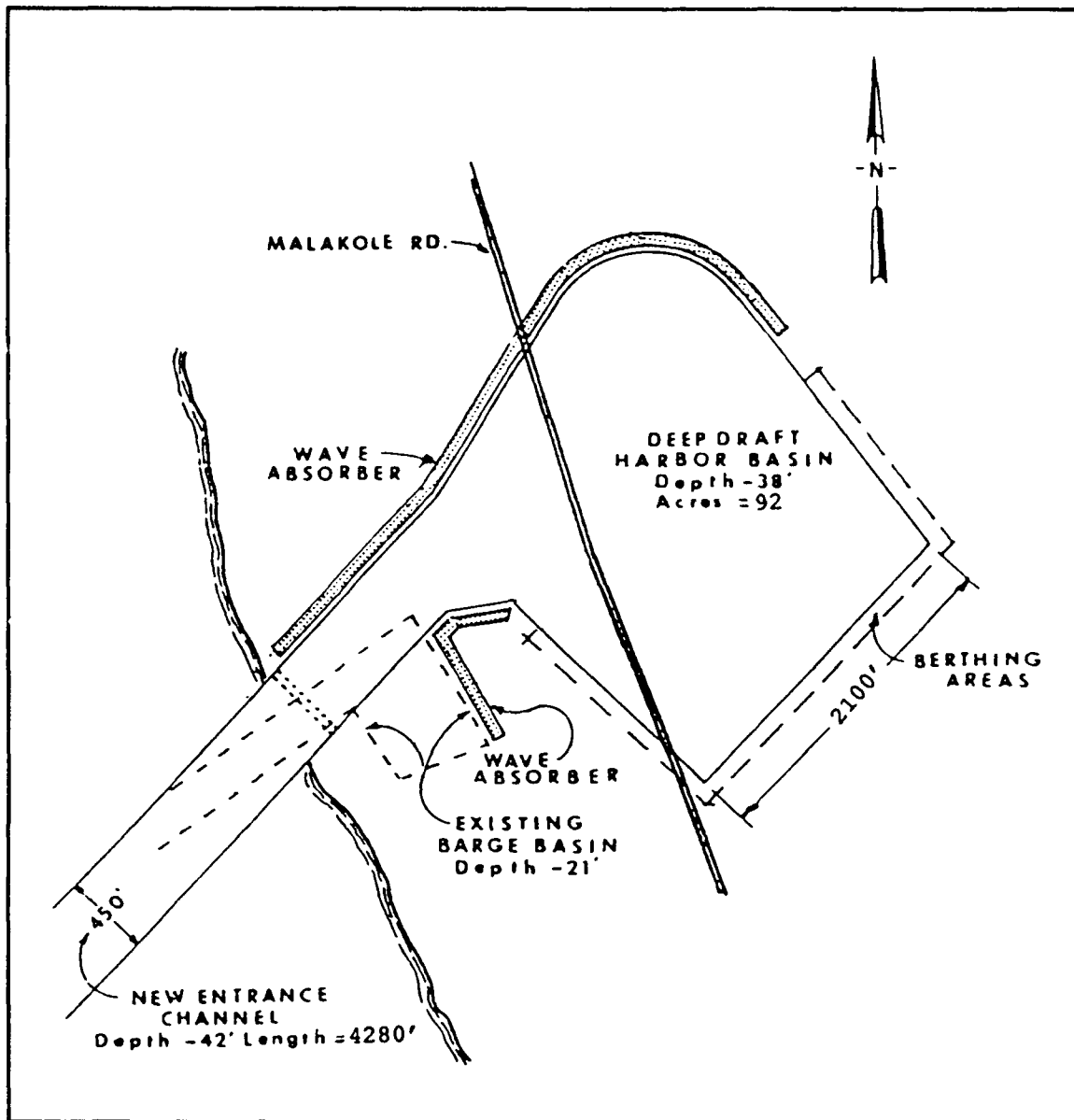
Figure 20. Numerical model study, 1978

model, however, adequately predicts the relative severity of various modes of oscillation. For further details on the theory of the numerical model used in this study, the reader is referenced to Durham (1978). A detailed description of the latest version of the harbor oscillation model is provided in Chapter 5 of this report.

Finite element grid

The finite element grid used to model the deep-draft harbor is shown in Figure 21. The grid included the deep-draft harbor, entrance channel, and barge harbor. The semicircular ocean boundary extended approximately 385 ft offshore. The total number of elements (triangles) and nodes (triangular corners) were 2,334 and 1,277, respectively. The largest elements were designed with an approximate eight elements per wavelength resolution based on a local wavelength of 20 sec. Smaller dimensions were selected for elements along docking facilities and wave absorbers as well as in the areas of depth and alignment changes in the channels and basins. Water depths were assigned to the centroid of each element; therefore, the chosen water depth represented a mean value over the element. Grid bathymetry was obtained from Plate 2 of Barbers Point Harbor Design Memorandum No. 1, Plan Formulation (USAED, Honolulu 1977).

For each incident wave condition, wave height amplification factors were saved from 30 nodes selected at locations in the harbor of major interest for navigation and ship mooring. The location and station number for the output nodes are shown in Figure 22. Station numbers 1 through 18 are located in the deep-draft harbor basin, 19 through 23 are located in the entrance channel, and 24 through 30 are located in the barge harbor. Wave height amplification factors at each node over the entire grid were also saved for incident wave periods resulting in resonant modes of oscillation. The data were used to create contour plots of wave amplification over the entire harbor.

Test wave conditions

Historical wave characteristics, based on hindcast statistics supplemented by wave observations and measurements, estimated that the barge harbor experienced long-period surging problems of approximately 2 min wave period. Therefore, the proposed deep-draft harbor was expected to be subjected to long period wave energy of at least 2 min. Test conditions consisted of incident waves from a direction parallel to the axis of the entrance channel (approximately 225.0-deg azimuth) with periods from 15 sec to 27 min. The initial values for the wave period increment over specified period ranges are listed in Table 5. Resonant peaks were identified within each wave period range, and the model was retested in increments of 0.02 to 0.01 sec about the identified resonant peaks to refine the peak wave periods of oscillation.

FINITE ELEMENT GRID

BARBERS POINT HARBOR STUDY
PROPOSED DEEP DRAFT HARBOR
PHASE 1

SCALE IN FEET

NOTE: NUMBER OF NODE POINTS = 1277
NUMBER OF ELEMENTS = 2334
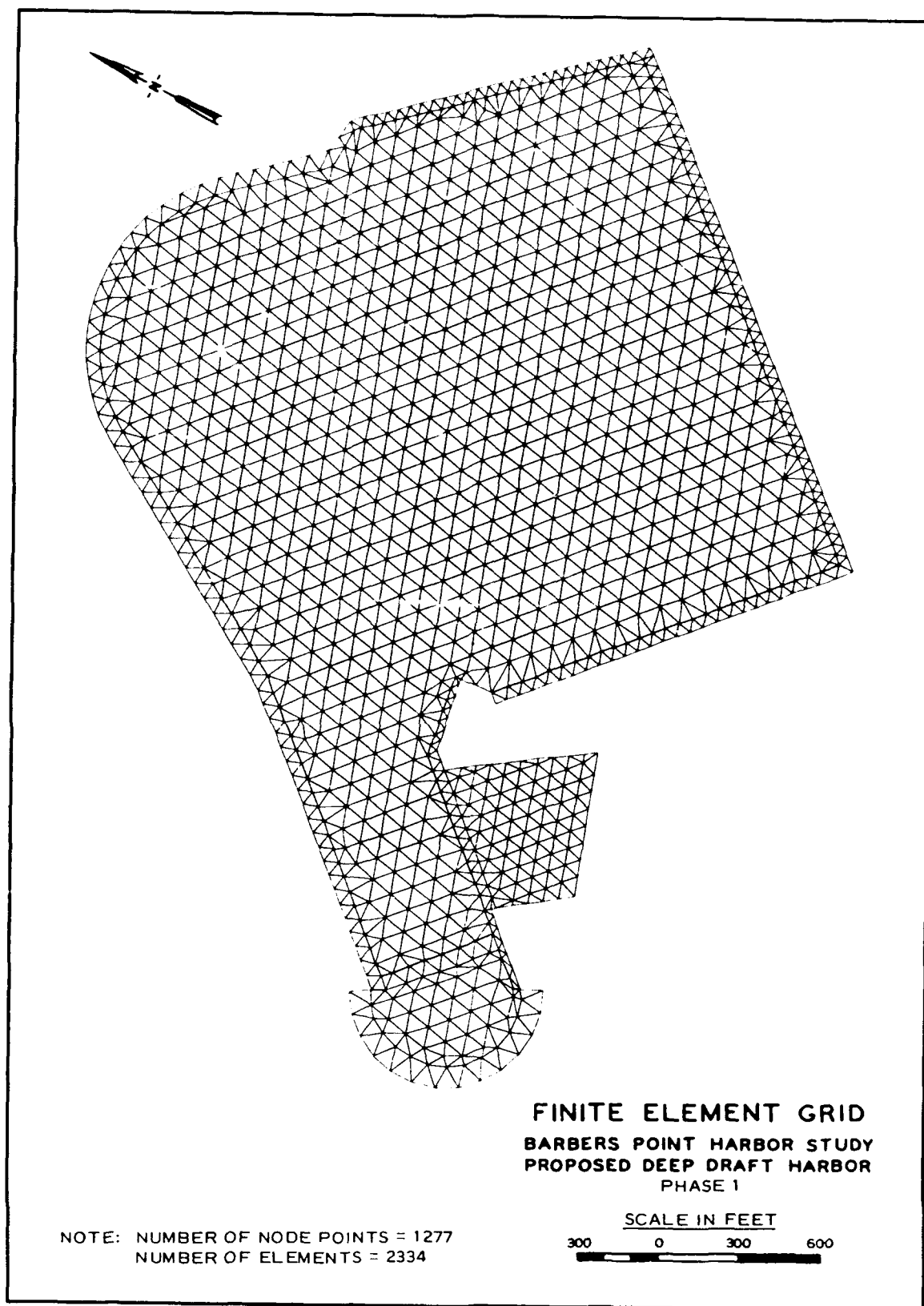
Figure 21. Finite element grid, 1978

FINITE ELEMENT GRID
BARBERS POINT HARBOR STUDY
PROPOSED DEEP DRAFT HARBOR
ELEVATION STATIONS, PHASE 1

LEGEND
● ELEVATION STATION
1 STATION NO.

NOTE: NUMBER OF NODE POINTS = 1277
NUMBER OF ELEMENTS = 2334

SCALE IN FEET
300   0   300   600
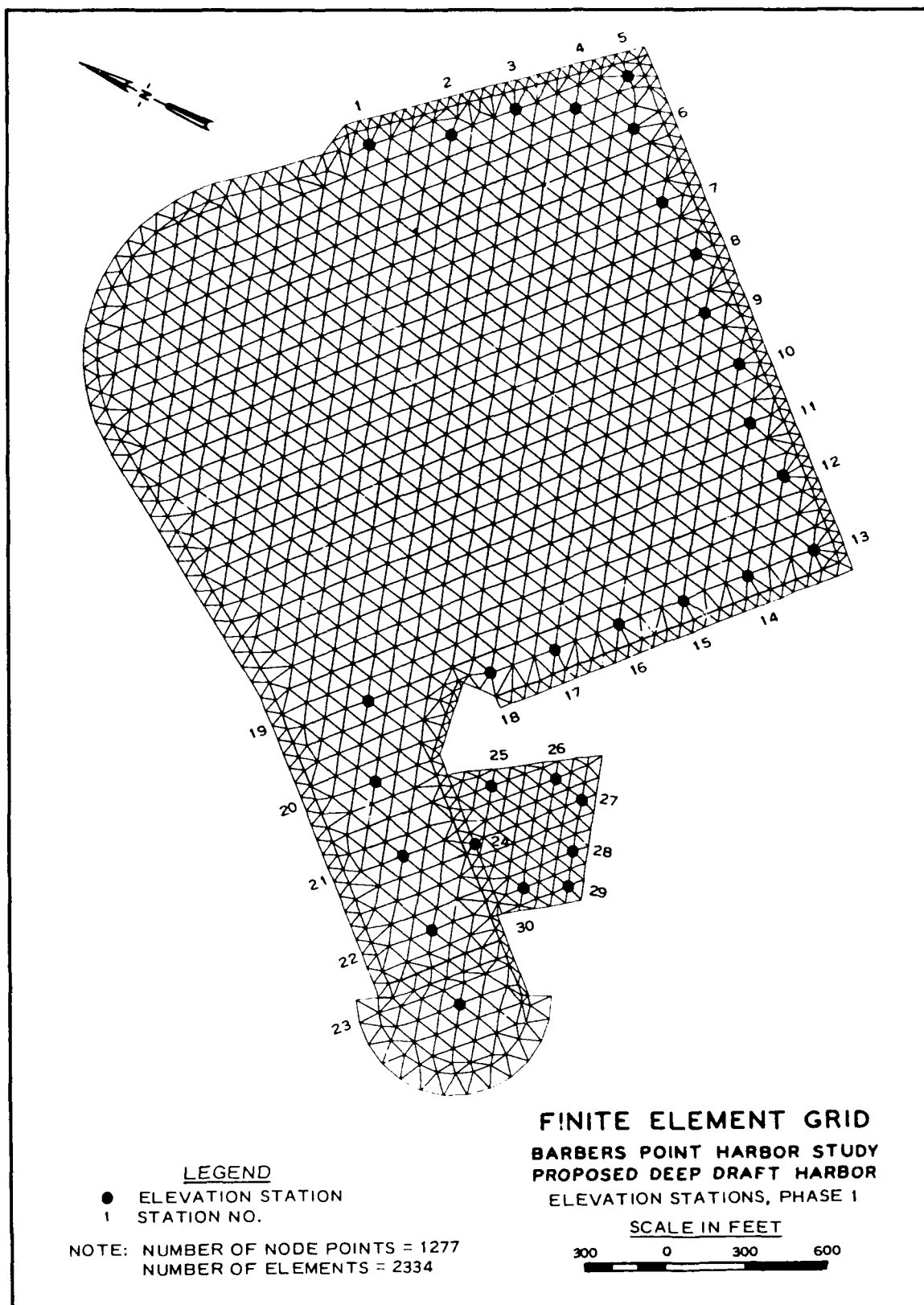
Figure 22. Numerical model output stations, 1978

Table 5
Initial Numerical Model Wave Period Increments

ΔT (sec)	Range of Wave Periods (sec)
1.0	15 - 68
2.0	70 - 100
2.5	102.5 - 200
5.0	205 - 360
10.0	370 - 720
20.0	740 - 1620

Numerical model results

For each of the 30 nodal points selected for output, a wave height amplification factor was calculated for wave periods from 15 sec to 27 min. The wave height amplification factor is defined as the ratio of the wave height to twice the incident wave height. This traditional definition results from the theory that a standing wave height for a straight coast with no harbor would be twice the incident wave height due to superposition of the incident and reflected waves. Frequency (wave period) response curves of predicted wave height amplification factors for each of the 30 output stations are provided in Durham (1978). Results from stations 1, 4, 14, 20, 22, 25, and 29 are shown in Figures 23 through 36.

Twenty-five resonant modes of oscillation ranging from 19.4 to 799.0 sec were identified. The wave periods of the 25 resonant modes, the corresponding wave height amplification factors, and the station number in which they occurred are listed in Table 6. The deep-draft harbor is characterized by the Helmholtz mode, which occurs at 799.0 sec (13.32 min). This mode exhibits amplification factors from 7.5 to 8.5 throughout the entire harbor. Resonant modes were also identified at wave periods of 145.0, 129.5, 107.2, and 81.9 sec, with amplification factors ranging from 4.35 to 14.45. These modes are close to the 120-sec (2-min) mode observed to excite the barge harbor. The remaining resonant modes occur between 63.0 and 19.4 sec. Contour plots of the resonant modes occurring at 799.0, 145.0, 129.5, 107.2, 81.9, 63.0, 58.6, 56.5, and 45.8 sec are shown in Figures 37 through 45.

FREQUENCY RESPONSE
WAVE HEIGHT AMPLIFICATION FACTOR
STATION 1

NOTE: R=WAVE HEIGHT AMPLIFICATION FACTOR
H=WAVE HEIGHT, FT
HCH=WAVE HEIGHT FOR CLOSED HARBOR, FT
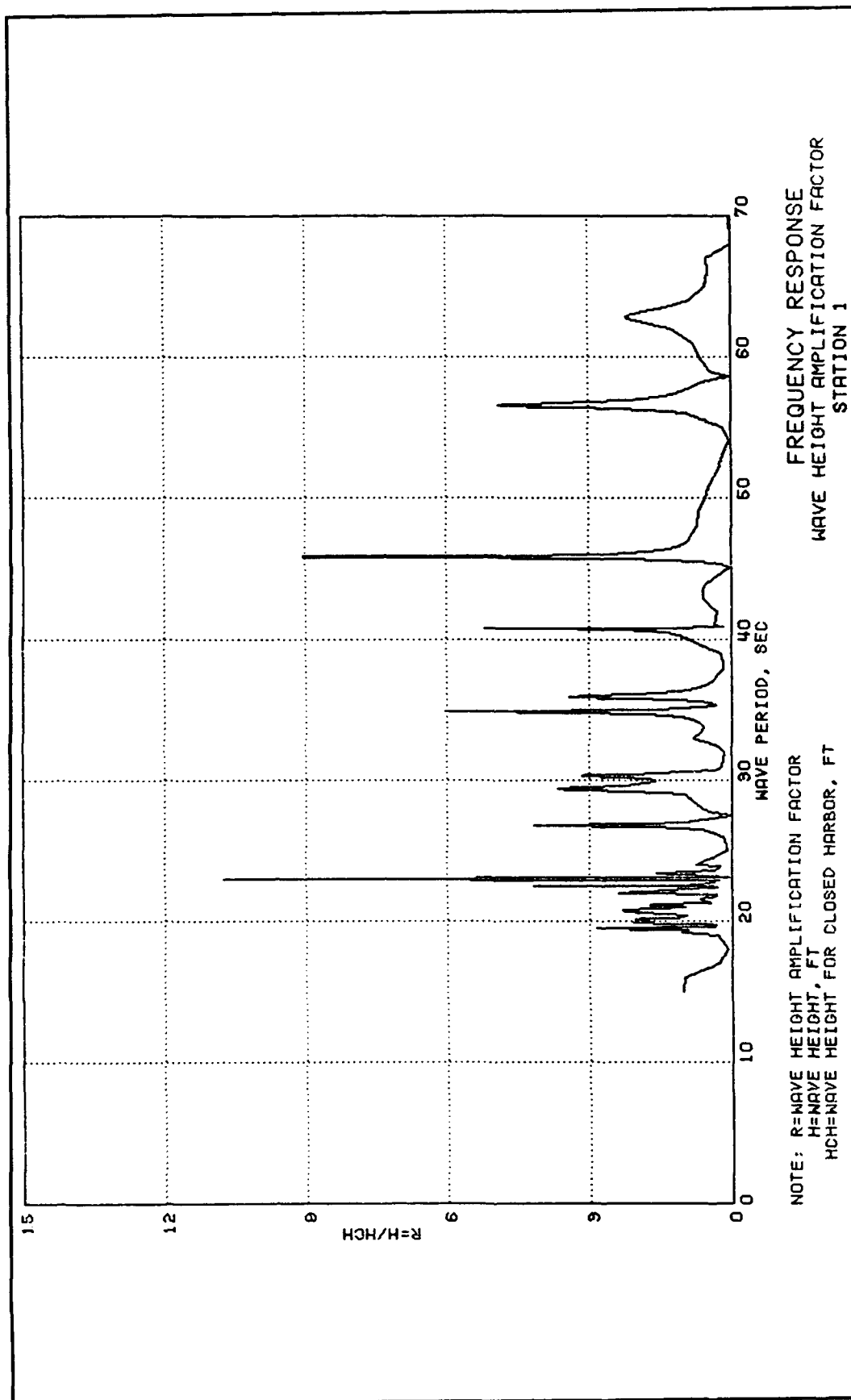
Figure 23. Frequency response curves, Station 1, 0-69 sec
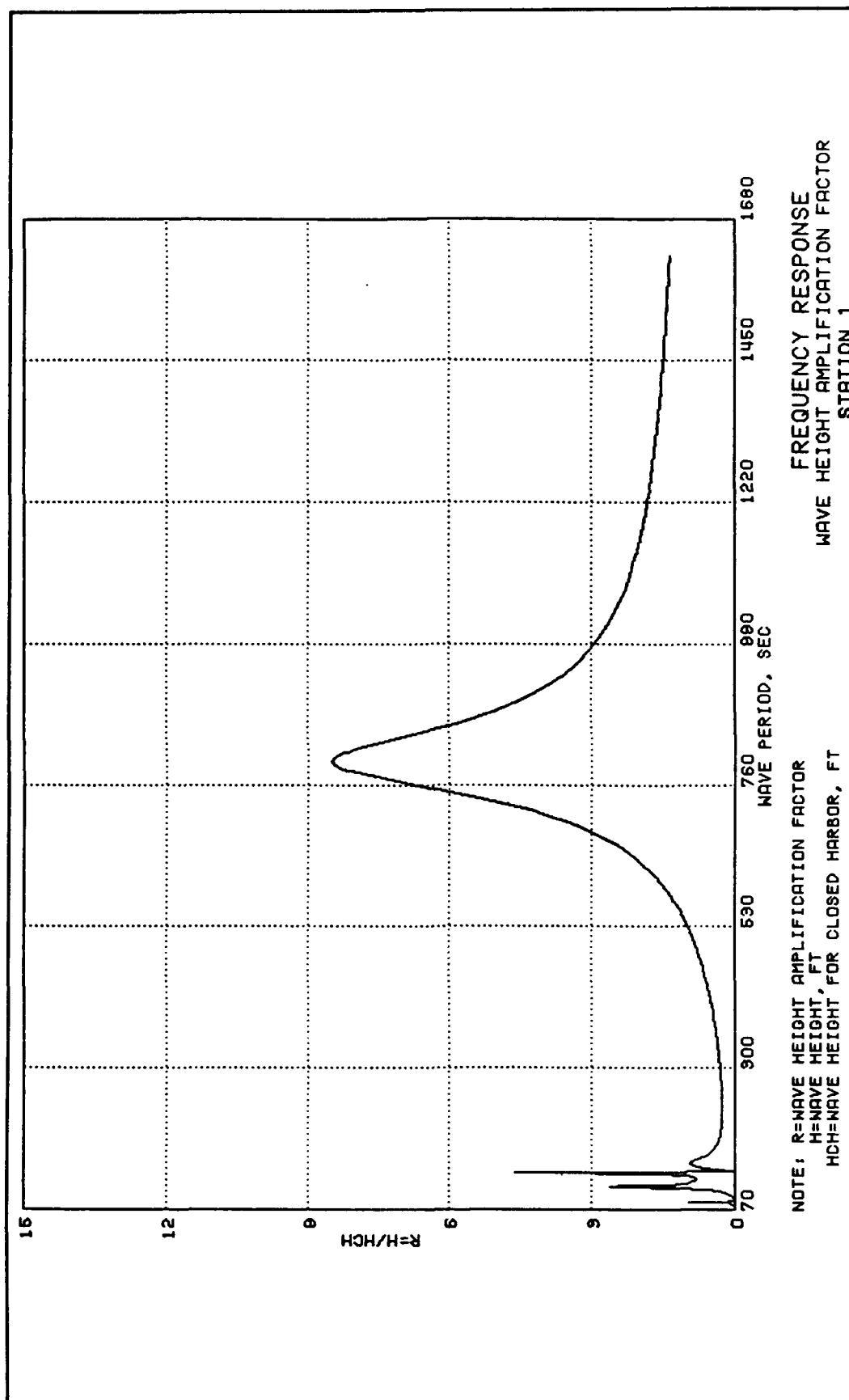
Figure 24. Frequency response curves, Station 1, 70-1680 sec
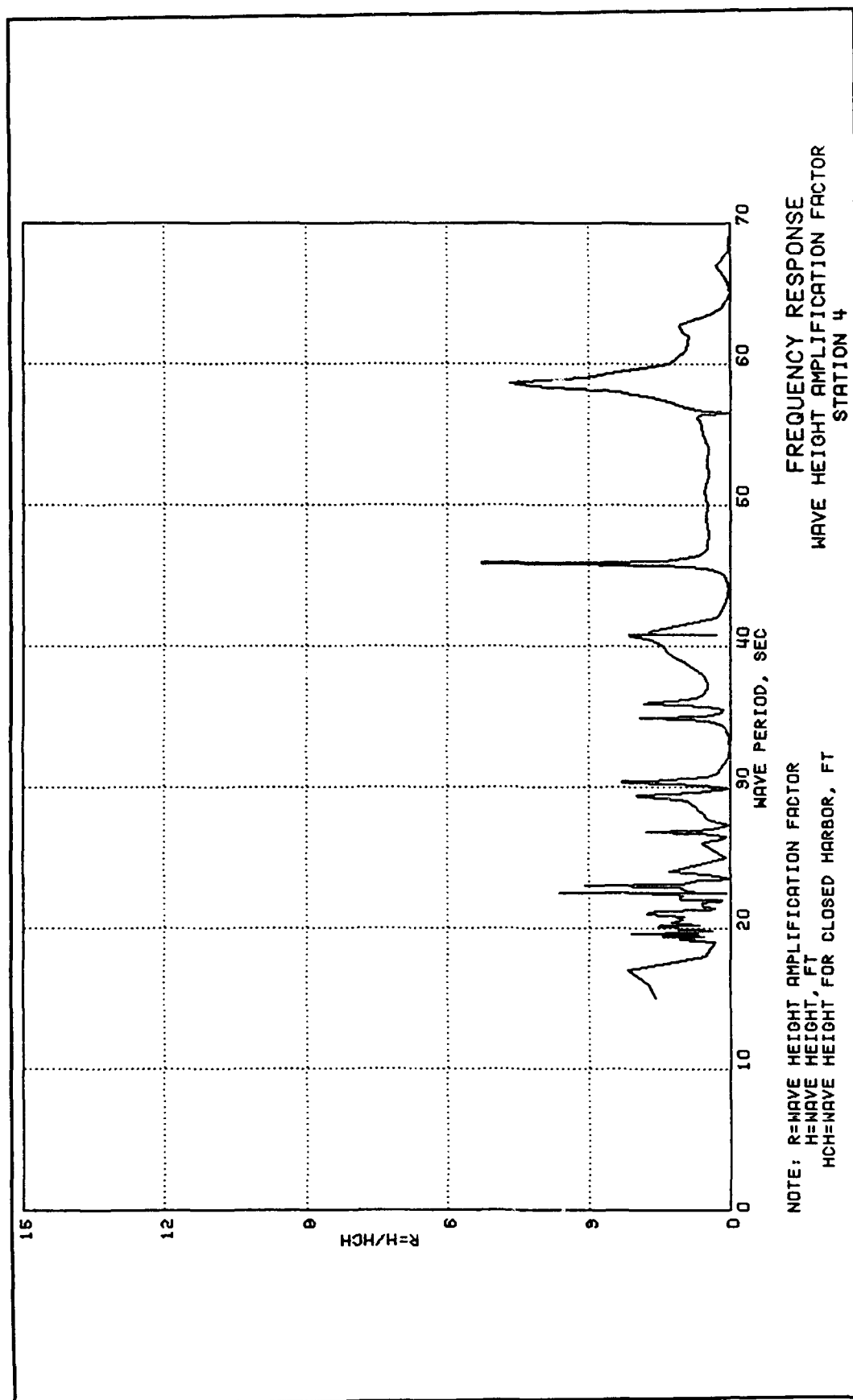
Figure 25. Frequency response curves, Station 4, 0-69 sec
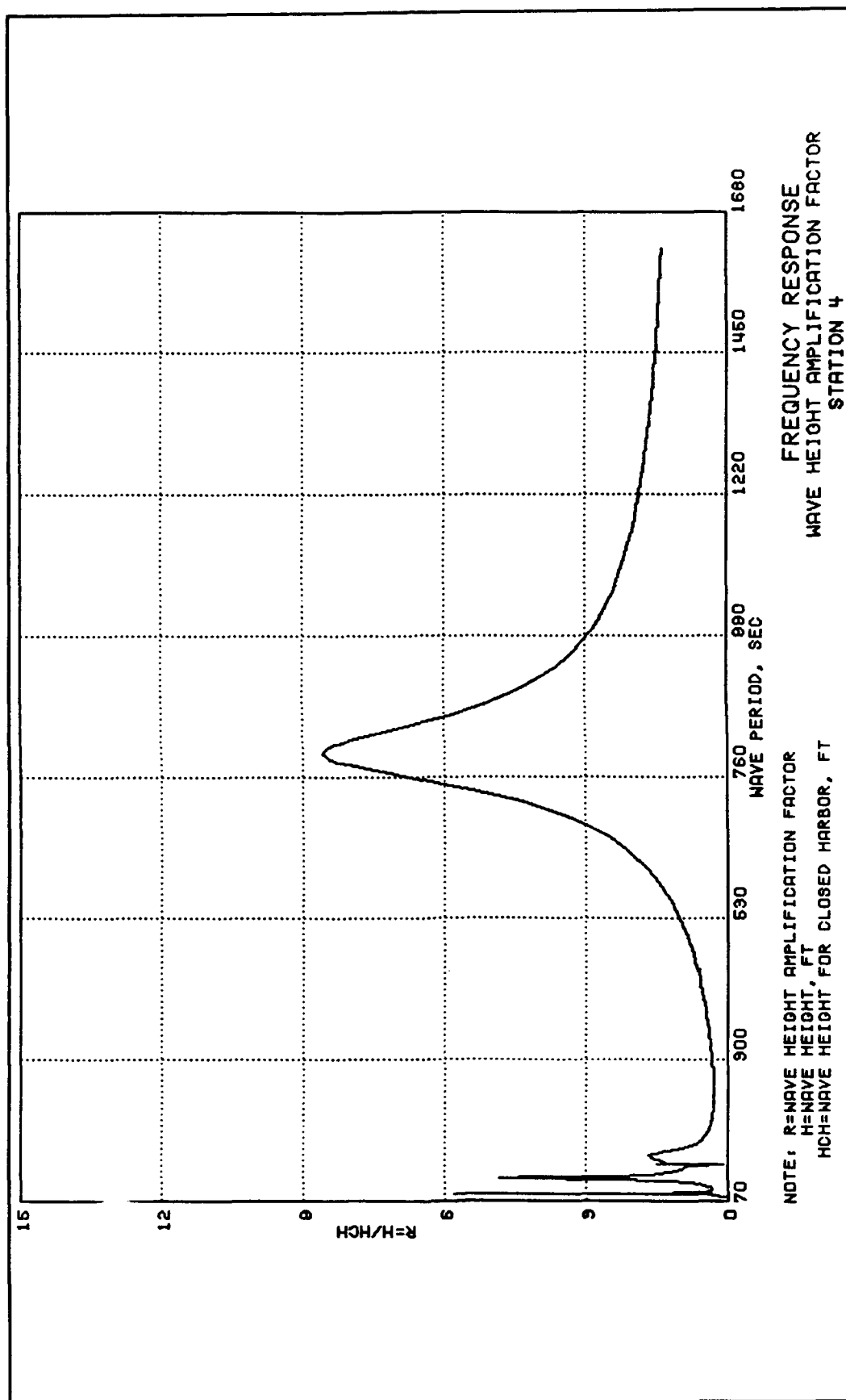
Figure 26. Frequency response curves, Station 4, 70-1680 sec

FREQUENCY RESPONSE
WAVE HEIGHT AMPLIFICATION FACTOR
STATION 14

NOTE: R=WAVE HEIGHT AMPLIFICATION FACTOR
H=WAVE HEIGHT, FT
HCH=WAVE HEIGHT FOR CLOSED HARBOR, FT
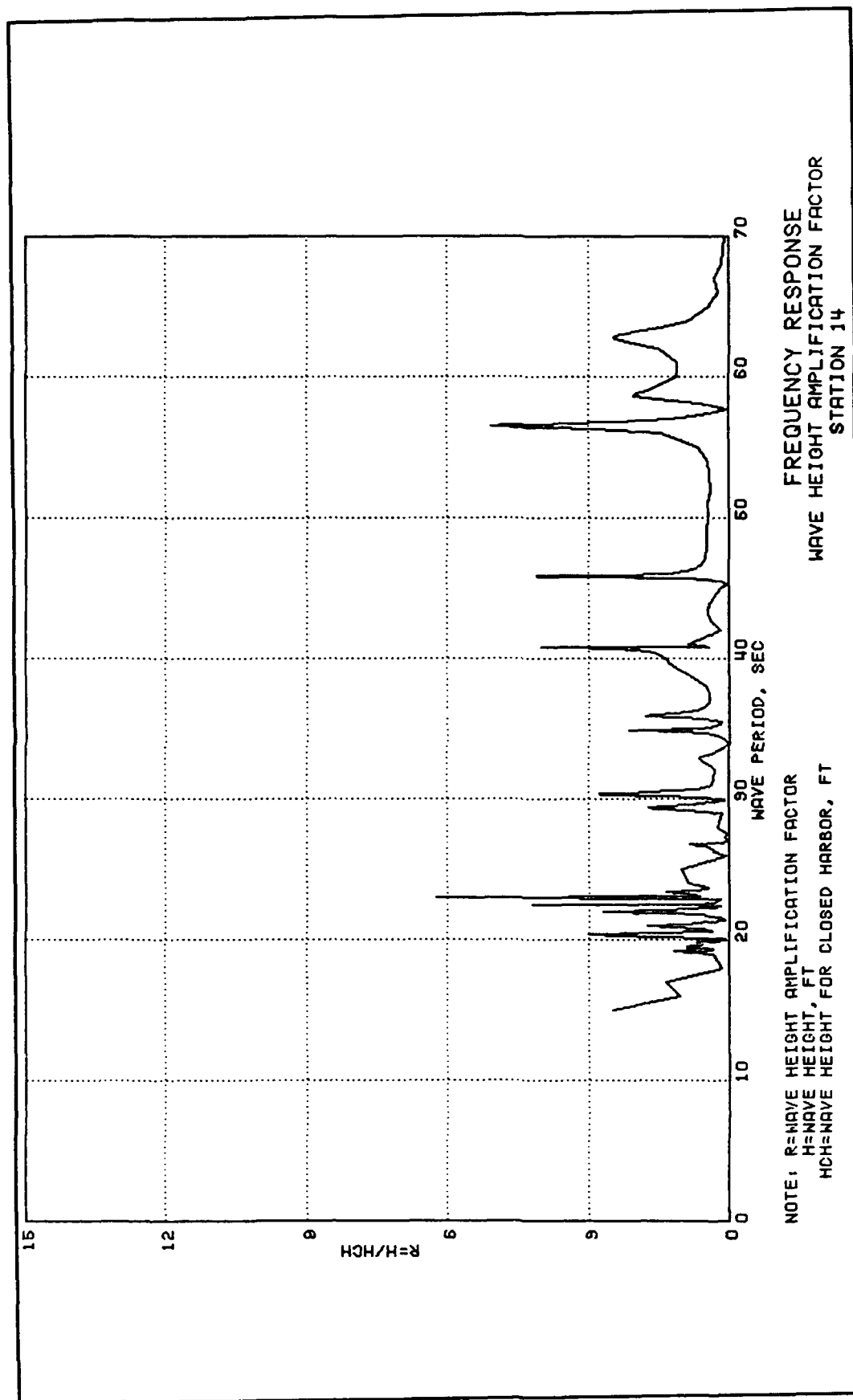
Figure 27.   Frequency response curves, Station 14, 0-69 sec

NOTE: R=WAVE HEIGHT AMPLIFICATION FACTOR
      H=WAVE HEIGHT, FT
      HCH=WAVE HEIGHT FOR CLOSED HARBOR, FT
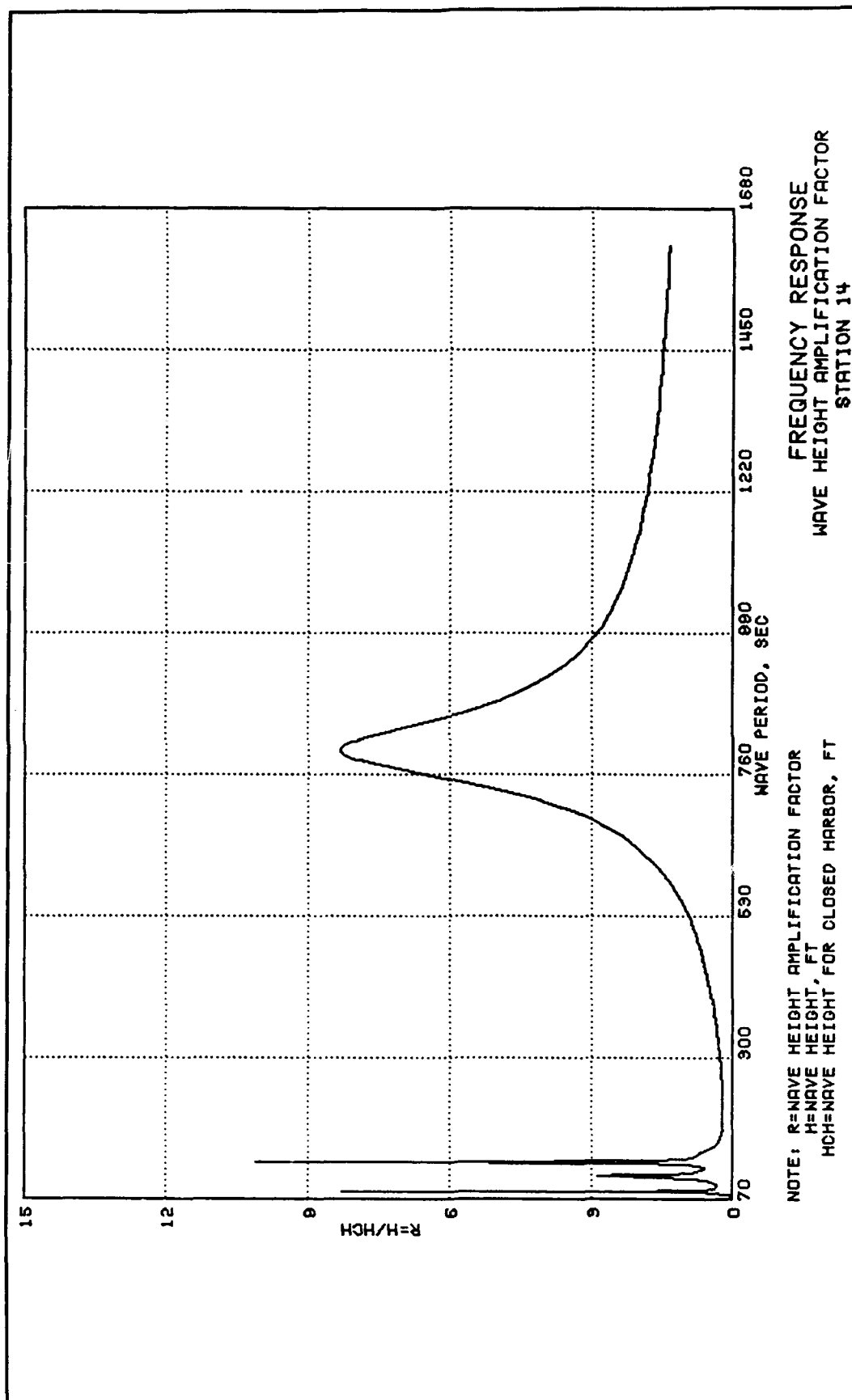
Figure 28.   Frequency response curves, Station 14, 70-1680 sec

FREQUENCY RESPONSE
WAVE HEIGHT AMPLIFICATION FACTOR
STATION 20

NOTE: R=WAVE HEIGHT AMPLIFICATION FACTOR
H=WAVE HEIGHT, FT
HCH=WAVE HEIGHT FOR CLOSED HARBOR, FT
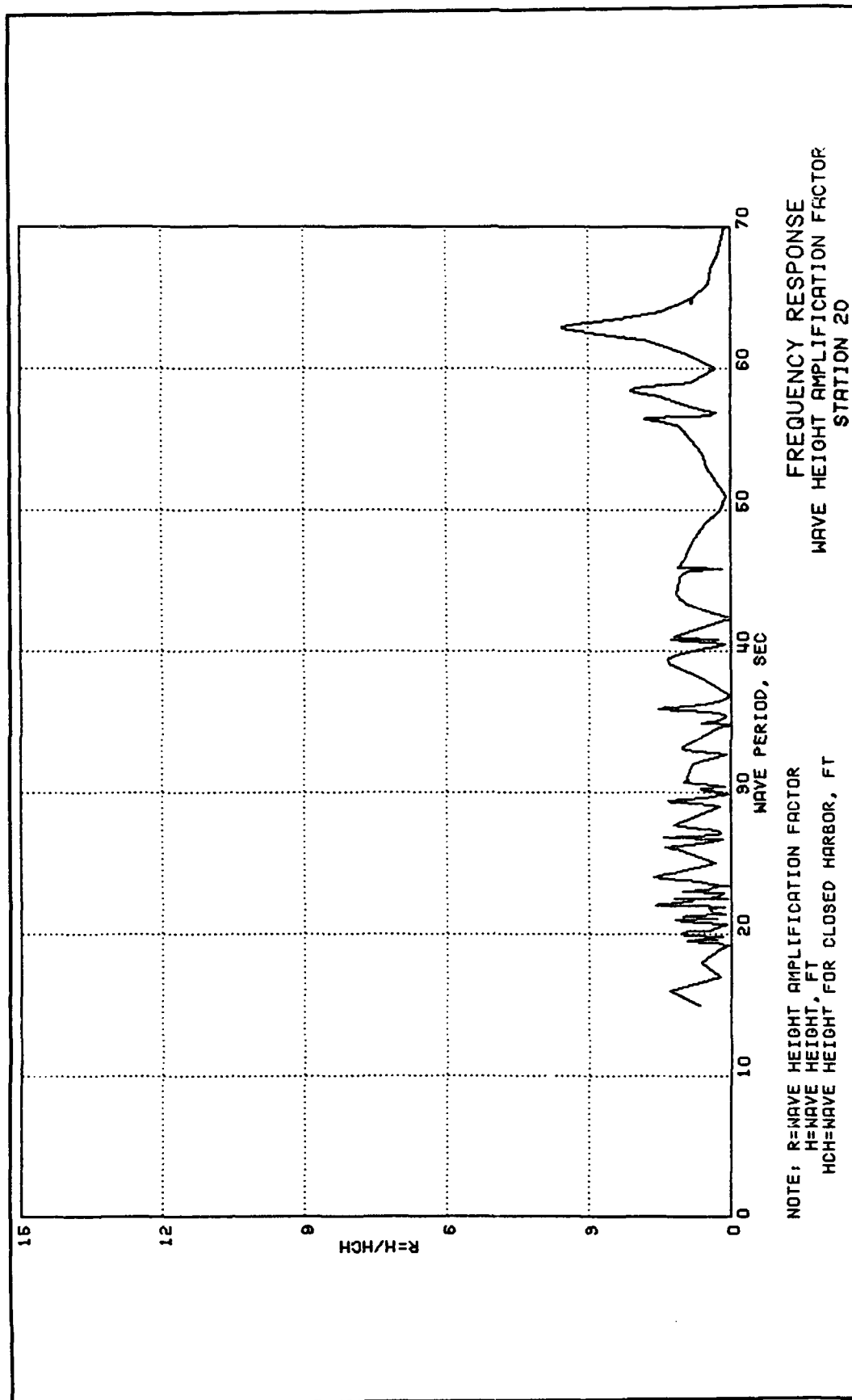
Figure 29. Frequency response curves, Station 20, 0-69 sec
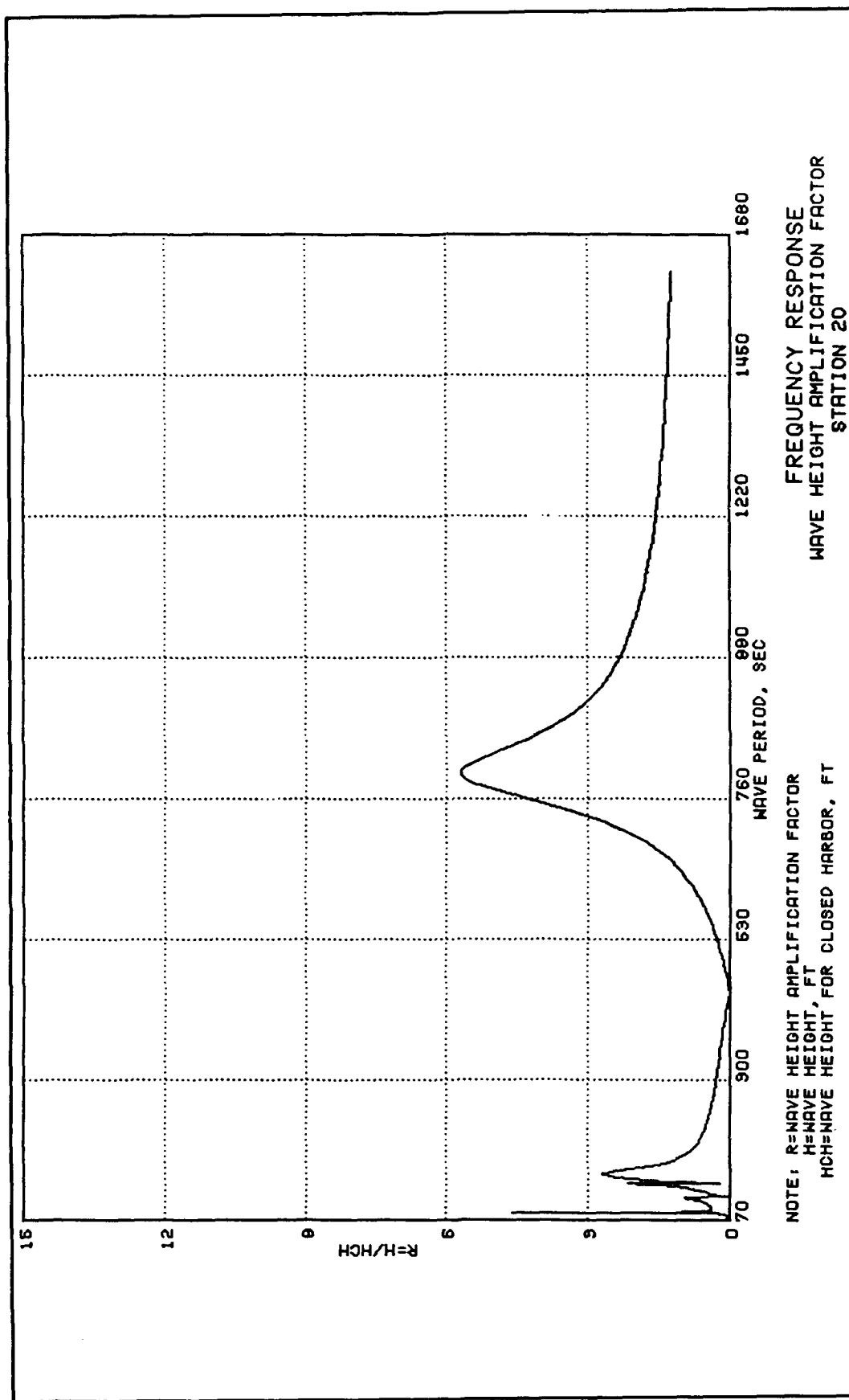
Figure 30. Frequency response curves, Station 20, 70-1680 sec

FREQUENCY RESPONSE
WAVE HEIGHT AMPLIFICATION FACTOR
STATION 22

NOTE: R=WAVE HEIGHT AMPLIFICATION FACTOR
H=WAVE HEIGHT, FT
HCH=WAVE HEIGHT FOR CLOSED HARBOR, FT
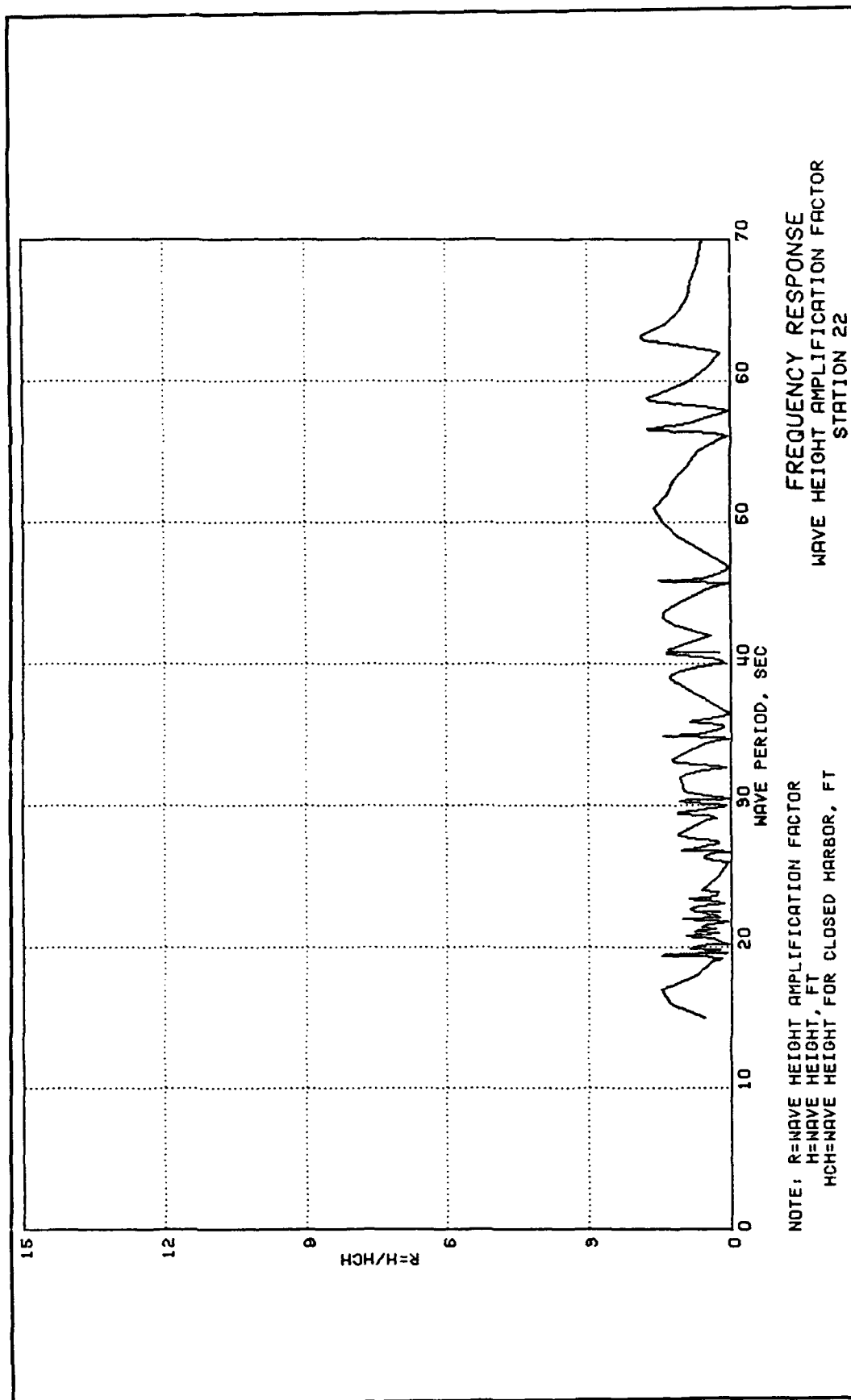
Figure 31. Frequency response curves, Station 22, 0-69 sec
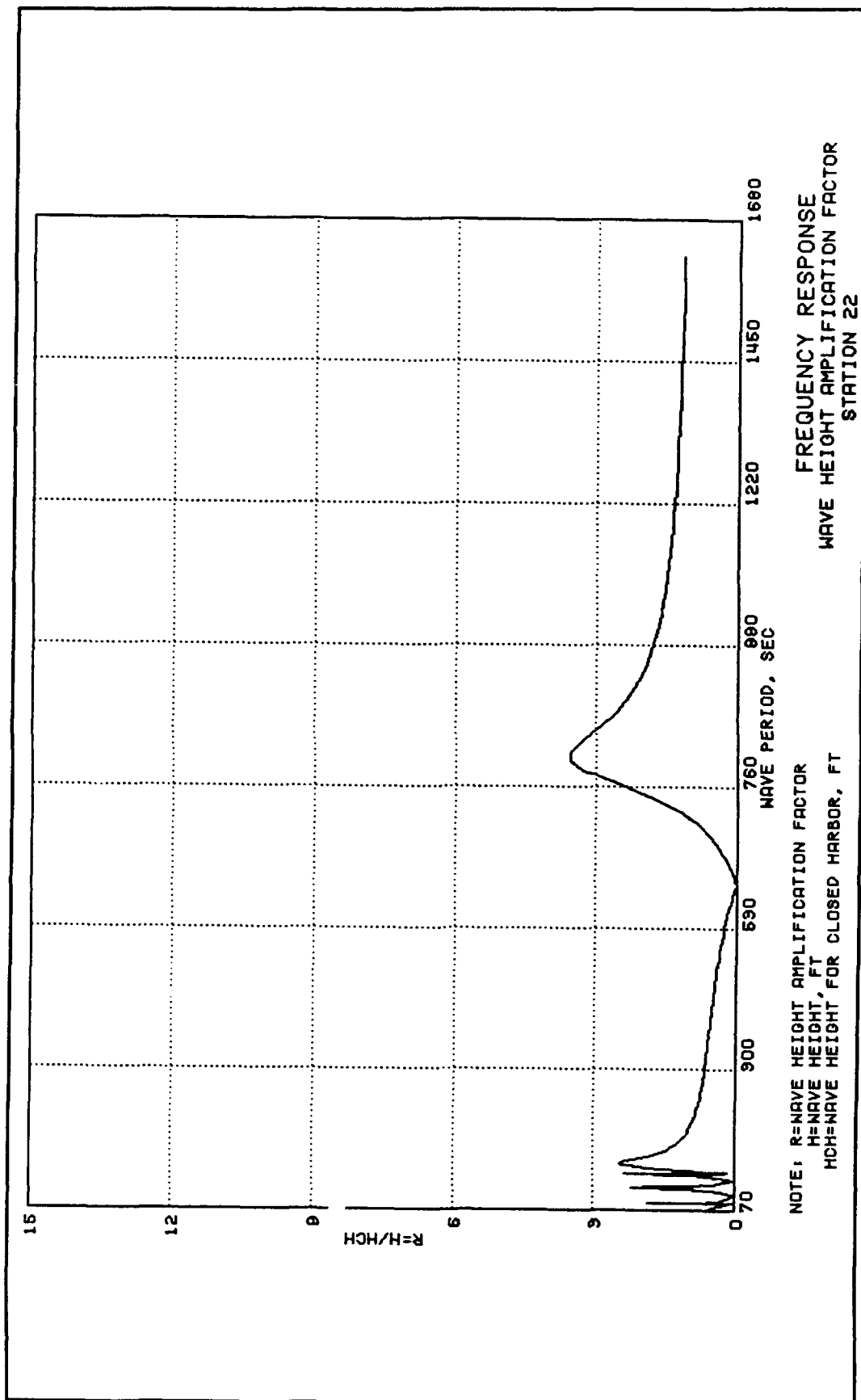
Figure 32. Frequency response curves, Station 22, 70-1680 sec
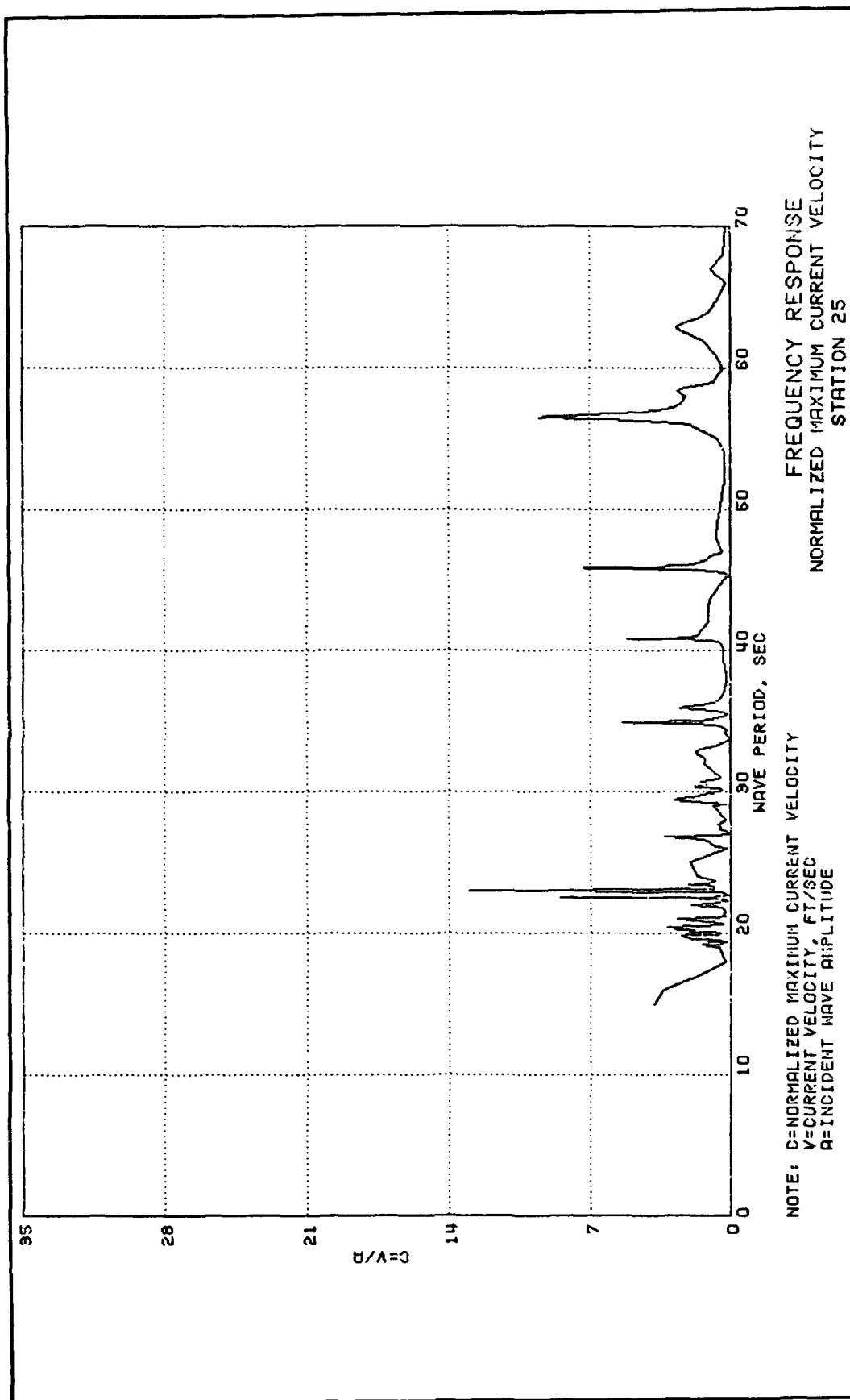
Figure 33. Frequency response curves, Station 25, 0-69 sec
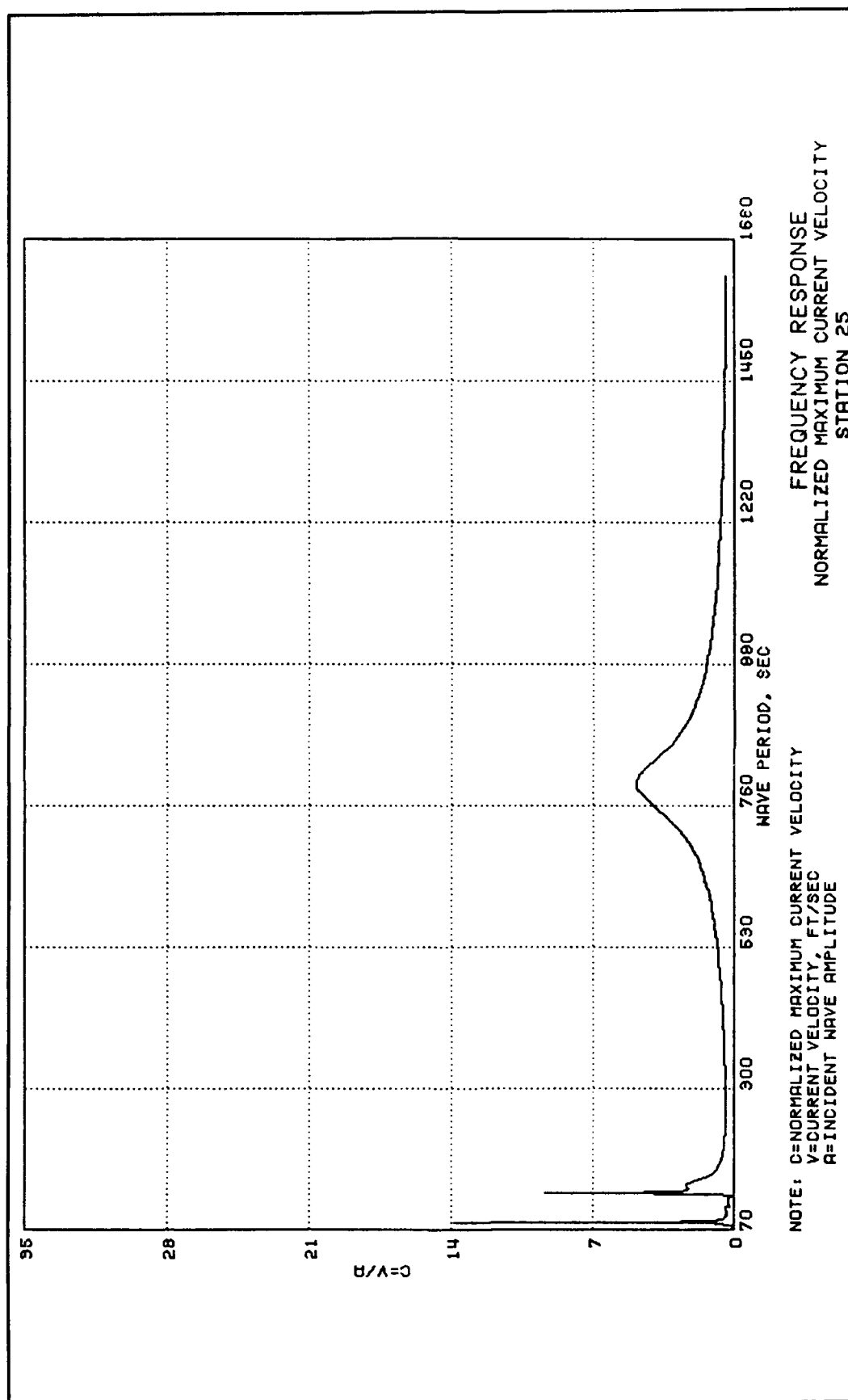
Figure 34. Frequency response curves, Station 25, 70-1680 sec

NOTE: C=NORMALIZED MAXIMUM CURRENT VELOCITY
      V=CURRENT VELOCITY, FT/SEC
      A=INCIDENT WAVE AMPLITUDE

FREQUENCY RESPONSE
NORMALIZED MAXIMUM CURRENT VELOCITY
STATION 29
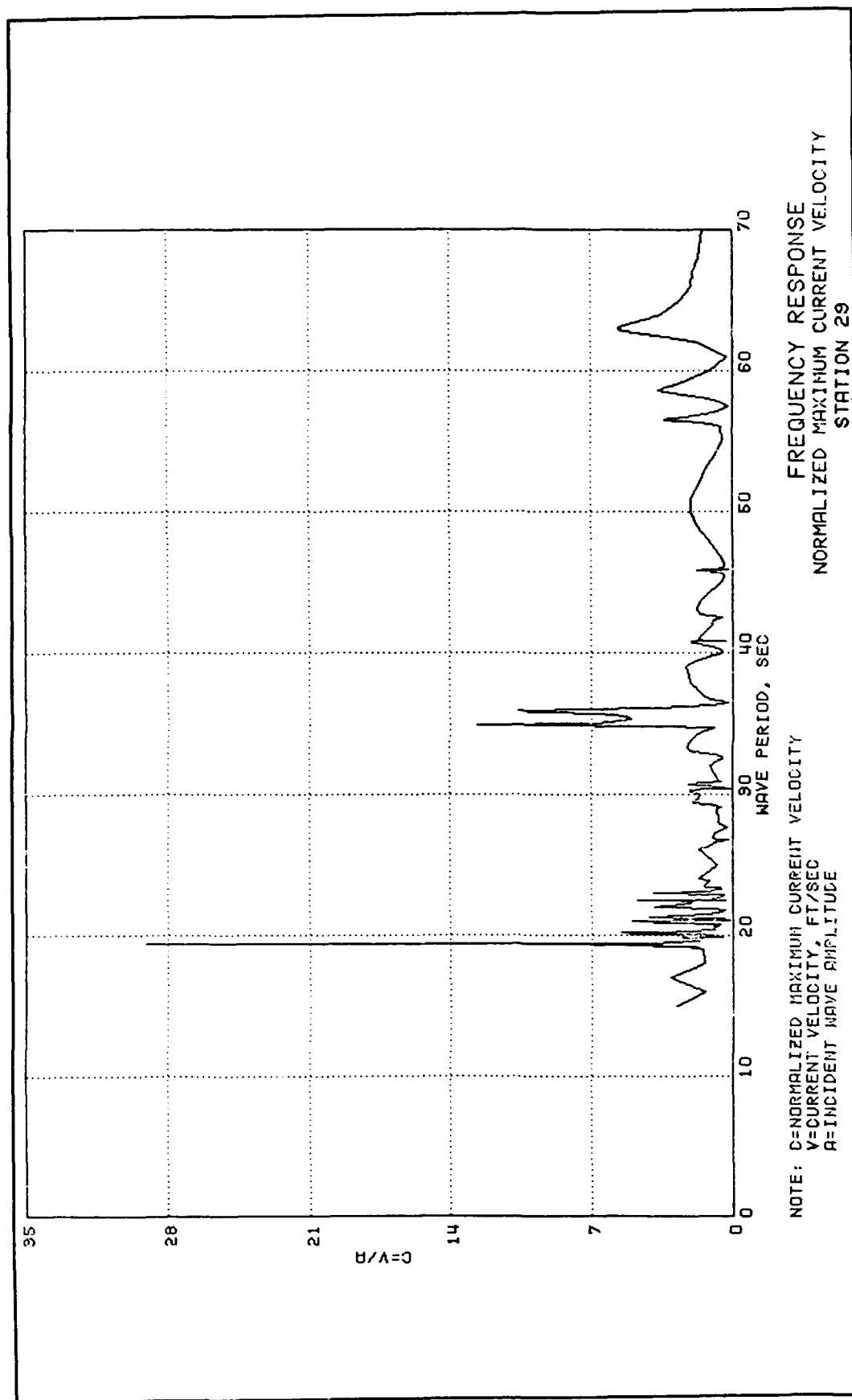
Figure 35. Frequency response curves, Station 29, 0-69 sec
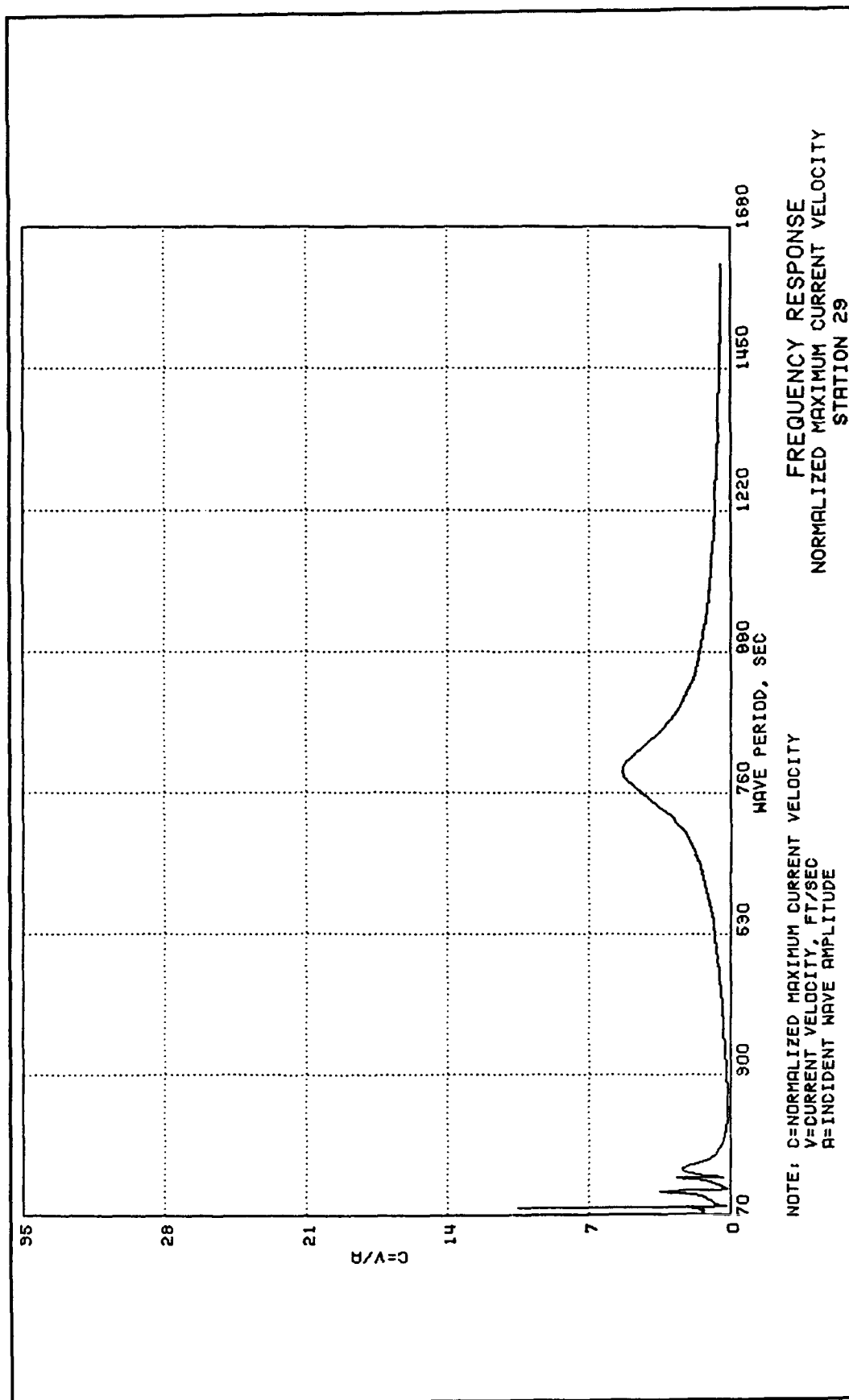
Figure 36. Frequency response curves, Station 29, 70-1680 sec

Table 6
Numerical Model Resonant Modes of Oscillation

Wave Period (sec)	Maximum Amplification	Nearest Gage
799.00	8.58	5
145.00	4.35	26
129.50	10.92	13
107.20	*5.50	27
81.90	14.45	27
63.00	6.30	27
58.60	5.99	5
56.55	8.63	13
45.85	11.51	5
40.80	13.71	15
35.92	10.22	29
34.92	12.93	29
33.05	3.00	DD
30.34	6.00	5
29.42	4.00	3
26.82	6.00	DD
23.40	3.50	5
23.00	19.62	13
22.48	13.75	5
22.02	3.75	5
21.12	3.00	DD
20.78	3.00	1
20.14	3.00	18
19.60	8.46	28
19.40	15.03	29

Hydraulic Model Study 1985

At the request of the West Beach Estates, Honolulu, HI, the University
of Hawaii performed a second hydraulic model study from April 1984 to
January 1985. The problems with which the model study was concerned
were of interest to POD, DOT, and West Beach Estates. The purposes of
the model investigation were to verify and refine design concepts of the
proposed small boat harbor to be located north of the deep-draft harbor,
and to investigate any adverse effects the small boat harbor may have on
the deep-draft harbor. Two types of model studies were conducted: (a) a
three-dimensional model including the deep-draft harbor, barge harbor,
small boat harbor, and adjoining ocean area; and (b) a two-dimensional
wave flume model to evaluate boundary designs for wave absorption. The
objective of the three-dimensional model study was to test wave character-
istics of three proposed entrance channel design concepts. The objective
of the two-dimensional flume tests was to evaluate wave reflection

54

BARBERS POINT HARBOR STUDY
PROPOSED DEEP DRAFT HARBOR, PHASE 1

CONTOURS OF
WAVE - HEIGHT AMPLIFICATION
799.00 – SEC WAVE PERIOD

SCALE IN FEET
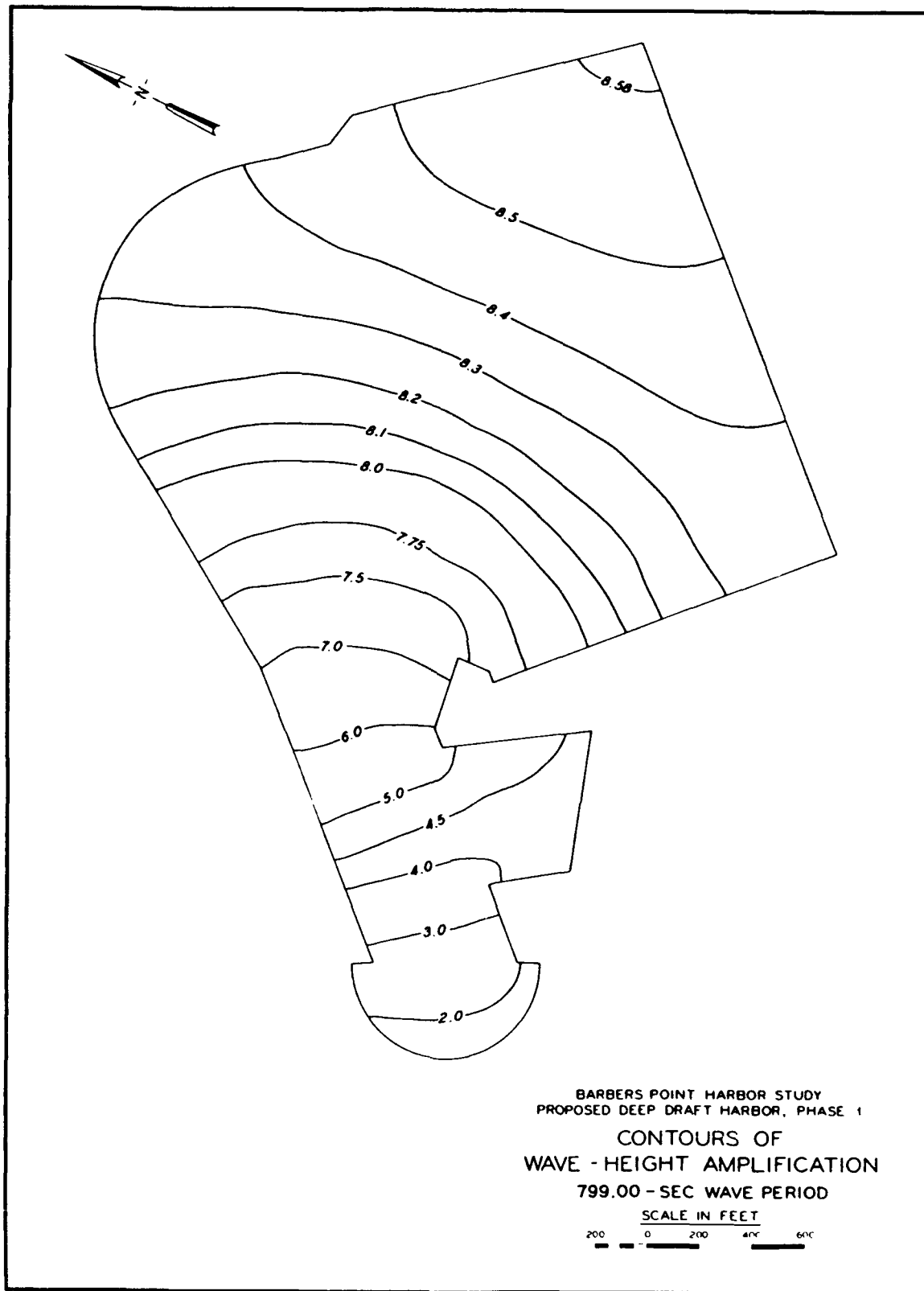
Figure 37.   Harbor resonance contour plot, 799.0 sec

BARBERS POINT HARBOR STUDY
PROPOSED DEEP DRAFT HARBOR, PHASE 1

CONTOURS OF
WAVE - HEIGHT AMPLIFICATION
145.00 - SEC WAVE PERIOD

SCALE IN FEET
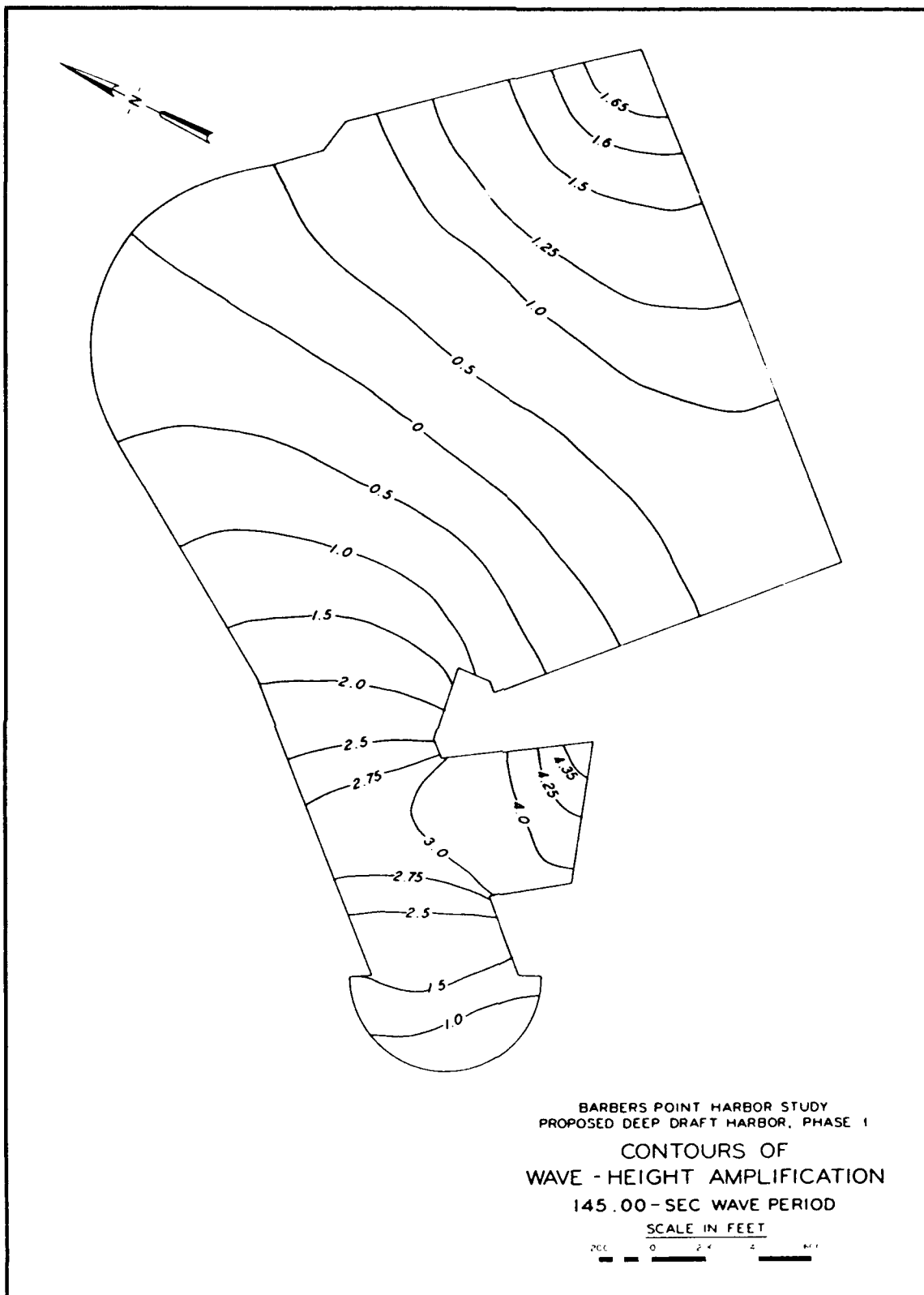
Figure 38.   Harbor resonance contour plot, 145.0 sec

BARBERS POINT HARBOR STUDY
PROPOSED DEEP DRAFT HARBOR, PHASE 1

CONTOURS OF
WAVE - HEIGHT AMPLIFICATION

129.50 - SEC WAVE PERIOD

SCALE IN FEET
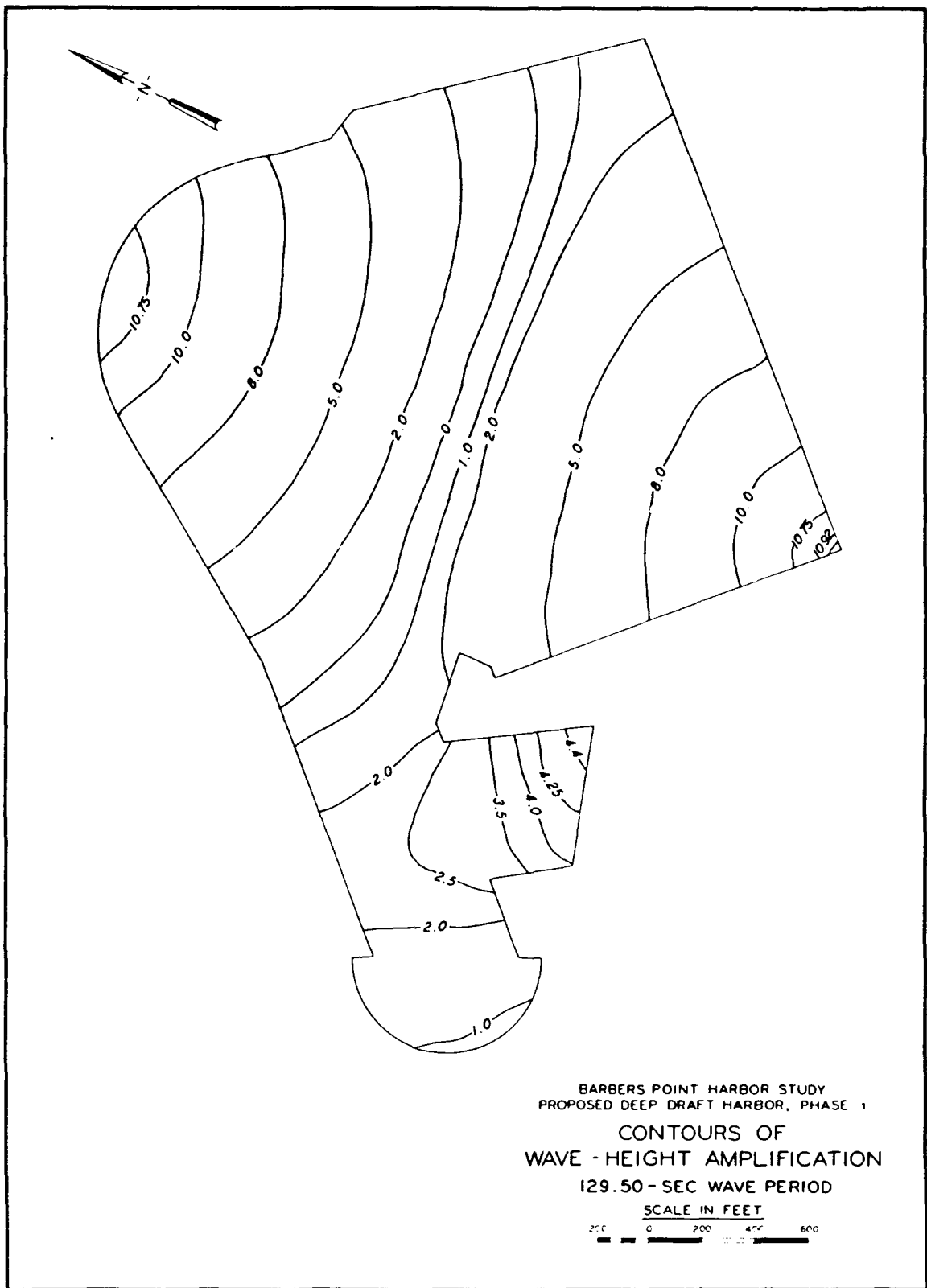
Figure 39. Harbor resonance contour plot, 129.5 sec

BARBERS POINT HARBOR STUDY
PROPOSED DEEP DRAFT HARBOR, PHASE 1

CONTOURS OF
WAVE - HEIGHT AMPLIFICATION

107. 20 - SEC WAVE PERIOD

SCALE IN FEET
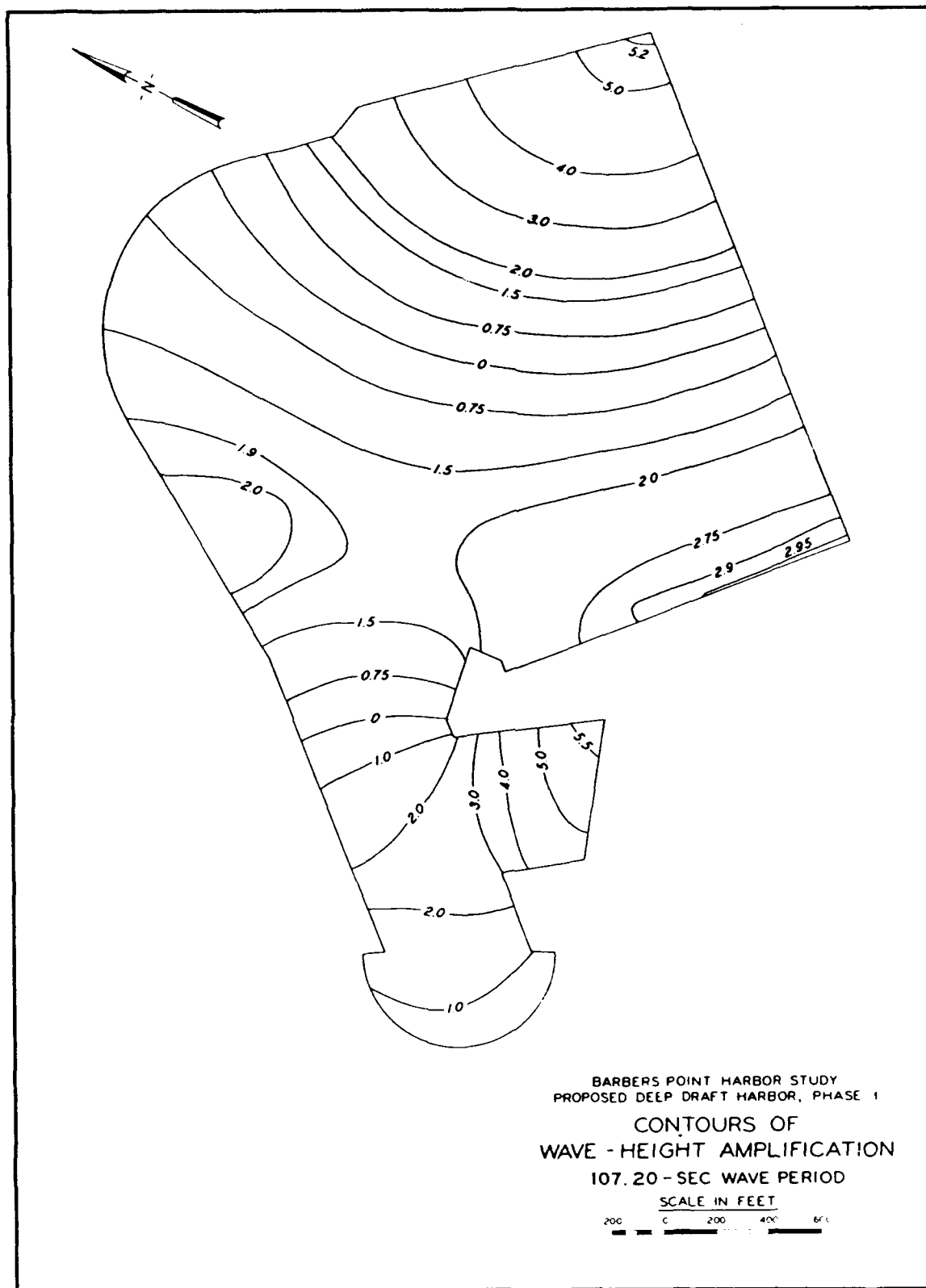
Figure 40.   Harbor resonance contour plot, 107.2 sec

BARBERS POINT HARBOR STUDY
PROPOSED DEEP DRAFT HARBOR, PHASE 1

CONTOURS OF
WAVE - HEIGHT AMPLIFICATION
81.90 - SEC WAVE PERIOD

SCALE IN FEET
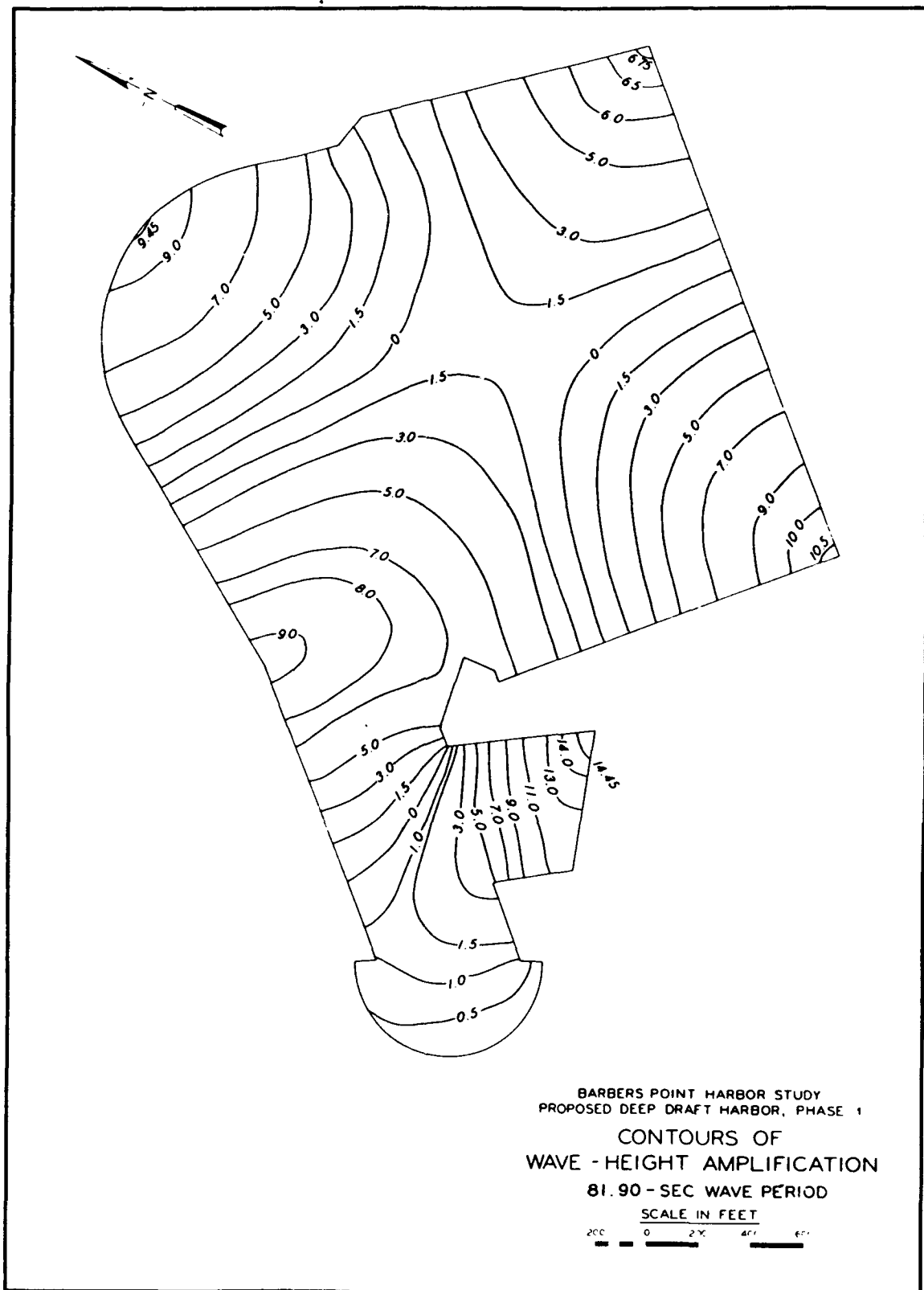
Figure 41. Harbor resonance contour plot, 81.9 sec

BARBERS POINT HARBOR STUDY
PROPOSED DEEP DRAFT HARBOR, PHASE 1

CONTOURS OF
WAVE - HEIGHT AMPLIFICATION

63.00-SEC WAVE PERIOD
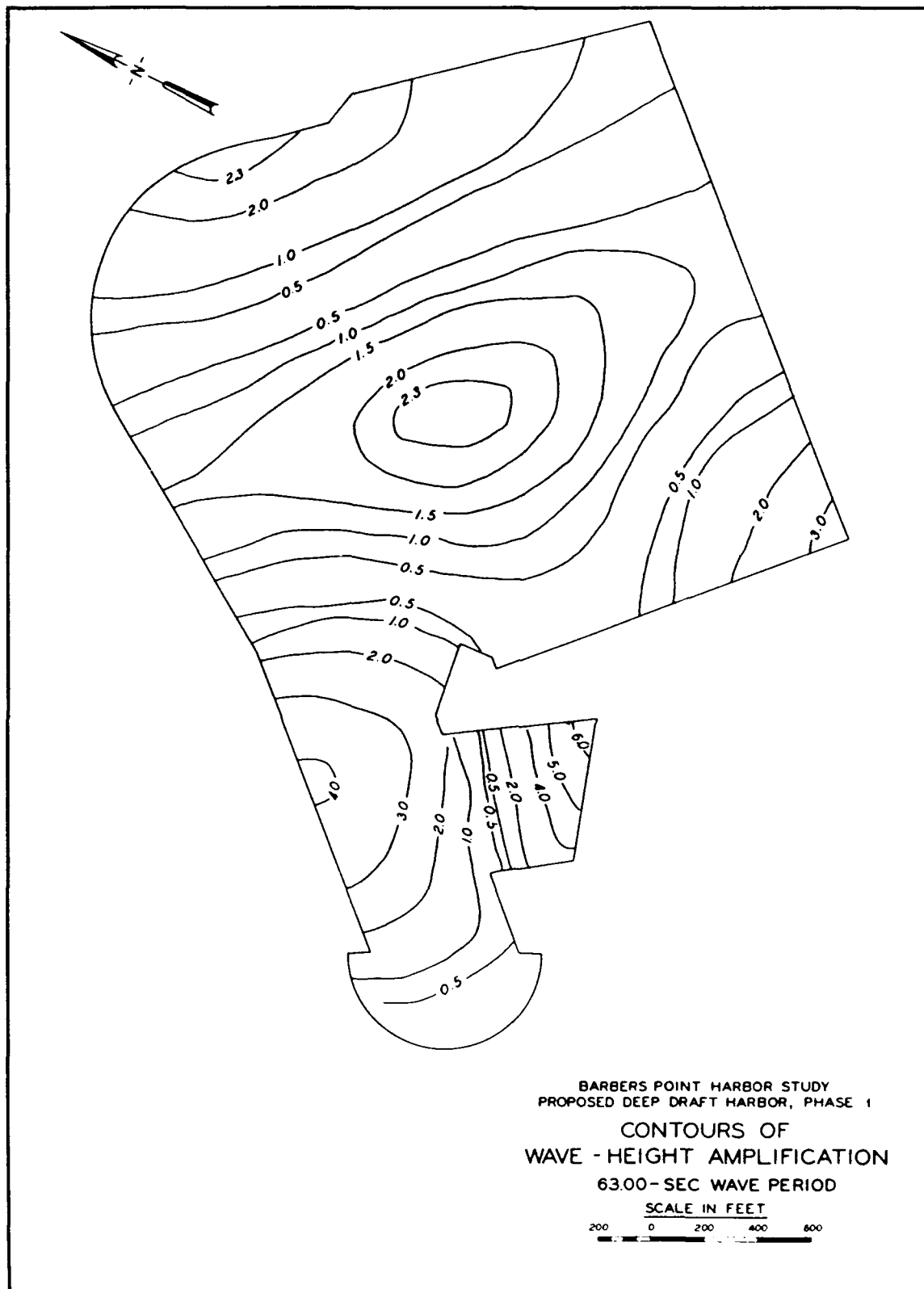
Figure 42.   Harbor resonance contour plot, 63.0 sec

BARBERS POINT HARBOR STUDY
PROPOSED DEEP DRAFT HARBOR, PHASE 1

CONTOURS OF
WAVE - HEIGHT AMPLIFICATION
58.60-SEC WAVE PERIOD

SCALE IN FEET
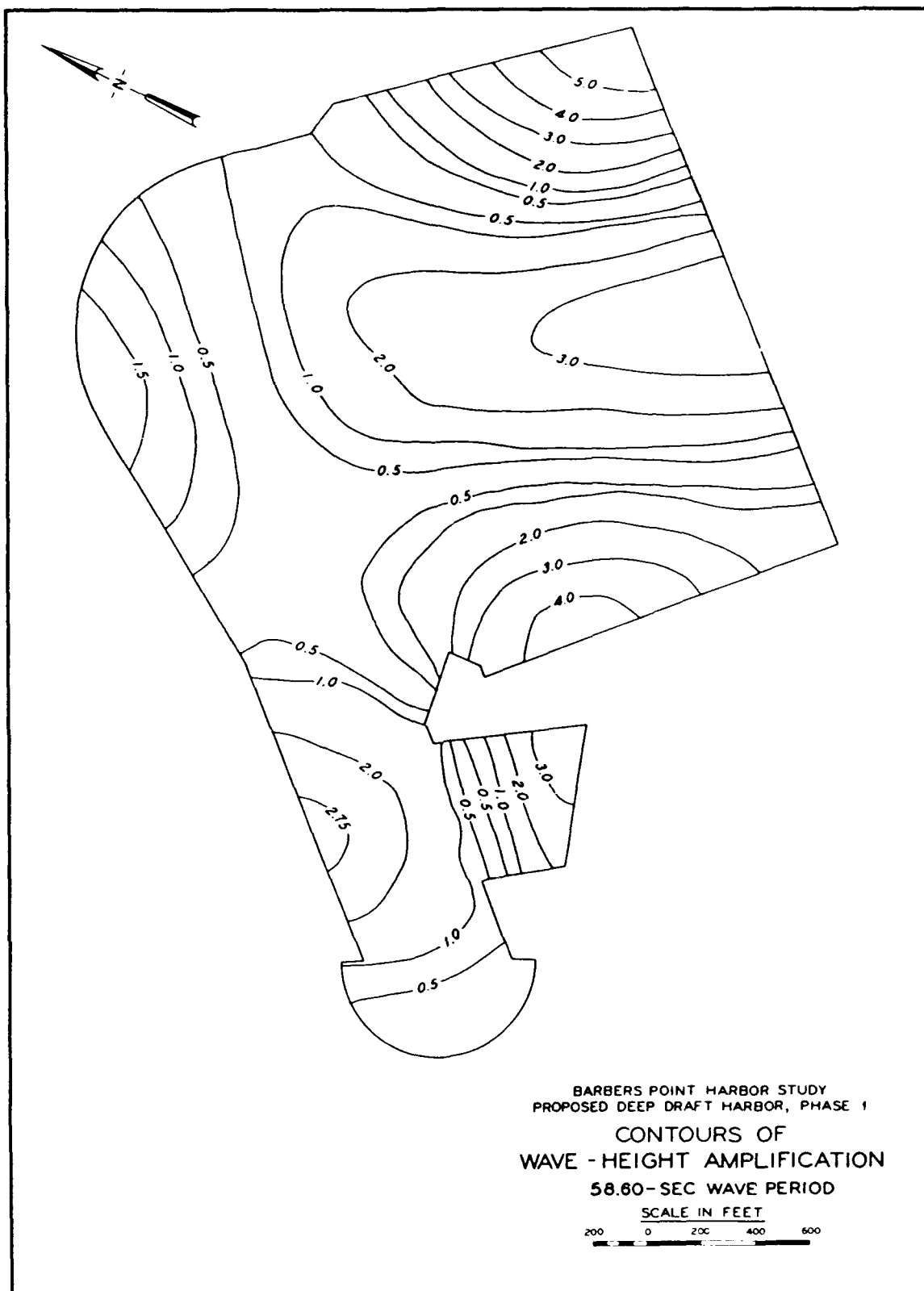
Figure 43. Harbor resonance contour plot, 58.6 sec

BARBERS POINT HARBOR STUDY
PROPOSED DEEP DRAFT HARBOR, PHASE I

CONTOURS OF
WAVE - HEIGHT AMPLIFICATION

56.55 - SEC WAVE PERIOD

SCALE IN FEET
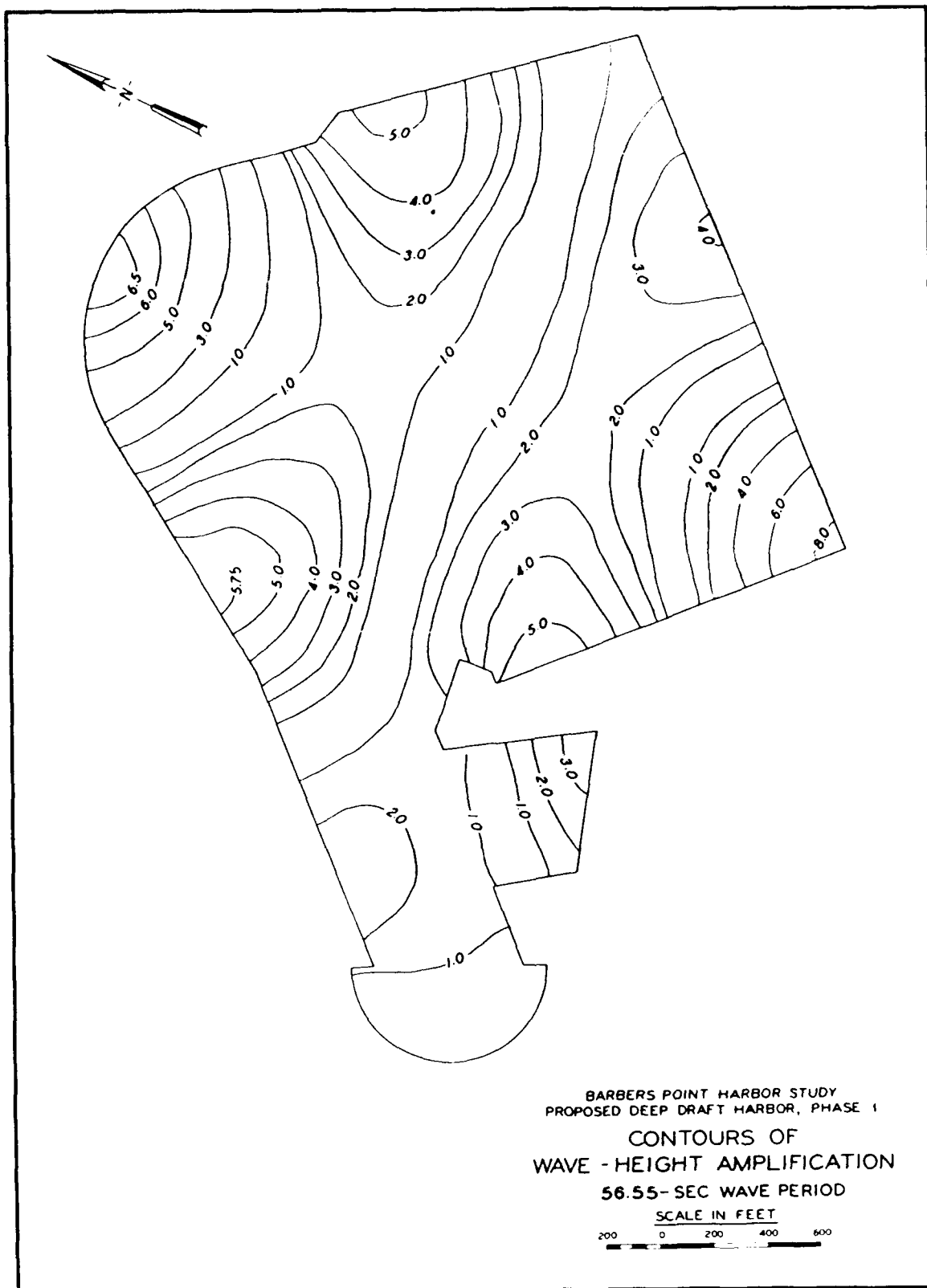
Figure 44.   Harbor resonance contour plot, 56.5 sec

BARBERS POINT HARBOR STUDY
PROPOSED DEEP DRAFT HARBOR, PHASE 1

CONTOURS OF
WAVE - HEIGHT AMPLIFICATION

45.85 - SEC WAVE PERIOD

SCALE IN FEET
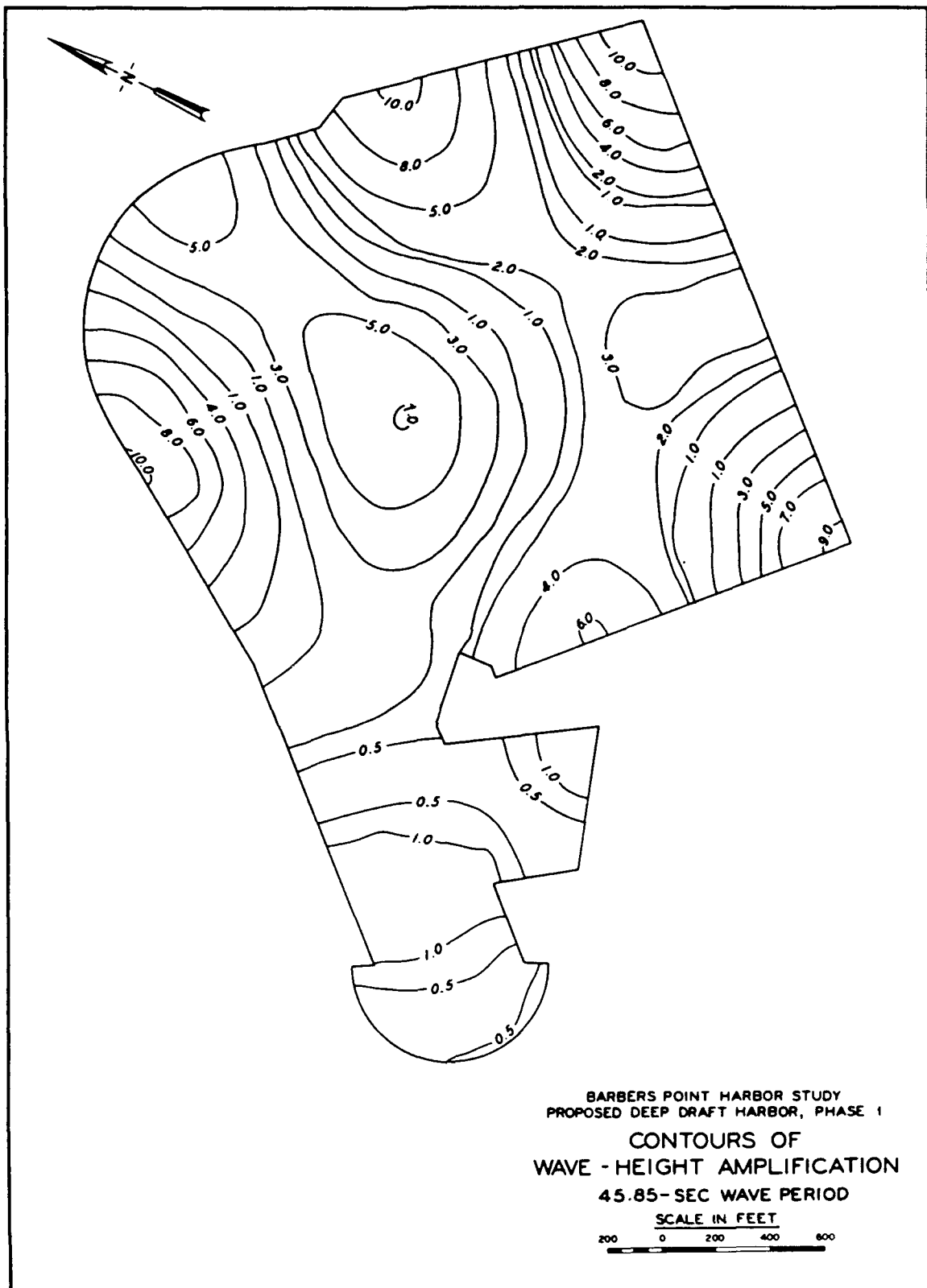
Figure 45. Harbor resonance contour plot, 45.9 sec

coefficients of various structures: a sloping spending beach, vertical walls, and wave absorbers. The description of the three-dimensional model study will be presented in this section, and the reader is referred to Lee (1985) for details of the two-dimensional wave absorber study.

Three-dimensional hydraulic model

The three-dimensional hydraulic model used in this study was the same 1:100 scale, model to prototype, model constructed for evaluating Plan V-A of the previous Barbers Point Deep-Draft Harbor model study conducted in 1970. A description of the three-dimensional deep-draft harbor model is provided in the "Hydraulic Model Study 1967" section of this chapter. The model test results were used to select the optimal small boat harbor design with: (a) minimal wave action within the small boat harbor boundaries; (b) minimum adverse effects on the deep-draft harbor; and (c) acceptable navigation conditions for vessels entering the small boat or deep-draft harbors.

For this study, the small boat harbor was redesigned to include an entrance area, wave absorbers, a spending beach, a short jetty, and a boat ramp. Three proposed entrance channel designs were evaluated and include: (a) an entrance perpendicular to the entrance channel of the deep-draft harbor; (b) an entrance parallel with the entrance channel of the deep-draft harbor; and (c) a separate entrance channel from that of the deep-draft harbor. The total area of the model with the redesigned small boat harbor was approximately 5,500 ft². The model was tested with four configurations. The base plan, Plan O, included only the deep-draft and barge harbors. The remaining configurations consisted of the deep-draft and barge harbors with the proposed perpendicular, parallel, and separate entrance channel designs, Plans I, II, and III, respectively. During testing of the base plan, Plan O, the small boat harbor was blocked off and filled to eliminate its effects on testing the deep-draft and barge harbors only. The four configurations tested are shown in Figure 46.

Wave heights were measured at selected locations in the model. Plan O used a total of nine gages; one near the wave generator to measure incident waves, one at the deep-draft harbor entrance, six in the deep-draft harbor basin along the perimeter, and one in the barge harbor. For the tests which included the small boat harbor, a total of eight gages were used. One incident wave gage near the wave generator, one at the deep-draft harbor entrance, two in the deep-draft harbor basin, one at the entrance passage area of the small boat harbor, and two in the small boat harbor basin. The gage locations for each configuration are shown in Figure 46.
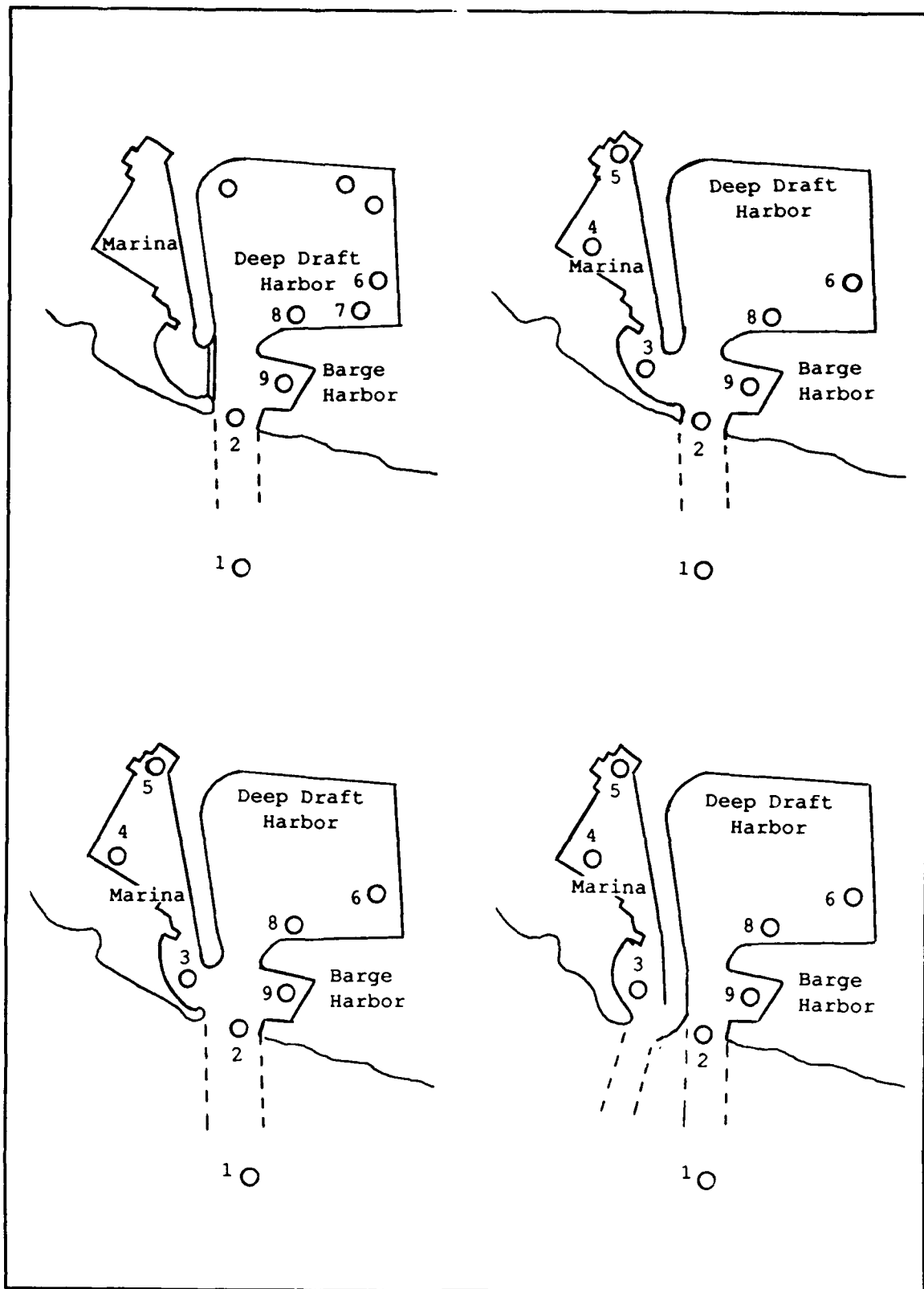
Figure 46. Small boat harbor configurations

Test wave conditions

The test wave conditions were selected through information from the following sources: (a) West Beach Estates consultants; (b) refraction diagrams developed during the 1967 Hydraulic Model study; (c) short-term wave measurements near the project site; and (d) hindcasts by the Marine Advisors (1964). A total of 154 test wave conditions were established and included wave periods of 6, 8, 12, 14, 15, and 20 sec, wave heights of 12, 18, and 36 ft, and wave directions approaching from the 202.5-, 225.0-, 247.5-, and 170.0-deg azimuth. The wave directions, i.e., wave generator positions, were determined from the refraction diagrams. The wave generator was located approximately at the 150-ft contour. The test conditions selected included normal, moderate, and storm wave conditions. The swl values were +3 ft above mllw for normal and moderate wave conditions and +4 ft above mllw for storm wave conditions.

The wave height criteria in the small boat harbor berthing area was specified by POD as 2.0 ft for a maximum-tolerable wave height and 1.0 ft for a desired-maximum limit. The criteria were developed for normal and moderate waves not to exceed a 20-ft incident wave height.

Summary of test results

The percentages of wave heights exceeding the POD wave height criteria are summarized below:

a Plan I - In the deep-draft and small boat harbors combined, 99 percent of the test wave conditions met the maximum tolerable wave height criteria and approximately 86 percent met the desirable maximum wave height criteria. Wave conditions in the barge harbor were more severe than in the deep-draft harbor.

b. Plan II - In the deep-draft and small boat harbors combined, 93 percent of the test wave conditions met the maximum tolerable wave height criteria and 63 percent met the desirable maximum wave height criteria. Wave conditions in the barge harbor were worse than in Plan I.

c. Plan III - In the deep-draft and small boat harbors combined, 90 percent of the test wave conditions met the maximum tolerable wave height criteria and 70 percent met the desirable maximum wave height criteria. The worst case wave conditions occurred in the barge harbor for this plan.

Overall, the inclusion of the small boat harbor had no significant adverse effect on the deep-draft harbor. Plan I is superior to the other plans from a wave impact point of view. Plan II, although less effective than Plan I, has acceptable wave conditions. Plan II has less acceptable wave conditions than the other plans. Plan I, which included the perpendicular

entrance to the deep-draft harbor entrance channel, was chosen as the final design plan for the small boat harbor.

An effort was made to determine the modes of oscillation in the three proposed design plans for the small boat harbor. It was found that the long period oscillation depended on the incident wave conditions, the location in the berthing area, and the configuration of the marina entrance. The evaluation determined that the modes of oscillation occur in the wave period ranges of 100 to 150 sec, 90 to 225 sec, and 90 to 240 sec for Plans I, II, and III, respectively. The proposed design plan, period of oscillation, and the gage in which they occur are listed in Table 7.

Table 7
Small Boat Harbor Peak Responses of Oscillation

Oscillation Period (sec)					
Plan I		Plan II		Plan III	
Gage #4	Gage #5	Gage #4	Gage #5	Gage #4	Gage #5
--	100	90	90	90	--
112	--		120	120	120
120	120		130	140	140
--	130		135	180	--
--	140		144	210	--
--	150		150	240	--
			155		
			160		
		165	--		
		180	--		
		225	--		

3 State-of-the-Art Numerical and Physical Model Efforts

Numerical Model Study

The numerical harbor wave-response model, HARBD, was used to estimate wave oscillations in the existing Barbers Point Harbor Complex. Model simulations were conducted both prior to and after inclusion of the small boat harbor. HARBD is a steady-state, finite element model that calculates linear wave oscillations in harbors of arbitrary configuration and variable bathymetry. The effects of bottom friction and boundary absorption (reflection) are included. Bottom friction is assumed to be proportional to flow velocity with a phase difference. The boundary reflection is based on a formulation similar to the impedance condition in acoustics and is expressed in terms of the wave number ($2\pi/L$ where L is the wavelength) and reflection coefficient of the boundary. The model uses a hybrid element solution method which involves the combination of analytical and finite element numerical solutions to determine the response of a harbor to an arbitrary forcing function. HARBD was originally developed for harbor oscillations (long period waves), and the general formulation was adapted for wind waves (short period waves) by Houston (1981). The mathematical formulations and numerical schemes are described in detail in Chen (1984 and 1986) and a user's manual (Chen and Houston 1987) is available. The model is accessible through the Coastal Modeling System (CMS) at the U.S. Army Engineer Waterways Experiment Station Coastal Engineering Research Center (CERC), and a CMS user's manual (Cialone et al. 1991) is available. The CMS is based on WES's CRAY-YM-P supercomputer.

The HARBD model has been tested and compared with known analytical solutions for a number of cases and the results are excellent (Chen 1984, Chen and Houston 1987). It has been applied in assessing the design or modification of the existing Barbers Point Harbor, Oahu, Hawaii (Durham 1978, Lillycrop and Briggs 1992); Agat Harbor, Guam (Farrar and Chen 1987); Kawaihae Harbor, Hawaii (Lillycrop, Bratos, and Thompson 1990); and Maalaea Harbor, Maui, Hawaii (Lillycrop et al. 1993). The model was instrumental in studying the effects of entrance channel

dredging at Morro Bay Harbor, California (Kaihatu, Lillycrop, and Thompson 1989), and analyzing harbor resonance at Los Angeles-Long Beach Harbor, California (Sargent 1989). The model was used to design coastal structures to provide optimal wave protection at Fisherman's Wharf, San Francisco, California (Bottin, Sargent, and Mize 1985); Green Harbor, Massachusetts (Weishar and Aubrey 1986); Los Angeles-Long Beach Harbor, California (Houston 1976); and to estimate the wave conditions in Indiana Harbor, Indiana, during a study of sediment disposal alternatives (Clausner and Abel 1986). HARBD was compared to laboratory data collected from the physical model study of Barcelona Harbor, Buffalo, New York (Crawford and Chen 1988) with encouraging results.

Boundary value problem

HARBD uses a hybrid element method in which a finite element solution in the interior region of the harbor is matched to an analytical solution in the exterior region. In the interior region, HARBD allows arbitrary depth (i.e., shallow, intermediate, and deepwater waves), variable bathymetry, and the effects of bottom friction and boundary absorption (reflection).

In model formulation for arbitrary depth waves, the entire water domain is divided into near and semi-infinite regions, A and B, respectively (Figure 47). The two regions are separated by an artificial 180-deg semicircular boundary δA located offsho.: of the harbor entrance as shown in the definition sketch of a harbor. The near region A is bounded by a wall boundary δC and includes the harbor and all marine structures and bathymetry of interest. The semi-infinite region B is a 180-deg semicircular ring, which is bounded by δA and the straight horizontal coastlines. The region extends to infinity in all directions, as shown in Figure 47. The semi-infinite region B is assumed to have a constant water depth and no bottom friction (Chen and Houston 1987).

The finite near region, which contains the area of interest, is subdivided into a mesh of nonoverlapping triangular-shaped elements. The length of side of each element is determined from the desired grid resolution and design wave parameters. The water depth and bottom friction coefficient are specified at the centroid of each element, and a reflection coefficient is assigned to each element along the solid near region boundaries. The model requires wave period and direction as input. The solution consists of an amplification factor (i.e., the ratio of local wave height to incident wave height) and a corresponding phase angle for each grid point in the near region. Phase angle represents the difference in phase between the grid point and the incident wave. Contour plots of the amplification factors and corresponding phase angles are used to illustrate the oscillation patterns occurring throughout the harbor.
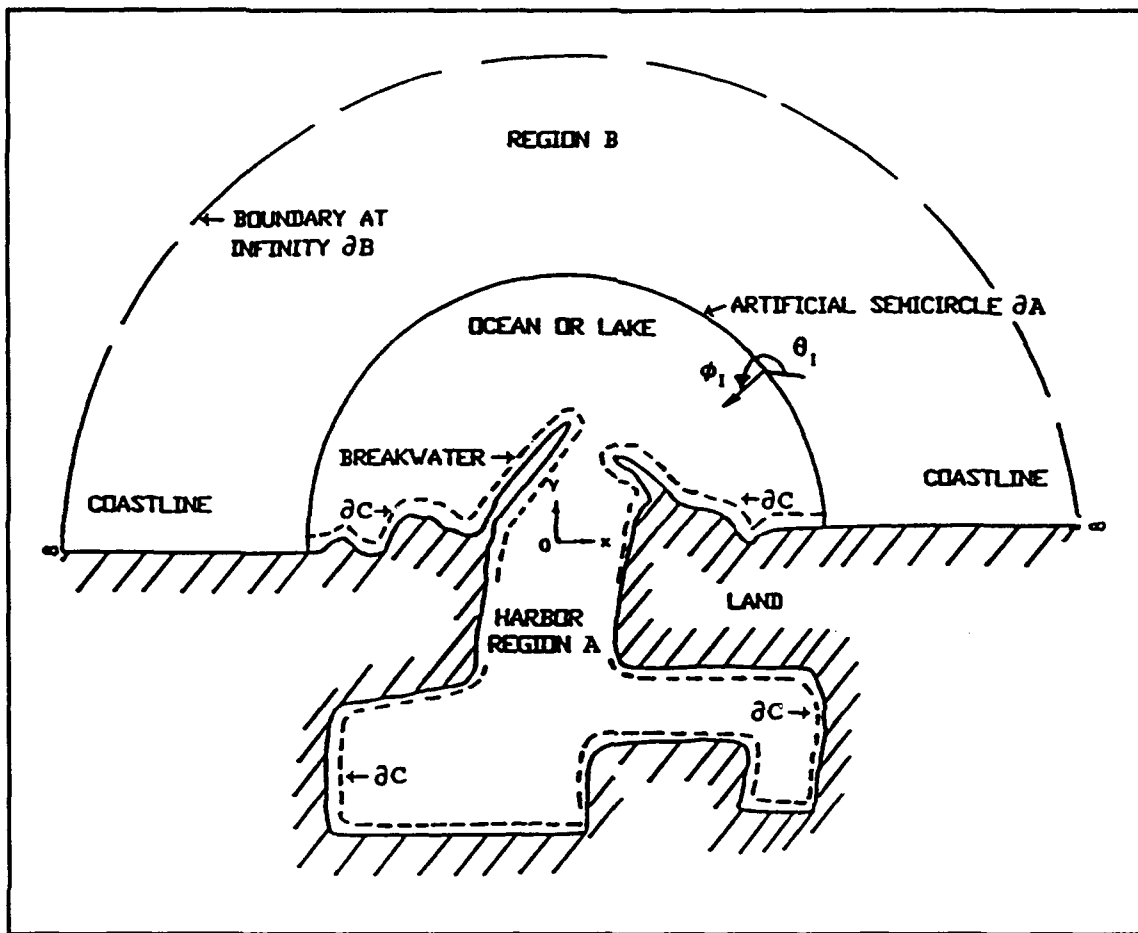
Figure 47. Definition sketch of a harbor

The governing partial differential equation is derived through application of linear wave theory to the continuity and momentum equations. All dependent variables are assumed to be periodic in time with angular frequency ω. These steps yield the following generalized Helmholtz equation (Chen 1986) in which the velocity potential ϕ is solved:

$$\nabla \cdot (\lambda c c_g \nabla \varphi) + \frac{c c_g}{c} \omega^2 \varphi = 0 \tag{1}$$

where

∇ = horizontal gradient operator

λ = complex bottom friction factor

c = wave phase velocity = (ω/κ)

ω = angular frequency

κ = wave number, $(2\pi/L)$, where L = wavelength

c_g = wave group velocity = $[c/2\{1 + (2\kappa h/\sinh 2\kappa h)\}]$

h = water depth

φ = velocity potential

The wave number is obtained from the dispersion relation,

$$\omega^2 = g\,\kappa\tanh(\kappa h) \tag{2}$$

where g = acceleration due to gravity

The complex bottom friction factor λ is assumed proportional to the maximum velocity at the bottom and is defined as:

$$\lambda \approx \cfrac{1}{1 + \cfrac{i\,\beta\,a_o}{h\,\sinh\kappa h}\,\exp(i\gamma)} \tag{3}$$

where

$i = (-1)^{1/2}$

β = dimensionless bottom friction coefficient that can vary spatially

a_o = incident wave amplitude

γ = phase shift between stress and flow velocity

The effects of bottom friction do not necessarily need to be included in the general solution. This is accomplished by setting $\beta = 0$, which results in $\lambda = 1$, and Equation 1 reduces to an expression that excludes bottom friction.

For the absorptive boundary condition along the solid harbor boundaries, the model adopts the impedance condition used in acoustics in terms of the boundary reflection coefficient K_r expressed as:

$$\frac{\partial\varphi}{\partial n} - \alpha\varphi = 0 \tag{4}$$

with

$$\alpha = i \kappa \frac{1 - K_r}{1 + K_r}$$

(5)

where

α = dimensional coefficient related to the boundary reflection

n = unit-normal vector directed outward from the fluid domain

Similar to the friction coefficient, when $K_r = 1$, then $\alpha = 0$ and Equation 4 reduces to a zero velocity potential normal to the boundary (Sargent 1989). This infers a perfectly reflecting boundary condition.

The HARBD model is intended to simulate waves that can be adequately described by the governing generalized Helmholtz equation (Equation 1). Model accuracy decreases as wave conditions approach those outside the validity of this governing equation. HARBD does not simulate nonlinear processes such as wave breaking, wave transmission and overtopping of structures, and wave current interaction; however, the model predicts wave heights accurately if these processes are not dominant. Since nonlinear processes naturally occur in the prototype, care and consideration of the effects must be taken in interpretation of results.

Finite element grids

The finite element grids generated to predict the harbor resonance modes prior to and after the completion of the small boat harbor are shown in Figures 48 through 50. Initially, Grid I was generated which included the deep-draft harbor, barge harbor, entrance channel, and the offshore area extending to the S_{xy} array location approximately 2,000 ft offshore. With this inclusion of the small boat harbor in August 1989, Grid I was modified to include the small boat harbor. The second grid is labeled Grid II. Generation of these grids was done by manually drawing, digitizing, and entering necessary information into ASCII files. The same procedure was used in the 1978 numerical model study of the harbor. Model simulations were conducted to predict harbor resonance modes using Grids I and II.

With the availability of automated finite element grid generation software, supercomputing facilities, and prototype and physical model data for calibration and comparisons, a third grid was generated to refine the harbor boundaries and to increase the resolution in the shallower depth barge and small boat harbors. The refined grid, Grid III, included the entrance channel, barge harbor, deep-draft basin, small boat harbor, and extended the same distance offshore as Grids I and II.
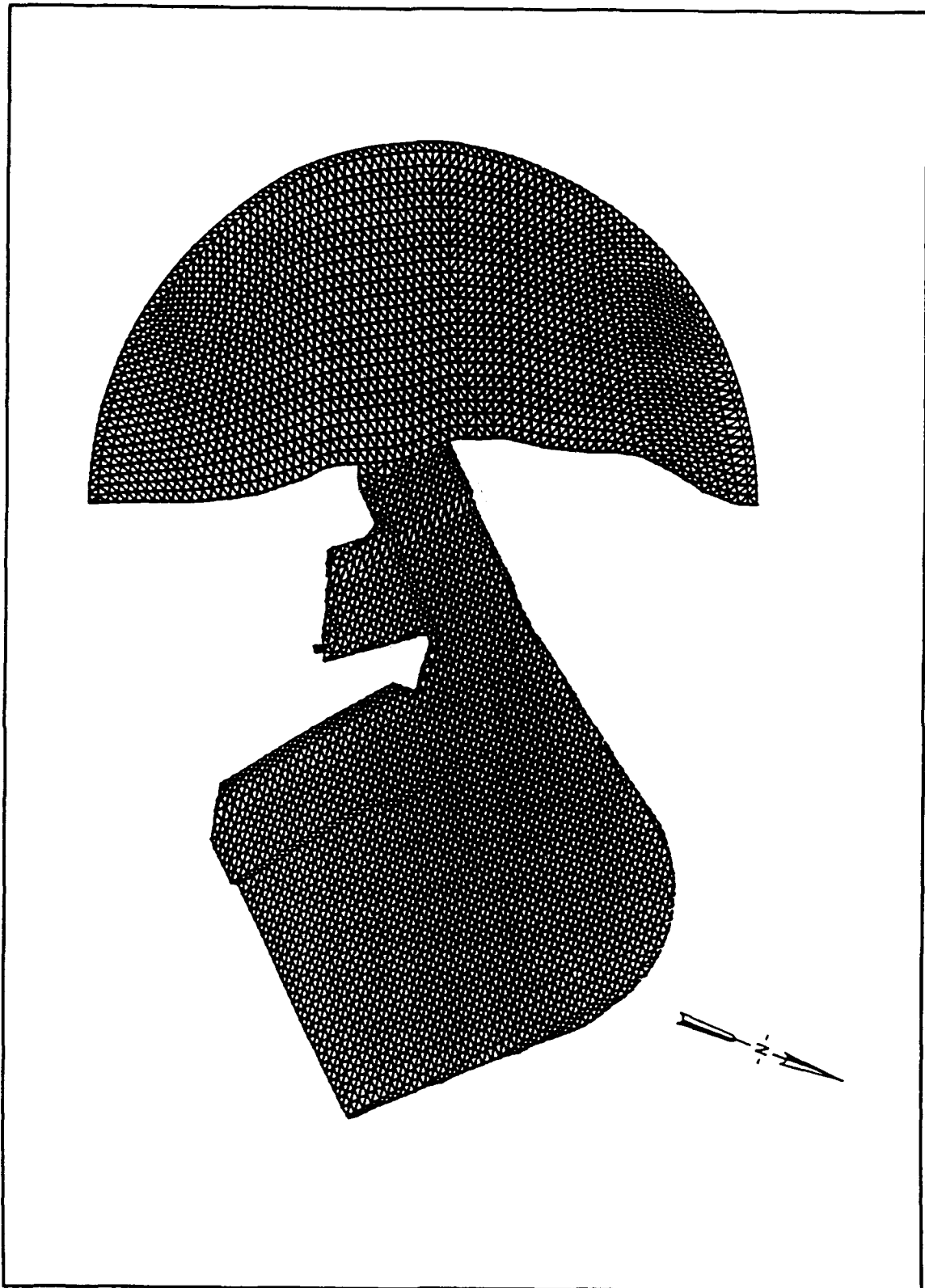
Figure 48. Finite element grid, Grid I
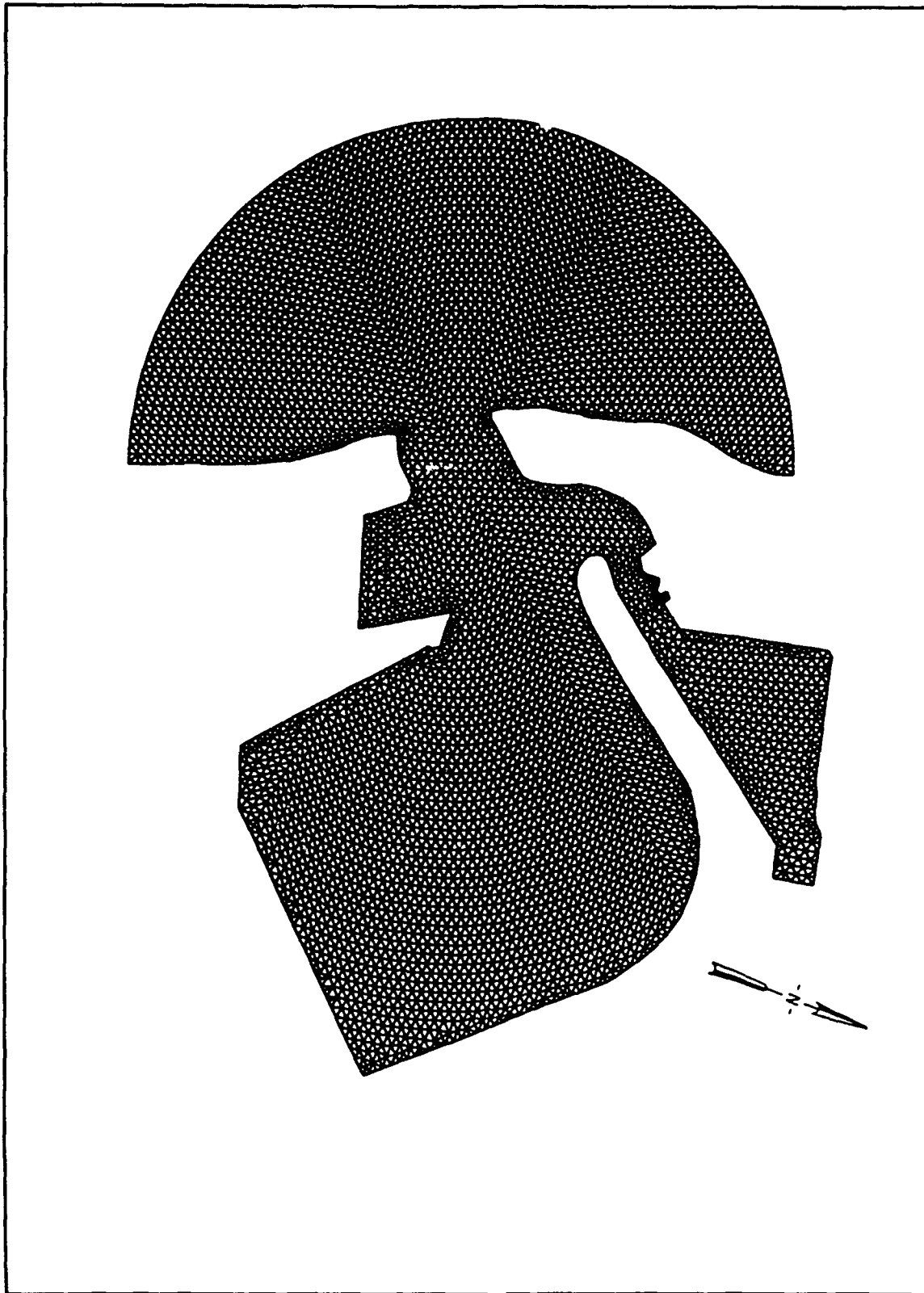
Figure 49. Finite element grid, Grid II
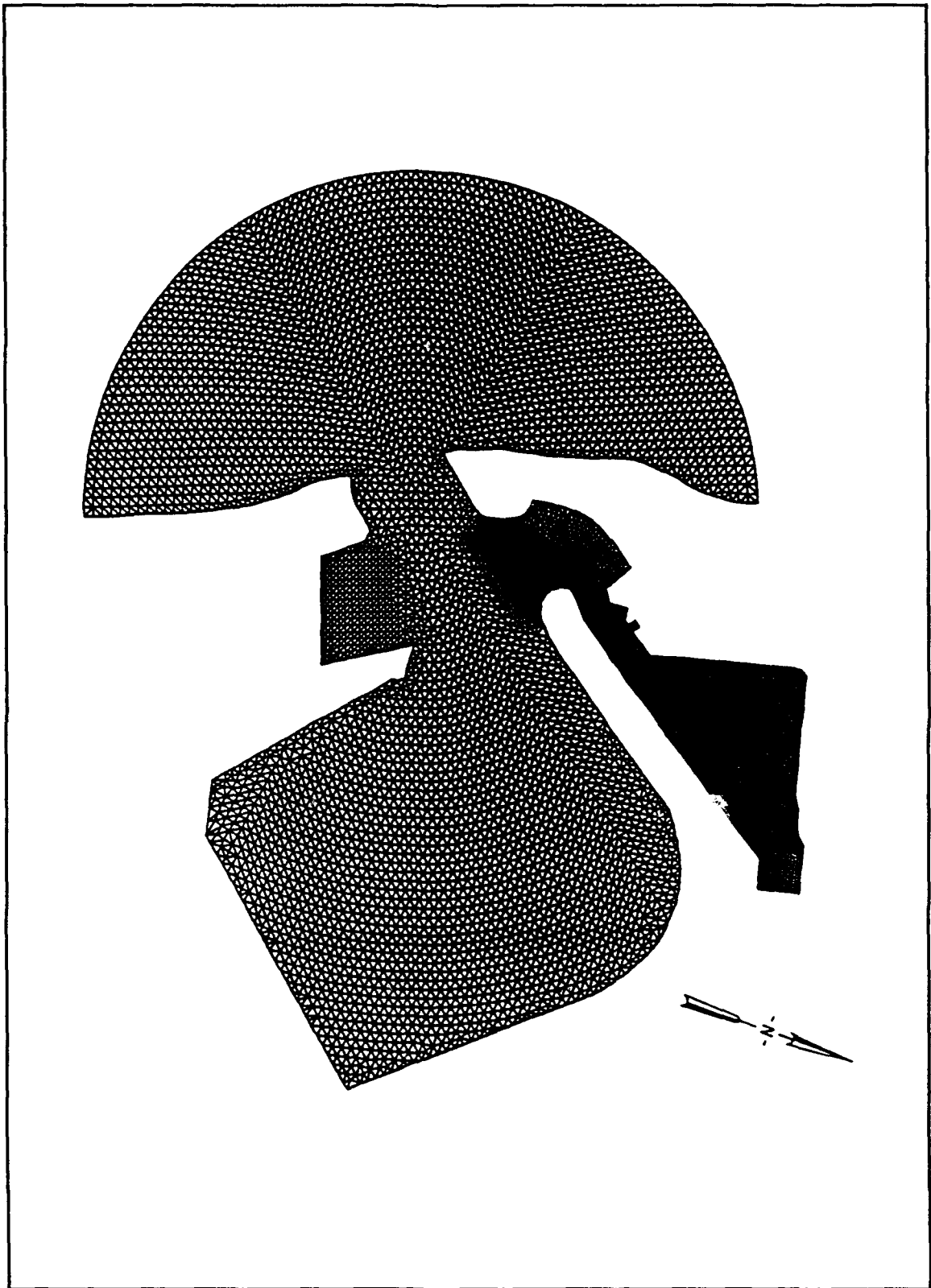
Figure 50.   Finite element grid, Grid III

All grids were designed with a resolution equal to approximately one sixth of the local wavelength, based on linear wave theory using a wave period of 10 sec and depths of 38, 21, and 16 ft in the deep-draft basin, barge harbor, and small boat harbor, respectively. Grid bathymetry was obtained from POD hydrographic surveys and referenced to mllw. The total number of elements (triangles), nodes (triangular corners), and boundary elements are given in Table 8. Because dissipative effects were not available in the numerical model study conducted in 1978, the effects of bottom friction and boundary absorption were not included (i.e., $K_f = 0.0$ and $K_r = 1.0$) in the simulations using Grids I and II. However, in calibrating the model for the evaluation of future modifications to the existing harbor, as mentioned in Chapter 1, bottom friction was incorporated into the model simulations using Grid III. A description of the tests including bottom friction are provided in the numerical model results section of this chapter.

Table 8
Grid Descriptions

Grid	# Elements	# Nodes	# Boundary Elements
I	7,784	4,079	261
II	8,677	4,581	372
III	11,694	6,155	503

To compare numerical model predictions to prototype measurements and physical model predictions, and to assist in identifying the harbor resonant modes, numerical model output locations were selected coincident with the prototype and physical model wave gage locations. Additional locations were selected to investigate the wave response in the barge harbor, small boat harbor, and through the harbor entrance channel. An output location is an area consisting of a specified number of elements from which the mean value of the results of those elements is calculated. The number of output locations selected for Grids I, II, and III were 17, 26, and 28, respectively, and are shown in Figures 51 through 53. The three grids included the following output locations. Nine locations correspond with the prototype wave gage positions shown in Figure 7. The three locations offshore of the harbor entrance represent the positions of slope array (S_{xy}) and offshore (Of) and onshore (On) wave gages. The remaining prototype wave gages in the deep-draft harbor entrance and basin are represented by the channel entrance (Ce), channel midpoint (Cm), south corner (Sc), north corner (Nc), and east corner (E1) and (E2), which were the two locations of the east corner wave gage. An additional output location was positioned at the center of the deep-draft harbor basin (Dc), and seven positions were selected to measure the response through the harbor entrance channel (C1 through C7).
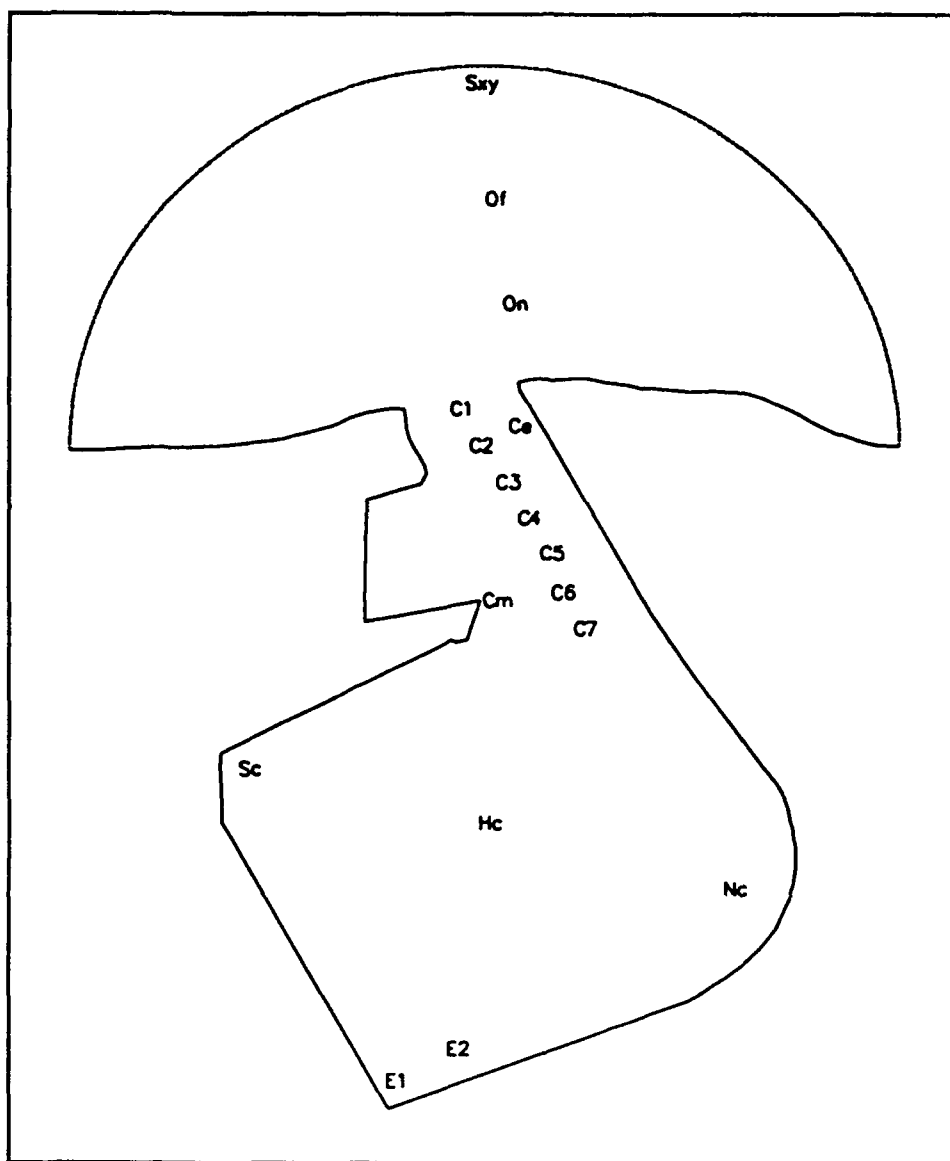
Figure 51. Output locations, Grid I

Additional output locations for Grids II and III were selected to evaluate the response in the barge and small boat harbors. The locations in the barge harbor are labeled barge east (Be) and barge south (Bs). The locations in the small boat harbor are labeled harbor entrance (He), harbor west (Hw), harbor north (Hn), and harbor center (Hc), and three locations were selected to measure wave amplifications through the channel (H1, H2, and H3). Grid III included two additional output locations which were not included in Grid II. They are located in the north corner of the barge harbor (Bn) and at the location of a proposed ferry terminal (Hf) along the northeast wall of the deep-draft harbor.
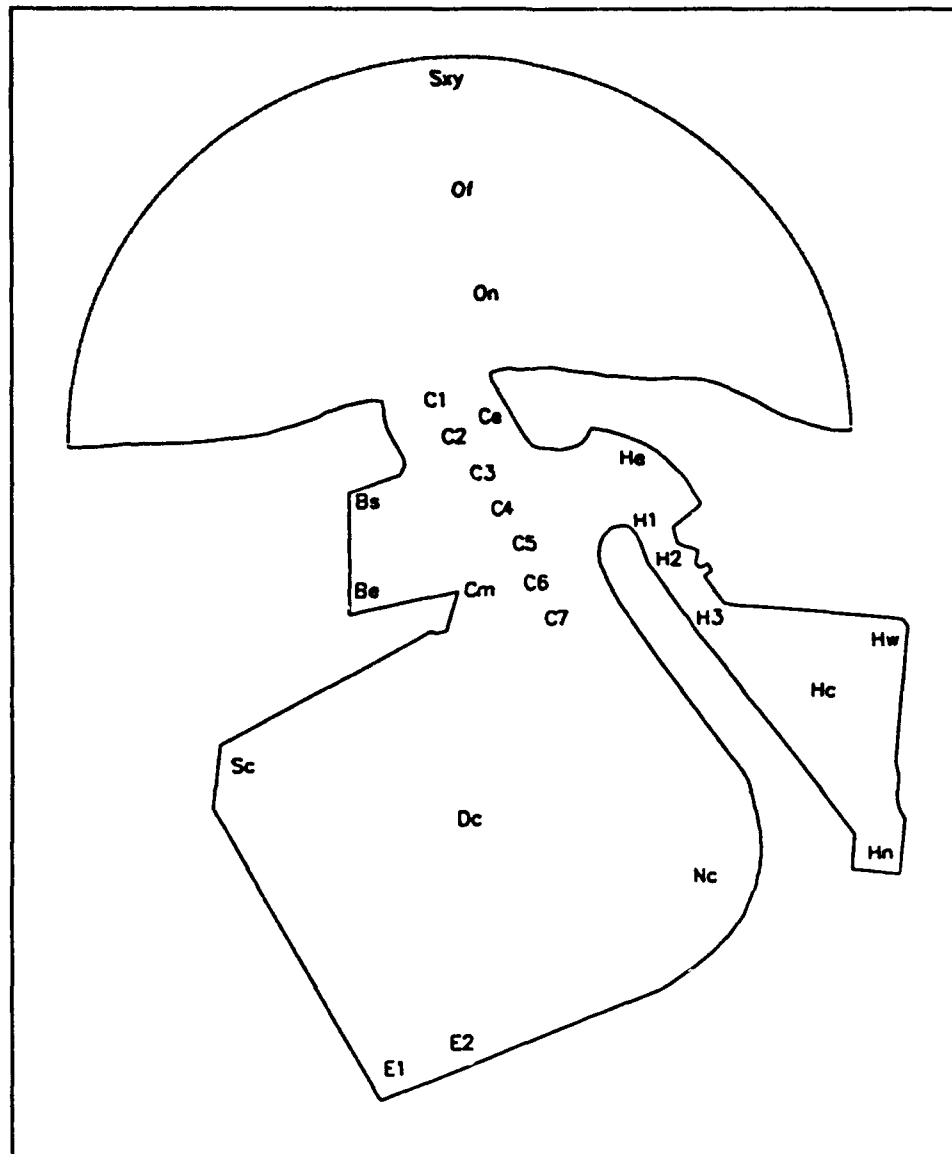
Figure 52. Output locations, Grid II

Wave height amplification factors were also obtained over the entire harbor grid for the long period resonant modes of oscillation. Contour plots of the wave height amplification factors were generated from the data for use in determining oscillation patterns and magnitudes of wave height amplification occurring during harbor resonance.
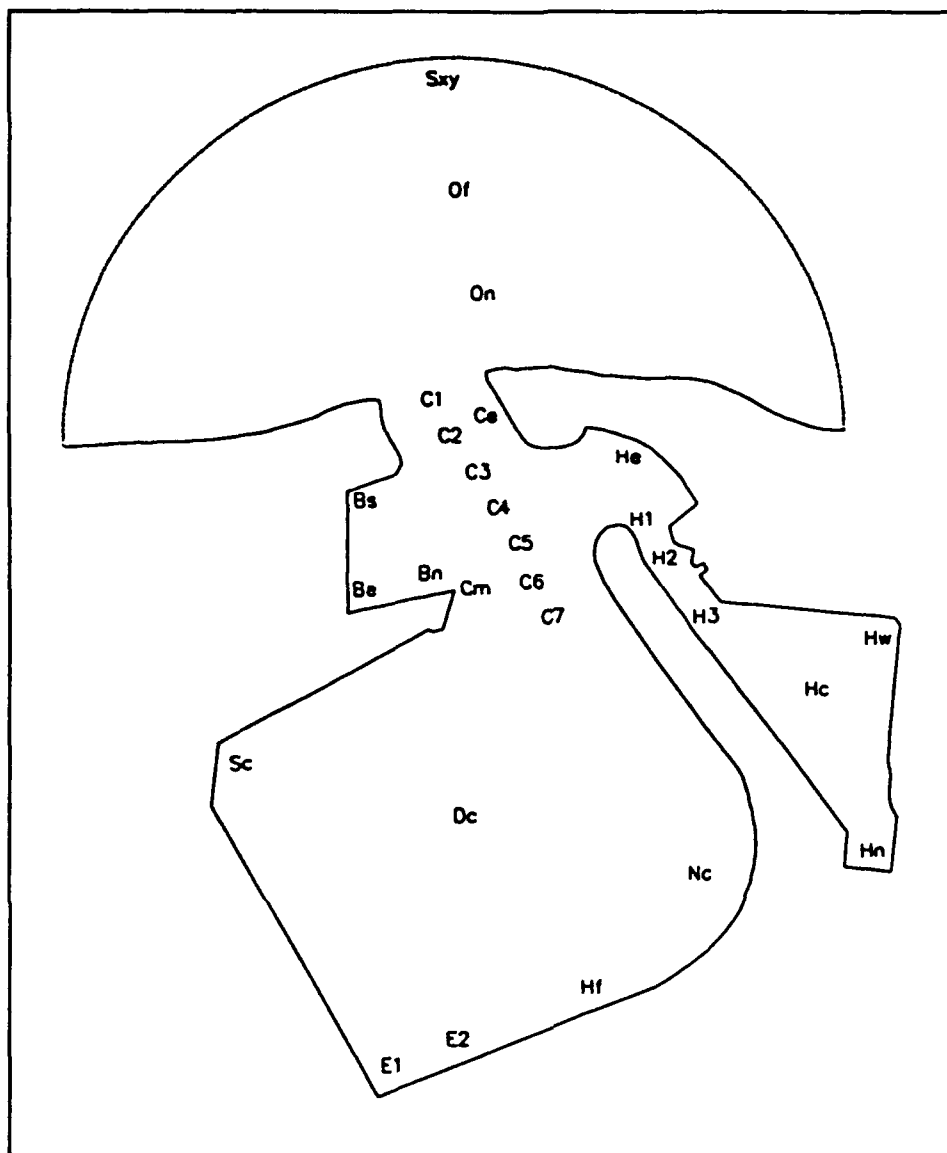
Figure 53. Output locations, Grid III

Model simulations

Grids I and II were tested with the wave period increments ΔT (Table 5) used in the 1978 numerical model study for a first pass evaluation of model performance. However, a different method was used to identify the resonant modes of oscillation since prototype data were available for comparison. The prototype data were analyzed with a spectral bandwidth of 0.000122 Hz (1/8197.7 sec) resolution; therefore, the numerical model was simulated using a resolution of three times the prototype resolution of 0.000041 Hz (1/24576.1 sec) to avoid the possibility of missing resonant peaks. The range of frequencies tested were from 0.000122 to 0.022 Hz

(24576.1 to 45.0 sec). The 0.022-Hz (45.0-sec) cutoff was selected because resonant modes no longer occurred beyond 45.0 sec in the prototype data. The incident wave direction was chosen perpendicular to the bottom contours since there was difficulty in distinguishing wave direction from the prototype measurements, as discussed in Chapter 4, and numerical tests showed insignificant differences in predictions from variable wave directions for the wave periods considered. The model predictions were averaged to obtain data sets that correspond to the resolution of the prototype data. All tests were run on the WES CRAY-YM-P supercomputer.

As mentioned previously, no dissipative effects due to bottom friction and boundary absorption (reflection) were used in the simulations using Grids I and II. Therefore, the magnitude of wave height amplification factors predicted by the numerical model will be larger than the prototype measurements. Also, as the incident frequency increases, or wave period decreases, the magnitude of numerical model amplitudes will increase due to dissipative effects becoming more dominant. The numerical model also predicts peak resonance modes at shorter wave periods and higher frequencies that do not occur in nature, since energy dissipation also impacts the occurrence of resonant peaks. For consistency with the 1978 numerical model study, the wave height amplification factors predicted by the model were divided by two, as explained in the section titled "Numerical Model 1978" in Chapter 2 of this report.

Results

Tables 9 through 18 provide listings of wave period and wave height amplification factors corresponding to the peak resonance modes identified from the numerical model simulations for each of the three grids. A blank entry in the table corresponds to a grid configuration not predicting a resonance mode that was predicted by another grid configuration. Tables 9 through 12 provide information for locations in the deep-draft harbor, Tables 13 though 15 provide information for locations in the barge harbor, and Tables 16 through 18 provide information for locations in the small boat harbor.

Table 9
Numerical Model Resonant Modes of Oscillation - South Corner

Grid I		Grid II		Grid III	
Wave Period (sec)	Amplification Factor	Wave Period (sec)	Amplification Factor	Wave Period (sec)	Amplification Factor
		1024.0	5.1	1024.0	5.2
910.2	5.8				
		585.1	2.1	585.1	3.2
132.1	2.3	132.1	3.2	132.1	3.2
107.8	1.3	107.8	1.9	107.8	2.3
83.6	5.0	81.9	3.7	85.3	0.9
		57.7	2.5	57.3	1.3
56.1	2.0	55.7	4.6		
46.5	3.0	46.5	2.4		

Table 10
Numerical Model Resonant Modes of Oscillation - East Corner

Grid i		Grid II		Grid III	
Wave Period (sec)	Amplification Factor	Wave Period (sec)	Amplification Factor	Wave Period (sec)	Amplification Factor
		1024.0	5.2	1024.0	5.3
910.2	5.9				
		585.1	2.2	585.1	3.4
				204.8	1.0
132.1	1.1	132.1	1.3		
107.8	1.9	107.8	2.9	107.8	3.3
83.6	4.3	81.9	2.6	85.3	0.7
70.0	3.4	70.0	1.2		
58.1	1.6	58.1	2.2	57.3	0.9
		55.7	3.1		
46.5	2.9	46.5	2.4		

Table 11
Numerical Model Resonant Modes of Oscillation - North Corner

Grid I		Grid II		Grid III	
Wave Period (sec)	Amplification Factor	Wave Period (sec)	Amplification Factor	Wave Period (sec)	Amplification Factor
		1024.0	5.1	1024.0	5.2
910.2	5.8				
		585.1	2.1	585.1	3.2
132.1	2.5	132.1	3.5	132.1	2.5
83.6	4.1	81.9	3.0	85.3	0.7
70.0	1.0				
		57.7	1.3		
		55.7	2.0		

Table 12
Numerical Model Resonant Modes of Oscillation - Channel Midpoint

Grid I		Grid II		Grid III	
Wave Period (sec)	Amplification Factor	Wave Period (sec)	Amplification Factor	Wave Period (sec)	Amplification Factor
		1024.0	4.2	1024.0	4.4
910.2	5.8				
		585.1	1.1	585.1	1.8
				204.8	1.4
		182.0	1.2		
167.2	1.5				
				143.7	0.9
		138.9	1.12		
				120.7	1.0
		113.8	1.3		
83.6	1.5	81.9	3.0	85.3	0.6
70.0	1.1				
		55.7	1.8		
		46.5	1.6		

Table 13
Numerical Model Resonant Modes of Oscillation - Barge South

Grid II		Grid III	
Wave Period (sec)	Amplification Factor	Wave Period (sec)	Amplification Factor
1024.0	3.6	1024.0	3.7
599.4	2.5	585.0	0.9
		204.8	2.4
182.0	1.8		
		143.7	1.5
138.8	1.9		
		124.1	1.5
113.8	2.3		
106.4	2.6	106.4	3.1
86.2	1.8		
81.1	1.6		
70.0	1.6		
45.8	1.3		

Table 14
Numerical Model Resonant Modes of Oscillation - Barge East

Grid II		Grid III	
Wave Period (sec)	Amplification Factor	Wave Period (sec)	Amplification Factor
1024.0	3.8	1024.0	3.7
599.4	2.5	585.1	1.1
		204.8	2.5
182.0	1.9		
		143.7	1.7
138.8	2.2		
		124.1	1.8
113.8	2.9		
106.4	3.0	106.4	3.7
86.2	2.5		
81.1	2.4	82.7	2.8
70.0	3.5		
56.1	2.1	57.7	1.4
47.9	2.0		
45.8	1.4		

Table 15
Numerical Model Resonant Modes of Oscillation - Barge North

Grid III	
Wave Period (sec)	Amplification Factor
1024.0	4.0
585.1	1.2
204.8	2.2
143.7	1.4
124.1	1.4
106.4	2.4

Table 16
Numerical Model Resonant Modes of Oscillation - Small Boat Harbor Entrance

Grid II		Grid III	
Wave Period (sec)	Amplification Factor	Wave Period (sec)	Amplification Factor
1024.0	4.5	1024.0	4.6
630.2	1.1	630.2	1.4
		204.8	1.4
178.1	2.2		
138.8	1.9		
		128.0	1.8
113.8	5.2		
86.2	2.1		
81.9	3.8		
60.2	1.7		
55.7	2.1		
47.9	1.3		

Table 17
Numerical Model Resonant Modes of Oscillation - Small Boat Harbor West

Grid II		Grid III	
Wave Period (sec)	Amplification Factor	Wave Period (sec)	Amplification Factor
1024.0	6.8	1024.0	6.5
630.2	8.6	630.2	13.6
138.8	1.6		
		125.0	1.5
113.8	4.2		
86.2	3.0		
81.9	3.8		
68.3	13.8		

Table 18
Numerical Model Resonant Modes of Oscillation - Small Boat Harbor North

Grid II		Grid III	
Wave Period (sec)	Amplification Factor	Wave Period (sec)	Amplification Factor
1024.0	7.0	1024.0	7.3
630.2	9.2	630.2	14.6
		143.7	4.2
138.8	7.2		
113.8	6.2		
86.2	2.1		
81.9	2.3		
68.3	12.3		
50.3	1.2		
47.9	2.3		
46.6	1.7		

Grid I. Frequency response curves of the predicted wave height amplification factors (i.e., normalized magnitudes), from the numerical model simulations using Grid I are shown in Figure 54 for the output locations in the four corners of the deep-draft basin. The resonant modes are identified by peaks occurring in the frequency response curves. The model predicted nine resonant peaks with normalized magnitudes greater than 1.0 for incident frequencies between 0.000122 and 0.22 Hz (24576.1 and 45.0 sec). Each of the four corners exhibit the long-period Helmholtz mode at 910.2 sec. Resonant modes were also identified at 167.2, 132.1, 107.8, 83.6, 70.0, 58.1, 56.1, and 45.6 sec. Tables 9 through 12 list the wave period and wave height amplification corresponding to peak resonance modes for each location in the deep-draft basin.
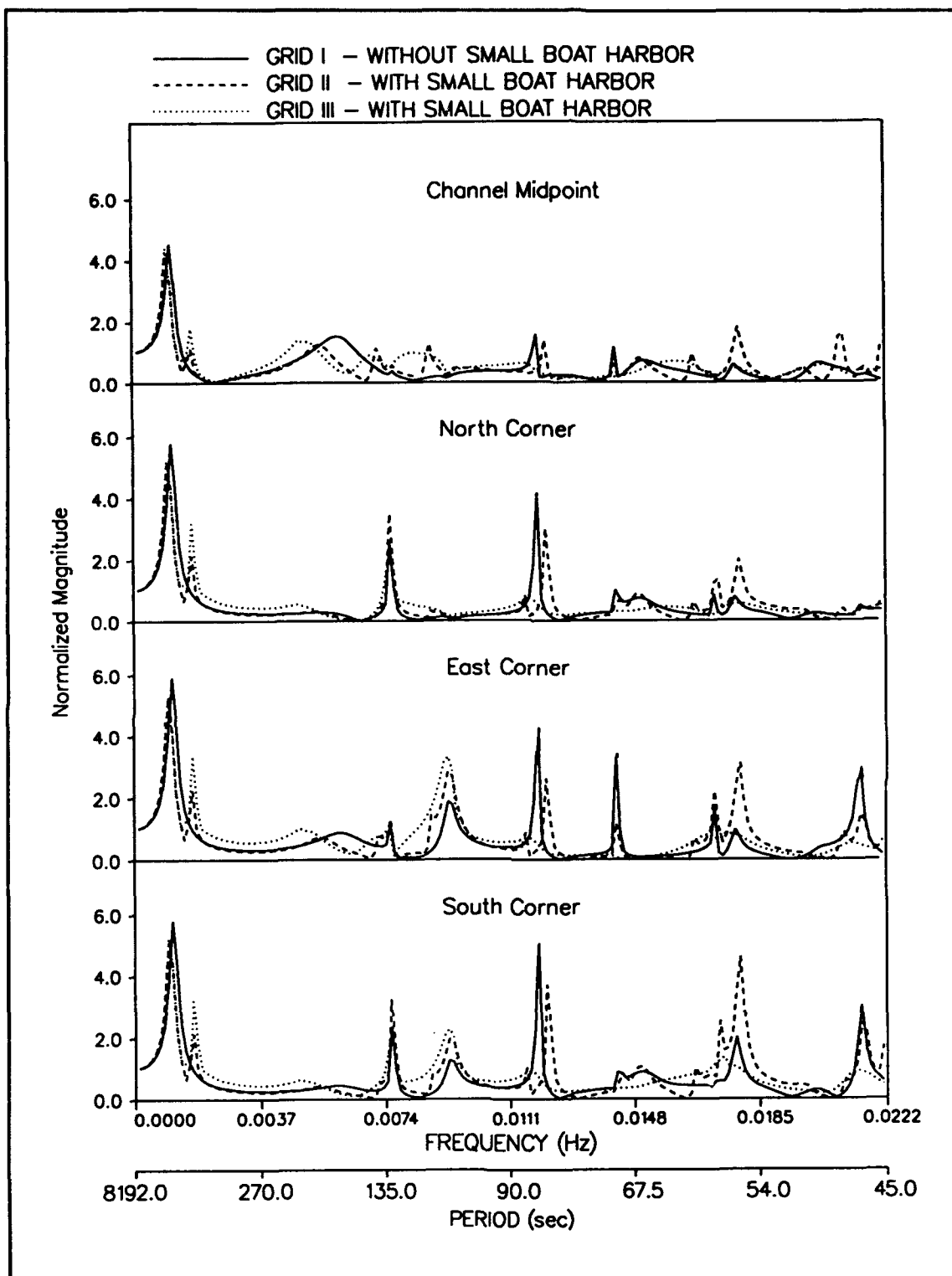
Figure 54. Numerical model frequency response curves for deep-draft harbor, Grids I, II, and III

Grid II. Model simulations of the harbor configuration that included the small boat harbor predicted 12 resonant peaks in the deep-draft basin, 12 resonant peaks in the barge harbor, and 13 resonant peaks in the small boat harbor. Wave periods and wave height amplifications corresponding to peak resonance modes are tabulated for each of the three harbor areas in Tables 9 through 14 and 16 through 18. The resonant peaks in the deep-draft harbor occurred at 1024.0, 585.1, 182.0, 132.1, 107.8, 138.9, 113.8, 81.9, 70.0, 57.7, 55.7, and 46.5 sec. Resonant peaks occurring in the barge harbor were 1024.0, 599.4, 182.0, 138.8, 113.8, 106.4, 86.2, 81.1, 70.0, 56.1, 47.9, and 45.8 sec, and resonant peaks occurring in the small boat harbor were 1024.0, 630.2, 178.1, 138.8, 113.8, 86.2, 81.9, 68.3, 60.2, 55.7, 50.3, 47.9, and 46.6 sec. Frequency response curves of the normalized magnitudes of amplification are shown in Figure 54 for the output locations in the deep-draft harbor, Figure 55 for the output locations in the barge harbor, and Figure 56 for the output locations in the small boat harbor. It should be noted that values along the y-axis of Figure 56 were increased to allow large magnitudes of amplification occurring in the small boat harbor.

The inclusion of the small boat harbor resulted in shifting the long-period Helmholtz mode from 910 sec to 1,024 sec as shown in Tables 9 through 12, and in the frequency response curves for all output locations. The output locations in the deep-draft harbor and small boat harbor also exhibit the appearance of a second long-period resonant mode occurring at 585.0 sec in the deep-draft harbor and 630.0 sec in the small boat harbor. Other significant differences resulting from the inclusion of the small boat harbor are the three resonant peaks that appear at the channel midpoint. Although the peak responses of the south, north, and east locations shift somewhat, the response at these locations is relatively unchanged.

Figure 55. Numerical model frequency response curves for barge harbor, Grids II and III

The inclusion of the small boat harbor resulted in shifting the long-period Helmholtz mode from 910 sec to 1,024 sec as shown in Tables 9 through 12 and in the frequency response curves for all output locations. Output locations in the deep-draft harbor and small boat harbor also exhibit the appearance of a second long-period resonant mode occurring at 585.0 sec in the deep-draft harbor and 630.0 sec in the small boat harbor. Other significant differences resulting from the inclusion of the small boat harbor are the three resonant peaks that appear at the channel midpoint.

88
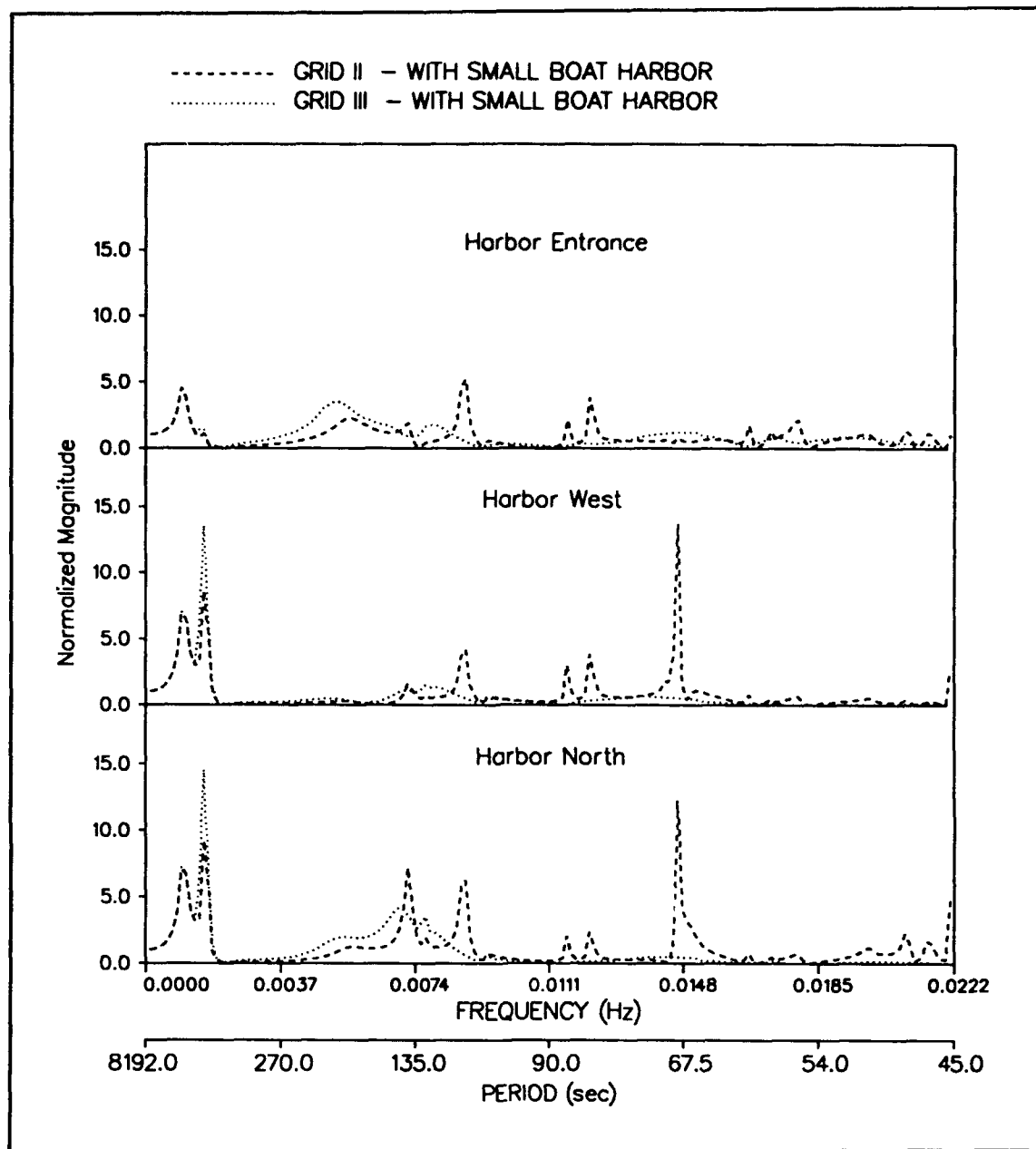
Figure 56. Numerical model frequency response curves for small boat harbor, Grids II and III

Although the peak responses of the south, north, and east locations shift somewhat, the response at these locations is relatively unchanged.

Grid III. The model simulations using Grid III were tested with the same input conditions as Grids I and II. However, it was necessary to calibrate the numerical model predictions with prototype measurements in order to evaluate proposed modifications to the existing harbor. Once it was determined that the model was predicting the resonant modes of

oscillation identified in the prototype measurements, the next task was to predict the magnitudes of wave height amplification. The HARBD model computes a standing wave for a given frequency. For a low frequency, or very long wavelength, the entire harbor responds as if it were a reflecting wall. A standing wave against a reflecting wall has a height of twice the incident wave. Therefore, the low frequency wave height amplitudes predicted by HARBD for input frequencies between 0.000122 and 0.001343 were divided by two. The cutoff for dividing by two was determined by the Helmholtz frequency.

The model was then tested at 0.00004069-Hz (1/24576.06-sec) frequency increments with varying bottom friction coefficients. The resulting wave height amplifications from each test were compared with the prototype measurements to investigate the reduction of wave energy due to the increase of bottom friction. This procedure was repeated until an accurate match of wave height amplification between the model predictions and prototype measurements was possible. This procedure established a correspondence between the incident wave period and dissipation due to bottom friction to accurately predict wave height amplitudes for the wave periods tested.

Once the bottom friction coefficients were identified for the range of wave periods tested, the model was retested using the identified coefficients corresponding to each wave period or frequency. The range of frequencies and wave periods and the corresponding bottom friction coefficient used to reduce the wave energy in the numerical model are given in Table 19.

Table 19
Numerical Model Bottom Friction Coefficients

Period Increments $T_1 - T_2$ (sec)	Frequency Increments $f_1 - f_2$ (Hz)	Friction Coefficient β
8192.02 - 744.73	0.000122 - 0.001343	0.0000
682.67 - 546.13	0.001465 - 0.001831	0.0000
512.00 - 204.80	0.001953 - 0.004883	0.0012
199.81 - 130.83	0.005005 - 0.007644	0.0025
128.00 - 106.39	0.007813 - 0.009399	0.0050
105.03 - 102.40	0.000952 - 0.009766	0.0100
101.14 - 66.06	0.009887 - 0.015138	0.0150
65.54 - 57.29	0.015258 - 0.017455	0.0200
56.89 - 49.95	0.017578 - 0.020020	0.0300

The frequency response curves corresponding to the normalized magnitudes of amplification for the deep-draft basin, barge harbor, and small boat harbor are provided in Figures 54 through 56. The simulations using the refined grid, which included energy dissipation, resulted in numerical model results that accurately predict the prototype measurements in the

deep-draft harbor. The wave period and wave height amplification of the predicted resonant peaks for the three harbor areas are listed in Tables 9 through 16. Grid III predicted nine resonant peaks in the deep-draft harbor. The peaks occurred at 1,024.0, 585.1, 204.8, 143.7, 132.1, 120.71, 107.8, 85.3, and 57.3 sec. The three peaks occurring at the channel mid-point location were 204.8, 143.7, and 120.7 sec. Six resonant peaks were predicted in the barge harbor at 1024.0, 585.1, 204.8, 143.7, 124.1, and 106.4 sec, and six resonant peaks in the small boat harbor at 1024.0, 630.2, 204.8, 143.7, 128.0, and 125.0 sec.

Contour plots of the wave height amplification throughout the harbor are useful in determining oscillation patterns during harbor resonance. Since the numerical model is time independent, the contour plots can be thought of as an instantaneous picture of the harbor oscillation patterns. Contour plots corresponding to the nine resonant modes occurring in the deep-draft harbor basin prior to the inclusion of the small boat harbor are provided in Figures 57 through 65. Contour plots of amplification factors for the resonant modes occurring after the inclusion of the small boat harbor, using Grid III, are shown in Figures 66 through 72. The plots of amplification factors occurring for the Helmholtz mode both prior to and after inclusion of the small boat harbor show how the water surface elevation rises up and down in unison throughout the harbor and marina. The second resonant mode occurring in the deep-draft harbor, 585.0 sec, occurs at 630.0 sec in the small boat harbor. This appears to be the pumping
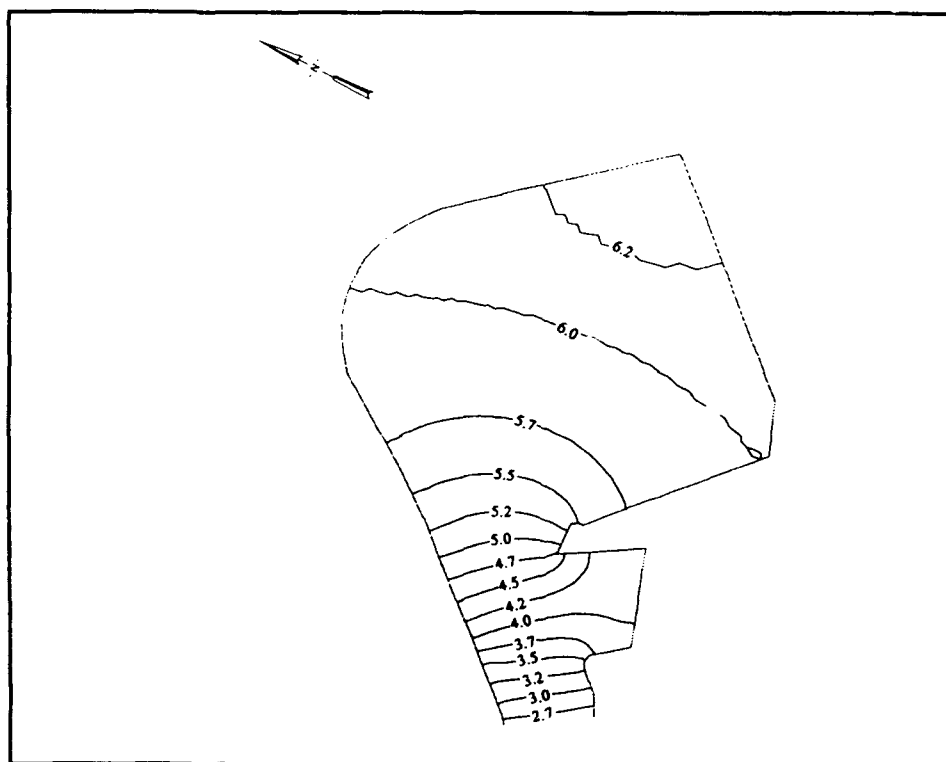
Figure 57. Harbor resonance contour plot, 910.2 sec
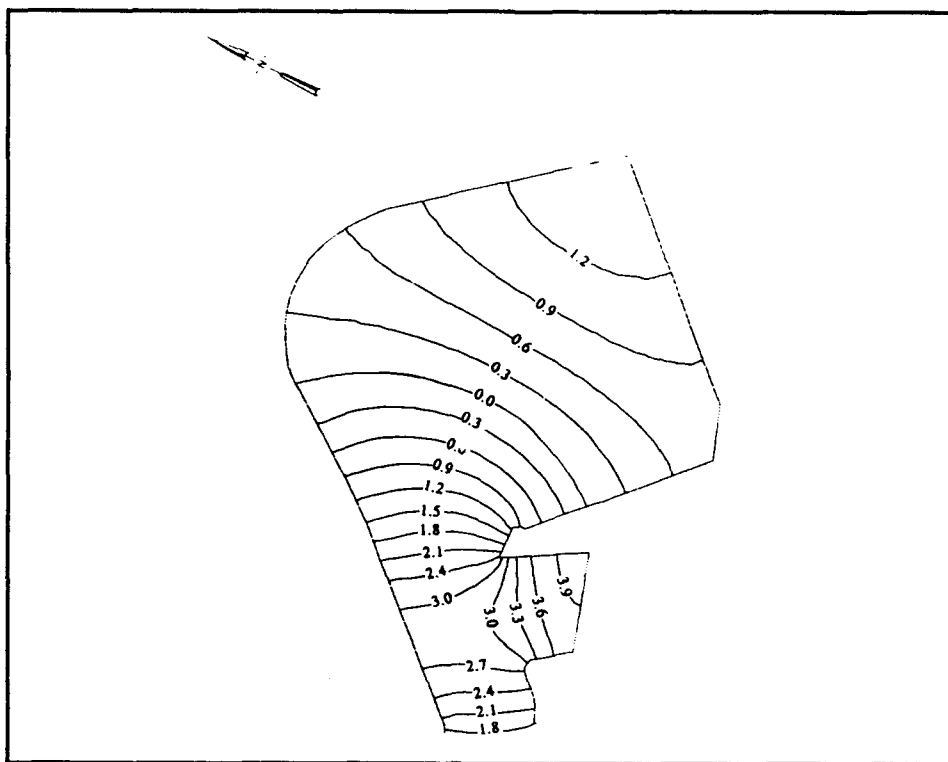
Figure 58. Harbor resonance contour plot, 167.2 sec
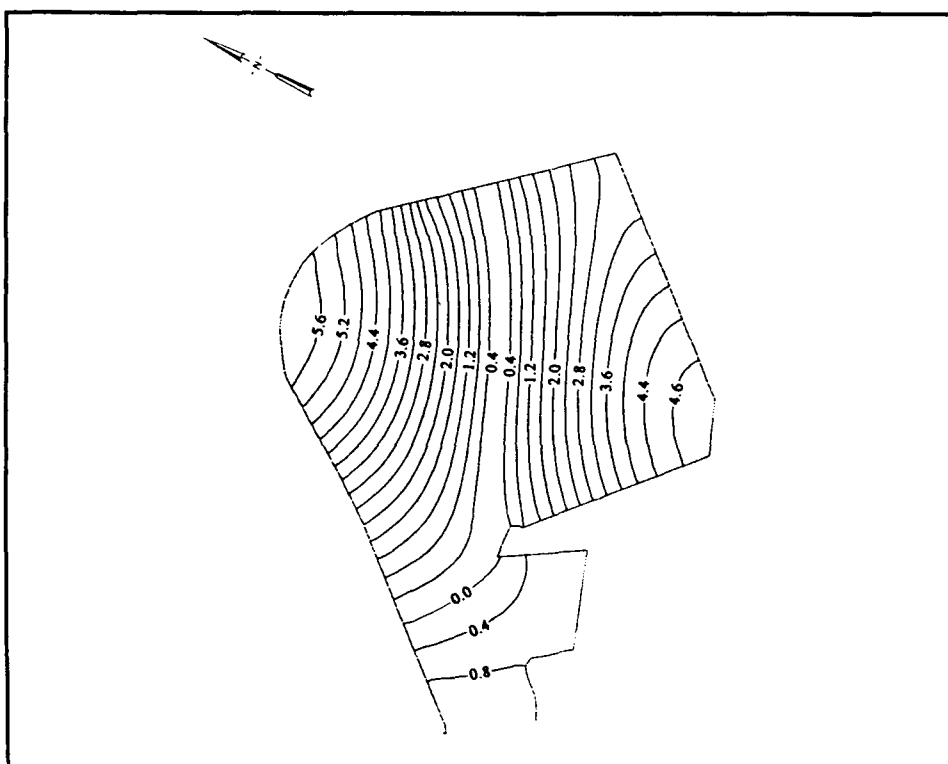
Figure 59. Harbor resonance contour plot, 132.1 sec
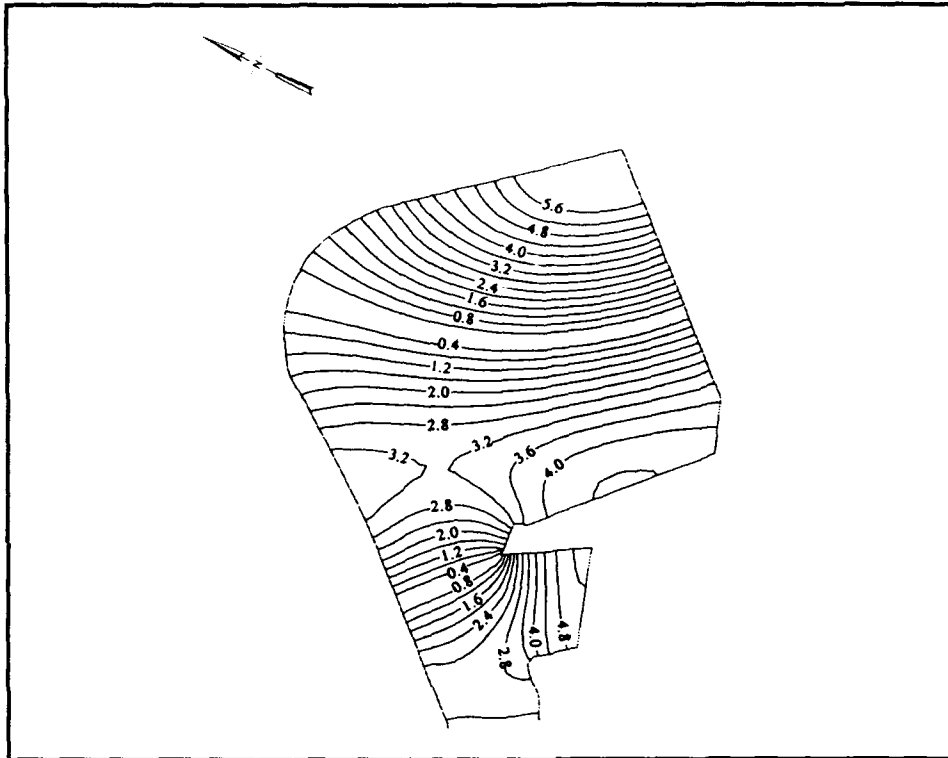
Figure 60.   Harbor resonance contour plot, 107.8 sec
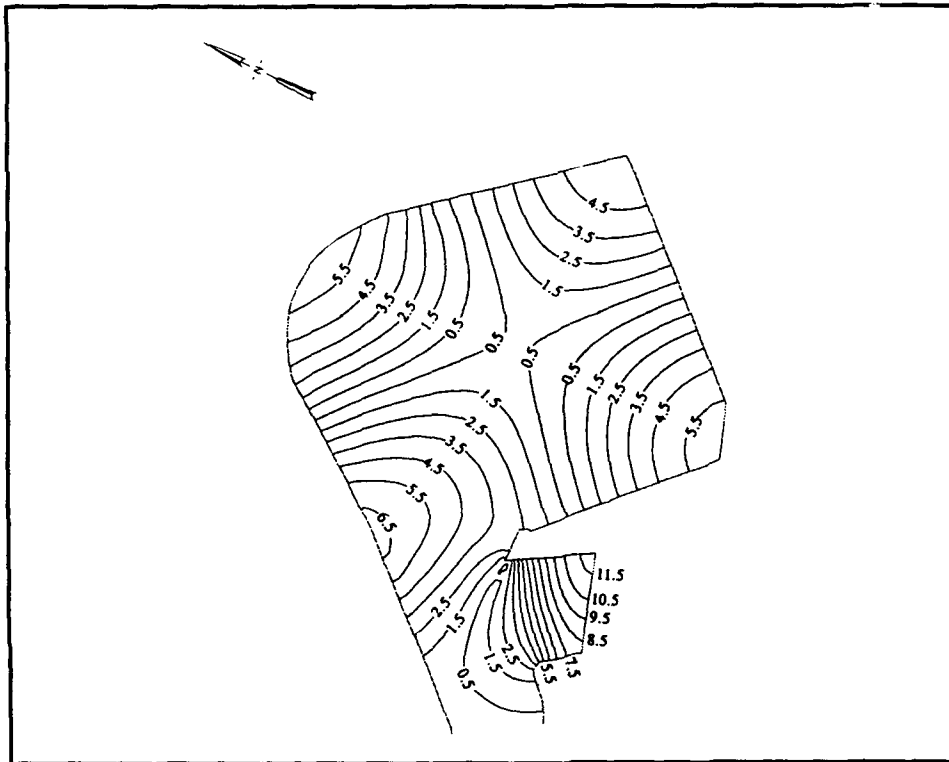
Figure 61.   Harbor resonance contour plot, 83.6 sec
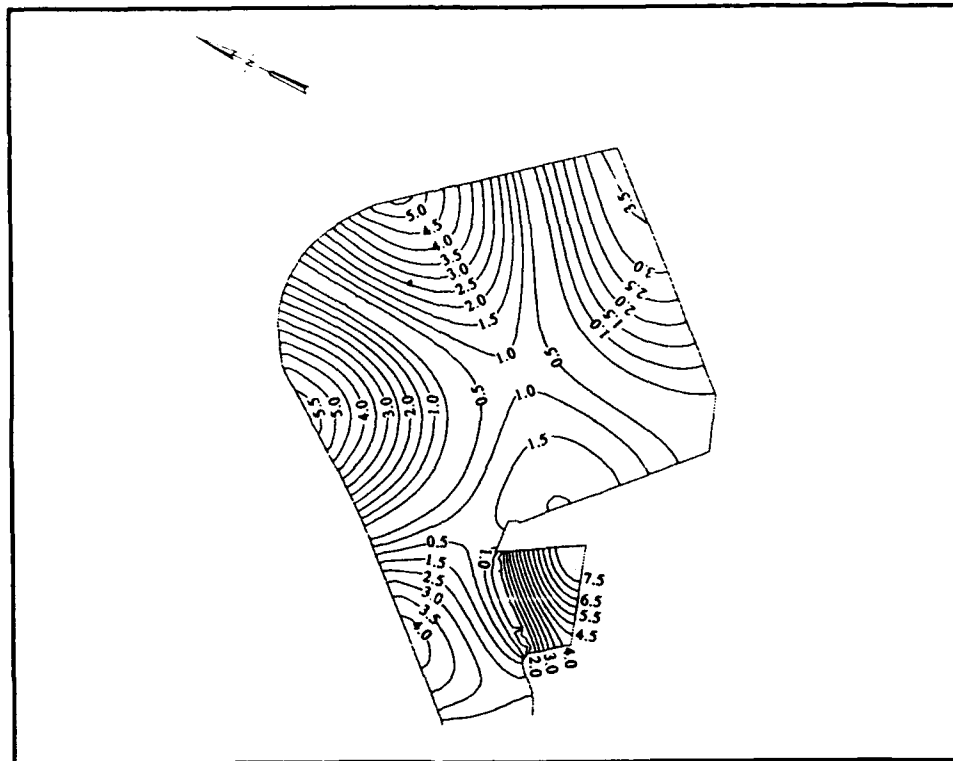
Figure 62. Harbor resonance contour plot, 70.0 sec
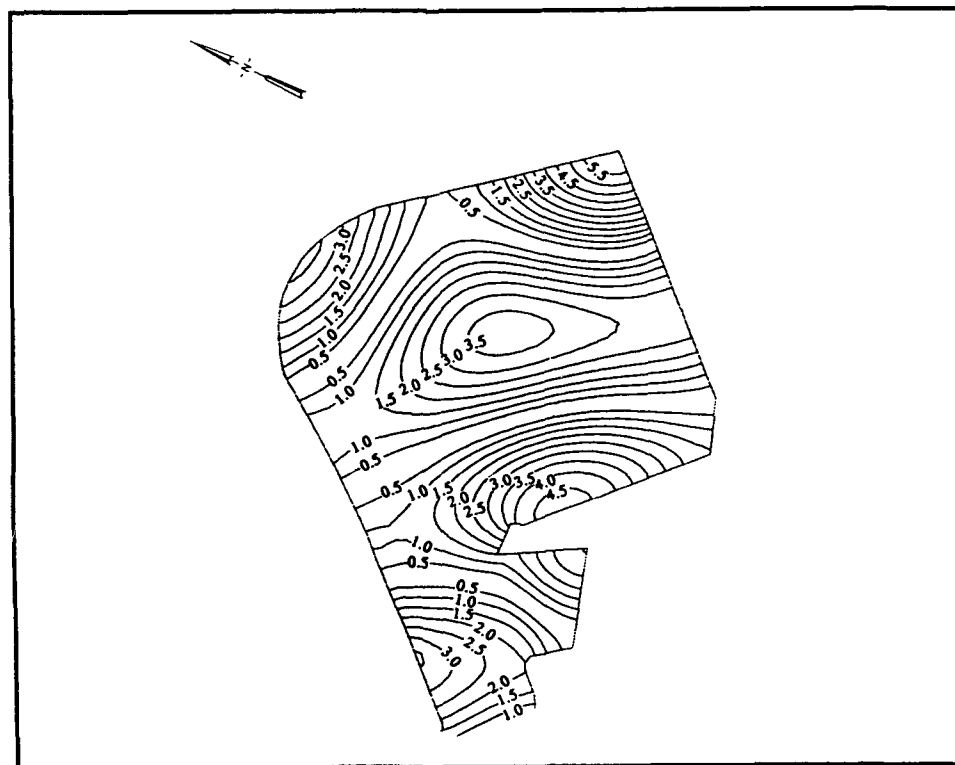
Figure 63. Harbor resonance contour plot, 58.1 sec
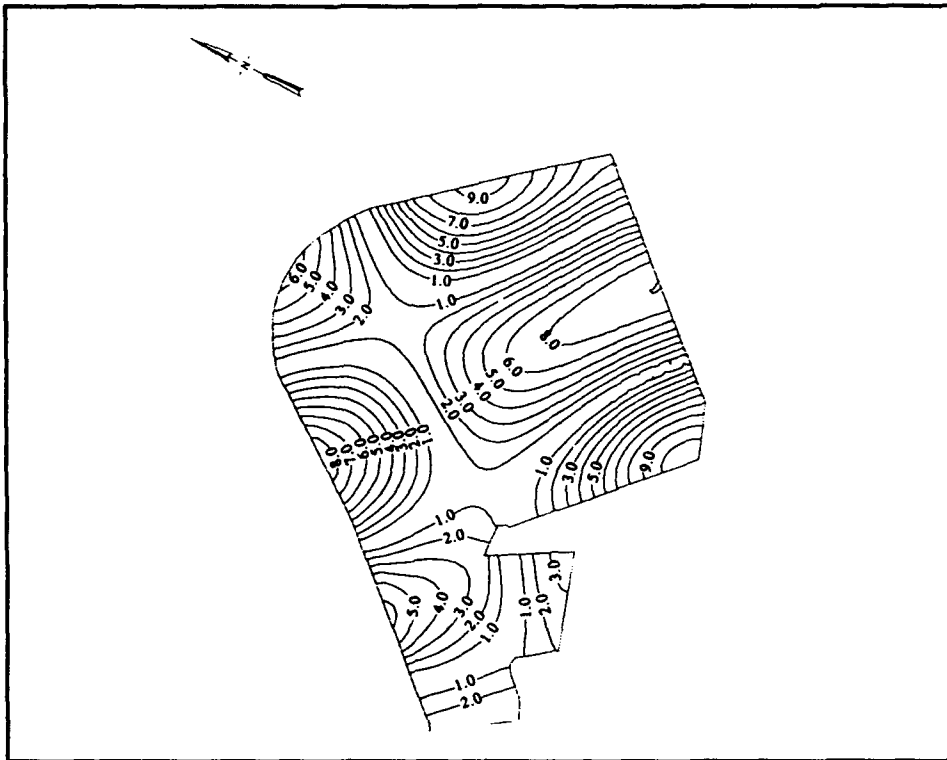
Figure 64. Harbor resonance contour plot, 56.1 sec
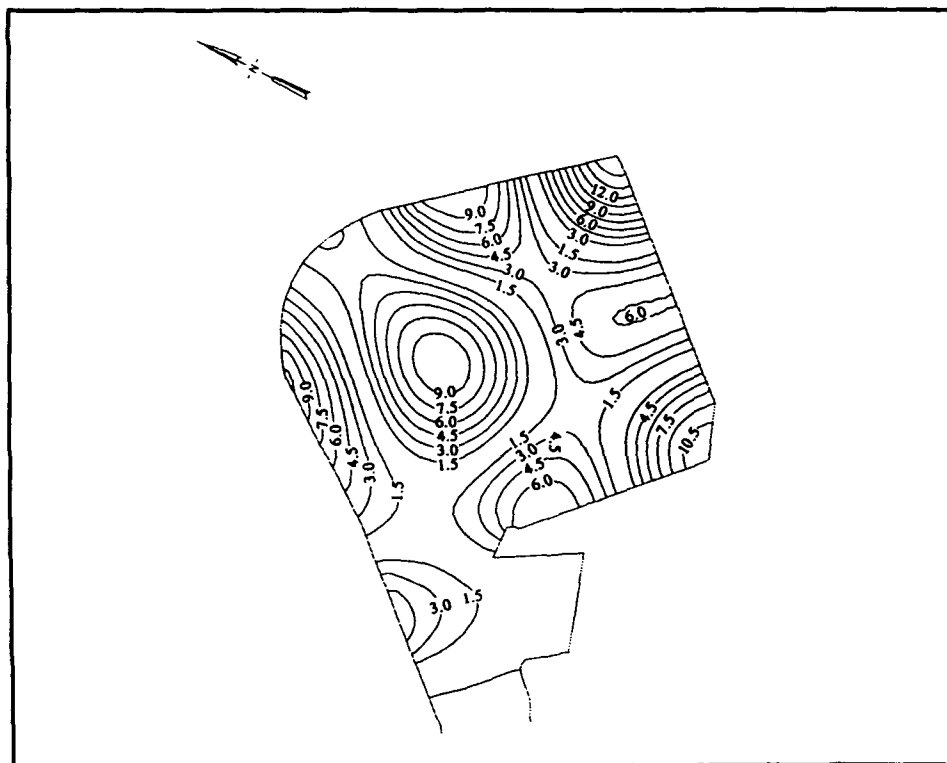
Figure 65. Harbor resonance contour plot, 45.6 sec
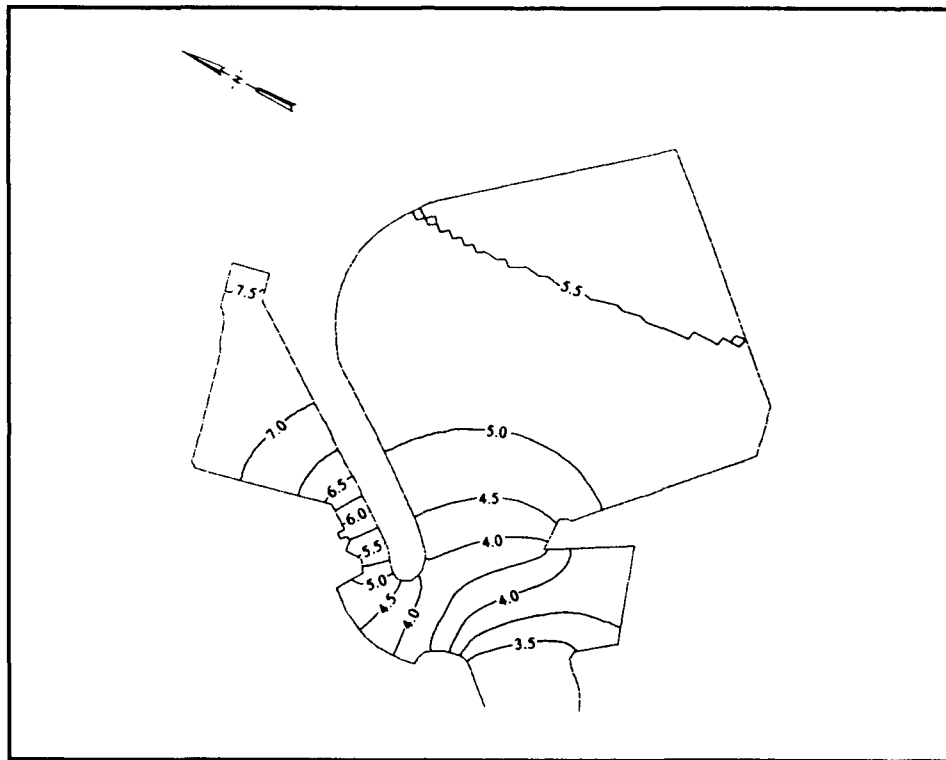
Figure 66. Harbor resonance contour plot, 1024.0 sec
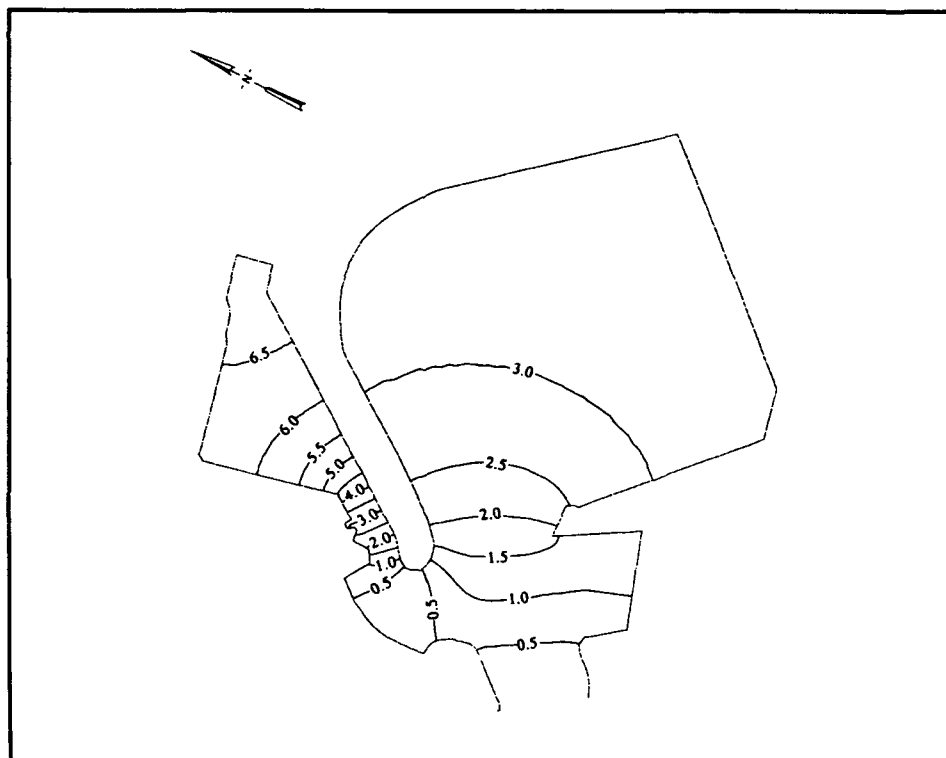
Figure 67. Harbor resonance contour plot, 585.1 sec
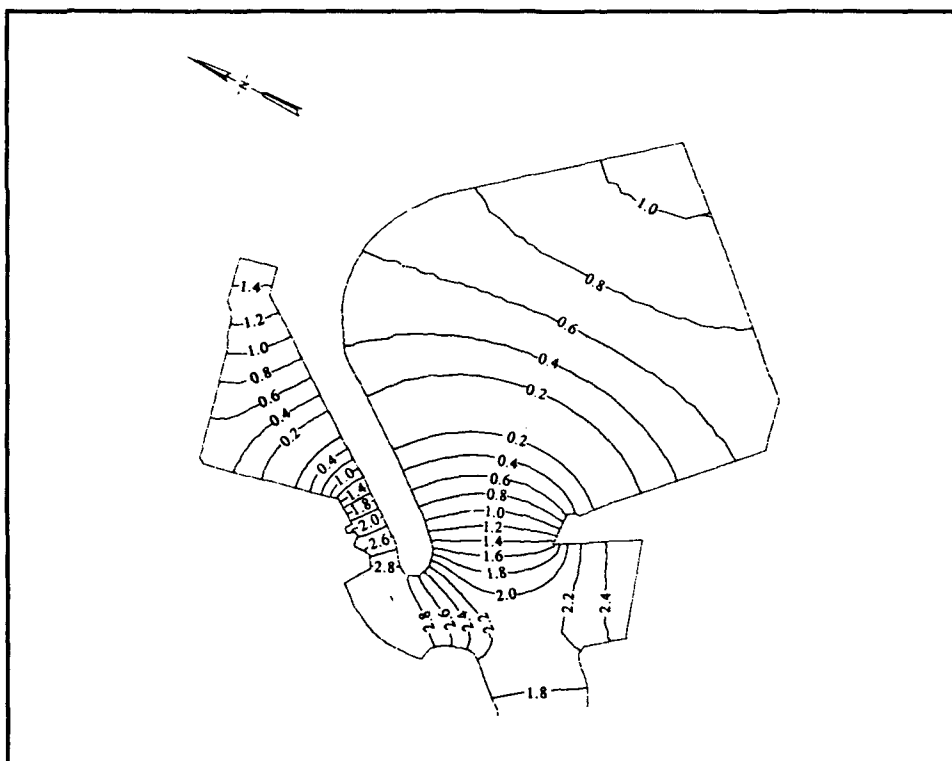
Figure 68. Harbor resonance contour plot, 204.8 sec
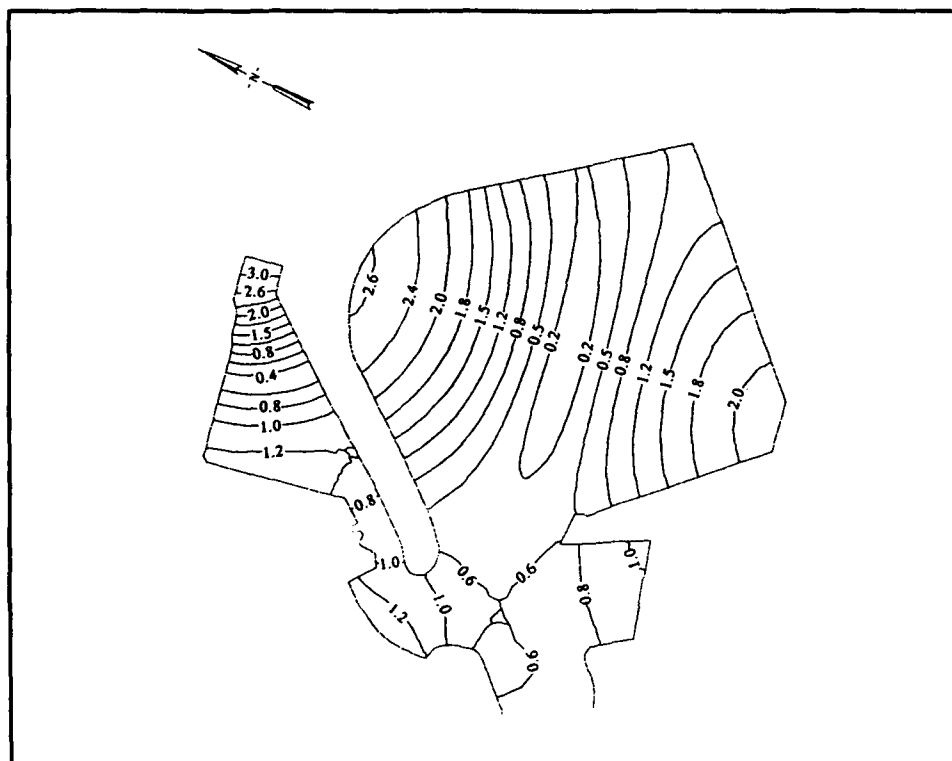
Figure 69. Harbor resonance contour plot, 132.1 sec
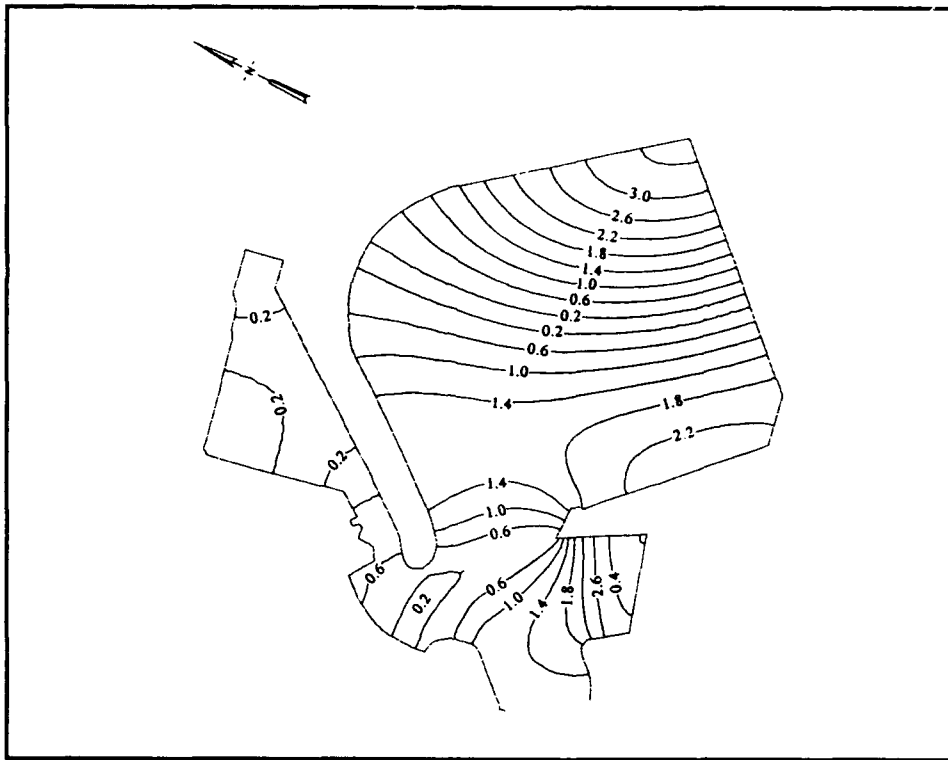
Figure 70. Harbor resonance contour plot, 107.8 sec
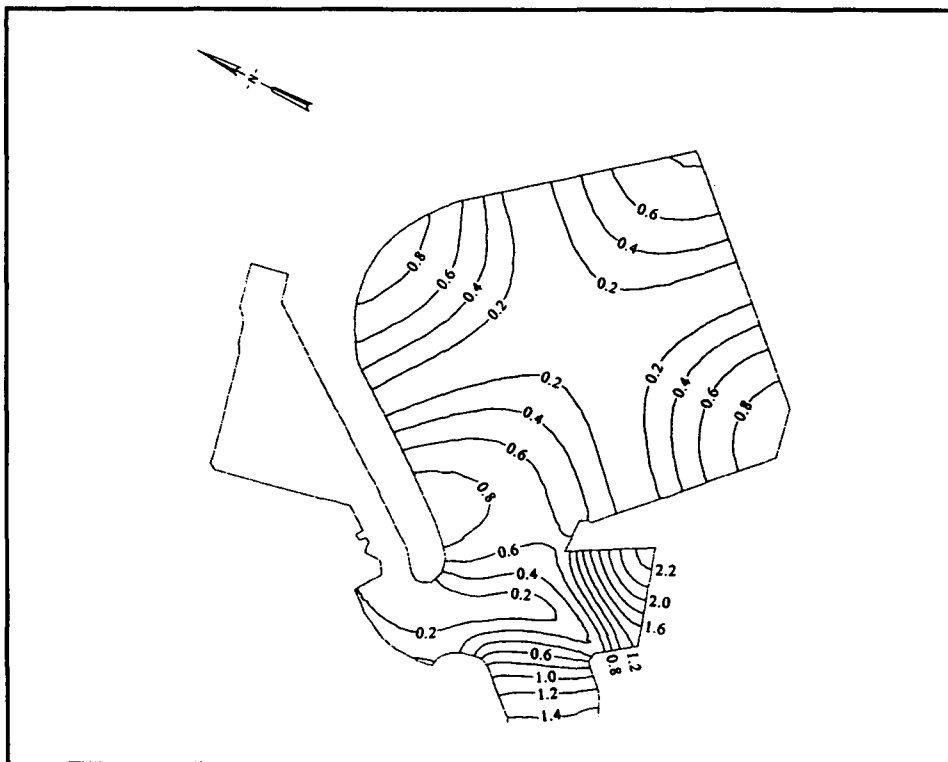
Figure 71. Harbor resonance contour plot, 85.3 sec
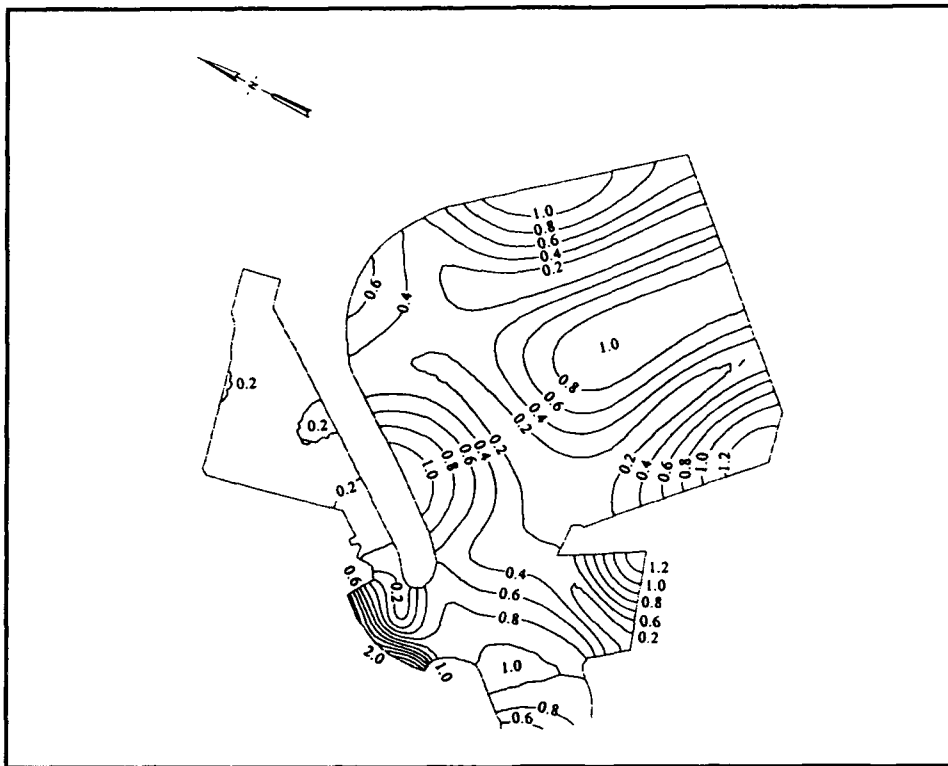
Figure 72.   Harbor resonance contour plot, 57.3 sec

mode of the small boat harbor. As Figure 67 shows, the elevation in the small boat harbor basin is uniform at this mode.

Physical Model Study

An undistorted, three-dimensional physical model of the Barbers Point Harbor complex (Figure 73) was constructed at a model-to-prototype scale $L_r = 1:75$, in accordance with Froude scaling laws (Stevens et al. 1942). It was patterned after the earlier physical model studies by Palmer (1970) and Lee (1985). The nearshore area extends to the 100-ft mllw contour and includes approximately 3,500 ft on either side of the entrance channel. Total area of the model was over 11,000 ft^2. The model scale was selected to allow proper reproduction of significant harbor features, typical storm waves and longshore currents, and a design containership (Briggs, Lillycrop, and McGehee 1992). The design containership was used in a navigation study which is described in Briggs et al. (in preparation).

The model was constructed using templates, sand filler, and a 2-in. mortar cap to mold the contours. The basin sides were lined with wave absorbers and one side was open to an adjacent basin to minimize reflections and cross-basin oscillations. The model is aligned with north in the prototype so that all harbor features, wave gages, and simulated wave

Figure 73. Physical model of Barbers Point Harbor complex

conditions correspond with those in the prototype (Briggs, Lillycrop, and McGehee 1992).

Wavemaker

Waves were generated with a unique wavemaker that can make waves from many different directions at once, typical of those occurring in nature. The directional spectral wave generator (DSWG) (Figure 74) is an electronically controlled, electromechanical system, designed and built by MTS Systems Corporation, Minneapolis, MN. The generator is 90 ft long and consists of 60 paddles, each 1.5 ft wide and 2.5 ft high. The 60 paddles are segmented into four portable modules with 15 paddles per module. Each wave paddle is independently driven at its joint by a 3/4-hp electric motor operating in piston mode. Flexible plastic plate seals between the paddles inhibit water from flowing between the paddles and produce a smoother, cleaner wave form (Outlaw and Briggs 1986, Harkins 1991).

Typical peak wave periods are 1.00 to 3.00 sec, with longer and shorter periods possible. The range of strokes is ± 12 in., corresponding to a ± 10-V input signal. Offset angles between paddles can be continuously varied within the range of 0 to 180 deg using the "snake principle" to produce directional waves at angles approaching ± 90 deg for most wave periods. The DSWG was aligned parallel to the 100-ft contour, at approximately 325 deg relative to north. This alignment permitted the greatest range of wave conditions and directions.

Figure 74. Directional Spectral Wave Generator (DSWG)

A Digital Corporation VAX 11/75 minicomputer was used to control the DSWG. It performs digital to analog conversion for the 60 paddles at run time, monitors paddle displacement and feedback, calibrates wave gages, and digitizes the measured data. A Digital Vax 3600 minicomputer was used to perform preliminary analysis of the measured wave data. A third computer, WES' CRAY-YM-P supercomputer, was used to calculate control signals for the wavemaker and do more advanced analysis of the data. All three computers are located in climate-controlled buildings and communicate through a fiber-optic network.

Instrumentation

Capacitance wave gages were used to measure surface elevations at the gage locations shown in Figure 75. Nine locations correspond with the prototype wave gage positions. The two locations labeled S_{xy1} and S_{xy2} represent the two positions of the slope array between 1986 and 1990. The two locations north of the entrance channel represent the offshore (Of) and onshore (On) wave gages. The remaining prototype wave gages in the deep-draft harbor entrance and basin are represented by the channel entrance (Ce), channel midpoint (Cm), south corner (Sc), north corner (Nc), and east corner (E1) and (E2), which were the two locations of the east corner wave gage. These locations correspond with output locations used in the numerical model study described in this chapter.
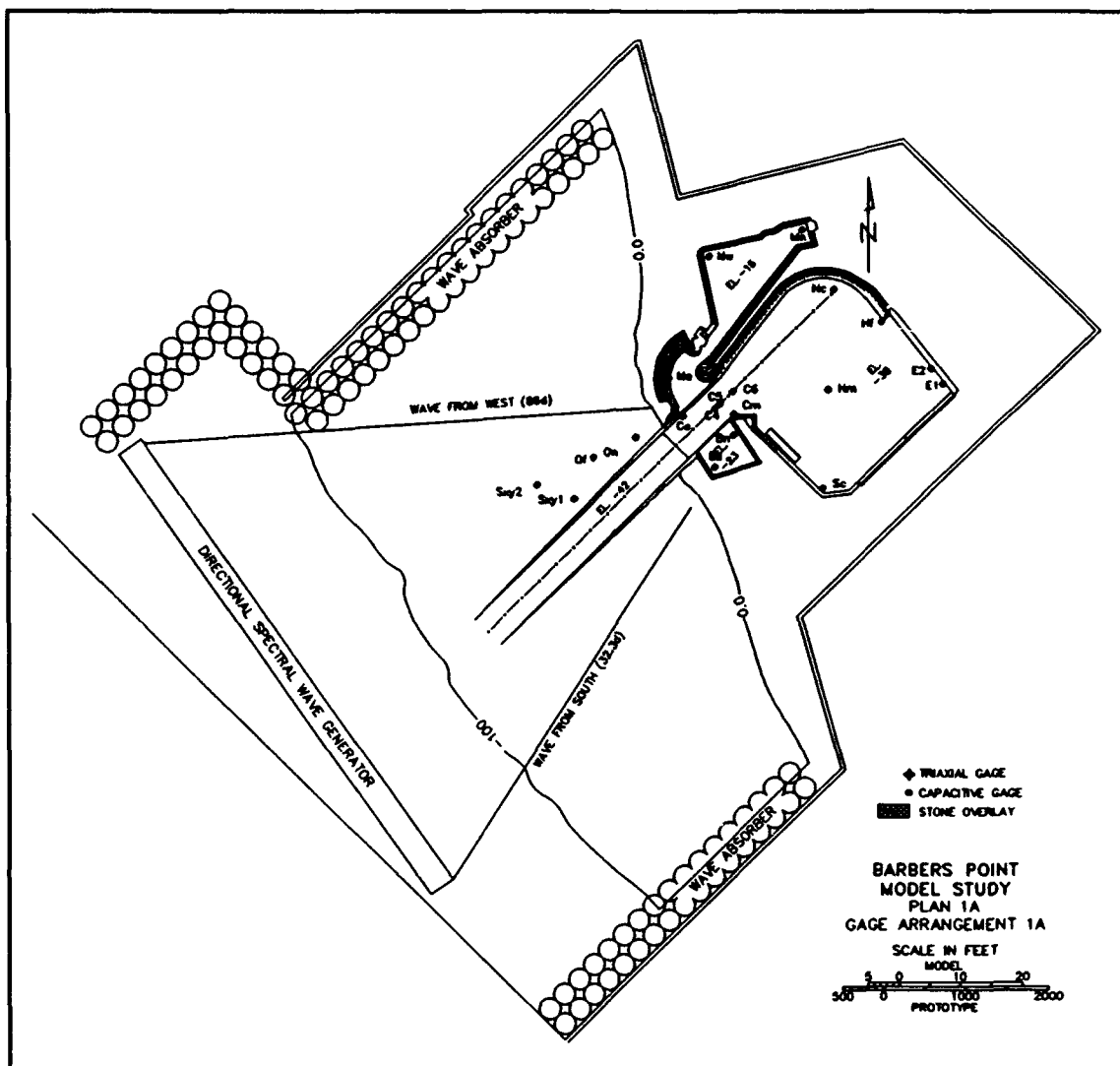
Figure 75. Physical model layout and gage locations

To measure reflection coefficients, three wave gages labeled C4, C5, and C6 were positioned in a Goda array and were located in the deep-draft harbor entrance channel. The remaining physical model wave gages were coincident with output locations of the numerical model study and were included to better quantify the harbor response. Two additional wave gages were located in the deep-draft harbor basin to measure wave conditions in the center of the basin and at the location of a proposed ferry terminal. These locations are labeled harbor center (Hc) and harbor ferry (Hf). Wave gages located in the small boat and barge harbors were used to evaluate wave conditions in the two harbors. These locations are labeled harbor north (Hn), harbor west (Hw), Harbor entrance (He), barge north (Bn), and barge south (Bs).

Wave gages were calibrated prior to each test with a computer-controlled procedure incorporating a least squares fit of measurements at 11 steps through the water column. After waiting a sufficient time for slower traveling high-frequency components to reach back wave gages, data were sampled at 10 Hz (i.e., $\Delta = 0.10$ sec) for 2,400 sec (24,000 points) (Briggs, Lillycrop, and McGehee 1992).

Test wave conditions

Table 20 lists the prototype wave conditions simulated in the physical model. The eight cases were selected from prototype wave measurements collected between July 1986 and March 1990. Simulated wave periods, heights, and directions range from 6 to 20 sec, 6 to 9 ft, and the 240- to 270-deg azimuth with directional spreading up to 10 deg, respectively. A water level of mllw was used for all cases. Selection of test wave conditions was based on: (a) preference given to the period after the small boat harbor was opened in July 1989 and the second slope array was installed; (b) obtaining the largest wave heights; (c) a representative range of wave period and direction; (d) maximum number of operational prototype wave gages for comparisons; and (e) reproducible wave directions due to physical model constraints. Each case is representative of wave conditions that could have occurred prior to or after opening of the small boat harbor. Therefore, for comparisons of long wave harbor response, all cases were tested in the physical model with the small boat harbor open (Briggs, Lillycrop, and McGehee 1992).

Table 20
Physical Model Selected Wave Conditions

No.	Date	Time	Peak Period sec	Significant Wave Ht deg	Average Direction deg	Range of Directions deg
1	16 Nov 89	1306	10-12	7.0	86	33-101
2	4 Nov 88	1600	6-8	9.8	45	45-86
3	2 Mar 89	0704	6-8	7.0	28	28-59
4	3 Mar 89	0104	8-10	7.4	54	38-92
5	3 Nov 86	1439	8-10	10.0	56	44-59
6	21 Jan 88	2006	16-18	7.8	46	46-77
7	22 Jan 88	0806	14-16	8.1	47	43-68
8	23 Jan 88	0206	12-14	7.1	49	37-62

Results

The relationship between wave conditions outside and inside the harbor can be expressed in terms of an amplification factor. In this study, amplification factor estimates were calculated for all gages located inside the harbor using incident wave conditions from the S_{xy2} gage. Estimates

of the amplification factors for each of the eight test wave conditions were calculated separately and averaged together. Three bands were band-averaged in the frequency domain to give a frequency resolution in model scale approximately equal to that of the prototype ($\Delta f = 3/2400$ sec = 0.00125 Hz model, $\Delta f = 0.000144$ Hz prototype). The degrees of freedom of these estimates are approximately $v = 48$, much less than the prototype amplification factor estimates. Therefore, accuracy of the physical model estimates is limited by the short duration of the data sets. Wave period and wave height amplification of the predicted resonant peaks for the deep-draft basin, barge harbor, and small boat harbor are listed in Tables 21 through 23, respectively. In the deep-draft harbor, the physical model predicted resonant modes at 207.9, 129.9, 109.4, 82.2, and 57.1 sec. The three peaks at the channel midpoint location were predicted at 207.9, 149.5, and 116.8 sec. The model predicted peaks at 207.9, 149.5, and 125.0 sec in the barge harbor, and 201.8, 180.7, 171.8, 152.8, 149.5, 129.9, 125.2, and 123.0 in the small boat harbor.

Table 21
Physical Model Resonant Modes of Oscillation - Deep-Draft Harbor

South		East		North		Midpoint	
Wave Per (sec)	Amp Fac	Wave Per (sec)	Amp Fac	Wave Per (sec)	Amp Fac	Wave Per (sec)	Amp Fac
						207.9	1.2
						149.5	1.1
129.9	1.0			129.9	1.0		
						116.8	1.0
109.4	1.4	109.4	2.4				
82.2	1.5	82.2	1.2	82.2	1.4		
57.1	1.0	57.1	1.3				

Table 22
Physical Model Resonant Modes of Oscillation - Small Boat Harbor

North		West		Entrance	
Wave Per (sec)	Amp Fac	Wave Per (sec)	Amp Fac	Wave Per (sec)	Amp Fac
				201.8	2.4
				180.7	2.0
				171.8	2.2
152.8	5.3				
		149.5	2.2		
129.9	1.7				
		125.2	1.8		
		123.0	1.6		

Table 23			
Physical Model Resonant Modes of Oscillation - Barge Harbor			
North		South	
Wave Per (sec)	Amp Fac	Wave Per (sec)	Amp Fac
207.9	2.0	207.9	1.9
149.5	1.6	149.5	1.6
123.0	1.4	123.0	1.5

Intercomparison of Results

Figure 76 is a comparison of the frequency response curves of amplification factor estimates from the numerical and physical model predictions from the four corners of the deep-draft basin. Resonant modes in the harbor are identified by peaks occurring in these estimates. The most noticeable difference between the two models occurs in the very long-period resonant peaks. The numerical model predicted these long-period resonant peaks at 1,024.0 sec, which is the Helmholtz or pumping mode of the harbor, and 585.0 sec, which is the Helmholtz mode of the small boat harbor. The physical model did not predict these modes since the physical model experiments were run for 40 min (model scale) and this run length did not provide sufficient resolution to identify these modes. The physical model run time can resolve waves with periods less than 400 sec. The agreement between the models for predicting the remaining resonant modes is good, although there is a difference in magnitudes of the peaks. Both models identified resonant peaks at about 204.0, 132.0, 107.0, 85.0, and 57.0 sec. As shown in Figure 76, the three peaks that appeared in the channel midpoint data after inclusion of the small boat harbor were also predicted by both models.

Results from the models at the locations in the barge harbor also followed similar trends. Frequency response curves of amplification factors for the barge south, east, and north locations are shown in Figure 77. The barge east location was not included in the physical model. In all three barge harbor locations, the numerical model identified the Helmholtz modes of the deep-draft and small boat harbors which are expected to occur throughout the harbor. Both models predicted three additional peaks in the barge harbor which also appear in the channel midpoint data after inclusion of the small boat harbor. The models also identified a 107.0-sec peak in the barge harbor, which is coincident with data from the east and south corners. Differences between the model predictions are a slight shift in frequency of occurrence and a larger magnitude of amplification in the numerical model data. Both models show larger magnitudes of amplification occurring in the barge harbor in comparison to the deep-draft harbor. This is due to wave diffraction into the barge harbor as energy enters and propagates throughout the harbor.
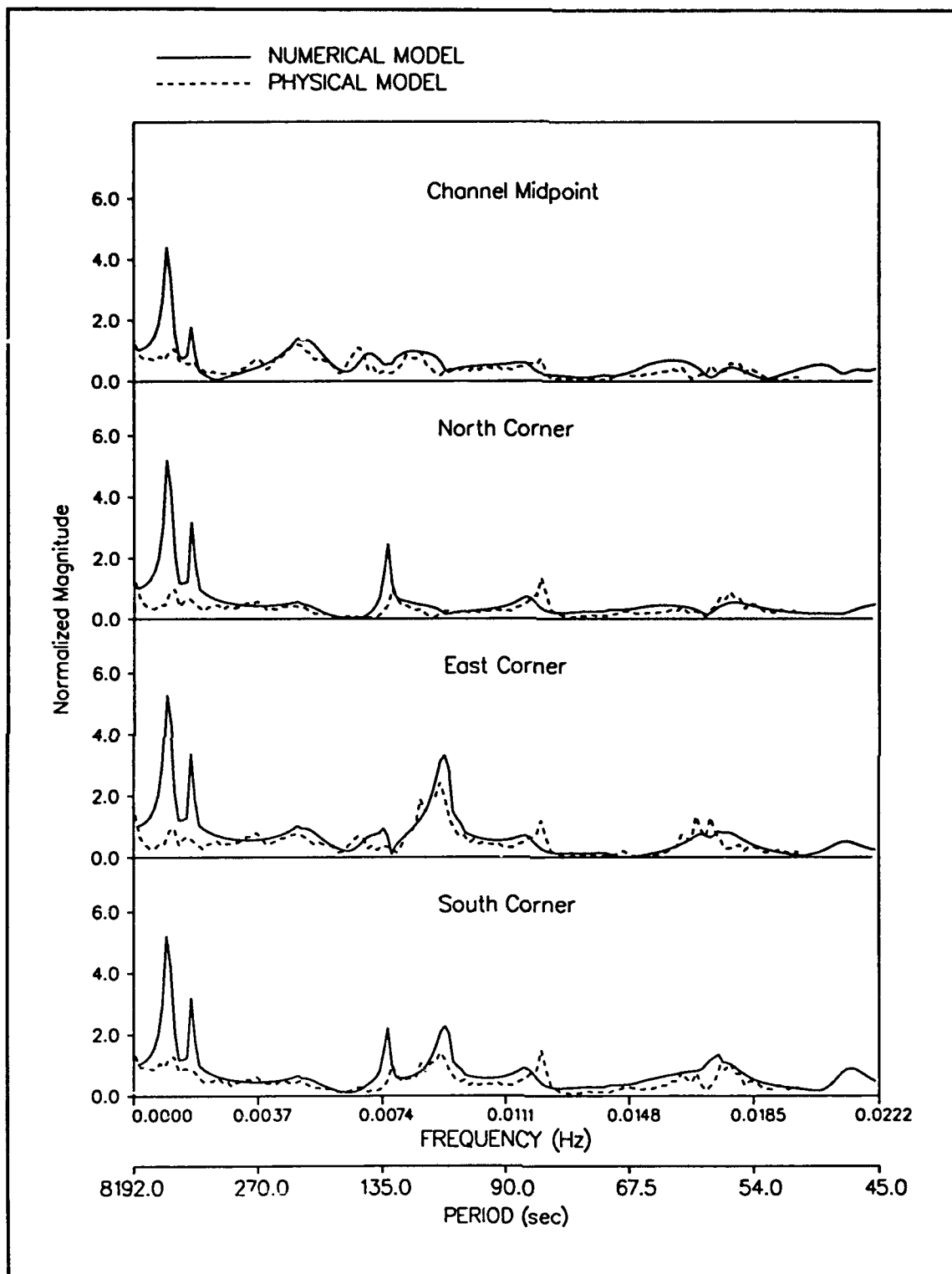
Figure 76. Numerical and physical model frequency response curves, deep-draft harbor
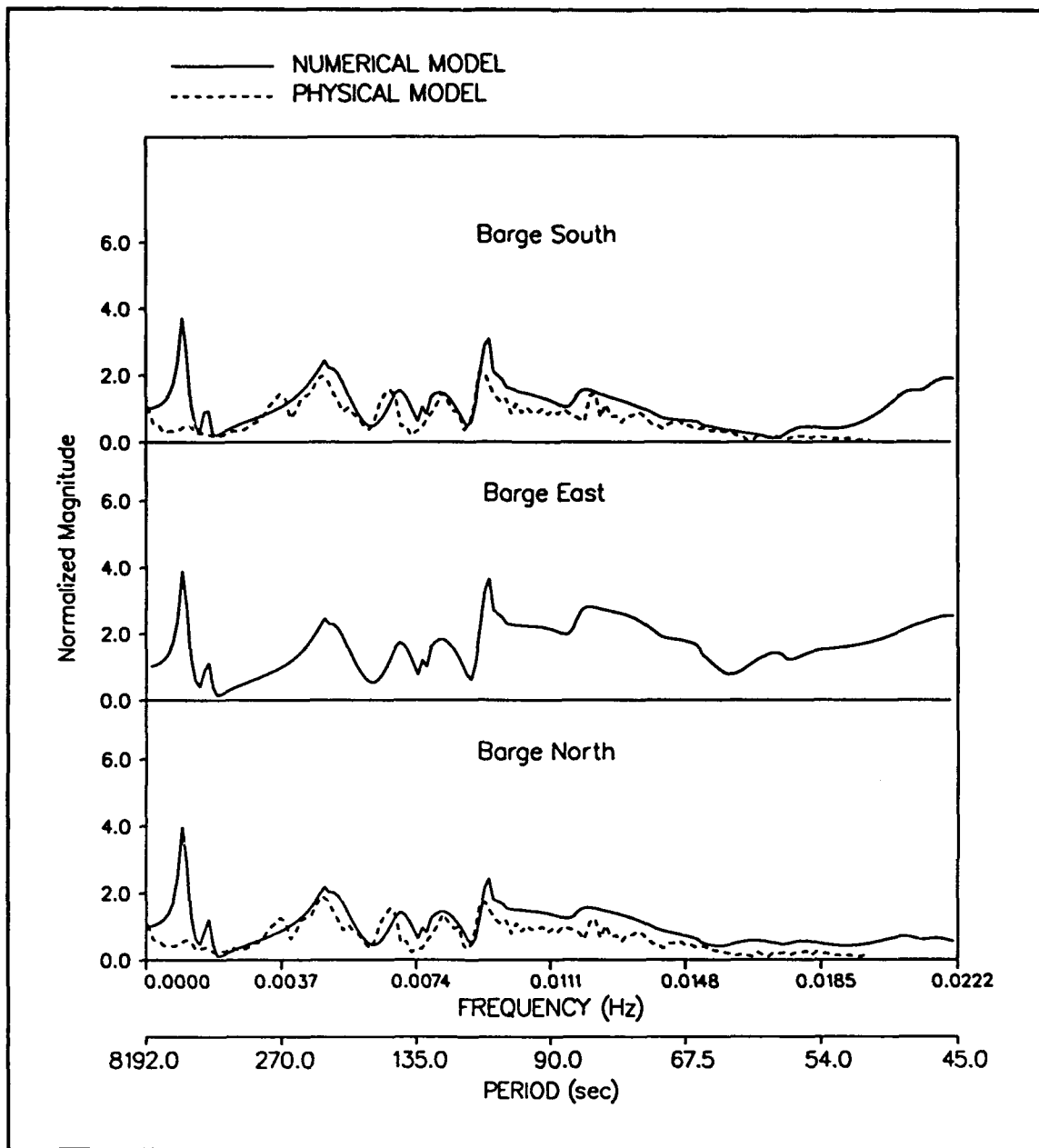
Figure 77. Numerical and physical model frequency response curves, barge harbor

The frequency response curves of amplification for the numerical and physical model predictions in the small boat harbor are shown in Figure 78. Again, the agreement between the models is good. It should be noted that values along the y-axis of this figure were increased since the models predicted larger magnitudes of amplification occurring in the small boat harbor than in the deep-draft and barge harbors. Noticeably, the resonant peak at 630.0 sec is larger than the 1024.0-sec peak. This is the Helmholtz mode of the small boat harbor. The remaining peaks appear at about 125.0, 167.0, and 204.0 sec.
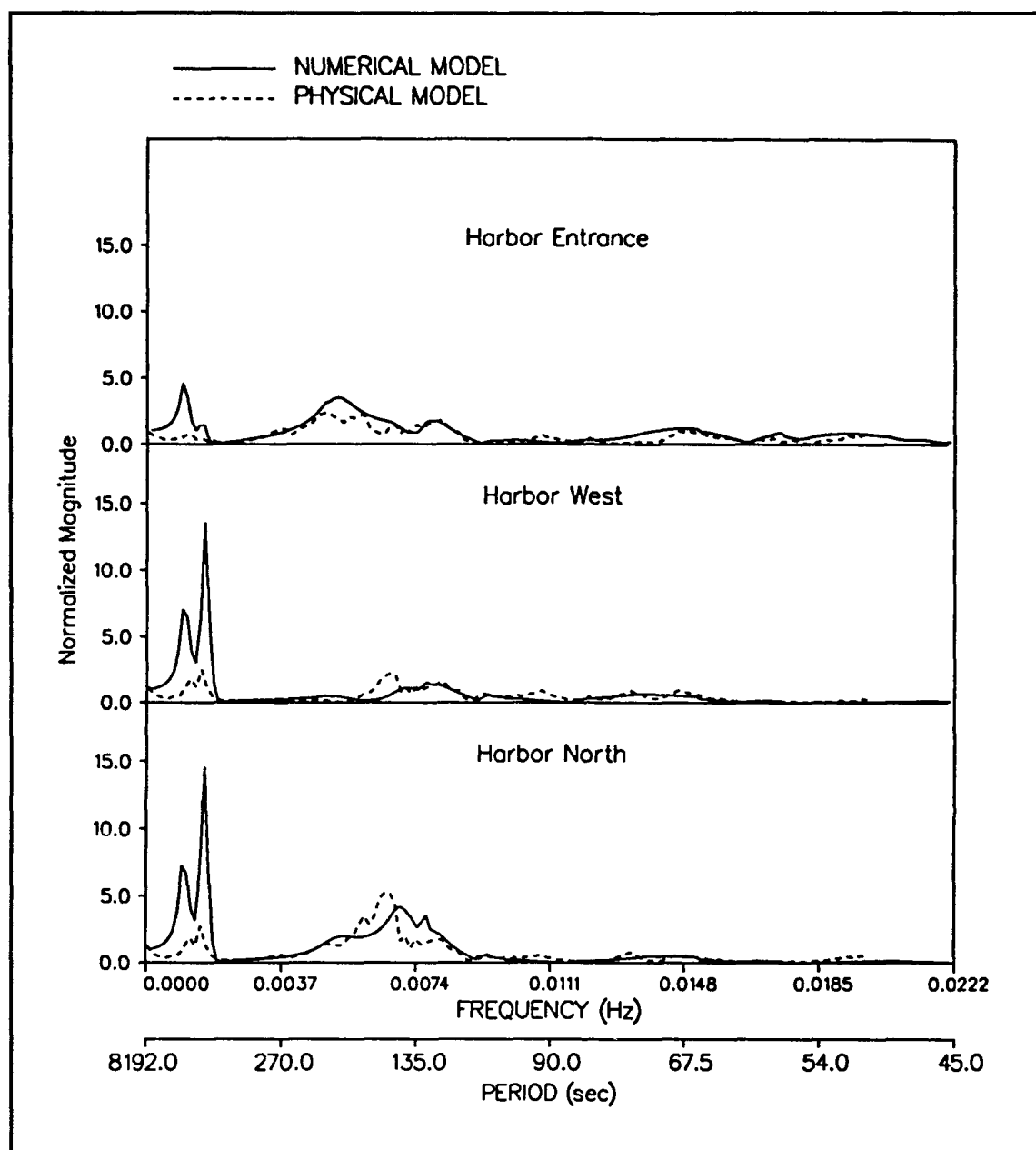
Figure 78. Numerical and physical model frequency response curves, small boat harbor

4 Monitoring Program

Monitoring Objectives

Objectives of the MCCP in monitoring Barbers Point Harbor were to:
(a) evaluate and validate the results of the model studies conducted for
harbor design; (b) perform wave gaging to measure wave climates in deep
water and nearshore areas, and long period oscillations of the harbor;
(c) relate the conditions outside the harbor to surge found inside the har-
bor; (d) evaluate the effectiveness of the wave absorber; and (e) compare
the measured data to the predictions of state-of-the-art physical and numer-
ical model studies.

Wave Gage Installation

Planning

Much planning was necessary in order to organize, coordinate, and
implement installation of wave gaging instruments at the project site. A
meeting was held with field wave gaging experts to develop a clear defini-
tion of the main monitoring goals of the project. Information pertaining
to the bathymetry, wave, and current conditions were useful in determin-
ing the method of gage installation. A log of existing equipment and
equipment that needed to be acquired was also generated at this meeting.
Coordination meetings were held with users of the facilities to notify
those involved of the monitoring plan; to obtain harbor usage and develop-
ment information; to determine the optimal location for a shore station, if
necessary; and to discuss uses of the acquired data with the local popula-
tion that utilize Barbers Point Harbor (Boc 1987).

Since Barbers Point Harbor was constructed in a relatively undevel-
oped area, complications were encountered in obtaining telephone and
electrical connections. An investigation of possible sources determined
that standard telephone and electrical connections would be costly. How-
ever, use of a cellular phone also proved to be an inviable option due to

the incompatibility of the data and the cellular phone signal; therefore, a standard telephone connection was utilized. To reduce costs, the telephone company provided a connection terminal at the closest telephone pole and the Corps installed the connections to the site. In reviewing sources for electricity, a solar electric system was utilized since the monitoring location is on the dry leeward side of the island with adequate direct sunshine. A photovoltaic system was designed and installed through a local contractor (Boc 1987).

Since there were no existing structures for housing the photovoltaic system, receiver, and phone connections at the site, a small wood building with a solar panel installed in the roof was constructed to house the equipment (Figure 79). The building orientation and roof angle were designed for compatibility with the solar electric system. A chain link fence topped with barbed wire provided security for the system (Boc 1987).

Installation

The entire installation including setup was completed in about one week. Setup included fabricating all mounting frames and the mounting and wiring of the gages with concurrent trenching and installation for the telephone lines. The majority of the equipment used in the monitoring is
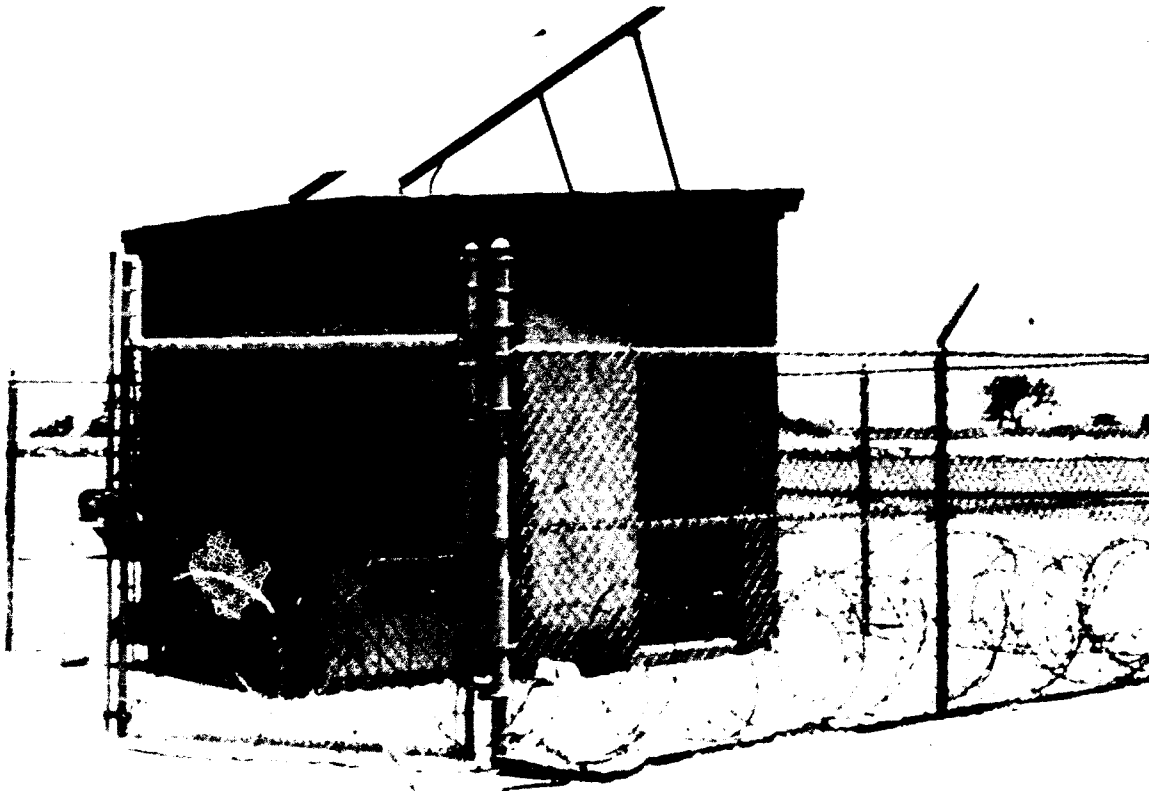
Figure 79. Shore station instrumentation building

110

extremely heavy so the use of mobile, mechanized equipment to handle the cable, array, and buoy was necessary (Boc 1987).

The wave rider buoy was the first instrument installed. Because data are transmitted to shore by radio, this was one of the easier installations. To install the directional array, float bags were attached to the frame and it was lowered to the water in the barge harbor by use of a crane (Figure 80). A work boat then towed the array to the site where divers assisted in completing the installation. A similar scenario occurred to install the remaining single point pressure gages (Boc 1987).

Wave Data Collection

Data collection began in July 1986 and continued through March 1990. During the monitoring effort, a total of ten instruments were deployed and data collected at various intervals. As with any attempt to collect data in the ocean, problems arose that resulted in the periodic loss of data, and the replacement or relocation of gages. The present work uses data from five of the near-bottom pressure gages in the harbor, one near-bottom pressure gage outside the harbor, and a Waverider buoy offshore in deep water. Data were typically collected every 6 hr; however, the location of
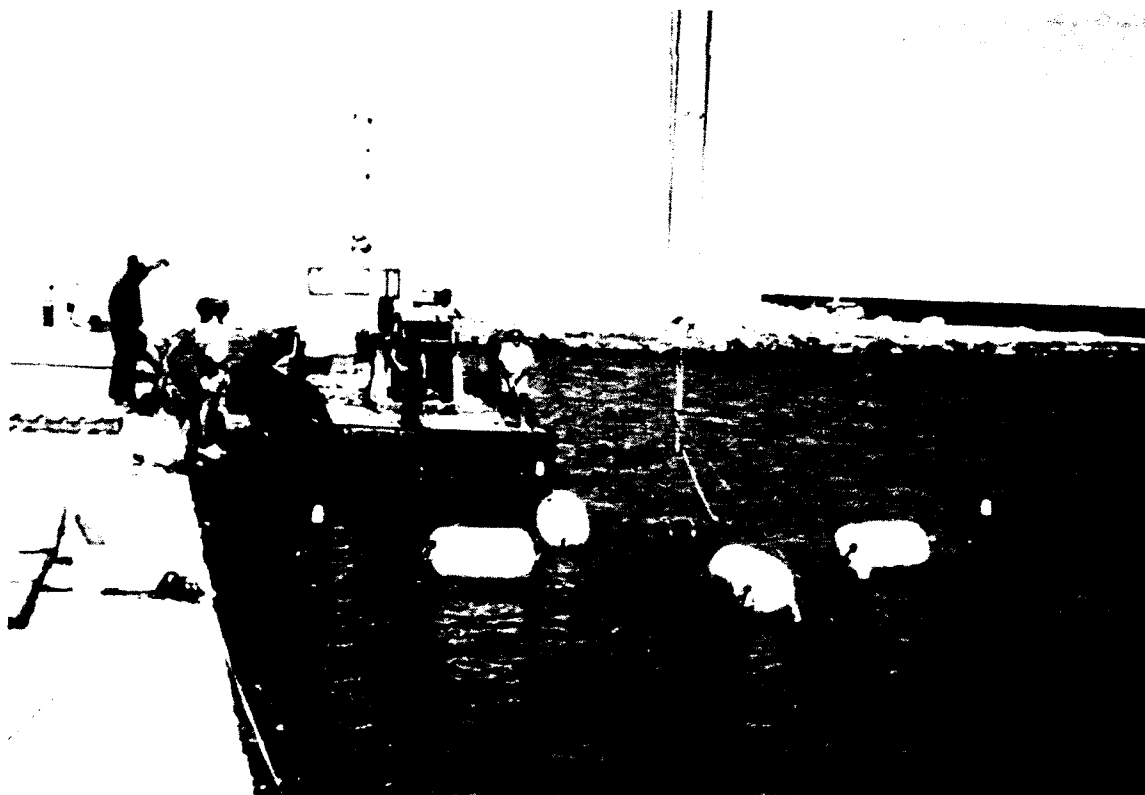
Figure 80. Lowering of directional wave array into barge harbor

some gages as well as data sampling frequency and record length were modified during the data collection period.

A Datawell Waverider buoy located approximately 1 mile offshore (21 20.1 deg N latitude and 158 9.0 deg W longitude) at a 650-ft (200-m) depth was installed to provide wave height and period data on the incident deepwater waves. This buoy was located in water deep enough to minimize the bathymetric effects on the measured waves. The Waverider buoy uses a vertically stabilized accelerometer to sense the vertical component of the buoy's motion. Vertical acceleration and displacement data are transmitted up to 31 miles (50 km) from shore.

To collect directional wave data, a slope array, which was developed by the Scripps Institution of Oceanography, was located near the edge of the reef at an approximate 40-ft (12-m) depth. The array consists of four single point pressure gages arranged in a 20-ft (6-m) square and uses a specially designed armored underwater cable for data and power transmission. The slope array requires reasonably straight, parallel offshore bottom contours, as is the case at Barbers Point. Details of the array are described by Higgins and Seymour (1978), and the analytical method for extracting wave directionality from the sea surface slope components measured by the array are described in Higgins, Seymour, and Pawka (1981). An estimate of the longshore component of radiation stress Sxy can be extracted when the surface elevation and components of sea surface slope are known at a point. The components of the slope are determined from the difference between a pair of gages (Hemsley 1985).

A single gage from the slope array was used to measure the incident conditions. Data transmission over long distances using satellite telephone links led to problems in obtaining complete data records from the slope array. It was determined that the lack of even a few data points subsequently leads to large problems in obtaining directional information from the slope array. The slope array occupied two positions during the data collection period (Slope 1 and Slope 2 in Figure 7). Initially the slope array was located directly alongside the dredged entrance channel (Slope 1, Figure 7). In June 1988, the slope array was moved northward (Slope 2, Figure 7) to a region of relatively regular bathymetric contours. The new positions of the slope array resulted in cleaner estimates of the incident wave conditions because of the reduction of the effects of wave refractions due to the steep sides of the dredged entrance channel.

Three single point pressure gages located in the deep-draft harbor are referred to by locations; north, south, and east corners (Figure 7). The gage located near the mouth of the harbor is referred to as channel entrance and the gage located along the channel between the channel entrance and north corner will be referred to as channel midpoint. After the opening of the small boat harbor, the east corner gage was moved northward.

112

During the data collection period, the geometrical configuration of the harbor changed. The small boat harbor located adjacent to the deep-draft harbor, with an entrance channel opening perpendicular to the deep-draft harbor entrance channel, was opened in July 1989.

A summary of the data collection sampling frequency and record length at each gage location is provided in Appendix A (Table A1) of this report.

Data Analysis

Wave data summary

Each wave data record was quadratically detrended to remove tidal and other very low frequency motions. Fourier coefficients of pressure time series were then calculated and converted to sea surface elevation using linear wave theory. Wave frequencies below 0.04 Hz were arbitrarily defined as infragravity energy while wave frequencies above 0.04 Hz were defined as sea-swell energy. Significant wave heights were defined as four times the standard deviation of the time series in each frequency range.

The significant wave heights for each data record from each location at Barbers Point are plotted as a function of time to show the data availability at each gage and the seasonal (monthly) trends. Sea-swell significant wave heights from the deepwater buoy and the offshore slope array are shown in Figures A1 through A4. Infragravity significant wave heights at the offshore slope array are shown in Figures A5 and A6 and at the harbor basin gages in Figures A7 through A16.

It is clear from these seasonal plots of significant wave heights that the wave conditions at Barbers Point are more energetic during the fall and winter months (October - March) than during the spring and summer months (April - September). In order to quantify these seasonal trends, cumulative probability functions were constructed. Data records were sorted into intervals according to their significant wave heights. The wave height interval for sea-swell heights was 20 cm and for infragravity heights it was 5 cm. The total number of occurrences (data records) at each height range were determined for each gage location during the entire period of operation of the gage. The cumulative height probability function was then constructed by summing all occurrences greater than or equal to the minimum interval value and dividing this sum by the total number of observations. Cumulative height probabilities were calculated using all the data available from each gage. Cumulative height probabilities were also calculated using the subset of fall-winter data and the subset of spring-summer data. These probability values are shown in Tables A2 through A9. The probability of exceeding a given wave height is

consistently larger in the fall-winter months than in the spring-summer months.

Harbor resonance

Harbor resonance (also called seiche, surge, or oscillations) is the phenomenon of trapping and amplification of wave energy in a semi-enclosed body of water. A harbor of a given geometrical configuration will have natural frequencies at which it oscillates. If the harbor is forced at one or more of these resonant frequencies, the amplitudes of the oscillations will increase until the rate of energy loss by friction, flow separation, boundary absorption, and radiation from the harbor mouth balances the energy input from the exciting sources. Harbor resonance can be viewed as a resonant standing wave system having nodal and anti-nodal patterns. Observations of this type of resonant standing wave phenomenon in lakes date back to the 1800's and were followed by studies of their oceanic counterpart in the 1930's.

Typical resonant periods are on the order of minutes (dependent on the size of the harbor) and are thus referred to as long waves when compared to wind wave and swell periods. In this section, a description of the frequencies and spatial configuration of the resonant modes at Barbers Point harbor will be given.

Data collected at Barbers Point Harbor during the period from February 1989 to March 1990 were used for analyzing the harbor resonant mode frequencies and amplification factors. During this time the greatest number of operational gages in the harbor was five. These harbor measurements were coincident with data from the offshore slope array (Slope 2, Figure 7). The gages used to measure the harbor response included the two gages in the entrance channel near the barge harbor (channel entrance and channel midpoint) and the three gages in the deep-draft basin (north, south, and east corner). The channel entrance gage failed in May 1989 and no data were available after that time. The east corner gage failed in April 1989 but was reinstalled approximately 250 ft northward in October 1989. Data from the north, south, and east corner gages, as well as the slope array, are available for the entire period being considered.

In addition to the presence of multiple operational gages, the individual time series records during this time frame were adequate in length to resolve the long resonant periods of the harbor. Time series records of up to 4.5 hr were obtained four times a day. The sample rate at the slope array and channel entrance gages was 1.0 Hz while the sample rate at the other gages was 0.5 Hz.

The time frame selected for analysis also encompassed the two configurations of the harbor basin; with and without the small boat harbor. The small boat harbor entrance channel is connected to the deep-draft

harbor entrance channel and is directly across from the barge harbor (Figure 7). The small boat harbor was opened in early July 1989.

Resonant frequencies

High resolution, smooth estimates of the power spectra at each gage location in the harbor were obtained by ensemble averaging over multiple 2.3-hr raw spectra, resulting in a spectral bandwidth of 0.00012 Hz.

The selection of segments that were ensemble averaged was based on the average depth during the 2.3 hr. Resonant periods for a basin the size of Barbers Point Harbor are typically on the order of a few minutes (i.e., shallow water waves) and are thus affected by the depth, which necessitated this separation. As an example of the effects of depth on the resonant frequencies of the harbor, smooth estimates of the normalized power spectra at low tide (solid line) and high tide (dashed line) from four of the basin gages (after the small boat harbor was open) are shown in Figure A17. Low-tide spectra were obtained by ensemble averaging over 122 raw spectra and the high tide spectra averaged 111 raw spectra. At high tide, the depth in the harbor is the greatest, the wave phase speeds are the highest, and the resonant modes are shifted to higher frequencies compared with the resonant modes at low tide levels.

The primary purpose of this ensemble averaging technique is to clearly demonstrate the existence of resonant modes in the harbor and to show the differences between the resonant frequencies as a function of the location in the harbor and due to changes in the physical geometry of the harbor.

Estimates of the average power spectrum at each of the gage locations in the harbor at mid-tide level (8.4 m $\leq$ slope array depth < 8.7 m) before and after the small boat harbor was opened are shown in Figures A18 and A19, respectively. The average power spectral density at frequencies greater than 0.02 Hz was typically very small and is not shown. The average power spectra for the time period when the small boat harbor was open were obtained by ensemble averaging over 277 mid-tide level 2.3-hr segments. All 277 time series at each location (north, south, and east corners, and mid-point) correspond to exactly the same time frame. The number of segments ensemble averaged to obtain the averaged spectra for the period when the small boat harbor was closed varied from 31 at the channel entrance and east corner, 44 at the north corner, and 91 at the channel mid-point and south corner due to incomplete data from all the gages. Comparisons between the magnitudes of the power spectral peaks are limited only to those estimates that correspond to the same time period (i.e., when the small boat harbor was open).

A common feature at all the gages in the harbor is the very low frequency resonant mode at 0.00098 Hz (1,024 sec) when the small boat harbor was open and 0.0011 Hz (910 sec) when the small boat harbor was closed. This low frequency mode is thought to be the Helmholtz or pumping

mode, which is theoretically characterized by an almost uniform rise and fall of the water surface level in the harbor with decreasing amplitudes in the entrance channel as the harbor mouth is approached. As shown in Figure A19, the average magnitudes of the peaks at 0.00098 Hz (1024 sec) at the north, south, and east corner locations are approximately equal. The same peak at the channel mid-point location is smaller in average magnitude than at the interior basin locations, consistent with the theoretical Helmholtz mode.

Normalized spectra from both harbor configurations (small boat harbor closed and open) are shown in Figure A20. A number of differences and similarities between the resonant frequencies for the two harbor geometries are apparent. The shift of the Helmholtz mode from 0.0011 Hz (910 sec) to 0.00098 Hz (1024 sec) when the small boat harbor was closed and open, respectively, is consistent with the physical change in geometry since the inclusion of the small boat harbor effectively increases the overall size of the harbor basin and therefore decreases the lowest resonant mode's frequency.

The presence of the small boat harbor also corresponded to the appearance of a resonant peak at approximately 0.0016 Hz (630 sec). Although there is some indication of energy at this frequency when the small boat harbor is closed, the presence of this mode is clearest when the small boat harbor is open, which suggests that it may be the lowest mode of this harbor. The presence of a small amount of energy at this frequency when the small boat harbor is closed may be due to the permeable boundary between the small boat harbor and the deep-draft harbor that existed during parts of the construction of the small boat harbor. Large boulders were placed along the small boat harbor entrance channel (dashed line in Figure 7) to close it off from the deep-draft harbor basin during the construction phase of the small boat harbor. These rocks did not completely seal off the small boat harbor from the deep-draft harbor. The rock barrier may have been transparent to the 0.0016-Hz (630-sec) mode, making it possible for the small boat harbor to resonate at this frequency even before the barrier between the small boat and deep-draft harbors was removed.

At higher frequencies, significant differences between the power spectra for the two geometrical configurations are most noticeable at the channel mid-point (Figure A20). When the small boat harbor is closed to the deep-draft harbor, the smoothed power spectrum shows a broad peak centered at approximately 0.006 Hz (167 sec). After the small boat harbor is opened, three resonant peaks appear centered at 0.005 Hz (200 sec), 0.006 Hz (167 sec), and 0.008 Hz (125 sec).

In the deep-draft harbor, the resonant frequencies appear unchanged as a result of the addition of the small boat harbor. The dominant resonant peaks in the deep-draft harbor appear at 0.0076 Hz (132 sec) and 0.009 Hz (110 sec). The presence and absence of these resonant peaks at various locations in the harbor basin are indicative of nodes and anti-nodes typical

of standing wave systems. Both the modes at 0.0076 Hz (132 sec) and 0.009 Hz (110 sec) are energetic at the south corner. In the north corner only the mode at 0.0076 Hz (132 sec) is present indicating a nodal point (or line) of the 0.009-Hz (110-sec) mode at this location. In the east corner the resonant mode at 0.009 Hz (110 sec) is very energetic whereas the mode at 0.0076 Hz (132 sec) has negligible energy at this location. The phase relationships of these resonant frequencies at different locations in the deep-draft harbor as well as the location of nodes and anti-nodes were further investigated by means of cross-spectral analysis.

Phase relationships

Cross-spectral analysis (Bendat and Piersol 1986) was used to determine the phase relationships of the resonant frequencies at different locations in the deep-draft harbor. From these, node and anti-node locations were inferred. The 4.5-hr time series records collected at the basin gages were not all time synchronized. However, the time series did overlap and it was possible to obtain 2.3-hr-long records from each gage that were concurrent with all the other gages. Smooth estimates of the auto and cross-spectral density functions were obtained by ensemble averaging the raw spectral density functions obtained from multiple 2.3-hr-long time series records. No frequency band merging was used because it was necessary to preserve the highest frequency resolution possible in order to resolve the very low frequency modes of the harbor. The time series records that were used to compute the smoothed spectra, phase, and coherence are the same mid-tide level records used previously to calculate the resonant frequencies.

Average spectra, phase, and coherence are plotted in Figures A21 through A30 for data from pairs of gages collected when the small boat harbor was closed and in Figures A31 through A36 for data taken when the small boat harbor was open. The 95-percent level of the null hypothesis is also indicated by a dashed line in each coherence plot (the value of the coherence exceeded with 5 percent probability by randomly related records). Observed values of coherence less than this value should not be regarded as significantly different from zero (Bloomfield 1976).

It is clear from the plots of phase that most of the energy in the deep-draft basin is due to standing waves with phases θ of 0 or 180 deg. At the lowest resonant frequencies (0.00098, 0.0011, and 0.0016 Hz or 1024, 910, and 630 sec) the signals from all the gages in the harbor are in phase ($\theta = 0$ deg).

At higher frequencies, the phase relationships between the resonant frequencies at different positions in the harbor are more complicated. When the small boat harbor was closed (Figures A21 through A30) the energy centered at 0.006 Hz (167 sec) is in phase ($\theta = 0$ deg) at the channel entrance and midpoint. However, the phase between the channel entrance (as well as the midpoint) and the deep-draft basin gages (north, south, and

east corners) is 180 deg. The 180-deg phase between the channel locations and the deep-draft basin indicates the existence of a nodal line separating the two regions.

The structure of the resonant mode at 0.0076 Hz (132 sec) is most clearly illustrated in Figures A29 and A35. These figures show the phase between the south and north corner when the small boat harbor is closed (Figure A29) and when it is open (Figure A35). The 0.0076-Hz (132-sec) mode is present at both the north and south corners with approximately the same magnitude. The phase at this frequency is 180 deg indicating the existence of a nodal line between these two locations. The absence (or very small amount) of energy and decrease in coherence at this frequency at the east corner and channel midpoint locations (see Figures A27, A30, A33, and A36) imply that the nodal line at 0.0076 Hz (132 sec) may extend from west to east across the harbor.

The resonant mode at 0.00098 Hz (1024 sec) is most energetic at the south and east corners (Figures A30 and A36). At this frequency the phase between the south and east corners is 180 deg, indicating a nodal line between these two corners. The absence of any significant energy at the north corner (Figures A29 and A35) at this frequency implies that a nodal line runs from the north corner to a point along the southeast wall.

When the small boat harbor is open, three low-frequency peaks appear at approximately 0.005, 0.006, and 0.008 Hz (200, 167, and 125 sec) at the channel midpoint that are not apparent when the small boat harbor is closed. Small peaks at these frequencies also appear at the east corner location. Figure A33 shows the energy at these frequencies to be 180 deg out of phase at the mid-point and east corner locations.

Harbor amplification factors

The relationship between conditions outside and inside the harbor can be expressed by an amplification factor A(f) given by

$$G_{yy}(f) = A(f)\,G_{xx}(f)$$

where $G_{xx}(f)$ and $G_{yy}(f)$ are the input and output auto-spectral density functions, respectively.

In the following analysis, the data measured at the slope array (Slope 2, Figure 7) outside the harbor entrance were assumed to be the input conditions (expressed by the variable x), while the data measured at the gages inside the harbor were the output conditions (expressed by the y variable).

Estimates of the auto-spectral density functions $\hat{G}_{xx}(f)$ and $\hat{G}_{yy}(f)$ were obtained for each data record by breaking the 4.6-hr-long time series into two 2.3-hr records and ensemble averaging the two raw spectral density functions. No frequency band merging was used because it was necessary to preserve the highest frequency resolution possible in order to resolve the very low frequency modes of the harbor. Estimates of the amplification factors $\hat{A}(f)$ were then calculated from a linear regression on $\hat{G}_{xx}(f)$ and $\hat{G}_{yy}(f)$ from all the records. The existence and strength of the relationship between the input and output conditions is measured by the correlation between $\hat{G}_{xx}(f)$ and $\hat{G}_{yy}(f)$.

The selection of the time series records that were regressed to obtain the amplification factors was based on a number of factors. First, the data were separated according to whether they were collected while the small boat harbor entrance was closed or open. The opening of the small boat harbor channel changed the overall configuration of the harbor basin and any effects should be noticeable after July 1989.

The time series records were also separated by the average depth measured at the slope array during the record. The tidal variation (about 1 m) at Barbers Point results in a range of depths being encountered and changes in the depth affect the resonant frequencies of the harbor. An increase in the depth will result in a shift (to higher frequencies) of the resonant frequencies, as discussed earlier (see Figure A17).

The results shown in the remaining figures are based on mid-tide level (8.4 m ≤ slope array depth < 8.7 m) data. The amplification factors and correlation coefficients between the slope array and each of the harbor locations during the time period when the small boat harbor was closed are shown in Figures A37 through A40 and for the case when the small boat harbor was open in Figures A41 through A45. The horizontal dashed line in the plots of the correlation coefficients are the 95-percent confidence level on the null hypothesis (i.e. zero correlation). Values of the correlation coefficient less than this level are not statistically significant and the corresponding amplification values shown should not be used (Dixon and Massey 1969).

The amplification factors between the slope array and each of the harbor locations for both the time period when the small boat harbor was closed and when it was open are shown in Figure A46. Some significant differences between the amplification factors when the small boat harbor was closed and open are apparent. An expected change occurs at the lowest resonant (Helmholtz) mode of the harbor. As shown in Figure A46, when the small boat harbor is open and the overall harbor basin increases in size, the lowest mode shifts from 0.0011 Hz or 910 sec (small boat harbor closed, solid line) to 0.00098 Hz or 1,024 sec (small boat harbor open, dotted line). The mode at 0.0016 Hz (630 sec) is clearly amplified at all locations in the harbor when the small boat harbor is open and not amplified when the small boat harbor is closed. Three distinct low frequency

modes at approximately 0.005, 0.006, and 0.008 Hz (200, 167, and 125 sec) also appear at the channel midpoint when the small boat harbor is open compared with a single broad (in frequency) peak at about 0.006 Hz (167 sec) when the small boat harbor is closed.

Nearshore coupling between infragravity and sea-swell frequencies

The nearshore wave climate outside the harbor at Barbers Point was based on data from a single gage in the offshore slope array. As discussed earlier, problems with data transmission of long records over great distances using satellite telephone links rendered much of the slope array data unusable for directional processing. However, estimates of frequency spectra and the general incident wave climate were obtained using a single gage from the slope array.

The seasonal (monthly) trends of significant wave heights outside the harbor were discussed earlier and are summarized in Figures A1 through A4 and in Tables A3 and A4.

The existence and characteristics of a coupling between energy at infragravity frequencies (< 0.04 Hz) and sea-swell frequencies (> 0.04 Hz) outside the harbor were investigated. Shown in Figures A47 and A48 are the infragravity significant wave height versus the sea-swell wave height for data records from the two positions of the slope array. In both cases the infragravity and sea-swell significant wave heights are correlated (correlation = 0.87 for Slope 1 and 0.90 for Slope 2). Wave records were further separated into three groups delineated by the frequency of the spectral peak in each record. As shown in Figure A48, for a given sea-swell significant wave height, the infragravity wave height is clearly larger for swell conditions (0.067 Hz) than for higher frequency (0.10 Hz) wind waves (particularly for energetic events). Similar observations have been reported by others (see Okihiro, Guza and Seymour (1992) for a list of references and additional discussion). This coupling between energy at sea-swell and infragravity frequencies outside the harbor will be further discussed in the section on the forcing mechanism of the harbor oscillations.

Deep water and nearshore coupling

The wave climate in deep water at Barbers Point was based on data collected by a Waverider buoy located at the 183-m (600-ft) depth at 21 20.1 deg north latitude and 158 09.0 deg west longitude. The seasonal (monthly) trends of significant wave heights in deep water were discussed earlier and are summarized in Figures A1 through A4 and in Table A2. The sea-swell significant wave heights from the deep water buoy were compared to the sea-swell significant wave heights measured at the slope array to determine the correlation between the wave conditions at the two

sites. The purpose of this comparison was to see if the sea-swell conditions in the nearshore at Barbers Point could be accurately estimated with data from an offshore buoy.

The sea-swell significant wave heights measured at the slope array are plotted against the sea-swell significant wave height at the buoy for all the data collected from July 1986 to January 1990 in Figure A49. There is a considerable amount of scatter in this plot and the correlation between the buoy and slope array wave heights is 0.87. As mentioned earlier, the offshore slope array at Barbers Point occupied two different positions during the data collection period (Figure 7). In Figure A49, the $\Box$ are used for records from the first position of the slope array (Slope 1, Figure 7) and * correspond to records obtained from the second position of array (Slope 2, Figure 7). Data from the two different slope array positions were separated and plotted in Figures A50 and A51. It is apparent from Figures A50 and A51 that much of the scatter in Figure A49 is due to the original position of the slope array. The correlation between the wave heights at the buoy and the original slope array position is 0.82. The correlation between the wave heights at the buoy and the second position of the slope array is 0.95. The proximity of the slope array to the dredged entrance channel in its original position apparently resulted in refractive effects that were not necessarily representative of the incident wave conditions. Data from the second position of the slope array, in a region of relatively regular bathymetric contours, resulted in a significantly higher correlation with wave heights measured by the buoy in deep water.

Forcing mechanism of harbor resonance

As discussed earlier, a harbor has natural frequencies at which it resonates. These frequencies correspond to waves which reflect from the harbor boundaries and interfere constructively. A harbor subjected to forcing at one or more of these resonant frequencies will exhibit amplifications of the waves at these frequencies. Possible sources of forcing for harbors include tsunamis, atmospheric pressure disturbances, nonlinearly locally generated infragravity waves, and free infragravity waves (other than tsunamis) generated at and radiated from distant shores.

Tsunamis and atmospheric pressure disturbances have both been shown in previous studies to cause harbor surge. However, they alone cannot account for seiche problems existing in many harbors. Infragravity motions coupled to higher frequency wind waves were first observed off of Scripps pier in La Jolla, California (Munk 1949). Munk called these low-frequency waves surf beat to reflect their relationship with the beat in the incident sea-swell waves and found that an increase in sea-swell wave height corresponded to an increase in surf beat height. He speculated in his original surf beat paper that these infragravity waves may be responsible for harbor seiche.

Observations of increased sea-swell activity occurring simultaneously with harbor surge have been reported in the literature (Clark 1974; Botes, Russel, and Huizinga 1982; Kirkegaard and Nielsen 1982) and a number of authors (Gravesen, Jensen and Sorensen 1978; Lundgren 1981; Sand 1982; Kirkegaard and Nielsen 1982; Jensen and Warren 1986) have attributed infragravity waves forced by sea-swell wave groups as being responsible for harbor oscillations. Although qualitative observations indicate that this may be true, quantitative evidence from real harbors directly linking the nonlinearly generated infragravity waves to harbor resonance has not previously been shown.

The infragravity significant wave heights measured at the harbor gages were compared with the infragravity significant wave height measured at the slope array in Figures A52 through A54 for the original position of the slope array (Slope 1, Figure 7) and in Figures A55 through A59 for the second position of the array (Slope 2, Figure 7) to determine under what conditions the wave energy inside the harbor was greatest.

In only one instance (shown by the symbol o in Figures A52 through A54) was a large wave height recorded in the harbor without a corresponding large infragravity wave height measured at the slope array. Wave spectra from the slope array, channel entrance, channel midpoint, and south corner for this record (02:17) as well as for the data records 6 hr before (20:17) and 6 hr after (08:17) are shown in Figure A60. Spectra from the harbor show that the increase in wave height is due to a significant increase in the energy at the lowest (0.0011 Hz or 910 sec) resonant mode (Helmholtz mode). The dramatic increase in the Helmholtz oscillation in the harbor is shown in time series plots in Figure A61 for the period just prior to and during the unusual event. Atmospheric pressure readings recorded nearby at the Barbers Point Naval Air Station show that a drop in atmospheric sea level pressure occurred at the same time that the increase in the Helmholtz oscillations was recorded. This one instance of an increase in wave height in the harbor without an increase in wave height outside the harbor may have been due to atmospheric pressure forcing or other meteorological effects. The lack of any similar events during the entire 4-year data collection period indicates the relative unimportance of these sources of harbor seiche forcing at Barbers Point.

The majority of the data shown in Figures A52 through A59 show that infragravity wave heights measured in Barbers Point harbor are highly correlated with the infragravity wave heights measured outside the harbor. These observations in conjunction with the observations shown in Figures A47 and A48 (sea-swell versus infragravity wave heights at the slope array) make it clear that an increase in harbor seiche (measured in terms of infragravity significant wave height) is associated with an increase in the sea-swell energy outside the harbor. Nonlinear processes (e.g., bound and edge wave generation) that are able to transfer energy from sea-swell waves to infragravity waves outside the harbor are clearly an important mechanism for harbor resonance forcing at this location. Details of the

coupling between sea-swell energy and infragravity energy outside the harbor can be found in Okihiro, Guza, and Seymour (1992).

Finally, the correlation between harbor seiche and sea-swell wave heights also rules out free long waves generated from distance sources as an important forcing mechanism at Barbers Point, since these free waves are not necessarily coincident with energetic sea and swell.

5 Evaluation of Harbor Design Model Studies

Objectives of the MCCP monitoring study pertaining to modeling efforts of Barbers Point Harbor included: (a) evaluation and validation of results from the model studies conducted for harbor design, and (b) comparison of the measured data to the predictions of state-of-the-art numerical and physical model studies. Results from the prototype wave data analysis of Barbers Point were compared with the reported results of the three model studies conducted in the planning and modification stages for harbor design. The model studies conducted were: (a) the Hydraulic Model Study 1967, (b) the Numerical Model Study 1978, and (c) the Small Boat Harbor Hydraulic Model Study 1985. Details of the previous studies are described in Chapter 2 of this report. Prototype data were also compared to the recently completed state-of-the-art numerical and physical model studies. These studies are described in Chapter 3 of this report. A comparison of the previous numerical model results with the state-of-the-art numerical model study was also conducted.

Hydraulic Model Study 1967

The hydraulic model study was conducted to establish a harbor design plan that met the criteria that wave heights in the deep-draft harbor not exceed the desired maximum limit of 2.5 ft or the maximum tolerable limit of 4.5 ft. The maximum tolerable and the desired maximum wave height limits in the small boat harbor were 2.0 and 1.0 ft, respectively. The input wave conditions for the model tests were sea-swell wave periods ranging from 4 to 20 sec. These wave conditions were selected from Table 3. Since the study was only interested in the resulting wave heights at various locations in the harbor, a comparison of the short period wave heights was attempted with the prototype data. However, it should be noted that the hydraulic model study was performed on a harbor configuration that was not actually constructed in the prototype (Figure 19). Also, the small boat harbor was located to the south of the deep-draft harbor rather than the prototype location to the north. Since the configuration in the model

study and the actual prototype harbor both had small boat harbors extending off the harbor entrance, a comparison between the wave heights inside the deep-draft harbor was conducted.

Wave heights from the hydraulic model study and prototype data were compared at the three coincident south, east, and north corner locations (Figure 7). The hydraulic model locations are labeled gage stations 10, 5, and 4 in Figure 19. Table 24 lists the incident wave period, wave height, wave generator position, and resulting wave height for the three prototype and model locations. Since difficulties were encountered in determining wave directions in the prototype data, as discussed in Chapter 4, the prototype wave heights corresponding to each incident wave period and wave height were calculated for each of the incident wave directions. Table 24 shows that none of the incident wave conditions result in exceedance of the 2.5-ft desired maximum or the 4.5-ft maximum tolerable wave height criteria in the hydraulic model study or the prototype measurements.

Table 24
Results for Plan V-A Versus Prototype

Period (sec)	Height (ft)	Resulting Wave Height (ft) by Location					
		Model Station 4	Prototype North	Model Station 5	Prototype East	Model Station 10	Prototype South
Generator Position 2							
6	4	1.0	0.4	0.2	0.1	0.1	0.2
8	8	0.6	0.6	0.1	0.2	0.0	0.3
10	12	0.6	1.3	0.1	0.2	0.1	0.2
12	16	1.2	0.3	0.2	0.2	0.2	0.2
14	14	0.8	0.3	0.2	0.2	0.1	0.1
14	20	1.4	0.4	0.4	0.4	0.4	0.2
16	4	0.0	0.1	0.0	0.4	0.0	0.1
Generator Position 4							
8	8	0.8	0.6	0.2	0.2	0.0	0.3
10	12	0.7	1.3	0.3	0.2	0.3	0.2
12	16	1.0	0.3	0.2	0.2	0.1	0.2
12	24	1.8	0.5	0.4	0.2	0.1	0.2
Generator Position 5							
10	14	0.9	1.5	0.4	0.3	0.3	0.3
12	12	1.0	0.2	0.4	0.1	0.1	0.1
12	16	1.1	0.3	0.3	0.2	0.1	0.2
18	8	0.7	0.5	0.3	0.2	0.1	0.9
18	12	0.8	0.7	0.4	0.2	0.3	1.3
20	6	0.6	0.2	0.2	0.4	0.1	0.2
20	20	1.4	0.6	0.4	1.2	0.3	0.8
							(Continued)

Table 24 (Concluded)							
		Resulting Wave Height (ft) by Location					
Period (sec)	Height (ft)	Model Station 4	Prototype North	Model Station 5	Prototype East	Model Station 10	Prototype South
Generator Position 6							
4	4	0.2	--	0.0	--	0.0	--
8	14	2.2	1.1	0.9	0.4	0.6	0.6
10	12	1.9	1.3	0.6	0.2	0.6	0.2
14	8	0.7	0.2	0.7	0.2	0.4	0.1
16	8	1.0	0.2	0.4	0.1	0.1	0.2
16	14	0.8	0.4	0.8	0.1	0.3	0.3
16	18	0.8	0.5	0.4	0.2	0.3	0.4
18	10	1.0	0.6	0.3	0.2	0.1	1.1
18	14	1.1	0.8	0.4	0.3	0.3	1.5
20	8	0.8	0.2	0.3	0.5	0.3	0.3
20	10	1.5	0.3	0.8	0.6	0.4	0.4
20	20	1.9	0.6	0.8	1.2	0.4	0.8
Generator Position 7							
8	10	2.4	0.8	0.6	0.3	0.1	0.4
10	8	2.4	0.9	0.7	0.2	0.3	0.2
12	10	1.2	0.2	0.4	0.1	0.3	0.1
14	10	1.4	0.2	1.0	0.2	0.4	0.1

Numerical Model Study 1978

The numerical simulations conducted in 1978 were based on design concepts resulting from the 1967 hydraulic model study. After completion of the hydraulic model study, it was determined that a larger basin was necessary than originally designed. The objective of the numerical model study conducted in 1978 was to determine the effects of enlarging the basin on surging in the harbor. Therefore, the study was designed to investigate the effects of long waves in the harbor rather than the short wind wave periods studied in the 1967 hydraulic model study. Test conditions consisted of incident waves from a direction parallel to the axis of the entrance channel (approximately the 225.0-deg azimuth) with wave periods from 15 sec to 27 min. Results were reported as wave height amplification factors. The resonant peaks occurring in the numerical data are listed in Table 6. Prototype wave gages located near the numerical model output locations were the channel entrance, channel midpoint, east corner, and south corner (Figure 7). The corresponding numerical model output locations are labeled stations 22, 20, 14, and 4 in Figure 22. The resonant frequencies and wave periods with amplification values greater than 1.0 from both the numerical model and the prototype are listed in Tables 25 through 28. Frequency response curves of amplification factors from the five

prototype locations inside the deep-draft harbor and entrance channel are plotted in Figure 81. Contour plots of numerical model amplification factors for the first nine identified resonant modes of oscillation are provided in Figures 37 through 45.

Table 25
Observed and Numerical Model (Durham 1978)
South Corner Amplification Factors

Prototype				Model			
Sensor Location	Frequency (Hz)	Period (sec)	Amplification Factor	Sensor Location	Frequency (Hz)	Period (sec)	Amplification Factor
South Corner	1.22×10^{-3}	819.7	7.3	Station 14	1.25×10^{-3}	799.0	8.5
	7.57×10^{-3}	132.1	3.2		7.72×10^{-3}	129.5	10.2
	9.16×10^{-3}	109.2	2.0		9.33×10^{-3}	107.2	8.3
					1.22×10^{-2}	81.97	3.0
	1.66×10^{-2}	60.2	1.1		1.59×10^{-2}	62.9	2.5
					1.71×10^{-2}	58.5	2.0
	1.75×10^{-2}	57.1	1.8		1.77×10^{-2}	56.5	5.0
	2.12×10^{-2}	47.2	1.3				

Table 26
Observed and Numerical Model (Durham 1978)
East Corner Amplification Factors

Prototype				Model			
Sensor Location	Frequency (Hz)	Period (sec)	Amplification Factor	Sensor Location	Frequency (Hz)	Period (sec)	Amplification Factor
East Corner	1.22×10^{-3}	819.7	6.9	Station 4	1.25×10^{-3}	799.0	8.5
					6.90×10^{-3}	144.9	1.7
	7.57×10^{-3}	132.12	1.4		7.72×10^{-3}	129.5	1.5
	9.16×10^{-3}	109.2	3.1		9.33×10^{-3}	107.2	5.8
					1.22×10^{-2}	81.97	8.5
	1.43×10^{-2}	69.9	1.2				
	1.67×10^{-2}	59.9	2.8				
					1.77×10^{-2}	56.5	4.6
	2.12×10^{-2}	47.2	1.3				

Table 27
Observed and Numerical Model (Durham 1978)
Channel Mid-point Amplification Factors

Prototype				Model			
Sensor Location	Frequency (Hz)	Period (sec)	Amplification Factor	Sensor Location	Frequency (Hz)	Period (sec)	Amplification Factor
Channel Midpoint	1.22×10^{-3}	819.7	5.7	Station 20	1.25×10^{-3}	799.0	5.6
	5.98×10^{-3}	168.2	1.5		6.90×10^{-3}	144.9	2.7
					7.72×10^{-3}	129.5	2.2
					1.22×10^{-2}	81.97	4.6
					1.59×10^{-2}	62.9	3.5
					1.71×10^{-2}	58.5	2.0
					1.77×10^{-2}	56.5	1.8

Table 28
Observed and Numerical Model (Durham 1978)
Channel Entrance Amplification Factors

Prototype				Model			
Sensor Location	Frequency (Hz)	Period (sec)	Amplification Factor	Sensor Location	Frequency (Hz)	Period (sec)	Amplification Factor
Channel Entrance	1.22×10^{-3}	819.7	4.2	Station 22	1.25×10^{-3}	799.0	3.6
	5.37×10^{-3}	186.2	2.2		6.90×10^{-3}	144.9	2.5
					7.72×10^{-3}	129.5	2.3
	9.28×10^{-3}	107.8	1.2		9.33×10^{-3}	107.2	2.2
					1.22×10^{-2}	81.97	1.8
	1.48×10^{-2}	67.6	2.0				
					1.59×10^{-2}	62.9	1.8
					1.71×10^{-2}	58.5	1.7
					1.77×10^{-2}	56.5	1.7
	1.89×10^{-2}	52.9	1.1				

Comparisons between the prototype and numerical model amplification factors should be treated with caution. A number of differences exist between the numerical model and the prototype, which may account for some of the differences in magnitude of the amplification factors. First, the numerical model output locations are near, but not positioned at, the locations of the prototype wave gages. Although similar locations in the model and prototype were used for comparisons, amplification factors can vary as a function of location. Model amplification factors were also calculated as the wave height measured inside the harbor normalized by twice the incident wave height, whereas the prototype amplification factors were normalized by the waves measured at the slope array. The model results are consistently larger than the prototype measurements.
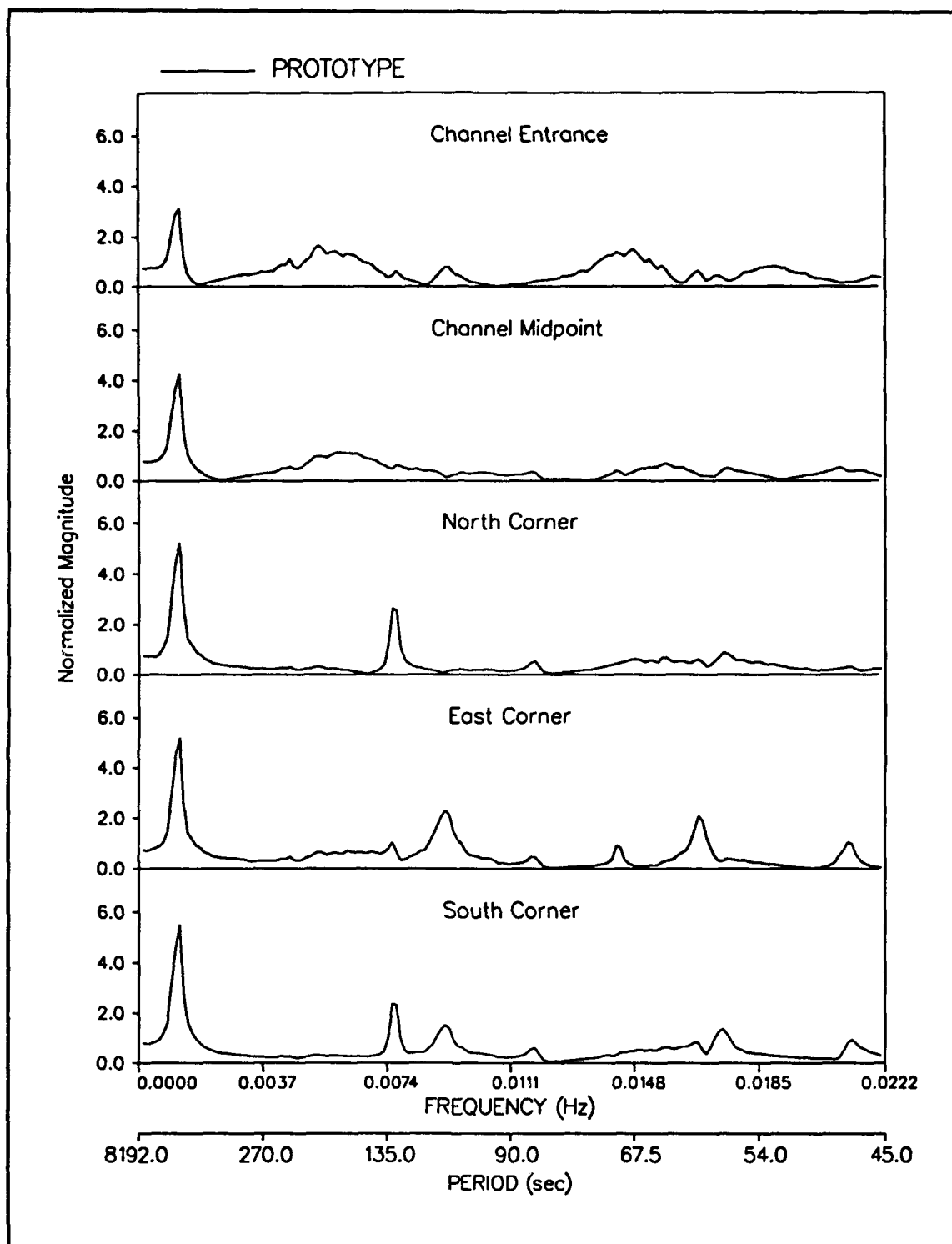
Figure 81. Prototype frequency response curves, deep-draft harbor

This is a result of excluding any wave energy dissipation mechanisms such as bottom friction and boundary absorption (reflection). Shoaling may also increase the numerical model amplification factors since the waves measured at the position of the slope array may be larger than the corresponding incident waves used in the numerical model. Finally, the prototype measurements are based on finite record lengths which limit the frequency resolution of the results. The prototype amplification factors correspond to a finite bandwidth whereas the numerical model amplification factors correspond to discrete frequencies.

Although the numerical model and prototype conditions differ, the model reasonably predicts the resonant peaks, spatial configurations, and magnitudes of the lowest resonant modes. The lowest frequency resonant mode is the Helmholtz mode, which occurs at 0.00125 Hz (799.0 sec) in the numerical model and significant amplification factors are present at all locations in the deep-draft harbor (Figure 37). The model amplifications at this frequency are relatively uniform in the main basin and range from 7.0 to 8.6 (Figure 37) with the maximum amplification occurring in the east corner. The lowest resonant mode observed in the prototype harbor occurred at 0.0011 Hz (910.0 sec). The observed amplification factors were 6.9 and 7.3 in the south and east corners, respectively, compared to model predictions of 8.5 at these locations (Tables 25 and 26). At the channel midpoint, the observed Helmholtz amplification factor was 5.7 compared to 5.6 in the model (Table 27). The amplification factors for this mode were lowest near the mouth of the harbor with observed and model values of 4.2 and 3.6 (Table 28), respectively. The numerical model results are consistent with the observations at the lowest resonant modes of the harbor.

The second resonant mode predicted by the numerical model occurs at 0.007 Hz (145.0 sec) and is most energetic in the region near the barge basin (Figure 38). Model amplification factors at this mode are less than two in the deep-draft harbor and between 2 and 4 near the channel entrance and midpoint. Amplifications in the prototype data also occur at this frequency at the channel midpoint. However, the observed amplification factors are peaked at slightly lower frequencies of 0.0054 Hz (186.2 sec) at the channel entrance (Table 28) and 0.006 Hz (167.2 sec) at the channel midpoint (Table 27). Both the observed and numerical model amplification factor peaks at 0.006 Hz (167.2 sec) are broad (in frequency) and show similar results. In the east corner, the numerical model predicts an amplification factor of 1.7 at 0.007 Hz (145.0 sec). Though the observed amplification is not greater than 1.0 at this location, the amplification in the east corner is twice that occurring in the south and north corners. This is consistent with the oscillation pattern shown in Figure 38.

A contour plot of numerical model amplification factors predicted at 0.008 Hz (130.0 sec) is shown in Figure 39. The largest amplification factors at this frequency occur in the north and south corners in the model and a nodal line runs from west to east. Figure 39 shows an amplification of 10.9 in the south corner and 10.7 in the north corner. Maximums in the

observed amplification factors occur at 0.0076 Hz (132.1 sec) at the south and north corners. The observed amplification factors of 3.2 in the south corner and 3.5 in the north corner are considerably smaller than the model-predicted amplifications of 10.9 and 10.7. In the east corner, the model predicted and observed amplifications of 1.4 and 1.5, respectively, are approximately equal (Table 26). The model amplification in the entrance channel is 2.0 whereas the prototype value is less than 1.0 (Table 28).

The next resonant mode from the numerical model data appears at 0.0093 Hz (107.2 sec). The corresponding contour plot of amplification factors is provided in Figure 40. Maximum amplifications occur in the east corner and barge harbor. Nodal lines run from north to south near the channel midpoint and from the north corner to the center of the south-east boundary. A peak in the observed amplification factors occurs at 0.0092 Hz (109.2 sec) at the south and east corners. Observed and model amplification factors are 2.0 and 3.0 (Table 25), respectively, at the south corner and 3.1 and 5.0 (Table 26), respectively, at the east corner. At the channel entrance, the observed amplification is 1.2 and the model predicted value is 2.2 (Table 28). The channel midpoint amplification is less than 1.0 for both the model and prototype.

The only low-frequency (long-period) resonant mode predicted by the numerical model but not identified in the prototype occurred at 0.012 Hz (82.0 sec). Contour plots of numerical data amplification factors are shown in Figure 41. Magnitudes of amplification are 9.5 to 10.5 in the north and south corners and 5.0 in the entrance channel. The east corner of the barge harbor shows amplitudes of 14.5. No amplification factors greater than 1.0 were observed at any of the prototype gages at this mode.

At frequencies greater than 0.015 Hz (67.0 sec), resonant modes with amplification factors greater than 1.0 were present in both the numerical model and the prototype. In general, the model amplifications were larger than those observed in the prototype. This is due to energy losses inherent in the prototype harbor (bottom friction and wave absorbing boundaries), which are more dissipative to energy at higher frequencies (shorter wave periods). Frequencies and amplification factors are tabulated in Tables 25 through 28, and contour plots are provided in Figures 42 through 45 for the remaining numerical model resonant peaks.

Hydraulic Model Study 1985

The hydraulic model used in the 1967 study described in Chapter 2 was also used to conduct the 1975 hydraulic model study to investigate long-period oscillations inside the small boat harbor. The small boat harbor entrance channel and basin configurations were redesigned and located north of the deep-draft basin as shown in Figure 46. Of three entrance channel configurations tested, the final design selected was the small boat harbor entrance channel located perpendicular and connected to the deep-draft

harbor entrance channel (Figure 46). Details of the study to develop the small boat harbor design are described in Chapter 2 of this report. The model tests to investigate long period oscillations involved sea-swell wave periods from 6 to 20 sec and the results were reported in terms of maximum wave heights at selected locations (Figure 46). Although the model test waves were short-period, long-period oscillation envelopes appeared in the time series records. These long period oscillations were found to vary with incident wave periods, height, and direction.

Using the measured time series from the model tests, an effort was made to determine the resonant modes of oscillation of the small boat harbor. The periods of oscillation for the final design plan, Plan I, varied from 112 to 120 sec at gage 4 and 100 to 150 sec at gage 5. The resonant peak periods for Plan I are listed in Table 7. Since no prototype wave gages were located in the small boat harbor during the monitoring study, data from the channel midpoint wave gage were used in an effort to compare the hydraulic model predictions to the prototype measurements. The channel midpoint location was selected for this comparison since it was the closest operational wave gage to the small boat harbor. The resonant oscillation periods ranging from 100 to 150 sec from the hydraulic model study including the small boat harbor configuration constructed in the prototype, Plan I, are qualitatively consistent with the 125- to 200-sec period resonant modes observed at the channel midpoint gage in the prototype harbor.

State-of-the-Art Numerical and Physical Model Studies

Results from the prototype wave data analysis were also compared with predictions from the recently completed state-of-the-art numerical and physical model studies to determine the resonant modes of oscillation. Model studies were conducted on the harbor configuration constructed in the prototype and included the small boat harbor. Details of these studies are described in Chapter 3 of this report.

Figure 82 provides a comparison of the prototype and numerical and physical model frequency response curves for the coincident channel midpoint and south, east, and north corner locations in the deep-draft harbor. These locations are shown in Figures 7, 53, and 75, respectively. Overall, the comparison is good between the prototype and the models. The most noticeable difference occurs between the physical model and the prototype and numerical model predictions at the very long Helmholtz modes of 1,024 sec for the deep-draft harbor and approximately 630 sec in the prototype and 585 sec in the numerical model for the small boat harbor. As explained in Chapter 3, the physical model run length of 40 min (model scale) was not sufficient to resolve these long period modes. The prototype and numerical model magnitudes of amplification are matched for
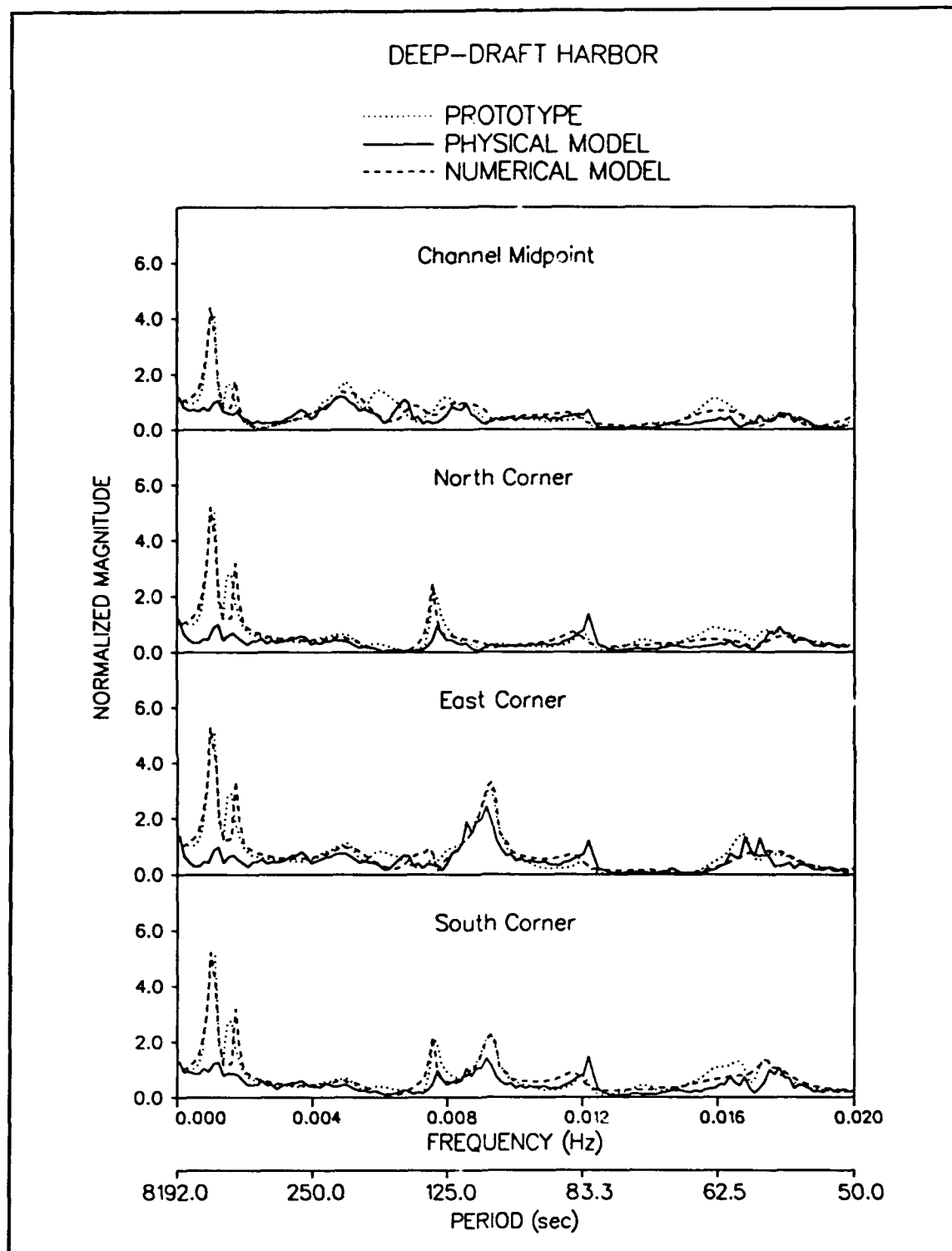
Figure 82. Comparison of prototype and numerical and physical model frequency response curves, deep-draft harbor

these first two resonance modes and are listed in Table 29. The values for the Helmholtz mode at the south, north, and east corners are approximately 5.1 in the prototype and 5.2 in the numerical model. The magnitude of amplification is lower at the channel midpoint and values are approximately 4.2 and 4.4 for the prototype and numerical model, respectively. Magnitudes of amplification for the next resonant peak are approximately 2.8 in the prototype and 3.2 in the numerical model for the three corner locations. Values at the channel midpoint are 1.6 prototype and 1.8 numerical model. Magnitudes of amplification for all resonant peaks are closely matched, as expected, since the numerical model was calibrated with the prototype data. Numerical model contour plots of amplification factors for these long-period modes are shown in Figures 66 and 67.

Five remaining prototype resonant modes occur in the deep-draft harbor at approximately 204, 132, 107, 85, and 57 sec. These modes were identified by both the numerical and physical models. Although magnitudes of amplification vary in the physical model with the prototype and numerical model, the prediction of these modes by both models is quite encouraging. The wave periods, corresponding frequency, and amplification factors for these five modes are listed in Table 29 for the prototype and numerical and physical models. Numerical model contour plots of these five modes (Figures 68 through 72) verify the oscillation patterns between the south and north corners, east and west corners, and south and east corners as described in detail in Chapter 4 and the previous Numerical Model 1978 section.

Table 29
Resonant Modes of Oscillation - Prototype, Numerical Model, Physical Model

South		North		East		Midpoint	
Wave Period (sec)	Amplification Factor	Wave Period (sec)	Amplification Factor	Wave Period (sec)	Amplification Factor	Wave Period (sec)	Amplification Factor
Prototype							
1024.0	5.1	1024.0	5.1	1024.0	5.1	1024.0	4.2
630.0	2.8	630.0	2.8	630.0	2.8	630.0	1.6
				204.0	1.1	204.0	1.7
132.0	2.1	132.1	2.2				
107.0	2.3			107.0	3.1		
85.0	0.8	85.0	0.7	85.0	0.5		
57.0	1.4	57.0	0.8				
Numerical Model							
1024.0	5.2	1024.0	5.2	1024.0	5.2	1024.0	4.4
630.0	3.2	630.0	3.2	630.0	3.2	630.0	1.8
				204.0	1.0	204.0	1.4
132.0	2.2	132.1	2.5				
107.0	2.3			107.0	3.3		
85.0	0.9	85.0	0.7	85.0	0.7		
57.0	1.4	57.0	0.9	57.0	0.8		
Physical Model							
						204.0	1.2
132.0	1.0	132.1	1.0				
107.0	1.4			107.0	2.4		
85.0	1.5	85.0	1.4	85.0	1.2		
57.0	1.0			57.0	1.3		

Additional resonant peaks occur at approximately 167 and 125 sec in the channel midpoint location in the prototype and numerical and physical model data (Figure 82). The differences between the numerical and physical model data and the prototype are slight shifts in the occurrence of these peaks and the magnitudes of amplification (Table 29). These peaks are due to the proximity of the small boat harbor. Frequency response curves of the response in the barge harbor and small boat harbor from the numerical and physical model data (Figures 77 and 78) verify the occurrence of these modes in these areas.

State-of-the-Art Numerical Model Versus Numerical Model Study 1978

In comparing the wave height amplification contour plots for the resonant modes of oscillation predicted by the Numerical Model Study 1978 and the state-of-the-art numerical model study recently completed, it can be concluded that both studies show the same patterns of oscillation occurring at approximately the same wave periods (frequencies). Comparisons are made with test results from the harbor configuration prior to inclusion of the small boat harbor. Both models predicted the Helmholtz mode; however, the peak occurred at 799 sec in the 1978 study and 910 sec in the recent study. Figures 37 and 57 provide contour plots of these oscillation modes and show that both studies predicted the same oscillation patterns; however, the 1978 magnitudes of amplification are larger than the recent study amplifications.

The remaining peak responses occur at approximately 145, 130, 107, 82, 63, 57, 56, and 46 sec from the 1978 study, and 167, 132, 107, 83, 70, 57, 56, and 46 sec from the recent study. Although the magnitudes of amplification are larger in the 1978 study results, and the occurrences of these peaks are at slightly different periods in some instances, the oscillation patterns match between the two model studies for the next four peaks as shown in Figures 38 through 41 for the 1978 study and Figures 58 through 61 for the recent study. There is no matching pattern for the 70-sec mode predicted by the recent study (Figure 62). Figures 42 and 63 show that the patterns for the 63-sec 1978 and 57-sec recent oscillation do match, and the recent 56-sec pattern seems to be a combination of the 57- and 56-sec 1978 study oscillation patterns, as shown in Figures 64, 43, and 44, respectively. Finally, the 46-sec oscillation patterns are matched between both model studies and are shown in Figures 45 and 65 for the 1978 and recent studies, respectively.

6 Evaluation of Wave Absorber

One of the objectives of the MCCP monitoring study at Barbers Point Harbor was to investigate the effectiveness of the wave absorber in dissipating wave energy inside the harbor. The 4,600 ft of rubble-mound wave absorber lines the side slopes of the northern side of the basin, entrance channel, and near the mouth of the harbor (Figure 83). The three-stone-thick wave absorber is placed on a 1:3 slope from a toe elevation of -11 ft mllw, to a crest elevation of +5 ft mllw. Below the wave absorber, basin walls were constructed on a 1:1.5 slope, which extends to the bottom. The stones vary from a 0.5- to 1-ton size at the innermost section of the harbor basin and increase to a 2- to 4-ton size towards the seaward sector of the harbor.

Figure 83. Rubble-mound wave absorber

The effectiveness of the wave absorber in dissipating wave energy inside the harbor was investigated in the physical model described in Chapter 2 of this report. Since prototype wave measurements excluding the wave absorber were unavailable, the physical model was used for this evaluation. To simulate the wave conditions only occurring in the deep-draft harbor, the small boat harbor was blocked off from the deep-draft harbor to eliminate its effects. The physical model layout is shown in Figure 84. The eight field wave conditions listed in Table 20 were also used in investigating the wave absorber.

The ability of the rubble-mound wave absorber to dissipate incident wave energy was evaluated using two approaches. The first method involved comparing predicted wave heights inside the harbor (from tests which excluded the wave absorber) to predicted wave heights inside the
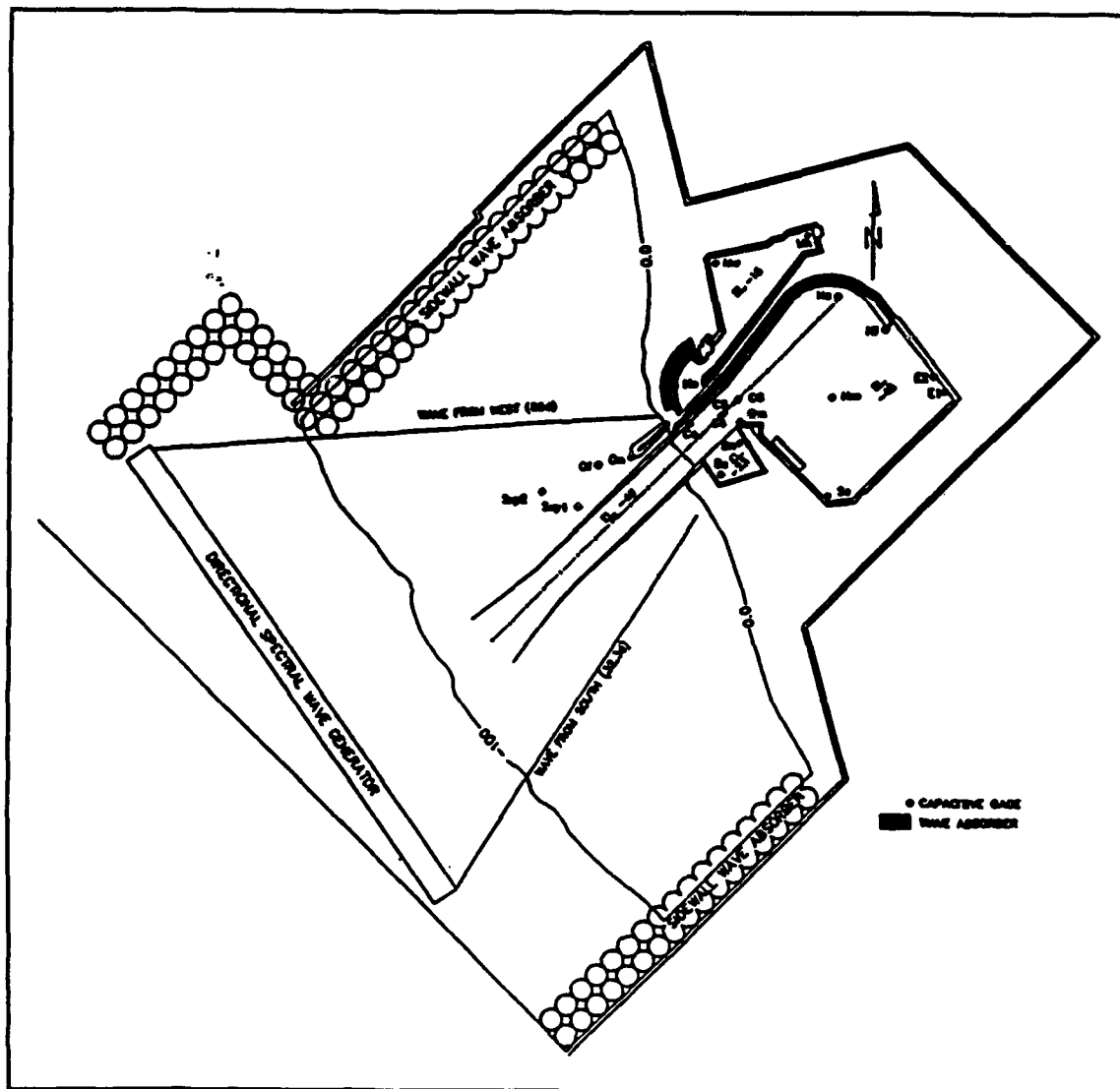
Figure 84. Physical model layout for wave absorber tests

harbor (from tests which included the wave absorber). This was accomplished by calculating the ratio of the significant wave height *Hmo* values excluding the wave absorbers to the *Hmo* values including the wave absorbers (Equation 6). The ratio indicates the change in wave energy and the dissipative characteristic of the rubble-mound wave absorber.

$$\frac{H_{m0}\ (w/o\ wave\,absorber)}{H_{m0}\ (w/\ wave\,absorber)} > 1.0$$

(6)

If the ratio is greater than 1.0, there is more energy inside the harbor with the wave absorber removed. The normalized *Hmo* values corresponding to the first four field cases are plotted in Figure 85, and values for the second four field cases are plotted in Figure 86. The average of all eight field cases is plotted in Figure 87. The graphs show that the S_{xy} and the *Of* and *Os* wave gages do not measure an appreciable amount of change in energy (i.e., *Hmo* values are close to 1.0), as expected since these gages are located outside the harbor. A measured increase in energy did occur at the wave gages located inside the harbor. For example, the *Ce* and *Cm* measurements increased approximately 35 percent, and the *Hf* and *Hm* measurements increased approximately 125 percent in some interior harbor locations when the wave absorber was removed. The percentage change in wave height was calculated using the equation:

$$\left(\frac{H_{m0}\ (\ w/o\ wave\,absorber)}{H_{m0}\ (\ w/\ wave\,absorber)} - 1\right) \times 100$$

(7)
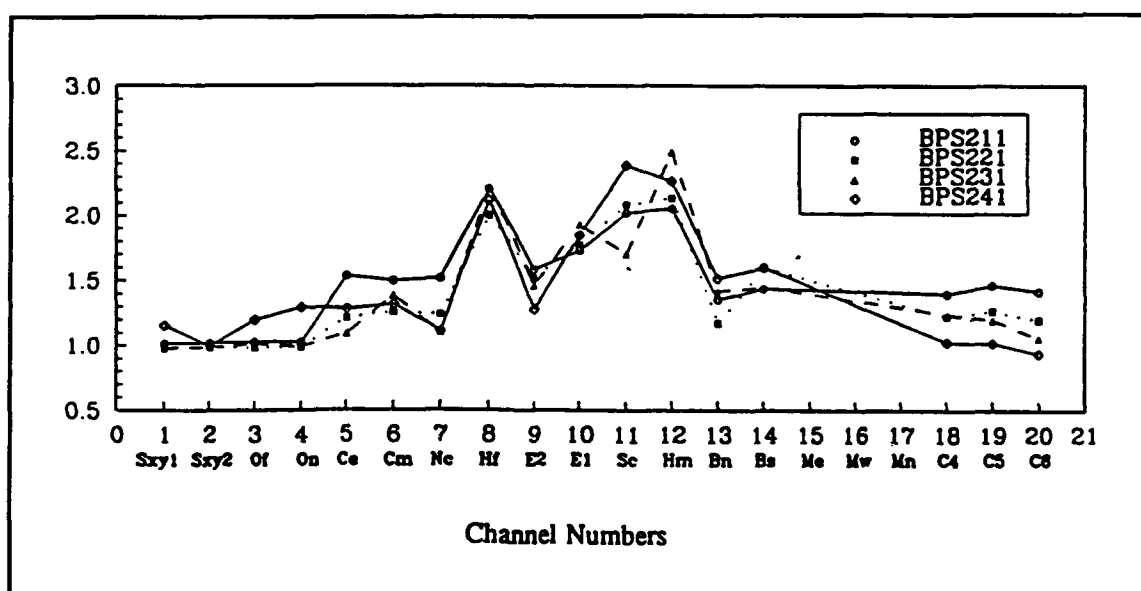
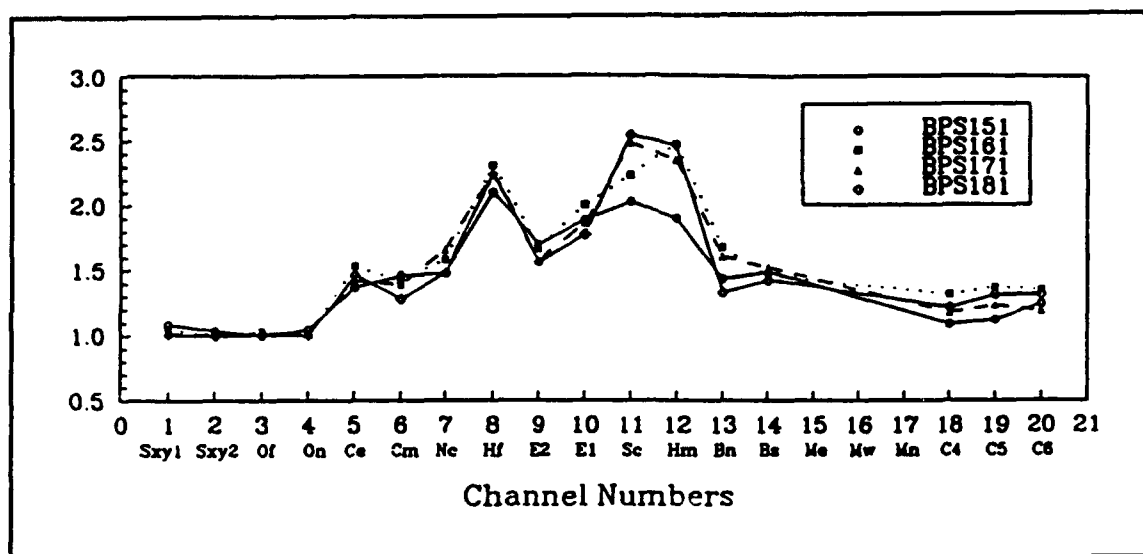Figure 85. Normalized *Hmo* values for the first four prototype wave cases

Figure 86. Normalized H_{mo} values for the second four prototype wave cases
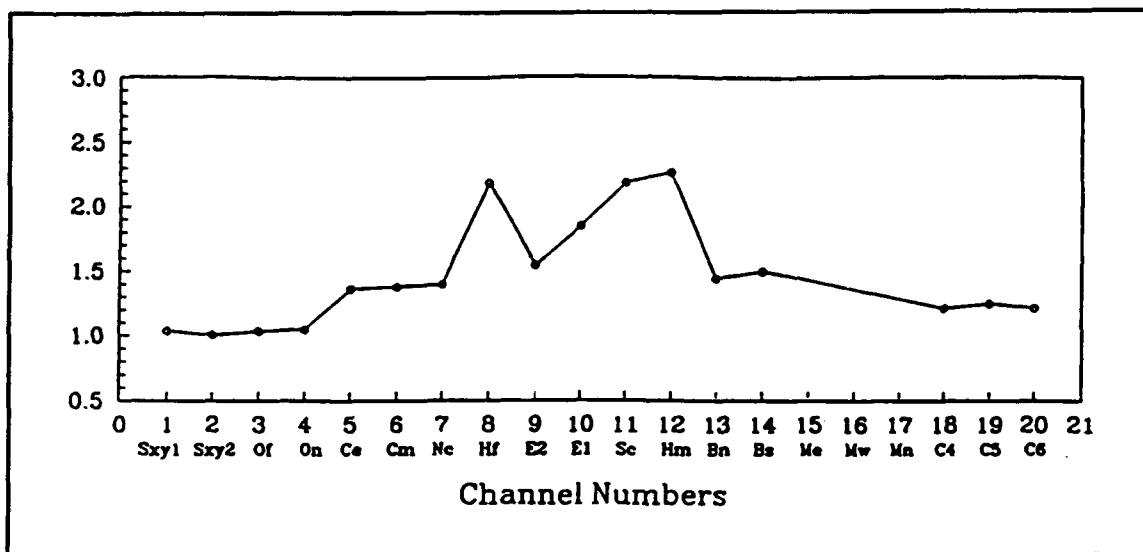

Figure 87. Averaged - normalized H_{mo} values for the eight prototype wave cases

Although the previous analysis technique indicates a dramatic change of wave energy inside the harbor, it does not directly show the change in reflection coefficient between the rubble-mound wave absorber and the reflective coral basin walls. An elevation of the rubble-mound wave absorber and the shape of the dredge cut of the coral basin wall is shown in Figure 88. The shape of the dredge cut provides some dissipation of wave energy; however, the data reveal that wave energy is not dissipated as effectively as with the rubble-mound wave absorber.
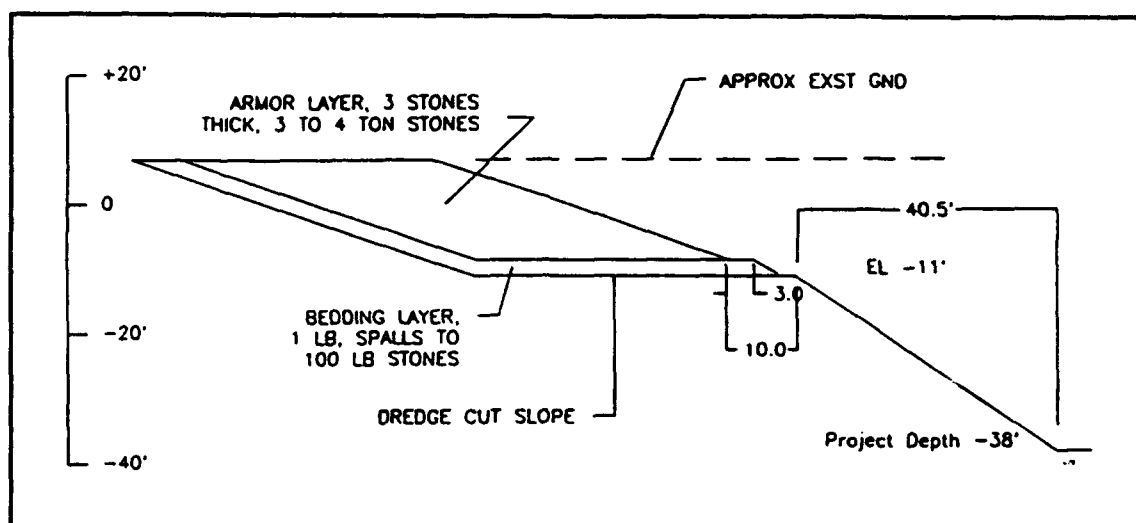
Figure 88. Elevation of wave absorber and shape of dredge cut

The second method for evaluating the efficiency of the wave absorber is described by Goda and Suzuki (1976). Goda showed that the incident and reflected wave spectra could be deduced by analyzing the time series from two separate wave gages. By incorporating a third gage, the frequency range over which the results are valid increases. Goda pointed out that this technique is valid only for a two-dimensional case in which the direction of wave propagation is parallel to the gage array. Waves propagating at an angle to the wave gage array are not accurately resolved.

For the purposes of this study, three gages were positioned in an array, as recommended by Goda, in the deep-draft harbor entrance channel. The array is referred to as the Goda array. Unfortunately, the wave directions in the deep-draft harbor basin are far from two-dimensional and the Goda array could not be used in evaluating the wave absorbers in the basin. However, the principal direction of wave propagation in the entrance channel can be considered two-dimensional and the predictions from the Goda array were used to calculate reflection coefficients from the wave absorber along the harbor entrance. The calculated reflection coefficients are presented in Table 30. The following equation was used to calculate the reflection coefficients:

$$K_r = \frac{Reflected\, H_{m0}}{Incident\, H_{m0}}$$

(8)

Although the results from the Goda array were contaminated by waves propagating at an angle to the array, it was possible to calculate reflection coefficients from the data. The result was that a higher proportion of incident wave energy was reflected when the wave absorber was removed.

Table 30
Physical Model Reflection Coefficients in Entrance Channel

Test Case	Plan With Wave Absorber	Plan Without Wave Absorber
151	0.22	0.44
161	0.30	0.50
171	0.27	0.47
181	0.31	0.49
211	0.30	0.49
221	0.19	0.34
231	0.22	0.38
241	0.26	0.44

Since the effectiveness of the rubble-mound wave absorber in dissipating wave energy is a function of the incident wave period, a third method to evaluate the wave absorbers is to investigate the spectral energy density values from the plan excluding the wave absorber normalized by values from the plan including the wave absorber. The values were averaged over the eight field wave cases and are plotted in Figure 89. Values above one indicate an increase in wave energy when the wave absorber was removed. These values were smoothed by band averaging Fourier coefficients to give an equivalent frequency band of 0.01 Hz. As shown in Figure 89, there is a small amount of variance in the averaged-normalized spectral density for the long period waves greater than 50 sec. This is because the wavelengths are too long to be affected by the wave absorber or
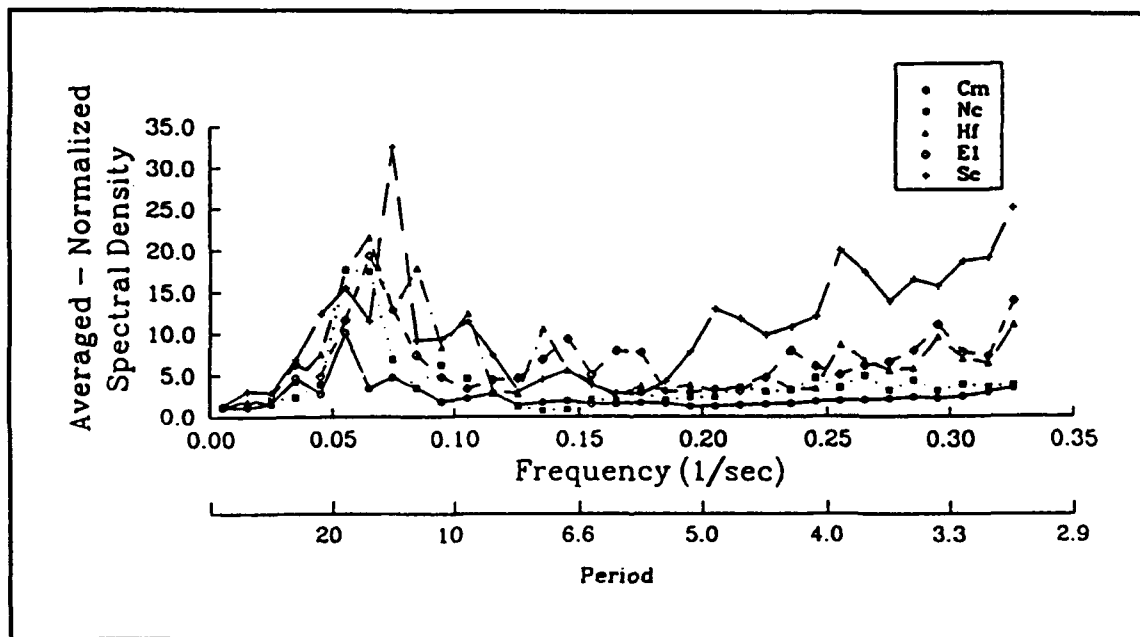
Figure 89. Averaged - normalized spectral density

other types of basin walls. Once the wave periods become increasingly
shorter, variation in the averaged-normalized spectral density decreases.
The variation in the 10- to 20-sec wave period range is dramatic, particu-
larly in the south corner gage.

Rubble-mound wave absorbers effectively reduce wave energy inside
the semi-enclosed harbor for wind-wave periods of 20 sec or less. The
wave absorbers were less effective in decreasing wave energy for the
longer waves with periods of 50 sec or greater. Results of this study indi-
cate that removing the wave absorbers will increase the H_{m0} wave heights
in the harbor basin by approximately 125 percent. Wave reflection analy-
sis also indicates that the wave absorber decreases reflection coefficients
up to approximately 50 percent.

7 Conclusions and Recommendations

Conclusions

To aid the reader in considering the study conclusions, a summary of the various model studies is provided in Table 31 below.

Table 31 Barbers Point Harbor Model Studies					
Model Study	Deep-Draft Harbor	Small Boat Harbor as Constructed	Small Boat Harbor	Short Waves	Long Waves
Hydraulic Model 1967	X		X	X	
Numerical Model 1978	X			X	X
Hydraulic Model 1985	X	X			X
Numerical Model (grid 1)	X			X	X
Numerical Model (grid 2)	X	X		X	X
Physical Model	X	X		X	X

The study conclusions are formulated based on the five study objectives as restated in *a* through *e* below:

a. Evaluate and validate the results of the model studies conducted for harbor design.

Results of the numerical model study show that the model did well in predicting the resonant modes of oscillation that were measured in the prototype harbor. Differences between the results are: (1) the numerical model resonant peaks occur at slightly offset periods from the prototype, which could result from differences in dimensions of the gridded harbor and the prototype configuration, and (2) the numerical model magnitudes of amplification are larger

144

than the prototype measurements, which is expected since the model neglected dissipative effects.

Difficulties were encountered in evaluating the results of the two hydraulic model studies; therefore, evaluation of this objective is limited and should be considered very general. Difficulties relating to the 1967 model study include: (1) only short period waves ranging from 4 to 20 sec were considered, (2) the configuration of the model did not correspond to the configuration constructed in the prototype, and (3) gage locations in the model and prototype were in the same vicinity but not coincident with each other. Difficulties relating to the 1985 study include: (1) differences between the model and prototype configurations, (2) model gages were located in the small boat harbor and the prototype gage was located in the entrance channel, and (3) incident wave directions were not available from the prototype data.

The 1967 hydraulic model and prototype results for short period waves did not exceed the desired maximum criteria of 2.5 ft or the maximum tolerable criteria of 4.5 ft in the deep-draft harbor. Generally, the model wave heights are larger than the prototype in the north and east corners; however, the prototype wave heights are larger in the south corner. The configuration of the small boat harbor tested for short waves was not constructed in the prototype; therefore, data are not available for comparison. As mentioned previously, no specific conclusions can be drawn to validate this study.

The 1985 hydraulic model study to evaluate various configurations of the small boat harbor using long waves as input determined that harbor oscillations would occur at periods between 100 and 150 sec in the small boat harbor. These resonant modes are consistent with the prototype data measuring oscillations occurring at approximately 110, 125, and 132 sec.

b. Perform wave gaging to measure the wave climate in deep water and nearshore areas, and long-period oscillations of the harbor.

Chapter 4 describes the prototype wave gaging effort to measure the wave climate in deep water, nearshore, and inside the harbor. Overall, the data show that the wave conditions at Barbers Point are more energetic during the fall and winter months (October to March) than during the spring and summer months (April to September).

A comparison of the sea-swell significant wave heights from the deepwater buoy and the slope array determined a correlation of 0.95; therefore, the sea-swell conditions in the nearshore at Barbers Point can be accurately estimated with data from the offshore buoy.

Long-period modes of harbor oscillation were identified both prior to and after inclusion of the small boat harbor. The resonant peaks prior to inclusion of the harbor occurred at approximately 910, 132, 110, 70, 60, and 47 sec. After inclusion of the small boat harbor, resonant peaks occur at approximately 1,024, 630, 200, 167, 132, 125, 110, 85, and 57 sec. The 1,024-sec peak is the Helmholtz mode of the deep-draft harbor, and the 630-sec peak is the Helmholtz mode of the small boat harbor.

c. Relate conditions outside the harbor to surge found inside the harbor.

Comparison of the infragravity significant wave heights measured inside the harbor with those measured at the slope array shows a high correlation between significant wave height inside and outside the harbor. It can be concluded that an increase in harbor seiche is associated with an increase in swell energy outside the harbor. Therefore, nonlinear processes which transfer energy from swell waves to infragravity waves outside the harbor are clearly an important mechanism for harbor resonance forcing at this location.

The high correlation between the harbor seiche and sea-swell wave heights rules out free long waves generated from distant sources as an important forcing mechanism at Barbers Point since these free waves are not necessarily coincident with energetic sea and swell.

d. Evaluate the effectiveness of the wave absorber.

The rubble-mound wave absorber effectively reduces the wave energy inside the harbor for wind-wave periods of 20 sec or less. The wave absorber is less effective in decreasing wave energy for longer waves with periods of 50 sec or greater.

Removing the wave absorber will increase wave heights at some locations inside the harbor by an estimated 125 percent (refer to equation 7). Analysis indicates that the wave absorber decreases the reflection coefficients up to 50 percent.

e. Compare measured data to the predictions of state-of-the-art physical and numerical model studies.

Overall, the comparison is good between the prototype measurements and the numerical and physical model predictions of the resonant modes of oscillation. The numerical model, which was simulated both prior to and after inclusion of the small boat harbor, was consistent with the prototype measurements in predicting the shift of the Helmholtz mode and the appearance of additional peaks with the inclusion of the small boat harbor. The physical model was not able to resolve the long period modes due to the length of simulations; however, the model accurately predicted the remaining resonant modes occurring in the harbor. Numerical model

146

magnitudes of amplification were consistent with the prototype amplifications since the model was calibrated to the measurements using bottom friction. The physical model magnitudes varied from the prototype depending on the wave period.

Physical and numerical models have strengths and limitations which must be recognized in making sound engineering judgements. Although both models can predict resonant modes of oscillation fairly well, the numerical model predicts the very long-period resonant modes better than the physical model. Long-period resonant modes may be under-represented in the physical model because duration of data collation is limited by economic concerns or by the size of the model. The physical model, however, more accurately predicts the shorter period waves. This is due to "built-in" dissipating factors in the physical model, whereas, in the numerical model, choosing correct boundary reflection (absorption) and bottom friction coefficients requires calibrated estimates.

Additional numerical model strengths include (1) ease of model setup and modifications, (2) availability of data throughout the modeled harbor grid, which permits visualization of the wave response over the entire gridded region, (3) quick response time, and (4) less cost to run the model. Limitations include simulation with (1) unidirectional regular waves without directional spreading effects, (2) neglect of nonlinear effects, and (3) lack of good reflection coefficient and bottom friction data for accurately calibrating the model.

Additional physical model strengths include the ability to simulate (1) directional wave spectra, (2) nonlinear wave-wave transformation as waves travel into harbors, (3) reflection, transmission, and overtopping of structures, (4) dissipation due to bottom friction within scale and depth limitations, (5) currents, and (6) navigation studies with model ships. Limitations are mainly due to the cost to construct and modify models and to collect data.

Long-period modes (resonance) cannot be effectively damped out once a harbor is constructed. A model investigation of resonant modes should be carried out before final project planning to ensure that the constructed harbor does not have unacceptable resonant modes of oscillation.

Recommendations

Through the use of prototype measurements, numerical and physical models were shown to be very effective tools in designing and evaluating Barbers Point Harbor. The combination of prototype and numerical and physical models verified the resonant modes of oscillation throughout the

harbor complex. These two modeling approaches should be used on other harbor projects where oscillations may occur.

It is recommended that harbor studies thoroughly investigate a full range of wave conditions to evaluate harbor oscillations, wind waves, and the effects of direction on those conditions.

This study demonstrated that both models, in conjunction with prototype data, accurately predict harbor wave response. Given the strengths and limitations of each model, it is recommended that both numerical and physical models be used to evaluate the response of a harbor to long and short period incident wave conditions.

It is recommended that as much prototype data as possible be obtained for a harbor study. In the design phase of a harbor, long-term wave gaging 's essential to collect the wave climate incident to the harbor. In monitoring the wave response of a harbor, or evaluating proposed modifications to a harbor, it is crucial that wave gaging be conducted to collect wave data incident to and within the entire harbor complex. Long-term wage gaging is essential to calculate probabilities of critical wave occurrences throughout the harbor complex.

Quantify or at least qualify the range of conditions that are to be measured prior to implementation of a data collection effort to ensure that sample durations are sufficient to resolve the study objectives. Long time series records are necessary for analysis of coupling between wind waves and infragravity motions outside and inside the harbor. Record lengths were originally collected for 1,024 sec (17 min), which was determined too short for the purpose of this study; therefore, record lengths were changed to 8,192 (2.3 hr) and 16,384 (4.5 hr). Time series records from all gages should also be synchronized in order to effectively cross-correlate results from various locations. When hardware restrictions prevent this, an alternative to synchronized records is to have accurate time-sampling of data. Record lengths of 4.5 hr were not synchronized at all gages; however, the records did overlap and it was possible to obtain 2.3-hr-long records, which were synchronized with other gages.

Correct placement of instruments is crucial and must be coordinated with overall study goals. Possibilities of channel, wall, etc., effects contaminating data and damage to instruments from vessels typical to the area must be carefully considered in deployment and placement of instruments. Also, an evaluation of the region is required to minimize the collection effort's intrusion into regional use.

It is recommended tha' wave gages be located in all areas of a study region. Partial coverage tends to raise more questions over the areas where data are not collected. In this study, the placement of the deep-draft harbor gages provided excellent data coverage to evaluate deep-draft harbor resonance modes, oscillation patterns occurring during harbor resonance, and to compare measured data to model study results. However, gages

148

were not located in the barge and small boat harbor. Prototype information in these areas would have aided in monitoring the harbor response, in calibrating the models, and in overall comparisons between prototype and model predictions.

Extra time should be added to project schedules when dealing with newer, advanced technical equipment. Data transmission over long distances (i.e., Oahu to California) using satellite telephone links can present problems in obtaining complete records. The lack of a few data points leads to surprisingly large problems in obtaining directional information from the slope array. The problem of incomplete records was corrected by repeating data transmission procedures until a complete record was obtained. This procedure was not cost-effective.

Accurate surveys of the entire harbor domain relative to the period of data collection are recommended to allow more accurate model simulations and comparisons to prototype data. Coordinates of pertinent features of the projects are also crucial for accurate model calibration and simulation. If possible, it is recommended that modelers use only as-built blueprints of the project site. Photographs and aerial photographs are invaluable aids to the model studies.

It is recommended that necessary research be conducted to establish boundary reflection (absorption) and bottom friction coefficients for various boundary and bottom types. This research is necessary, in general, and for the HARBD model. It is essential that specific research in this area be conducted for all models presently being applied and for those models in the development or proposed development phases. The relationship between coefficients for the numerical and physical models should also be investigated.

Regardless of location, a site visit prior to initiating the study has proven, many times over, to have been an asset to properly modeling the harbor. Experience and insight gained from site visits have helped overcome many difficulties in properly generating numerical grids, constructing the physical model, model simulations, and analyzing, interpreting, and comparing results. Modelers need to understand the processes they are simulating, particularly when prototype data are available and model prototype comparisons will be conducted.

References

Bendat, J. S., and Piersol, P. G. (1986). *Random data: Analysis and measurement procedure*. John Wiley & Sons, New York.

Bloomfield, P. (1976). *Fourier analysis of time series: An introduction*. John Wiley & Sons, New York.

Boc, S. J. (1987). "Barbers Point, Oahu, Hawaii deep-draft harbor monitoring program." *Proceedings, Coastal Zone '87 Conference*. American Society of Civil Engineers, Seattle, WA.

Botes, W. A. M., Russell, K. S., and Huizinga, P. (1982). "Resonance in South African harbours." *Proceedings, 18th International Conference on Coastal Engineering*, 439-53.

Bottin, R. R., Jr., Sargent, F. E., and Mize, M. G. (1985). "Fisherman's Wharf Area, San Francisco Bay, California, design for wave protection: Physical and numerical model investigation," Technical Report CERC-86-7, U.S. Army Engineer Waterways Experiment Station, Vicksburg, MS.

Briggs, M. J., Lillycrop, L. S., and McGehee, D. D. (1992). "Comparison of model results for Barbers Point Harbor." *Proceedings, Coastal Engineering Practice '92 Conference*. American Society of Civil Engineers, Long Beach, CA.

Briggs, M. J., Lillycrop, Linda S., Harkins, G. S., Thompson, E. F., and Green, Debra R. "Physical and Numerical Model Studies of Barbers Point Harbor, Oahu, Hawaii," in preparation, U.S. Army Engineer Waterways Experiment Station, Vicksburg, MS.

Chen, H. S. (1984). "Hybrid element modeling of harbor resonance." *Proceedings, 4th International Conference on Applied Numerical Modeling*, 312-16.

_____. (1986). "Effects of bottom friction and boundary absorption on water wave scattering," *Applied Ocean Research* 8,99-104.

Chen, H. S., and Houston, J. R. (1987). "Calculation of water oscillation in coastal harbors: HARBS and HARBD user's manual," Instruction Report CERC-87-2, U.S. Army Engineer Waterways Experiment Station, Vicksburg, MS.

Chen, H. S., and Mei, C. C. (1974). "Oscillations and wave forces in an offshore harbor," Report No. 190, Department of Civil Engineering, Massachusetts Institute of Technology, Cambridge, MA.

Cialone, M. A., Mark, D. J., Chou, L. W., Leenknecht, D. A., Davis, J. E., Lillycrop, L. S., and Jensen, R. E. (1991). "Coastal Modeling System (CMS) User's Manual," Intruction Report CERC-91-1, U.S. Army Engineer Waterways Experiment Station, Vicksburg, MS.

Clark, D. J. (1974). "The oscillations of Port Kembla Harbor," *The Dock & Harbour Authority*, 383-84.

Clausner, J. E., and Abel, C. E. (1986). "Contained aquatic disposal: Site location and cap material investigations for Outer Indiana Harbor and southern Lake Michigan," Appendix J in *Disposal alternatives for PCB-contaminated sediments from Indiana Harbor, Indiana*, Miscellaneous Paper EL-87-9, Vol II, U.S. Army Engineer Waterways Experiment Station, Vicksburg, MS.

Crawford, P. L., and Chen, H. S. (1988). "Comparison of numerical and physical models of wave response in a harbor," Miscellaneous Paper CERC-88-11, U.S. Army Engineer Waterways Experiment Station, Vicksburg, MS.

Dixon, W. J., and Massey, F. J., Jr. (1969). *Introduction to statistical analysis*. McGraw-Hill, New York.

Durham, D. L. (1978). "Numerical analysis of harbor oscillations for Barbers Point deep-draft harbor," Technical Report HL-78-20, U.S. Army Engineer Waterways Experiment Station, Vicksburg, MS.

Farrar, P. D., and Chen, H. S. (1987). "Wave response of the proposed harbor at Agat, Guam: Numerical model investigation," Technical Report CERC-87-4, U.S. Army Engineer Waterways Experiment Station, Vicksburg, MS.

Gaveson, H., Jensen, J., and Sorensen, T. (1978). "Harbour resonance generated by storm waves." 7th *International Harbour Congress*. Vol. 1.

Goda, Y., and Suzuki, Y. (1976). "Estimation of incident and reflected waves in random wave experiments." *Proceedings, 15th Coastal Engineering Conference*. American Society of Civil Engineers, 828-48.

Harkins, G. S. (1991). "Sensitivity analysis for multi-element wavemakers," M.S. thesis, University of Delaware, Newark.

Hemsley, J. M. (1985). "Monitoring completed coastal projects." *Proceedings, Coastal Zone '85 Conference*. American Society of Civil Engineers, Baltimore, MD.

Hemsley, J. M., Boc, S. J., and Okihiro, M. S. (1988). "Monitoring waves and surge at Barbers Point, Hawaii." *Proceedings, Pacific Congress on Marine Science and Technology Conference*. Marine Technology Society, Honolulu, HI.

Higgins, A. L., and Seymour, R. J. (1978). "Deep water direction from an intensity array," *Proceedings, Sixteenth Coastal Engineering Conference*. American Society of Civil Engineers, Hamburg, Germany.

Higgins, A. L., Seymour, R. J., and Pawka, S. S. (1981). "A compact representation of ocean wave directionality," *Applied Ocean Research* 75(33), 6778-801.

Houston, J. R. (1976). "Long Beach Harbor numerical analysis of harbor oscillations; Report 1, Existing conditions and proposed improvements," Miscellaneous Paper H-76-20, U.S. Army Engineer Waterways Experiment Station, Vicksburg, MS.

_____. (1981). "Combined refraction and diffraction of short waves using the finite element method," *Applied Ocean Research* 3(4),163-70.

Jensen, J., and Warren, I. R. (1986). "Modelling of waves in harbours - review of physical and numerical methods," *The Dock and Harbour Authority*, 123-29.

Kaihatu, J. M., Lillycrop, L. S., and Thompson, E. F. (1989). "Effects of entrance channel dredging at Morro Bay, California," Miscellaneous Paper CERC-89-3, U.S. Army Engineer Waterways Experiment Station, Vicksburg, MS.

Kirkegaard, J., and Nielsen, A. H. (1982). "Hydraulic studies of Bintulu deepwater port," *Portech* 1982.

Lee, T. T. (1985). "Proposed West Beach Marina hydraulic model investigation," TR No. 59, Univ. of Hawaii, Look Lab-85-1, Honolulu, HI.

Lillycrop, L. S., Bratos, S. M., and Thompson, E. F. (1990). "Wave response of proposed improvements to the shallow-draft harbor at Kawaihae, Hawaii" Miscellaneous Paper CERC-90-8, U.S. Army Engineer Waterways Experiment Station, Vicksburg, MS.

Lillycrop, L. S., Bratos, S. M., Thompson, E. F., and Rivers, P. (1993). "Wave response of proposed improvements to the small boat harbor at Maalaea, Maui, HI," Miscellaneous Paper CERC-93-4, U.S. Army Engineer Waterways Experiment Station, Vicksburg, MS.

Lillycrop, L. S., and Briggs, M. J. (1992). "Capabilities in harbor design and monitoring: A case study," CETN-I-54, U.S. Army Engineer Waterways Experiment Station, Vicksburg, MS.

Lundgren, H. (1981). "Natural sea states in maritime engineering." *Conference on hydraulic modeling applied to maritime engineering problems.*

Marine Advisers. (1964). *Characteristics of deep water waves in the Oahu area for the typical year.*

Munk, W. H. (1949). "Surf beats," *Eos Trans. American Geophysical Union,* 30(6), 849-54.

Noda, E. K., and Associates, Inc. (1988). "Evaluation of surge forces for the Barbers Point deep-draft harbor," prepared for Nakamura and Tyau, Inc., and DOT, Harbors Division, State of Hawaii.

Okihiro, M. S., Guza, R. T., and Seymour, R. J. (1992). "Bound infragravity waves," *Journal of Geophysical Research* 97(C7), 11453-69.

Outlaw, D. G., and Briggs, M. J. (1986). "Directional irregular wave generator design for shallow wave basins." *21st American Towing Tank Conference,* August 7, Washington, D.C., 1-6.

Palmer, R. Q. (1970). "Study of proposed Barbers Point Harbor, Hawaii: Hydraulic model investigation," TR No. 8, U.S. Army Engineer District, Honolulu, HI.

Sand, S. E. (1982). "Wave grouping described by bounded long waves," *Ocean Engineering* 9(6), 567-80.

Sargent, F. E. (1989). "Los-Angeles - Long Beach Harbor Complex 2020 plan harbor resonance analysis: Numerical model investigation," Technical Report CERC-89-16, U.S. Army Engineer Waterways Experiment Station, Vicksburg, MS.

Sea Engineering, Inc. (1980). "Measure of coastal currents, Waianae, Oahu, HI," Waimanalo, HI.

_____. (1983). "Wave and current data collection for coastal engineering analysis and design," Waimanalo, HI, prepared for West Beach Estates, Oahu, HI.

Shore Protection Planning and Design. (1966). 3rd ed., U.S. Army Engineer Waterways Experiment Station, Coastal Engineering Research Center, U.S. Government Printing Office, Washington, D.C.

Stevens, J. C., et al. (1942). "Hydraulic models," *Manuals of Engineering Practice No. 25,* American Society of Civil Engineers, New York.

U.S. Army Engineer District, Honolulu. (1976). "Barbers Point Harbor," Design Memorandum No. 1, Plan Formulation, Honolulu, HI.

_____. (1977). "Barbers Point Harbor," Design Memorandum No. 1, Phase II - Project Design, Honolulu, HI.

Weishar, L. L., and Aubrey, D. G. (1986). "A study of inlet hydraulics at Green Harbor, Marshfield, Mass.," Miscellaneous Report CERC 88-10, U.S. Army Engineer Waterways Experiment Station, Vicksburg, MS.

Wyrtki, K., Graefe, V., and Patzert, W. (1969). "Current observations in the Hawaiian Archipelago," Report No. HIG-69_15, Hawaii Institute of Geographics.

Appendix A
Monitoring Program

Table A1
Data Sampling Configuration

Sensor	Date	Sample Frequency (Hz)	No. of Samples	Record Length (s)
Buoy	Jul 86 - Aug 87 Sep 87 - May 88 Jun 88 - Jan 90	1.0 1.0 1.0	1024 2048 8192	1024 2048 8192
Slope 1	Jul 86 - Jan 88 Jul 86 - Aug 87 Sep 87 - Jan 88	0.125 1.0 1.0	2048 1024 8192	16384 1024 8192
Slope 2	Jun 88 - Jan 89 Jun 88 - Jan 89 Feb 89 - Mar 90	0.125 1.0 1.0	2048 8192 16384	16384 8192 16384
Entrance	Jul 86 - Jan 89 Jul 86 - Nov 86 Sep 87 - Jan 89 Feb 89 - May 89	0.125 1.0 1.0 1.0	2048 1024 8192 16384	16384 1024 8192 16384
Mid-point	Jul 86 - Jan 89 Jul 86 - Jun 87 Sep 87 - Jan 89 Feb 89 - Mar 90	0.125 1.0 1.0 0.5	2048 1024 8192 8192	16384 1024 8192 16384
North	Feb 89 - Mar 90	0.5	8192	16384
East	Feb 89 - Mar 90	0.5	8192	16384
South	Feb 87 - Apr 88 Feb 87 - Jul 87 Aug 87 - Apr 88 Feb 89 - Mar 90	0.125 1.0 1.0 0.5	2048 1024 8192 8192	16384 1024 8192 16384

Table A2
Cumulative Height Probability of Exceedence Offshore Buoy
July 1986 - January 1990

Significant Height (cm)	All Data	Winter (Oct-Mar)	Summer (Apr-Sep)
20.0	1.0000	1.0000	1.0000
40.0	0.9995	1.0000	1.9990
60.0	0.9360	0.9716	0.9021
80.0	0.6193	0.7749	0.4711
100.0	0.3085	0.4710	0.1536
120.0	0.1549	0.2694	0.0458
140.0	0.0829	0.1541	0.0151
160.0	0.0464	0.0885	0.0062
180.0	0.0243	0.0486	0.0010
200.0	0.0123	0.0251	0.0000
220.0	0.0064	0.0131	0.0000
240.0	0.0027	0.0055	0.0000
260.0	0.0008	0.0016	0.0000
280.0	0.0000	0.0000	0.0000
300.0	0.0000	0.0000	0.0000
320.0	0.0000	0.0000	0.0000

Table A3
Cumulative Height Probability of Exceedence Slope Array
July 1986 - March 1990

Significant Height (cm)	All Data	Winter (Oct-Mar)	Summer (Apr-Sep)
20.0	1.0000	1.0000	1.0000
40.0	0.8979	0.9576	0.880
60.0	0.5091	0.6870	0.306
80.0	0.2576	0.4082	0.1064
100.0	0.1310	0.2277	0.0338
120.0	0.0705	0.1288	0.0120
140.0	0.0400	0.0755	0.0044
160.0	0.0237	0.0467	0.0005
180.0	0.0142	0.0283	0.0000
200.0	0.0065	0.0130	0.0000
220.0	0.0033	0.0065	0.0000
240.0	0.0019	0.0038	0.0000
260.0	0.0011	0.0022	0.0000
280.0	0.0003	0.0005	0.0000
300.0	0.0003	0.0005	0.0000
320.0	0.0003	0.0005	0.0000

Table A4
Cumulative Height Probability of Exceedence Slope Array
(Infragravity) July 1986 - March 1990

Significant Height (cm)	All Data	Winter (Oct-Mar)	Summer (Apr-Sep)
0.0	1.0000	1.0000	1.0000
5.0	0.4436	0.5592	0.3257
10.0	0.1079	0.1826	0.0318
15.0	0.0418	0.0789	0.0039
20.0	0.0213	0.0417	0.0006
25.0	0.0130	0.0258	0.0000
30.0	0.0061	0.0121	0.0000
35.0	0.0022	0.0044	0.0000
40.0	0.0008	0.0016	0.0000
45.0	0.0003	0.0005	0.0000
50.0	0.0000	0.0000	0.0000

Table A5
Cumulative Height Probability of Exceedence Channel Entrance
July 1986 - May 1989

Significant height (cm)	All Data	Winter (Oct-Mar)	Summer (Apr-Sep)
0.0	1.0000	1.0000	1.0000
5.0	0.4719	0.5859	0.3221
10.0	0.1207	0.1863	0.0346
15.0	0.0452	0.0762	0.0045
20.0	0.0204	0.0353	0.0009
25.0	0.0106	0.0187	0.0000
30.0	0.0071	0.0125	0.0000
35.0	0.0031	0.0055	0.0000
40.0	0.0024	0.0042	0.0000
45.0	0.0012	0.0021	0.0000
50.0	0.0004	0.0007	0.0000

Table A6
Cumulative Height Probability of Exceedence Channel Mid-Point
July 1986 - March 1990

Significant height (cm)	All Data	Winter (Oct-Mar)	Summer (Apr-Sep)
0.0	1.0000	1.0000	1.0000
5.0	0.3766	0.4718	0.2546
10.0	0.0667	0.1056	0.0168
15.0	0.0247	0.0378	0.0079
20.0	0.0118	0.0152	0.0074
25.0	0.0067	0.0062	0.0074
30.0	0.0044	0.0025	0.0068
35.0	0.0023	0.0012	0.0037
40.0	0.0009	0.0000	0.0021
45.0	0.0000	0.0000	0.0000
50.0	0.0000	0.0000	0.0000

Table A7
Cumulative Height Probability of Exceedence North Corner
January 1989 - March 1990

Significant Height (cm)	All Data	Winter (Oct-Mar)	Summer (Apr-Sep)
0.0	1.0000	1.0000	1.0000
5.0	0.3567	0.4081	0.2877
10.0	0.0456	0.0733	0.0085
15.0	0.0134	0.0223	0.0014
20.0	0.0043	0.0074	0.0000
25.0	0.0024	0.0043	0.0000
30.0	0.0006	0.0011	0.0000
35.0	0.0006	0.0011	0.0000
40.0	0.0000	0.0000	0.0000
45.0	0.0000	0.0000	0.0000
50.0	0.0000	0.0000	0.0000

Table A8
Cumulative Height Probability of Exceedence East Corner
January 1989 - March 1990

Significant Height (cm)	All Data	Winter (Oct-Mar)	Summer (Apr-Sep)
0.0	1.0000	1.0000	1.0000
5.0	0.6080	0.5989	0.7826
10.0	0.1620	0.1636	0.1304
15.0	0.0659	0.0682	0.0217
20.0	0.0292	0.0307	0.0000
25.0	0.0173	0.0182	0.0000
30.0	0.0076	0.0080	0.0000
35.0	0.0032	0.0034	0.0000
40.0	0.0022	0.0023	0.0000
45.0	0.0000	0.0000	0.0000
50.0	0.0000	0.0000	0.0000

Table A9
Cumulative Height Probability of Exceedence South Corner
February 1987 - March 1990

Significant Height (cm)	All Data	Winter (Oct-Mar)	Summer (Apr-Sep)
0.0	1.0000	1.0000	1.0000
5.0	0.5911	0.6778	0.4728
10.0	0.1129	0.1722	0.0319
15.0	0.0382	0.0627	0.0048
20.0	0.0142	0.0246	0.0000
25.0	0.0057	0.0100	0.0000
30.0	0.0024	0.0041	0.0000
35.0	0.0007	0.0012	0.0000
40.0	0.0007	0.0012	0.0000
45.0	0.0003	0.0006	0.0000
50.0	0.0003	0.0006	0.0000
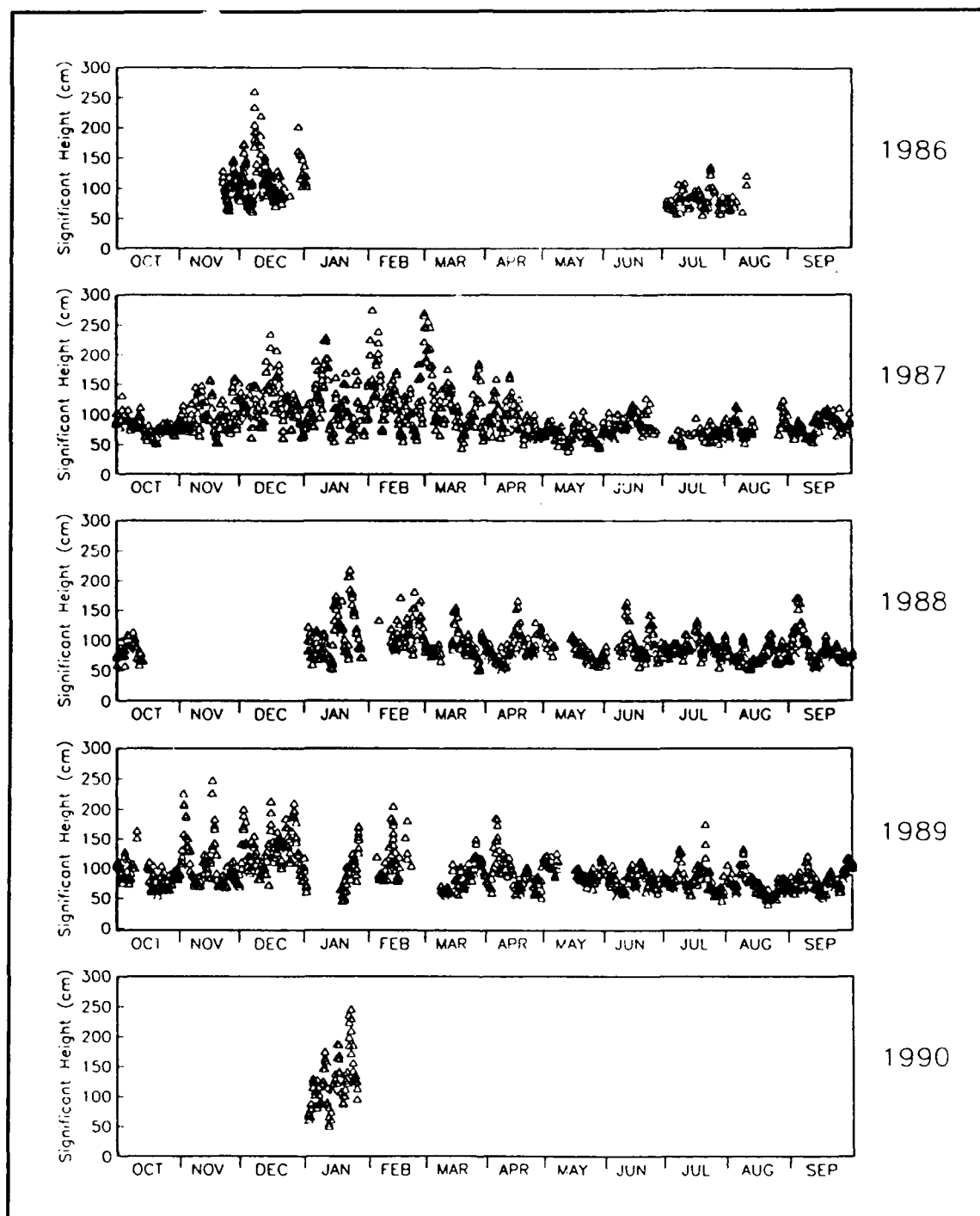
Figure A1. Offshore buoy sea-swell significant wave heights for all data records available
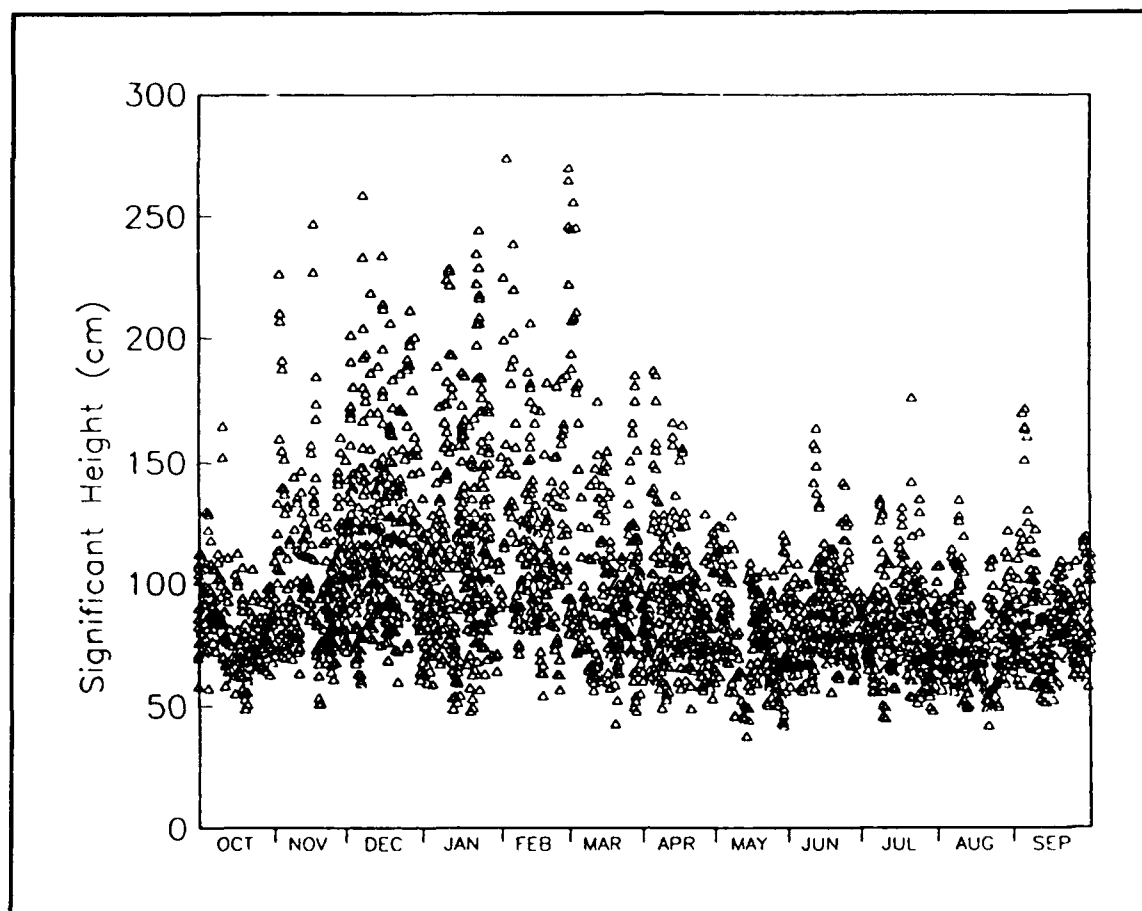
Figure A2. **Offshore buoy** sea-swell significant wave heights for **July 1986 - January 1990**
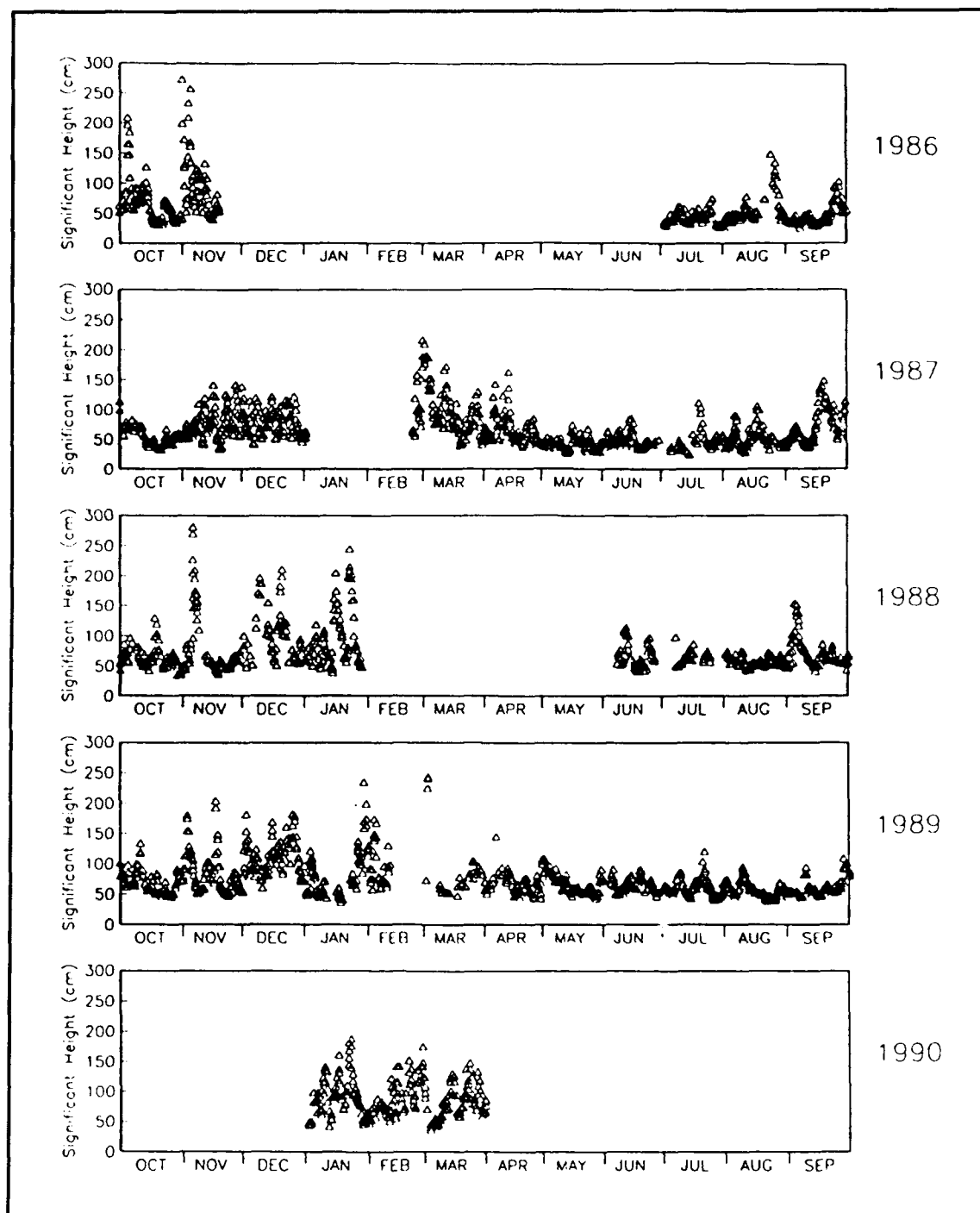
Figure A3. Slope array sea-swell significant wave heights for all data records available
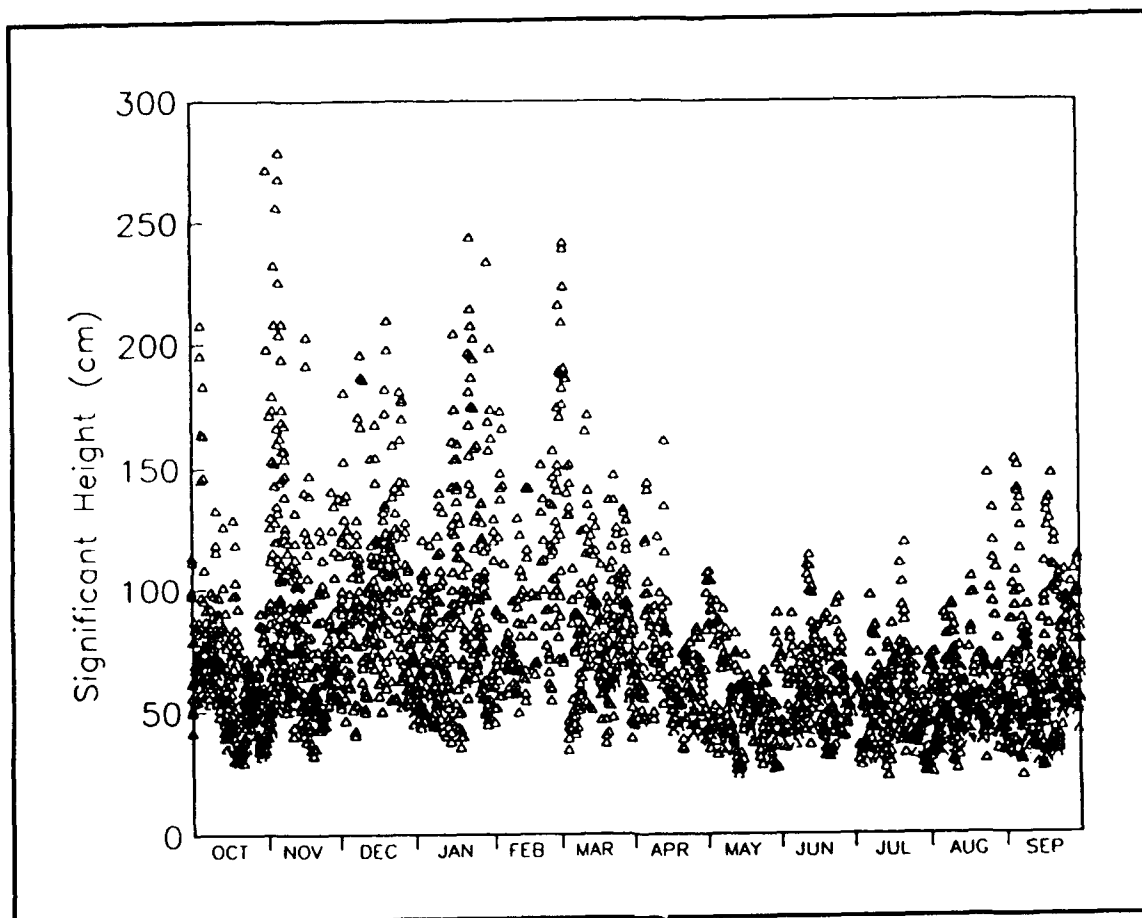
Figure A4. Slope array sea-swell significant wave heights for July 1986 - March 1990
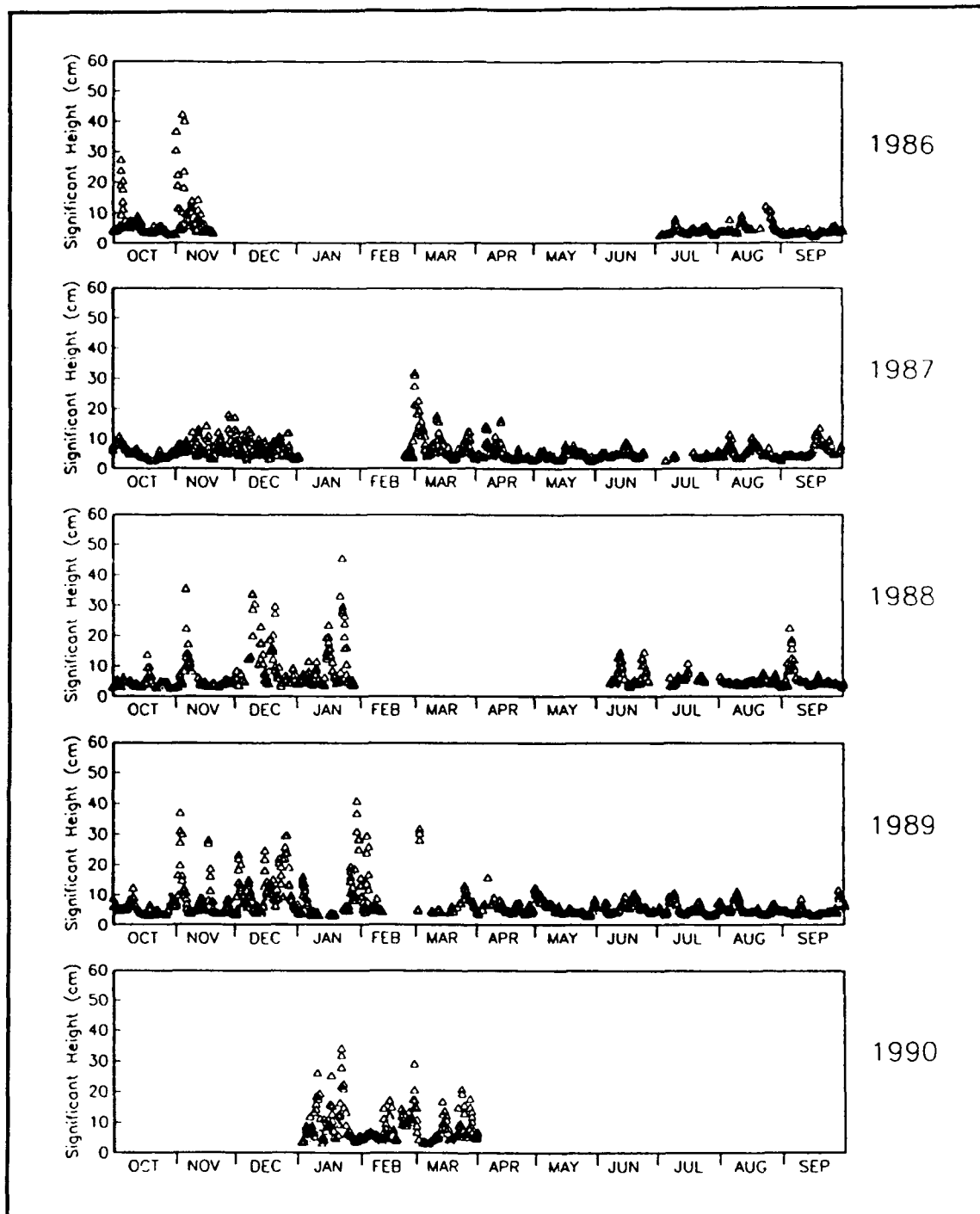
Figure A5. Slope array infragravity significant wave heights for all data records available
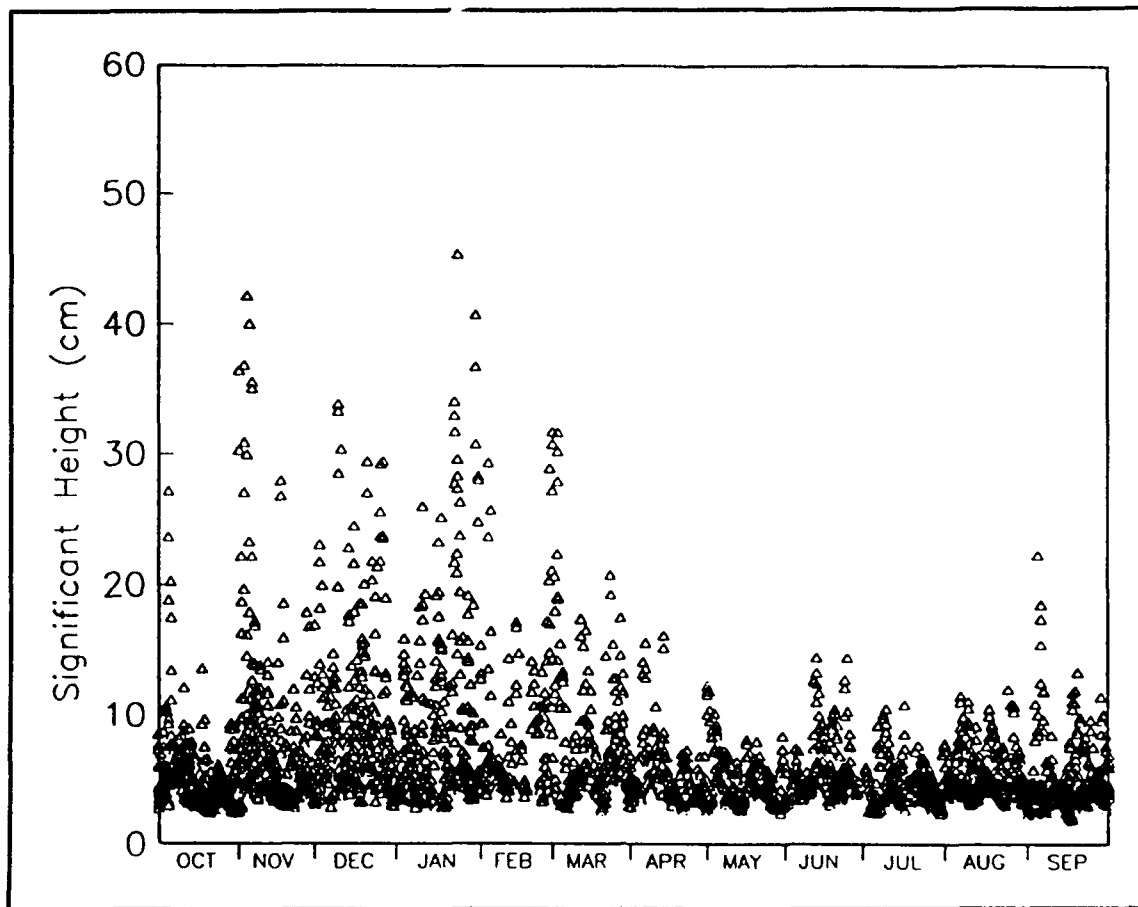
Figure A6. Slope array infragravity significant wave heights for July 1986 - March 1990
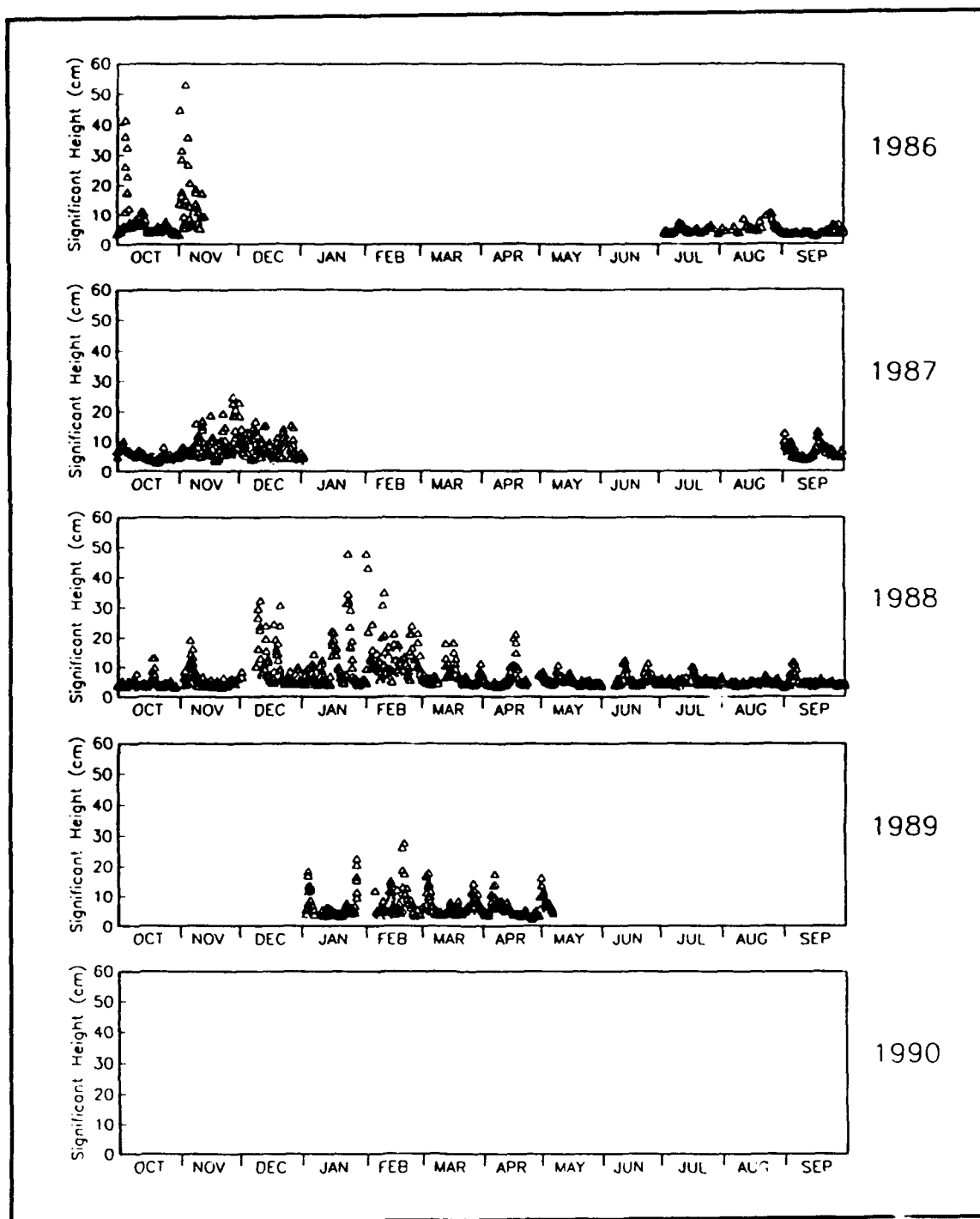
Figure A7. Channel entrance infragravity significant wave heights for all data records available
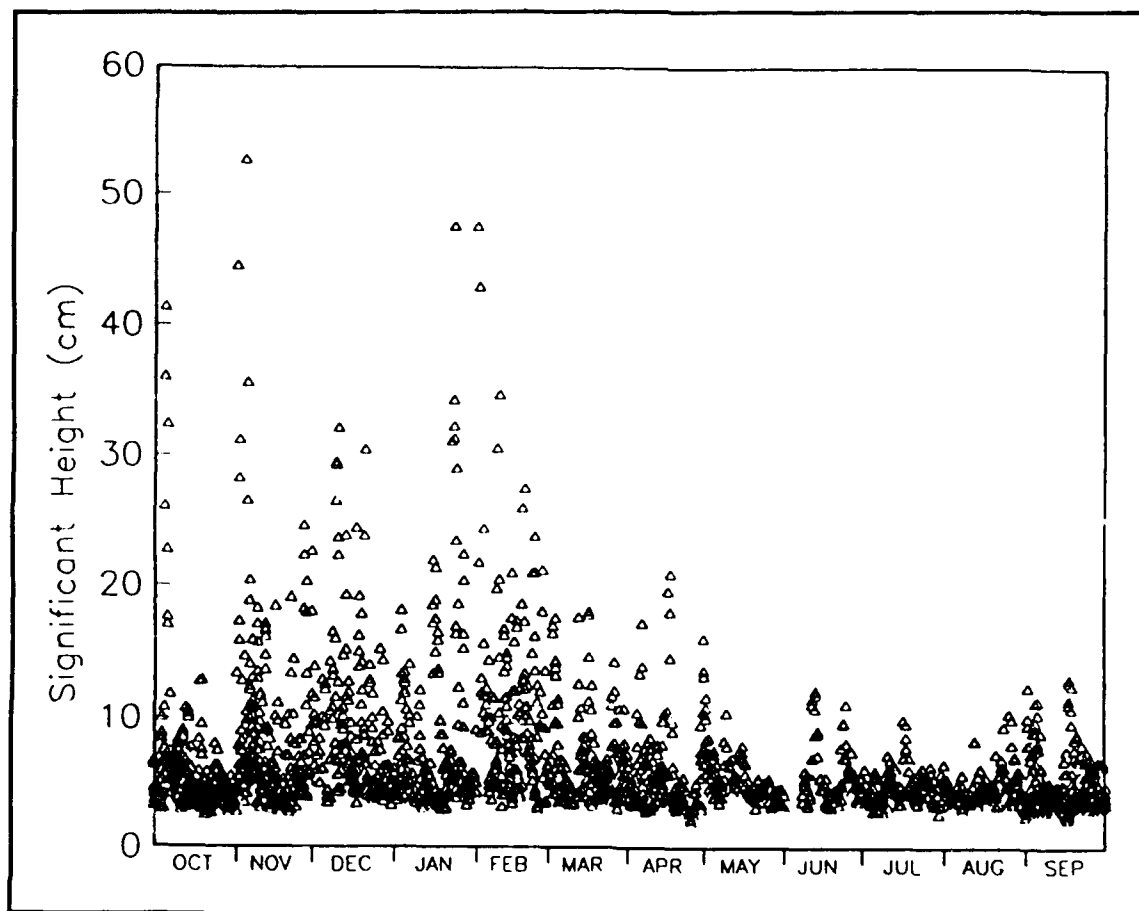
Figure A8. Channel entrance infragravity significant wave heights for July 1986 - May 1989
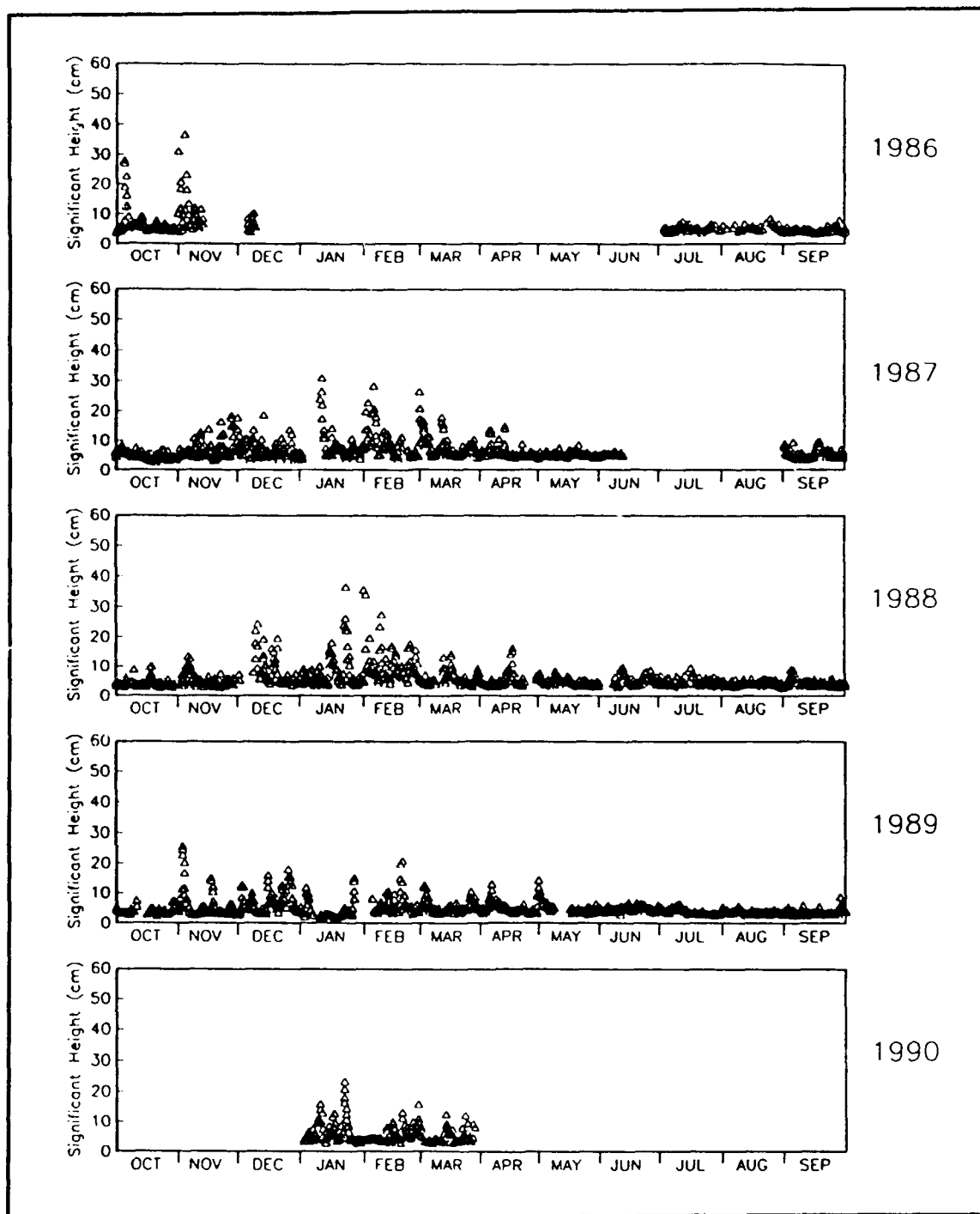
Figure A9. Channel midpoint infragravity significant wave heights for all data records available
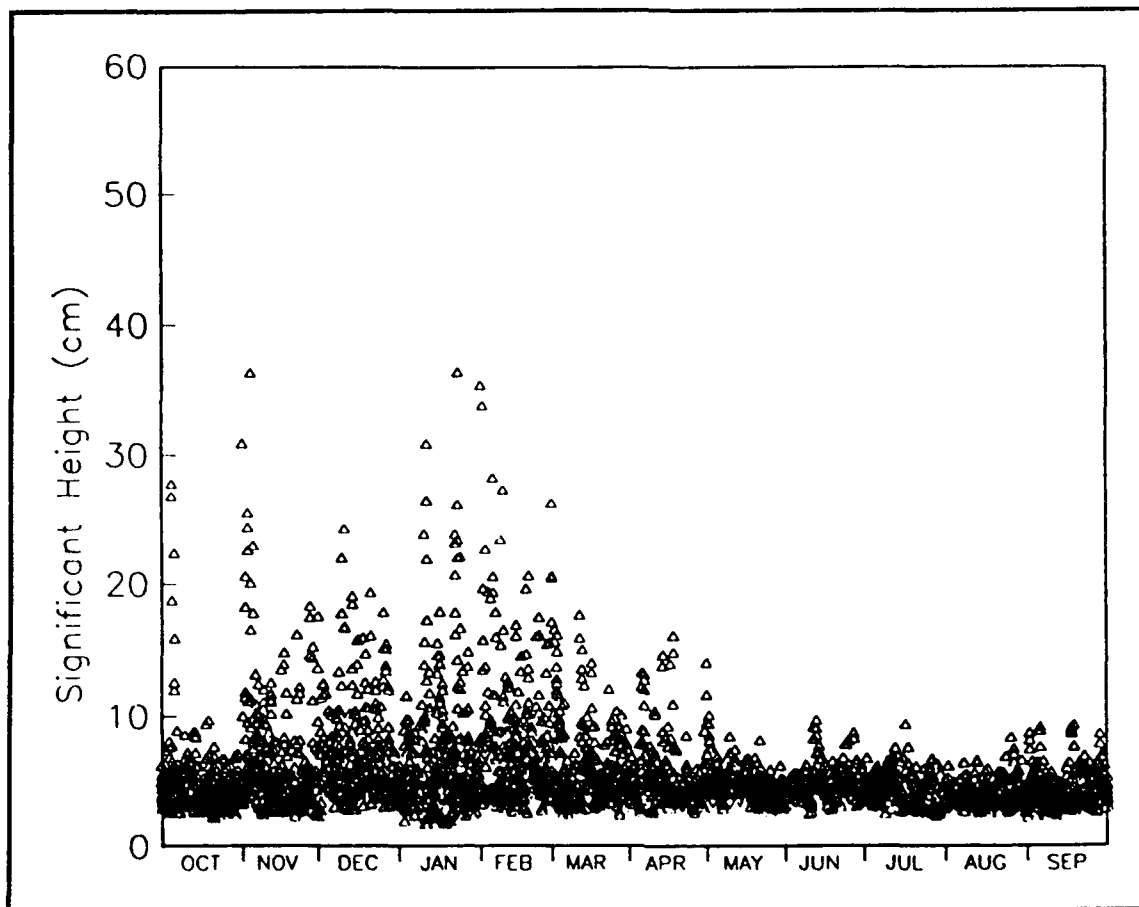
Figure A10. Channel midpoint infragravity significant wave heights for July 1986 - March 1990
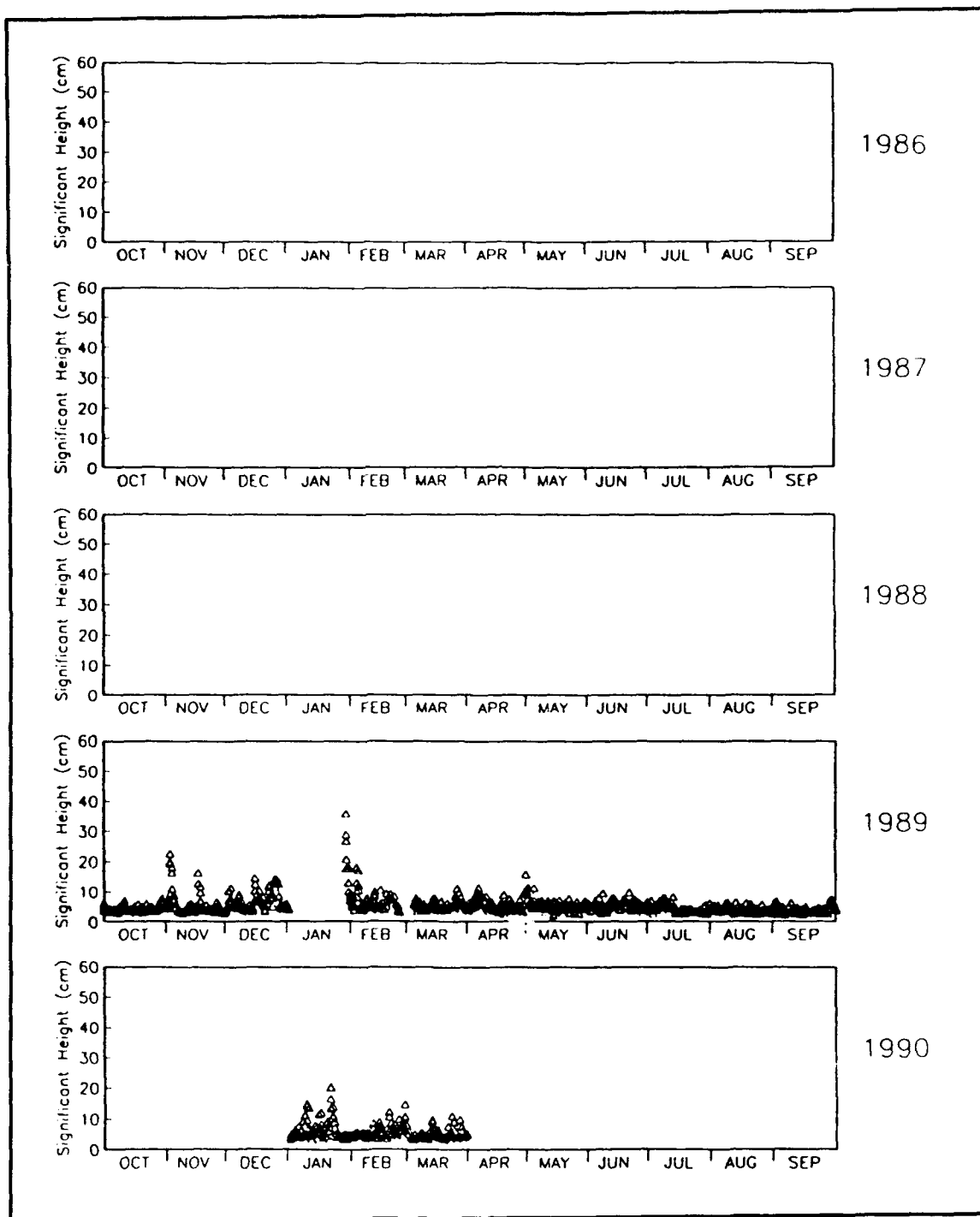
Figure A11. North corner infragravity significant wave heights for all data records available
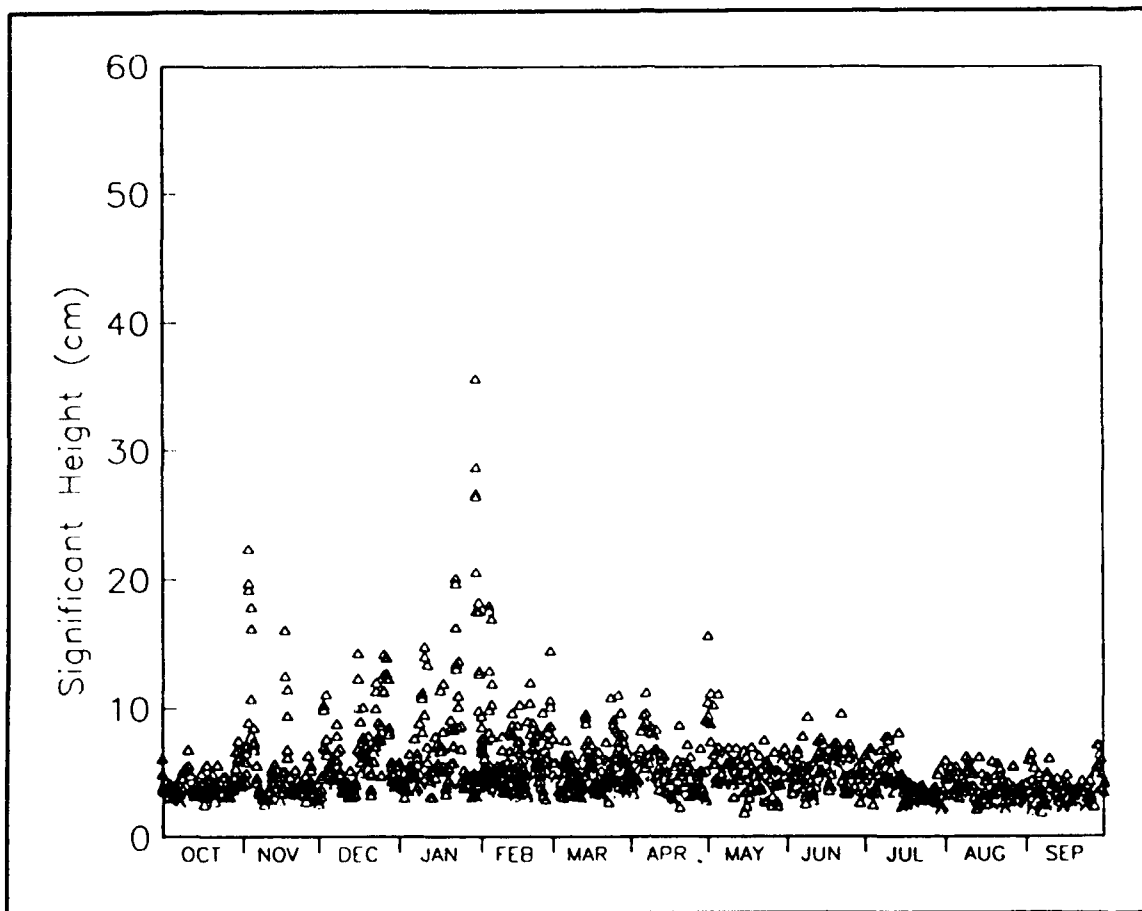
Figure A12. North corner infragravity significant wave heights for January 1989 - March 1990
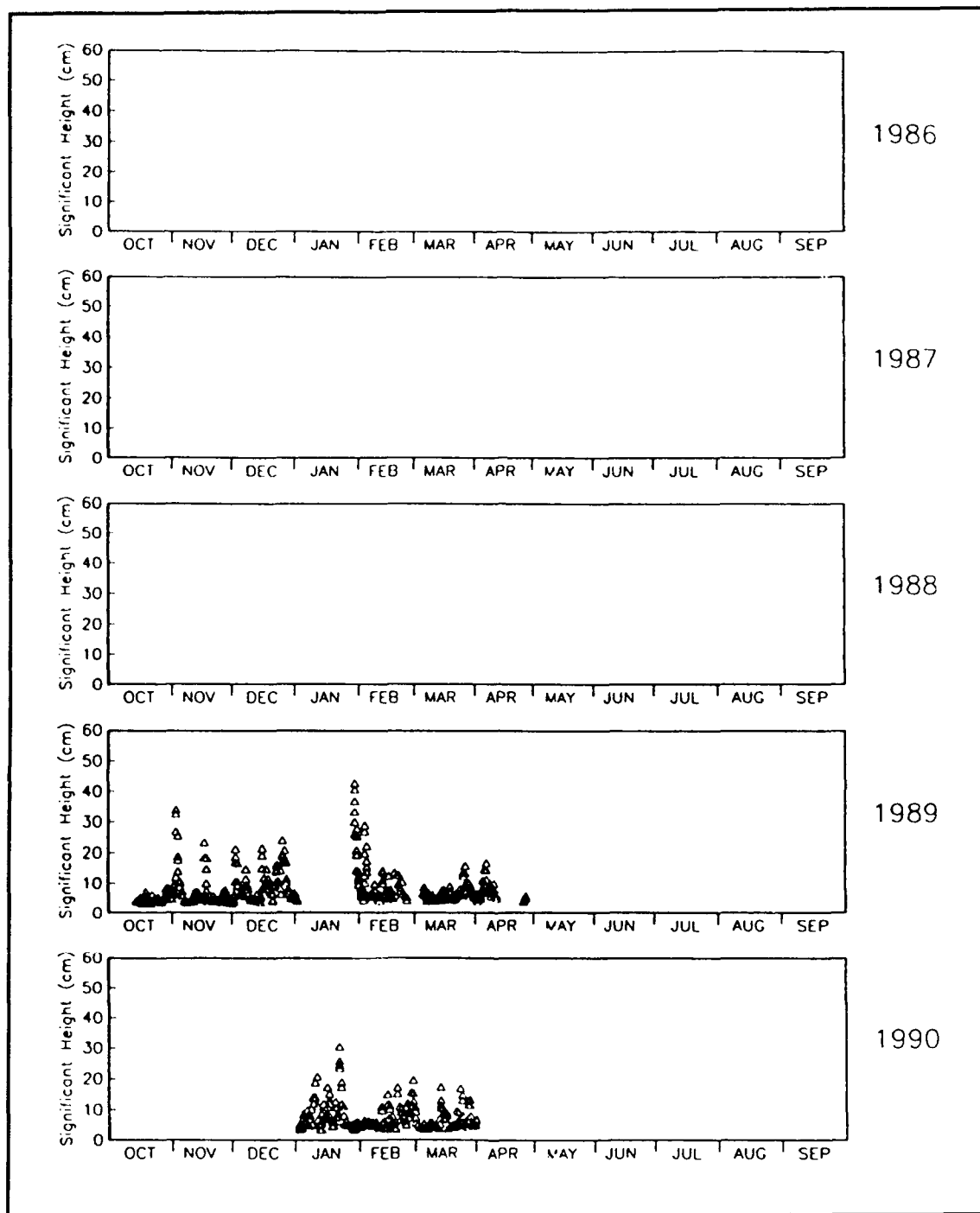
Figure A13. East corner infragravity significant wave heights for all data records available
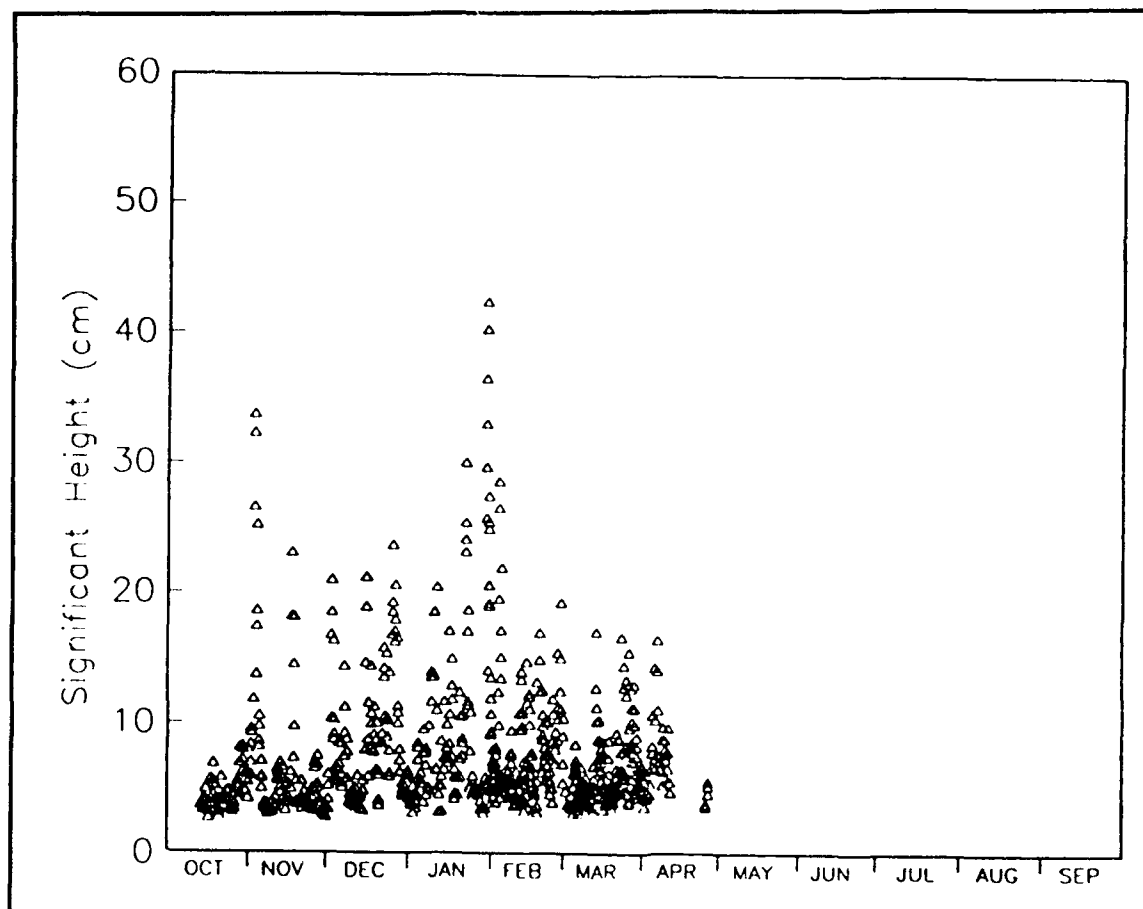
Figure A14. East corner infragravity significant wave heights for January 1989 - March 1990
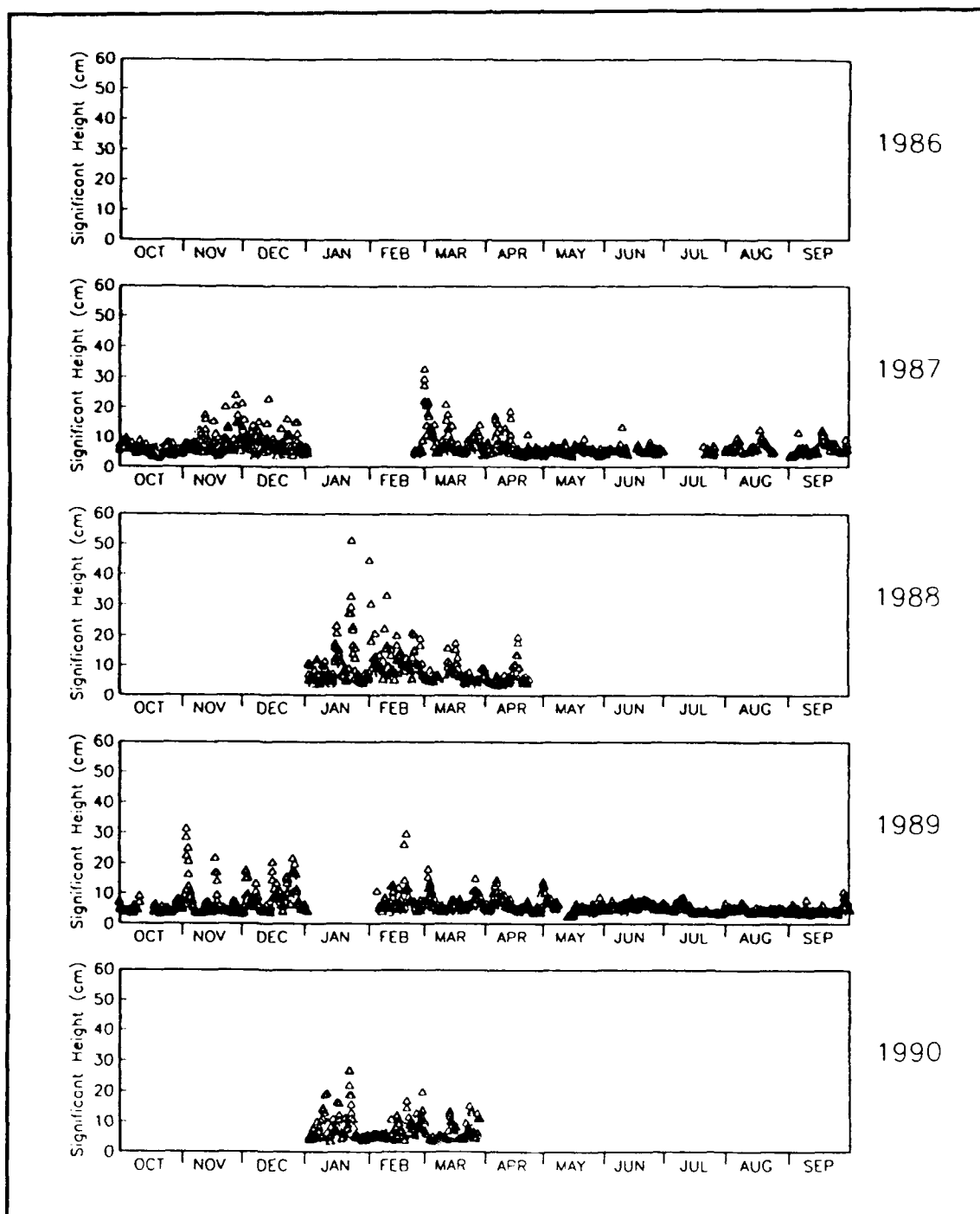
Figure A15. South corner infragravity significant wave heights for all data records
available
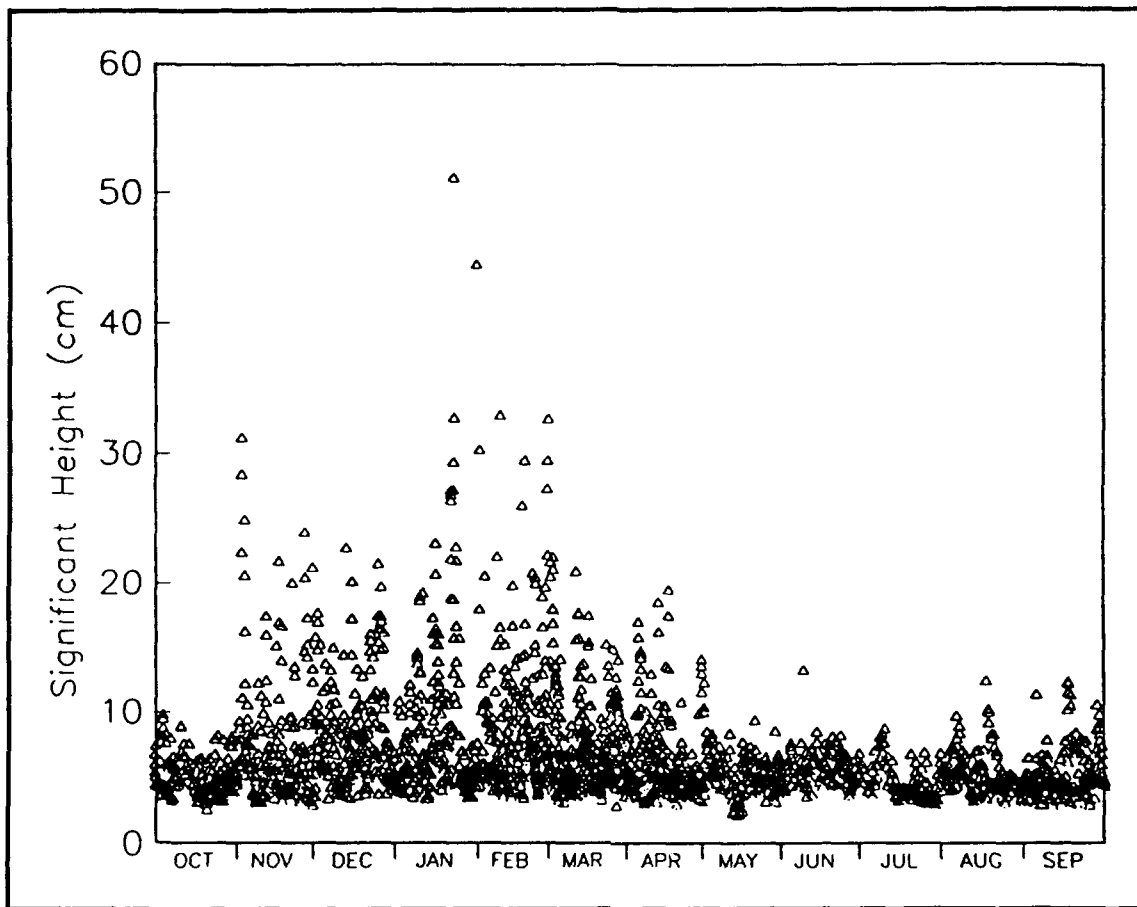
Figure A16. South corner infragravity significant wave heights for February 1987 - March 1990
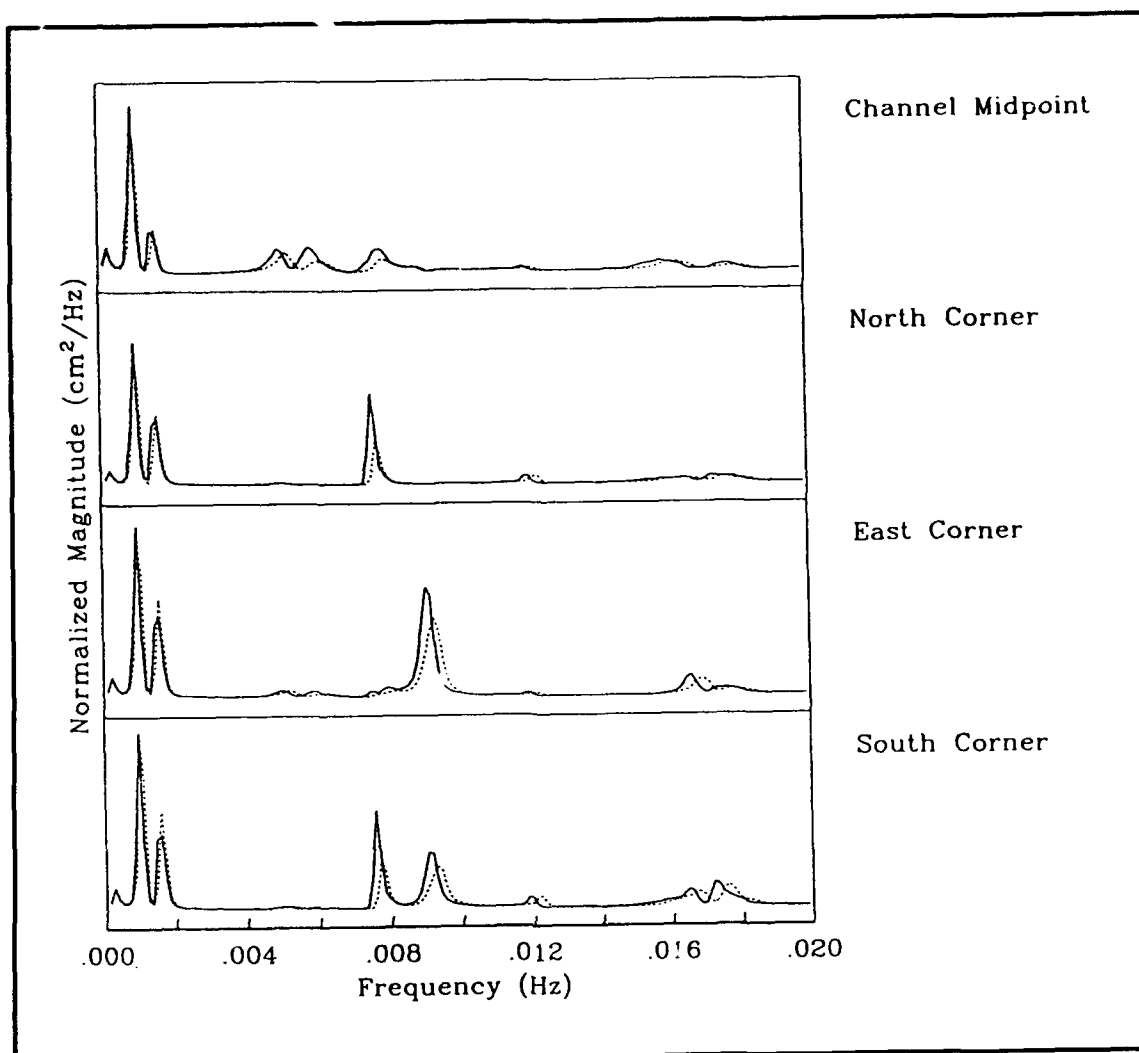
Figure A17. Resonant modes at low tide (solid line) and high tide (dashed line), small boat harbor open (October 1989 - March 1990)
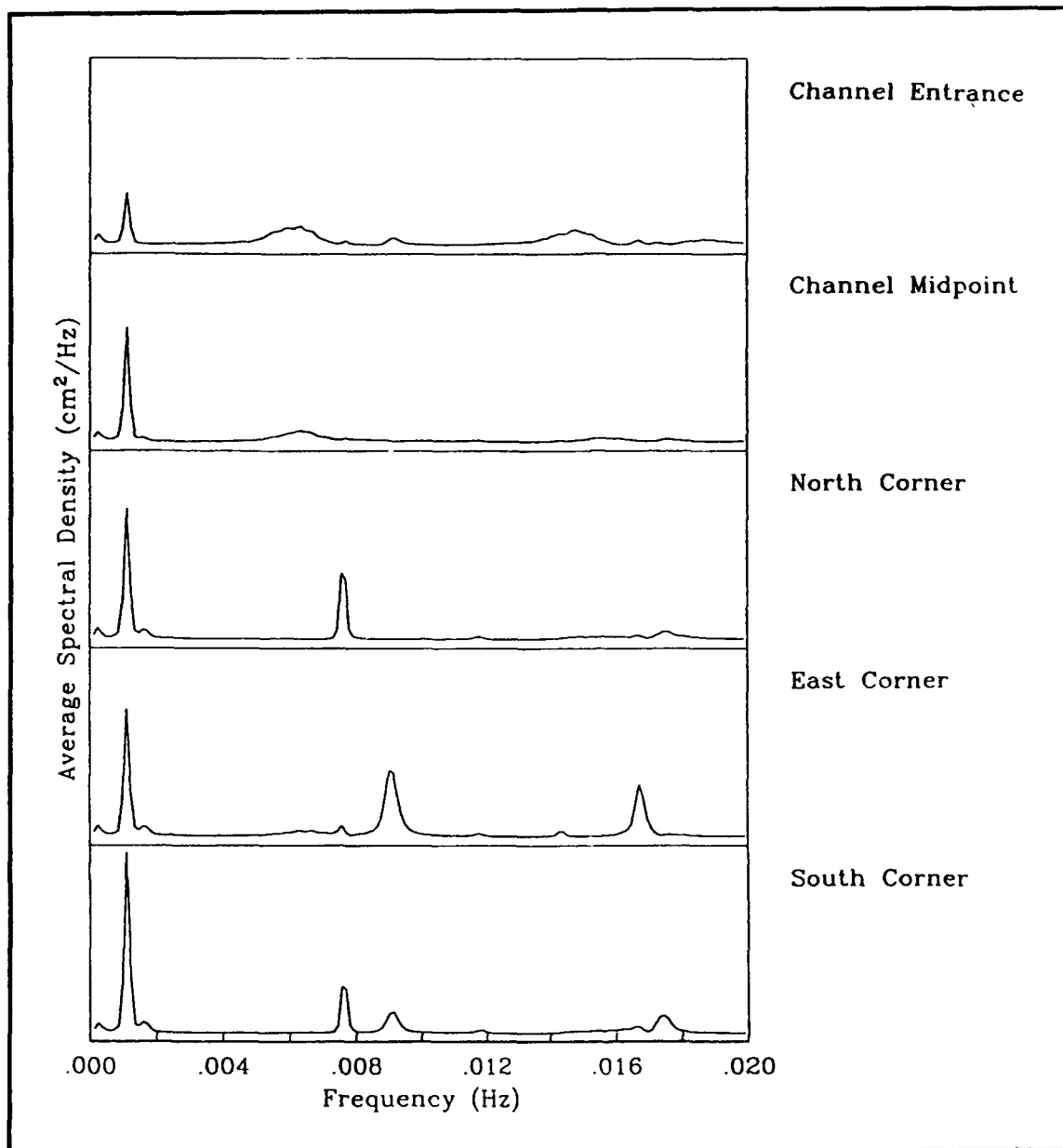
Figure A18. Resonant modes at mid-tide level, small boat harbor closed (February 1989 - July 1989)
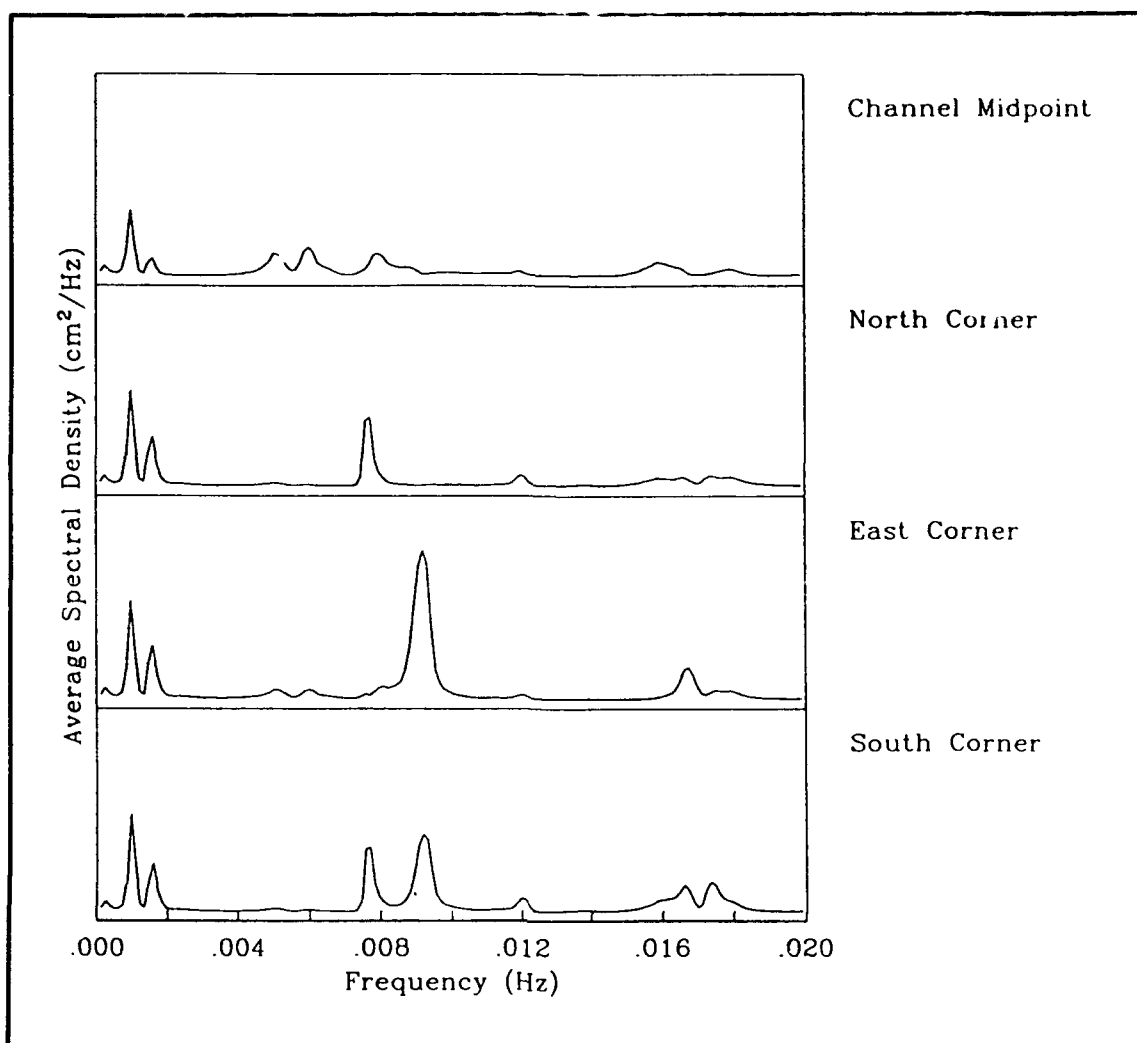
Figure A19. Resonant modes at mid-tide level, small boat harbor open (October 1989 - March 1990)
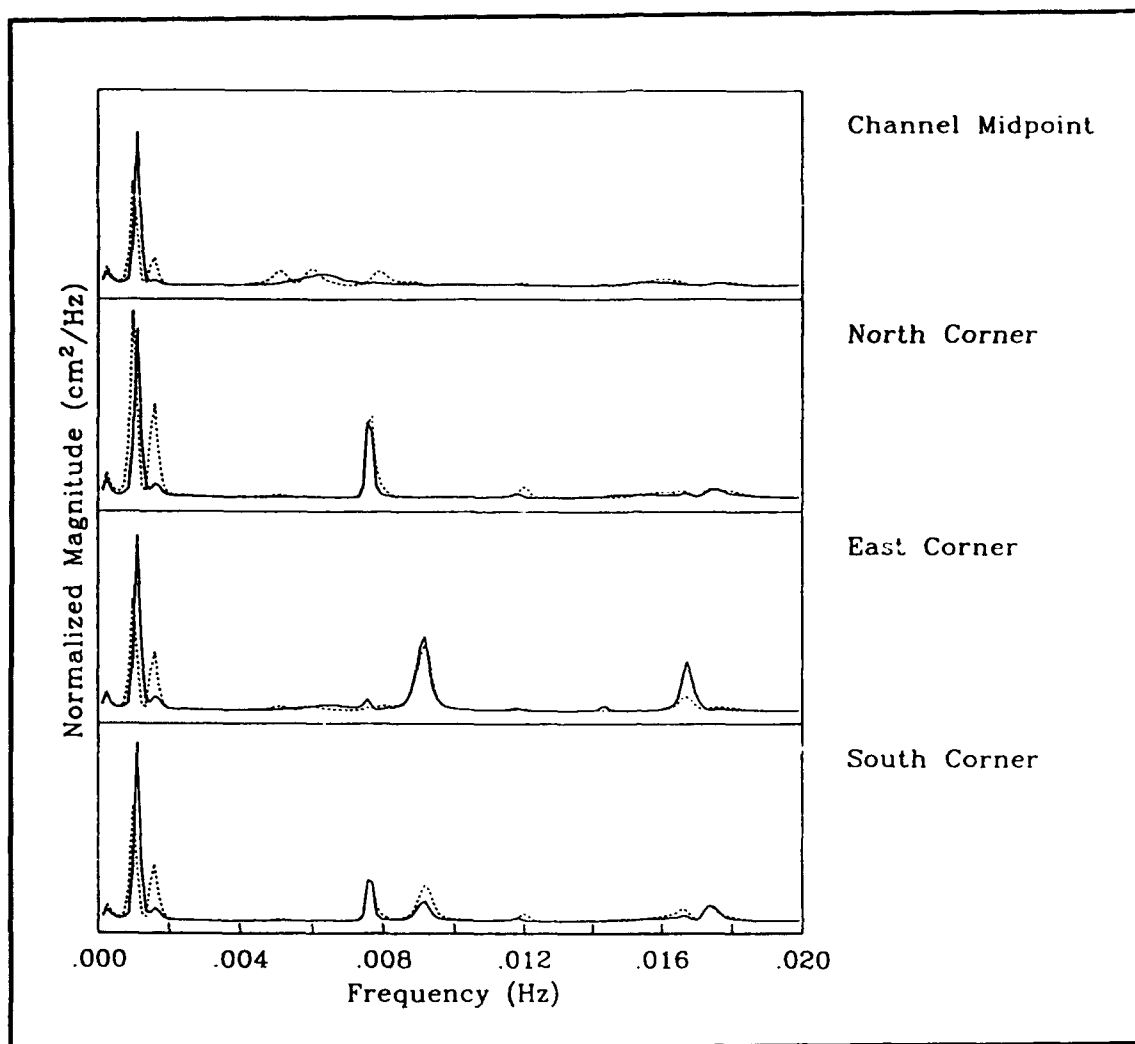
Figure A20. Resonant modes for different harbor geometries, small boat harbor closed (solid line) and open (dashed line)
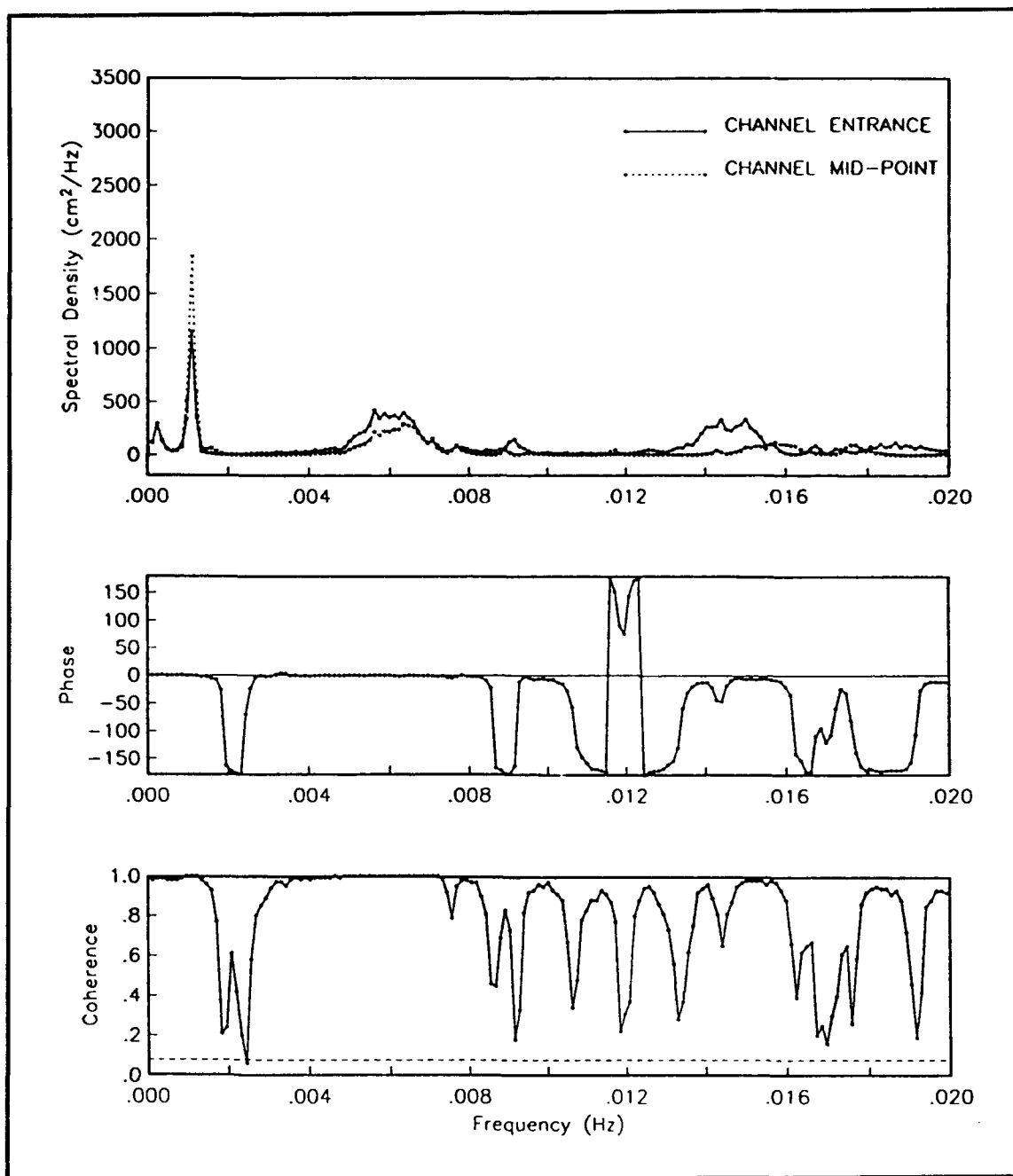
Figure A21. Average spectra, phase, and coherence at the channel entrance and channel midpoint. Small boat harbor closed (February 1989 - July 1989), 37 records averaged
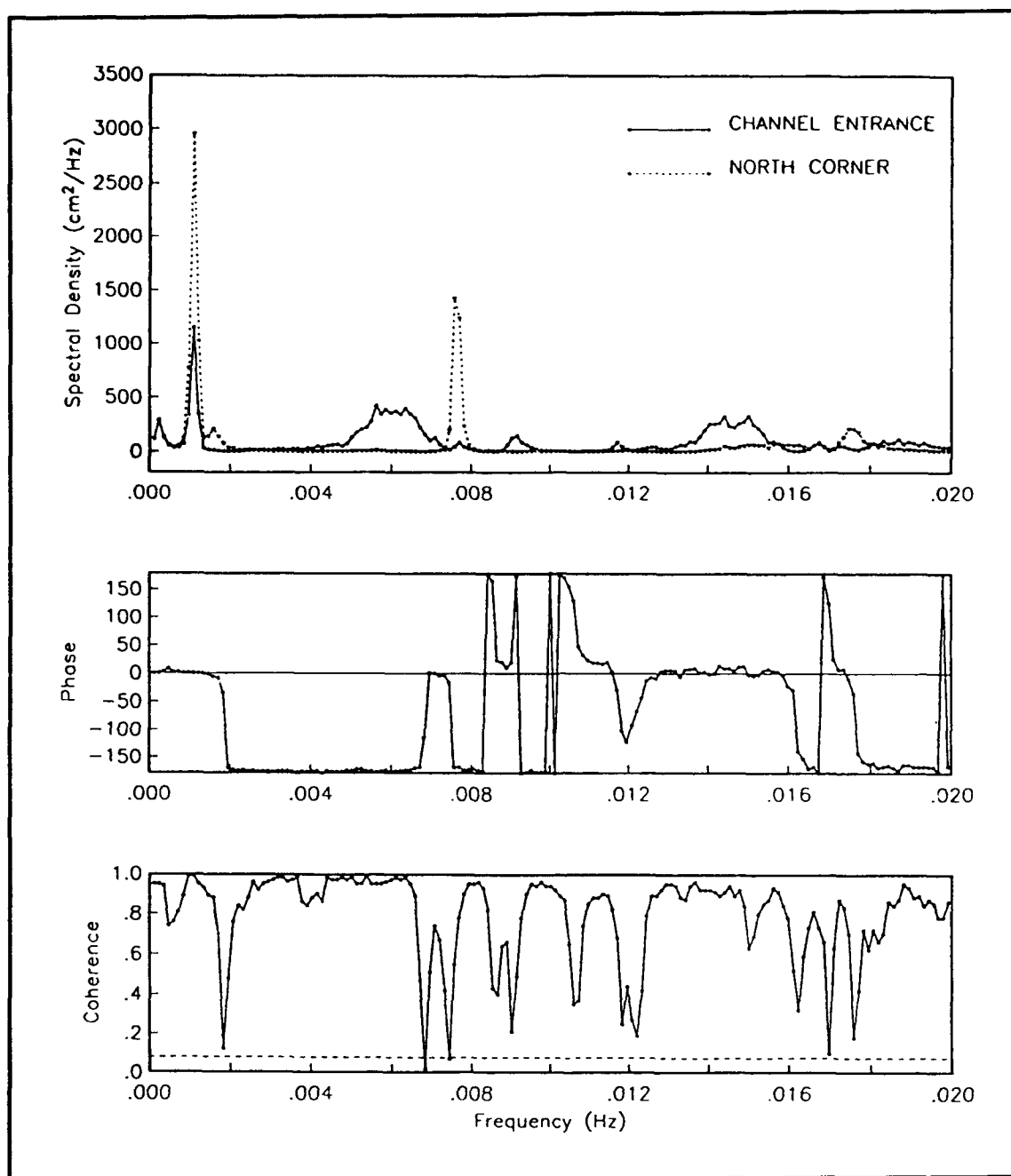
Figure A22. Average spectra, phase, and coherence at the channel entrance and north corner. Small boat harbor closed (February 1989 - July 1989), 37 records averaged
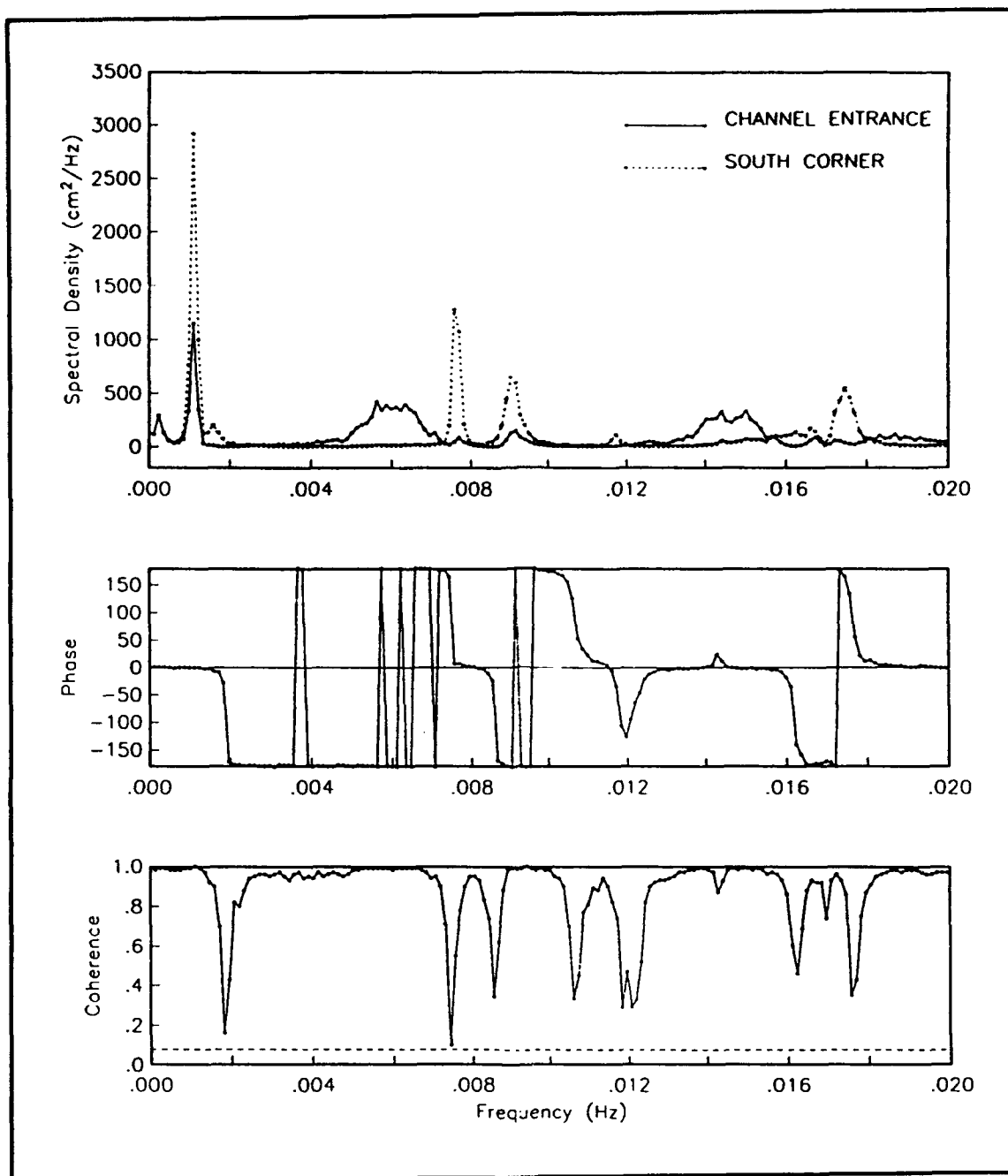
Figure A23. Average spectra, phase, and coherence at the channel entrance and south corner. Small boat harbor closed (February 1989 - July 1989), 37 records averaged
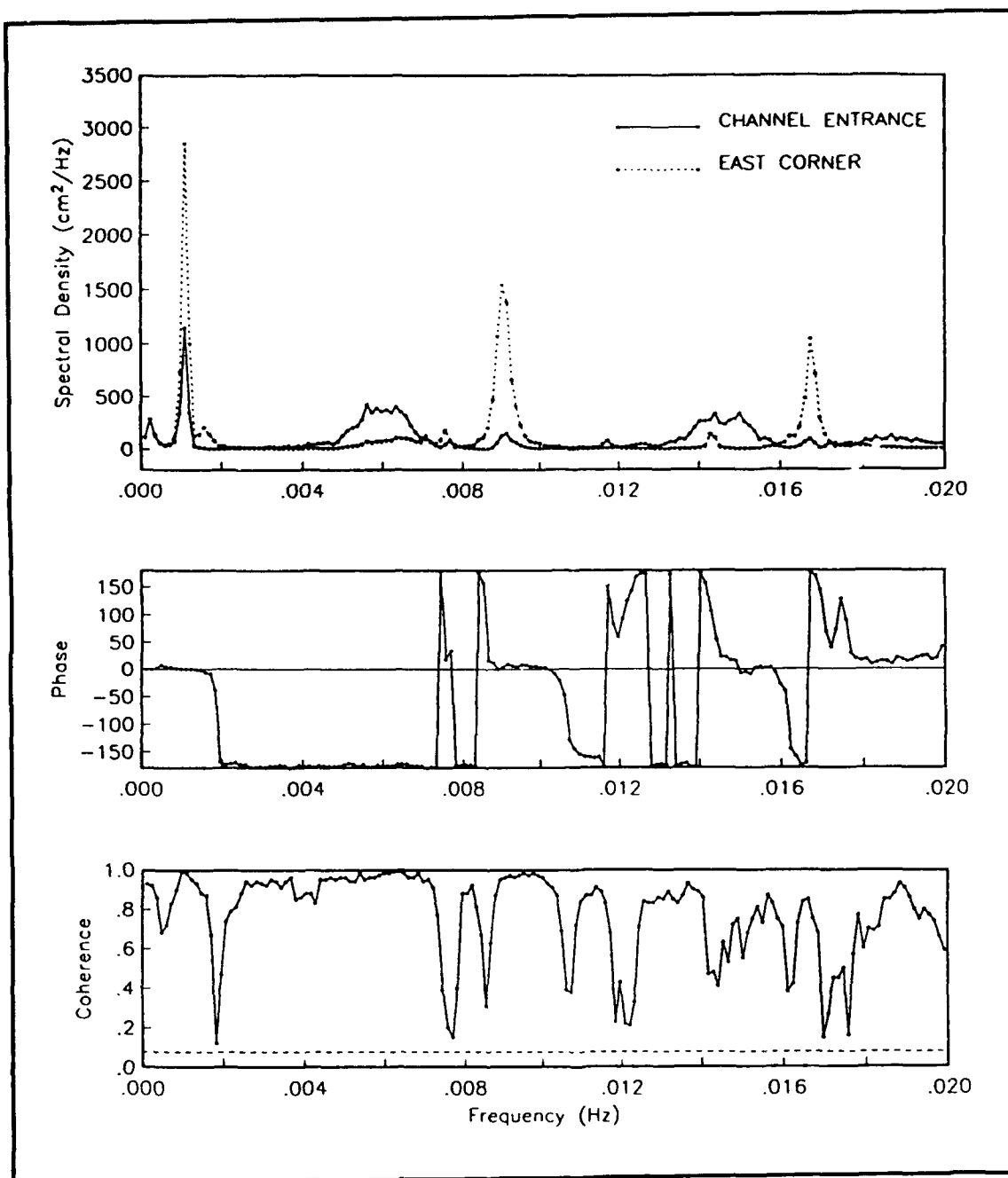
Figure A24. Average spectra, phase, and coherence at the channel entrance and east corner. Small boat harbor closed (February 1989 - July 1989), 37 records averaged
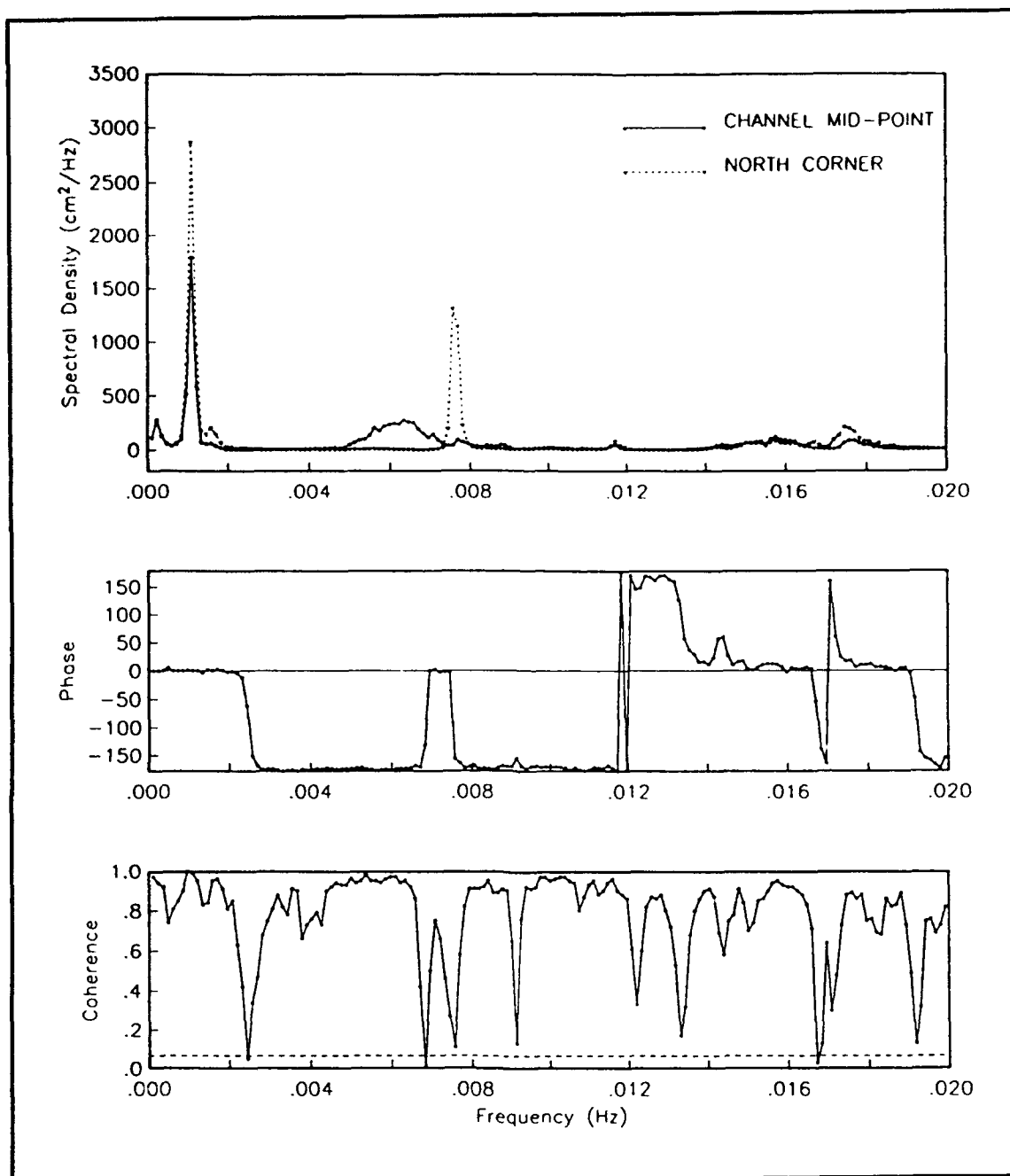
Figure A25. Average spectra, phase, and coherence at the channel midpoint and north corner. Small boat harbor closed (February 1989 - July 1989), 44 records averaged
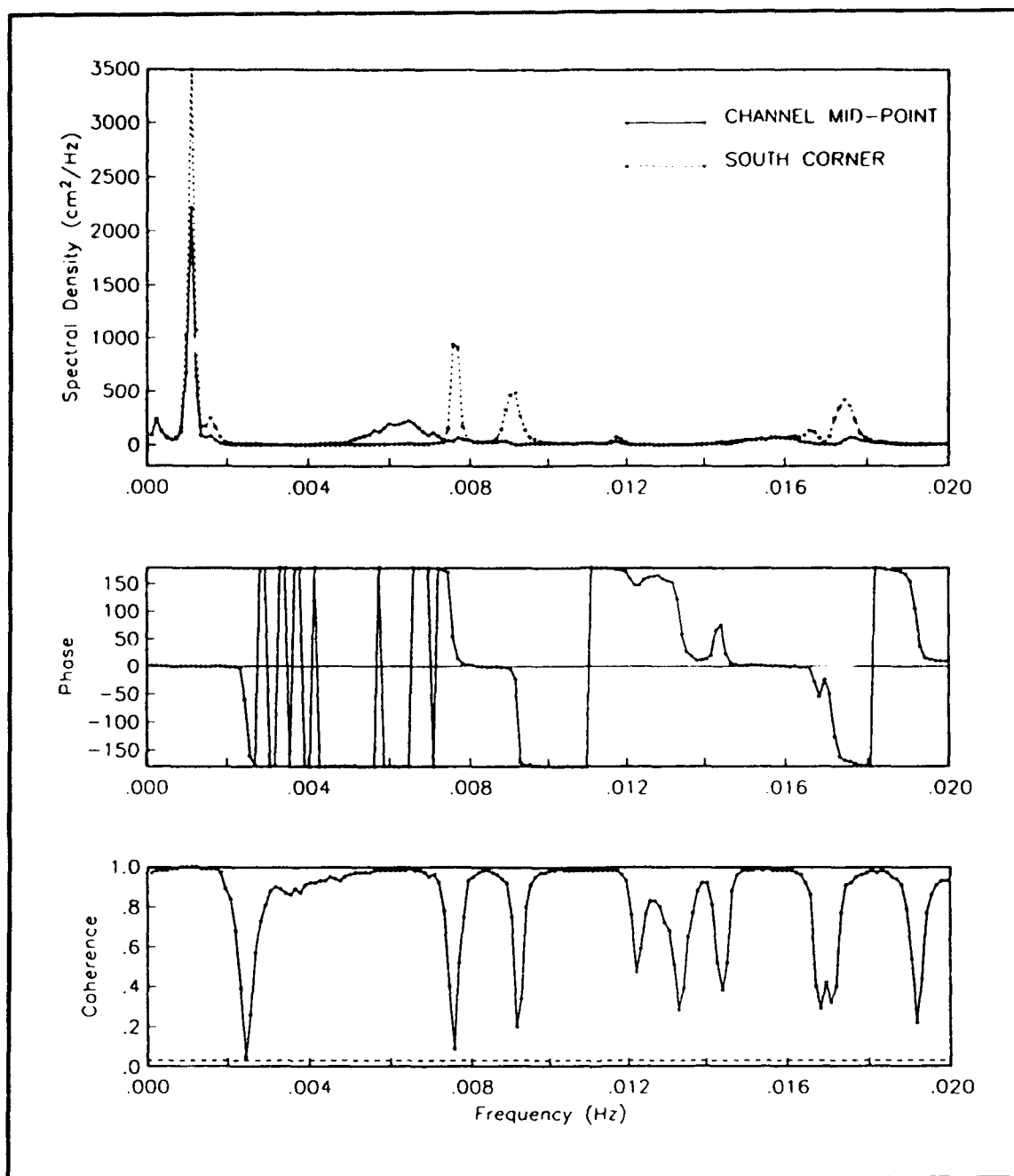
Figure A26. Average spectra, phase, and coherence at the channel midpoint and south corner. Small boat harbor closed (February 1989 - July 1989), 91 records averaged
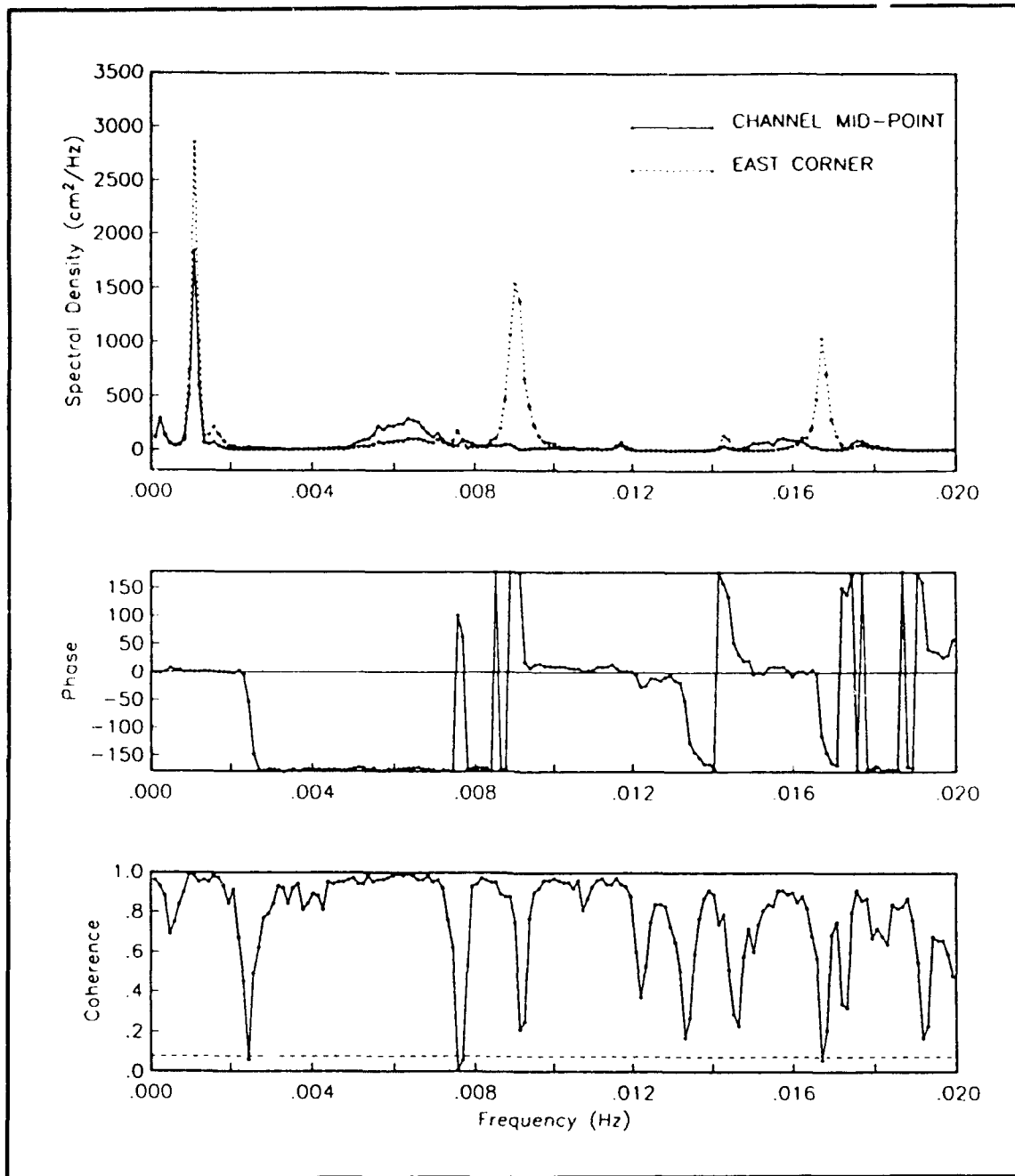
Figure A27. Average spectra, phase, and coherence at the channel midpoint and east corner. Small boat harbor closed (February 1989 - July 1989), 37 records averaged
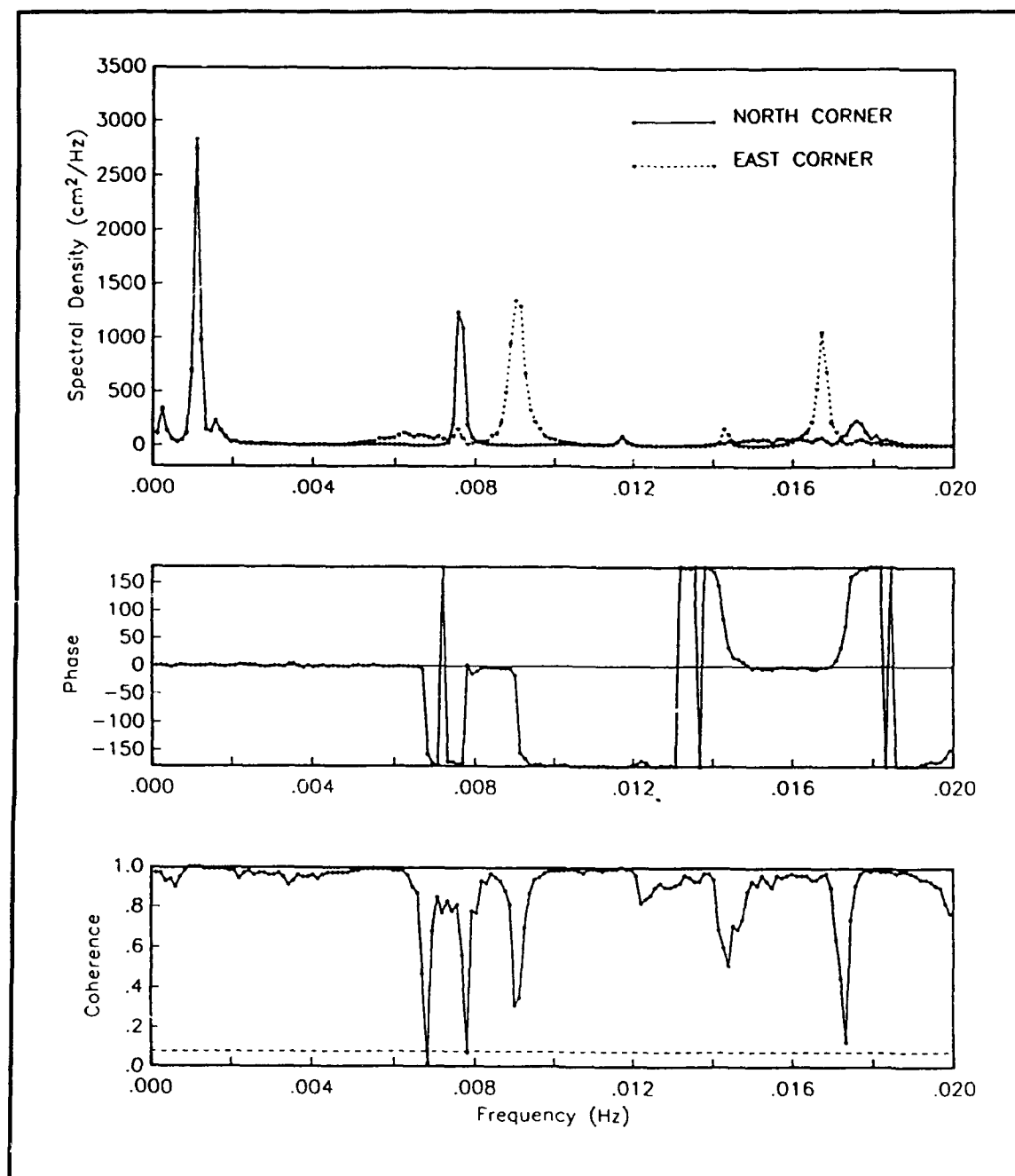
Figure A28. Average spectra, phase, and coherence at the north corner and east corner. Small boat harbor closed (February 1989 - July 1989), 37 records averaged
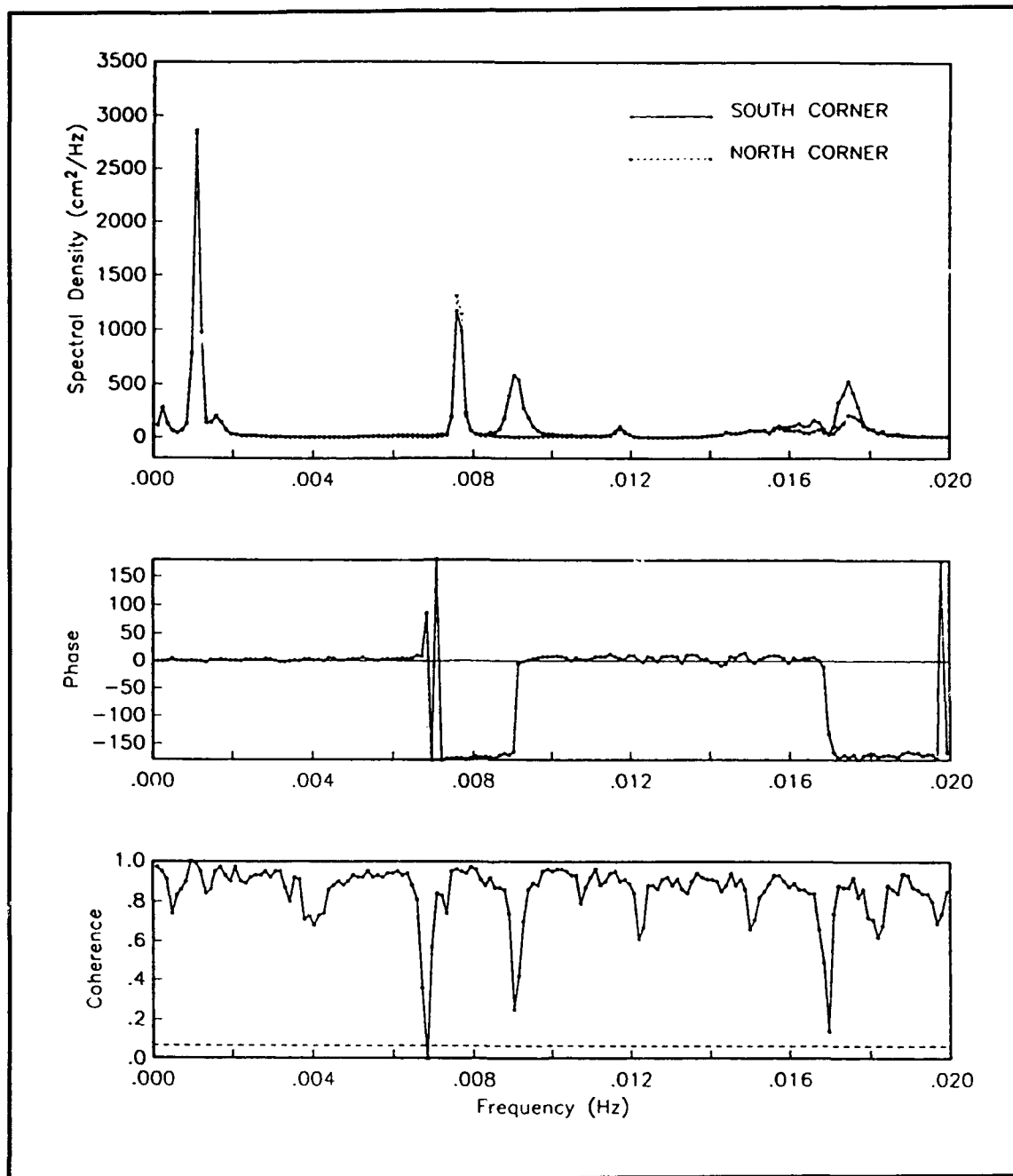
Figure A29. Average spectra, phase, and coherence at the south corner and north corner. Small boat harbor closed (February 1989 - July 1989), 44 records averaged
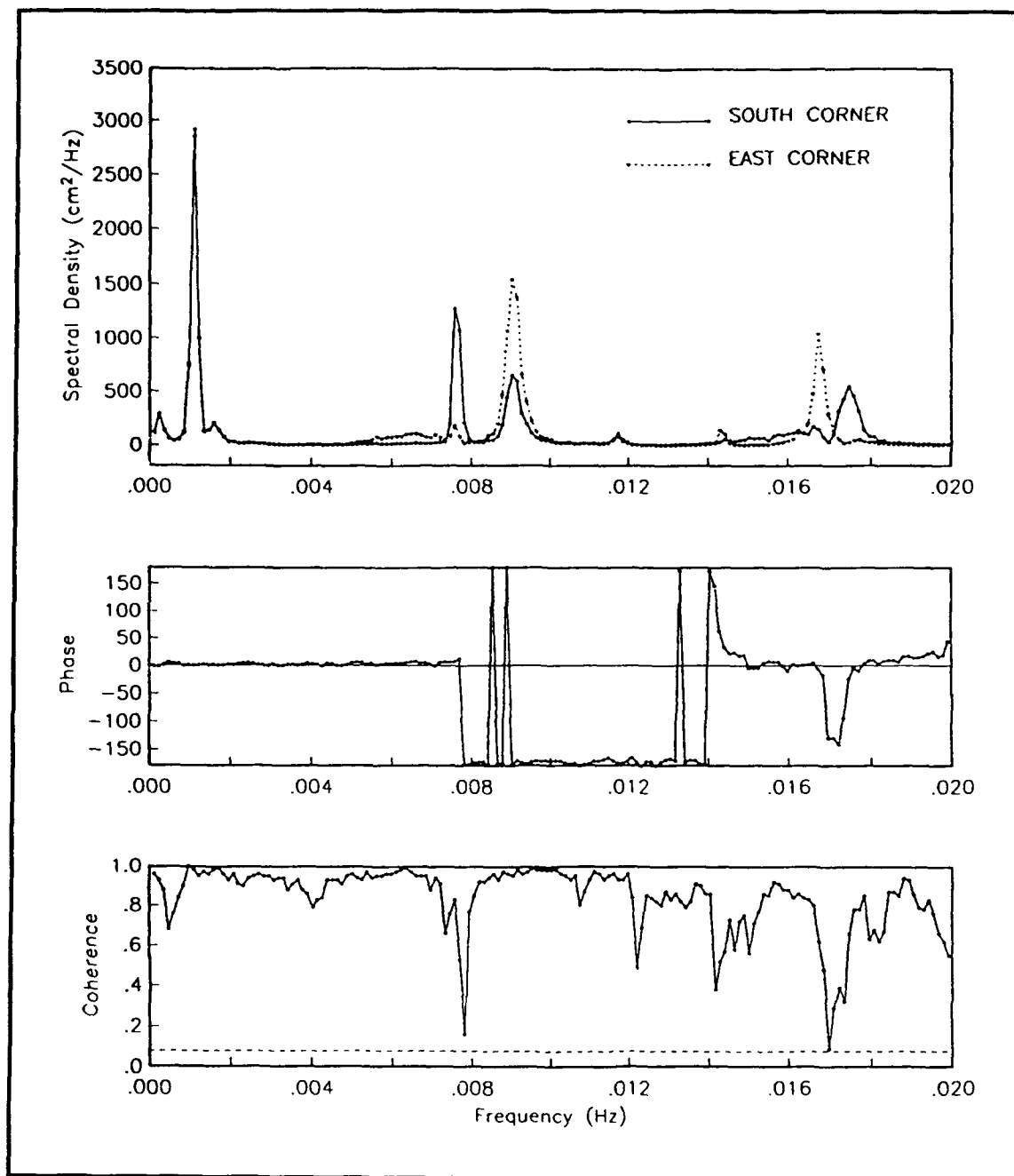
Figure A30. Average spectra, phase, and coherence at the south corner and east corner. Small boat harbor closed (February 1989 - July 1989), 37 records averaged
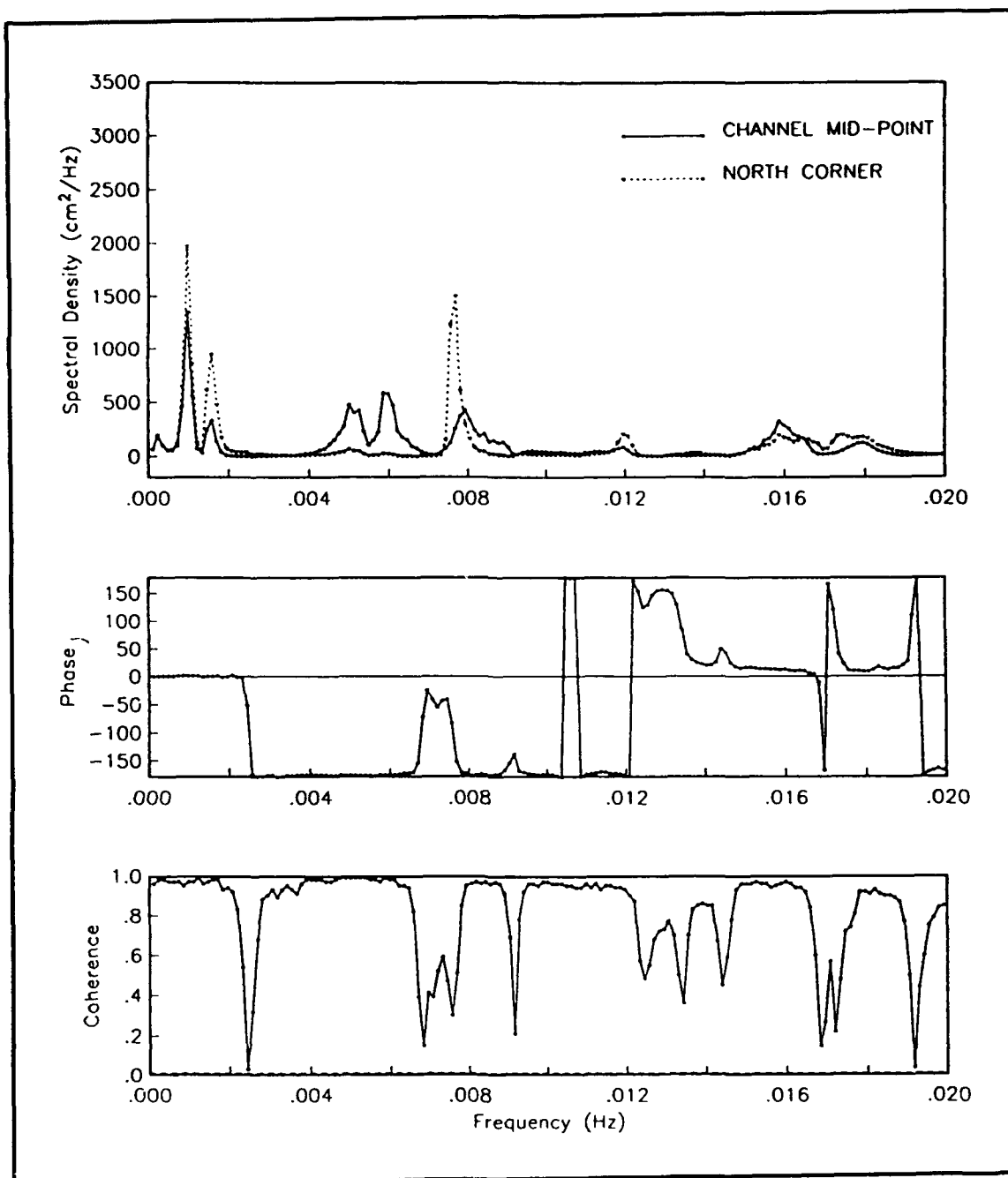
Figure A31. Average spectra, phase, and coherence at the channel midpoint and north corner. Small boat harbor open (October 1989 - March 1990), 277 records averaged
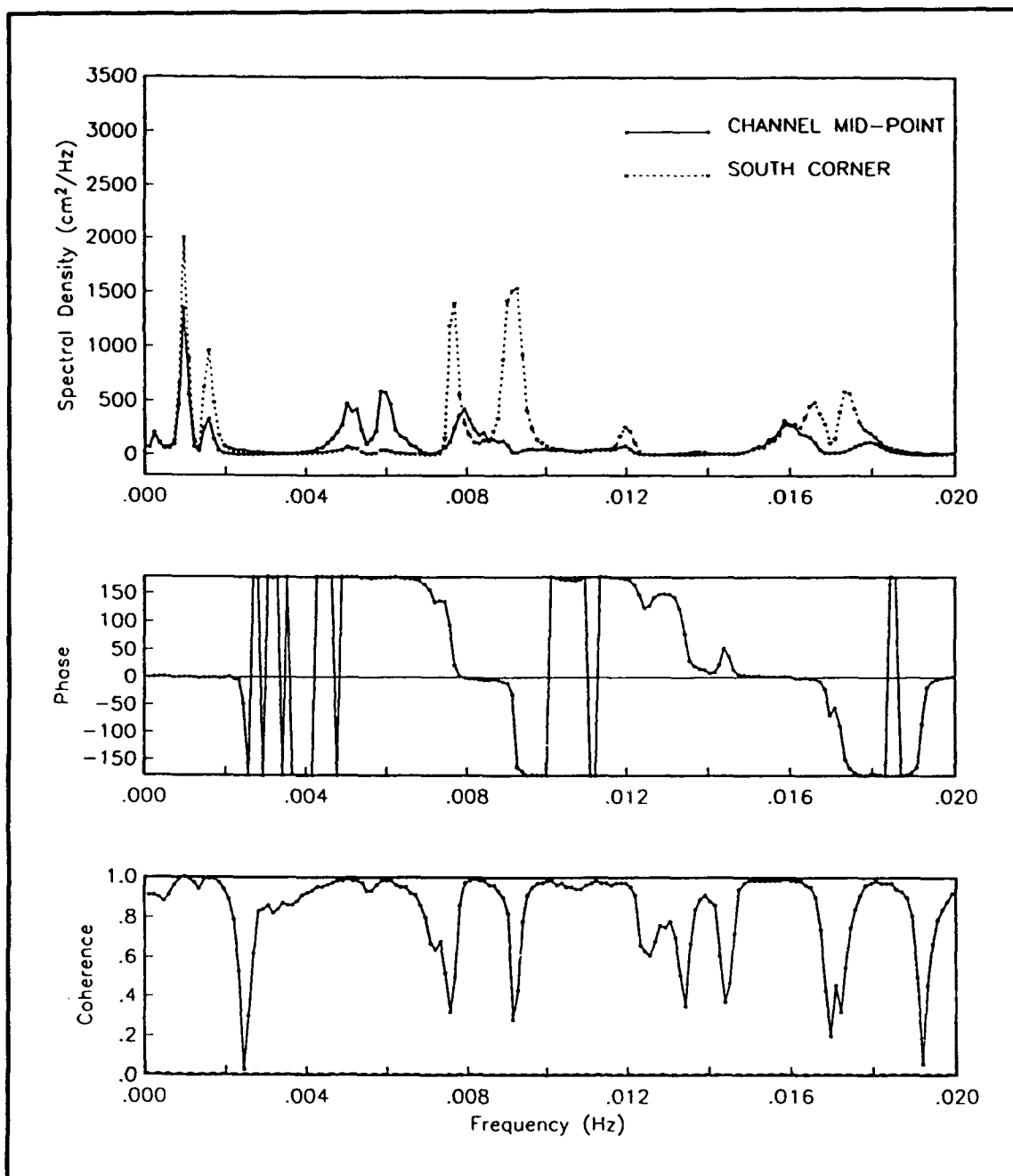
Figure A32. Average spectra, phase, and coherence at the channel midpoint and south corner. Small boat harbor open (October 1989 - March 1990), 277 records averaged
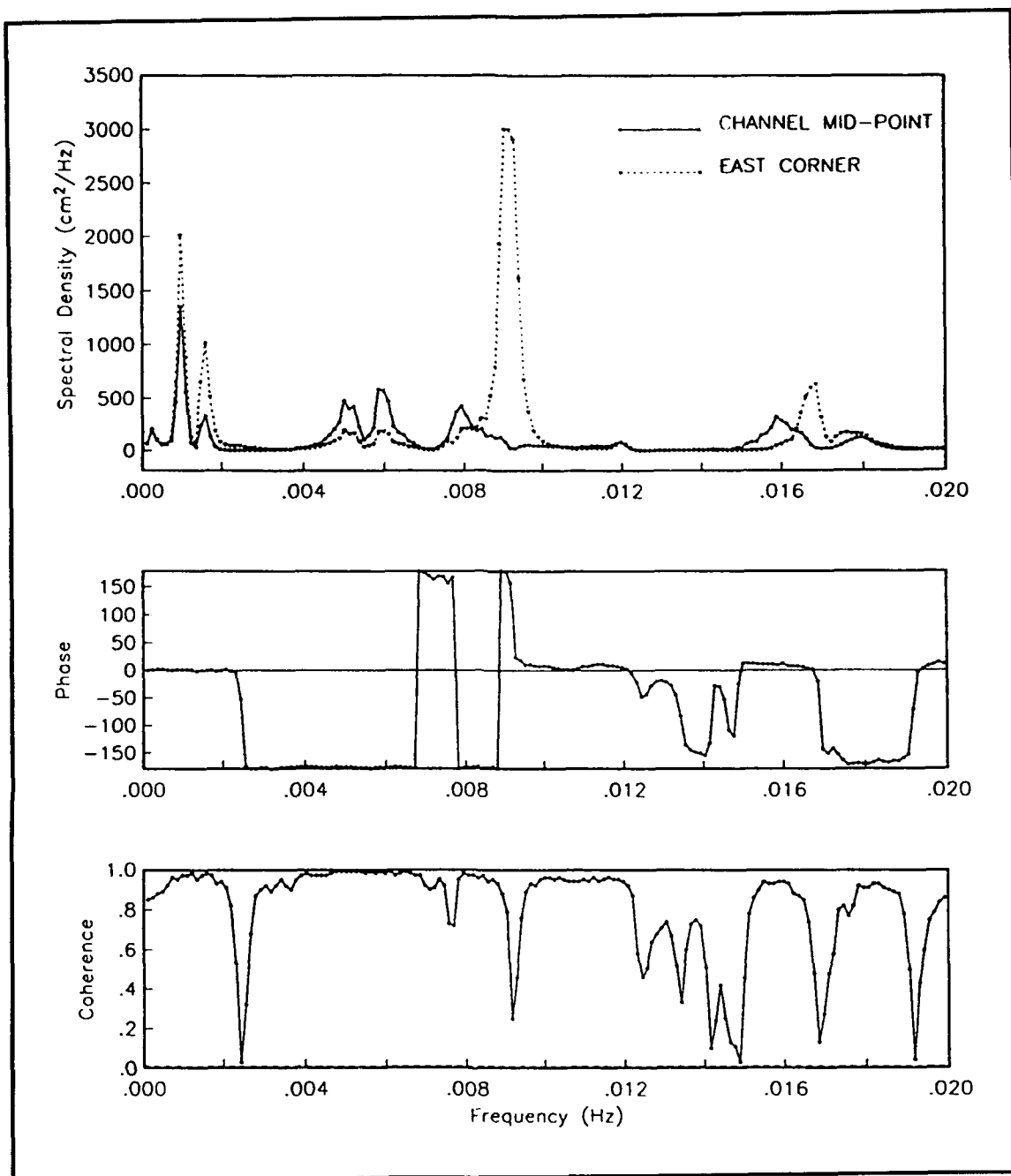
Figure A33. Average spectra, phase, and coherence at the channel midpoint and east
corner. Small boat harbor open (October 1989 - March 1990), 277 records
averaged
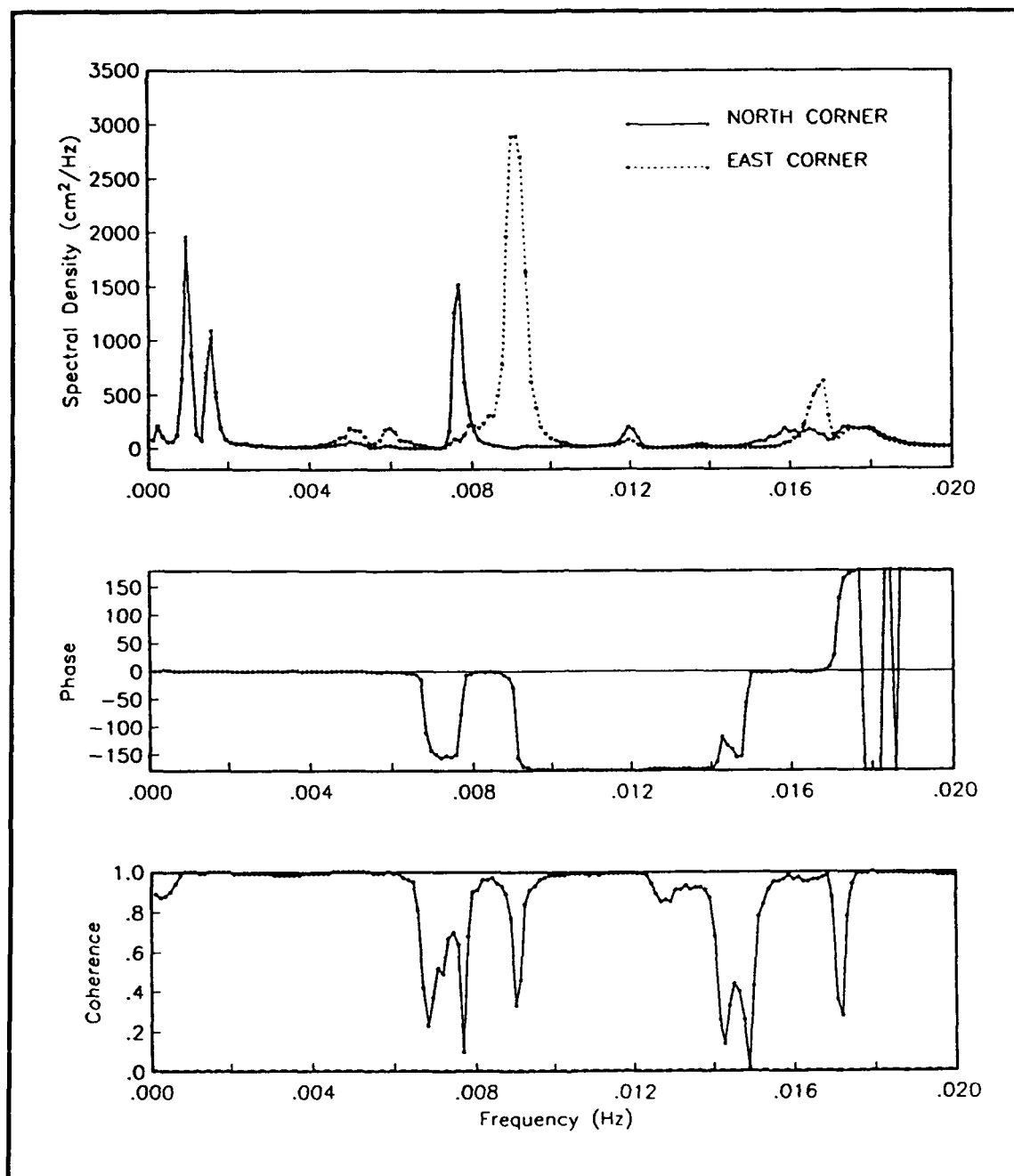
Figure A34. Average spectra, phase, and coherence at the north corner and east corner. Small boat harbor open (October 1989 - March 1990), 277 records averaged
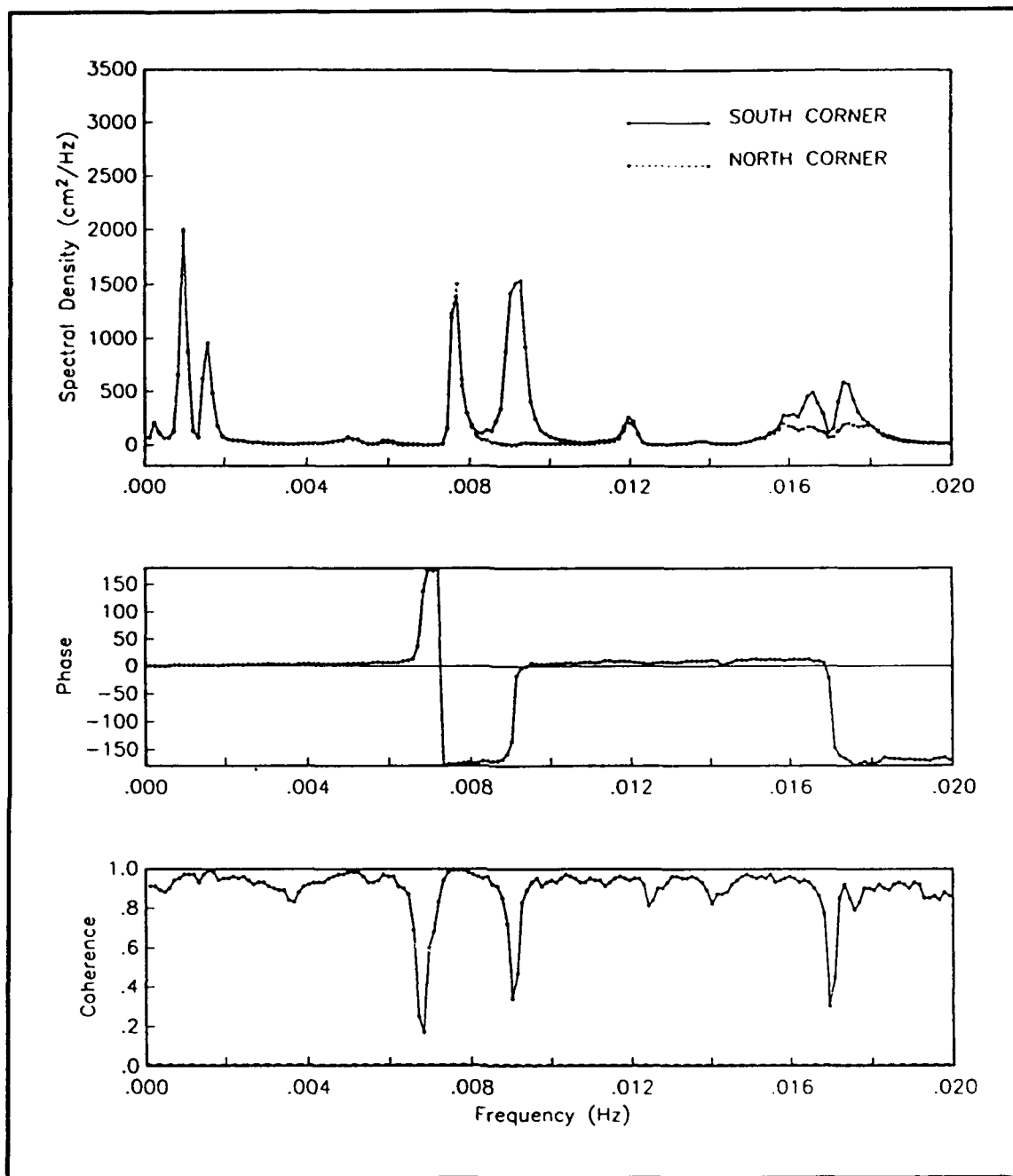
Figure A35. Average spectra, phase, and coherence at the south corner and north corner.
Small boat harbor open (October 1989 - March 1990), 277 records averaged
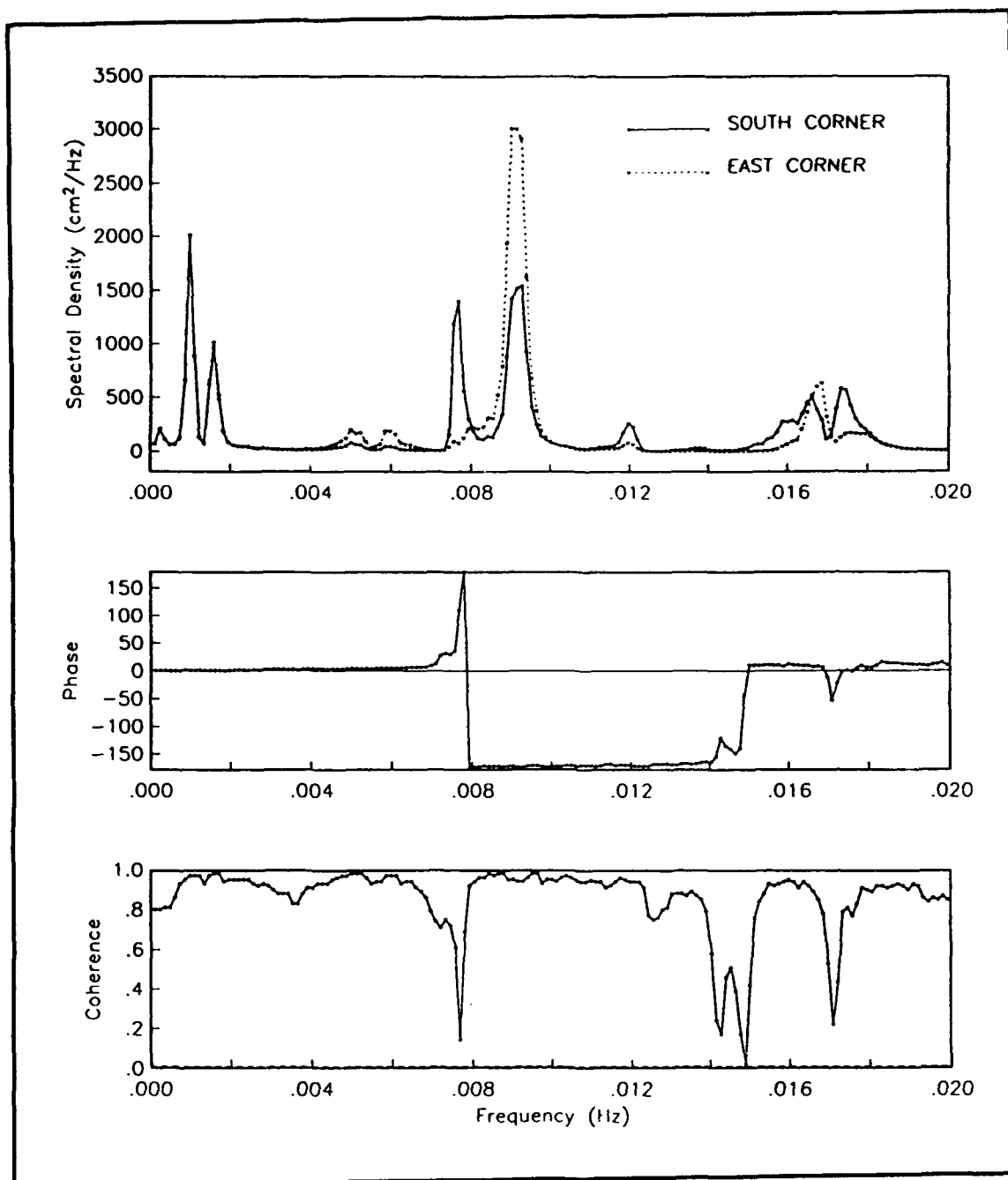
Figure A36. Average spectra, phase, and coherence at the south corner and east corner. Small boat harbor open (October 1989 - March 1990), 277 records averaged
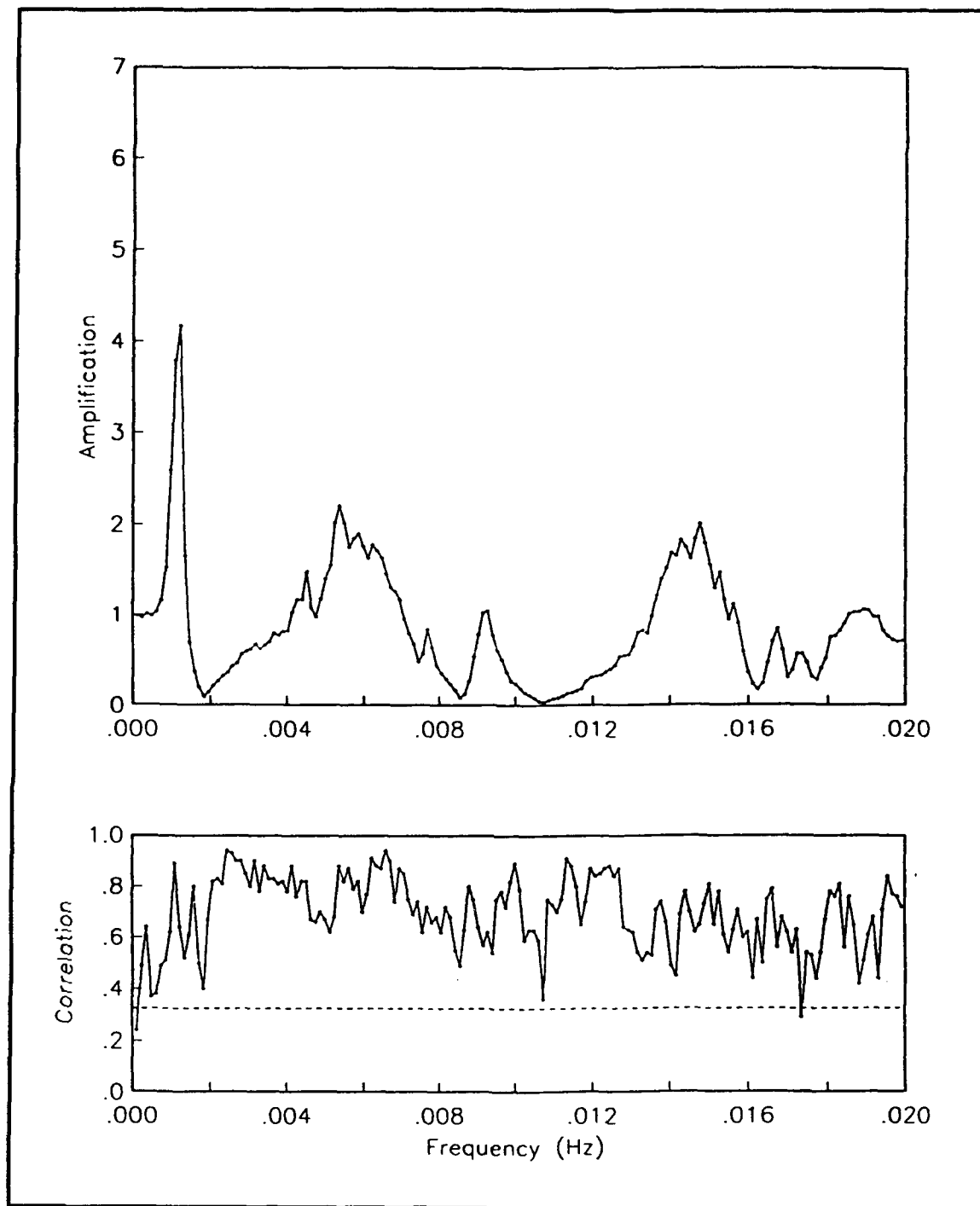
Figure A37. Amplification factors and correlation coefficients, channel entrance, small boat harbor closed (February 1989 - July 1989), 37 records averaged
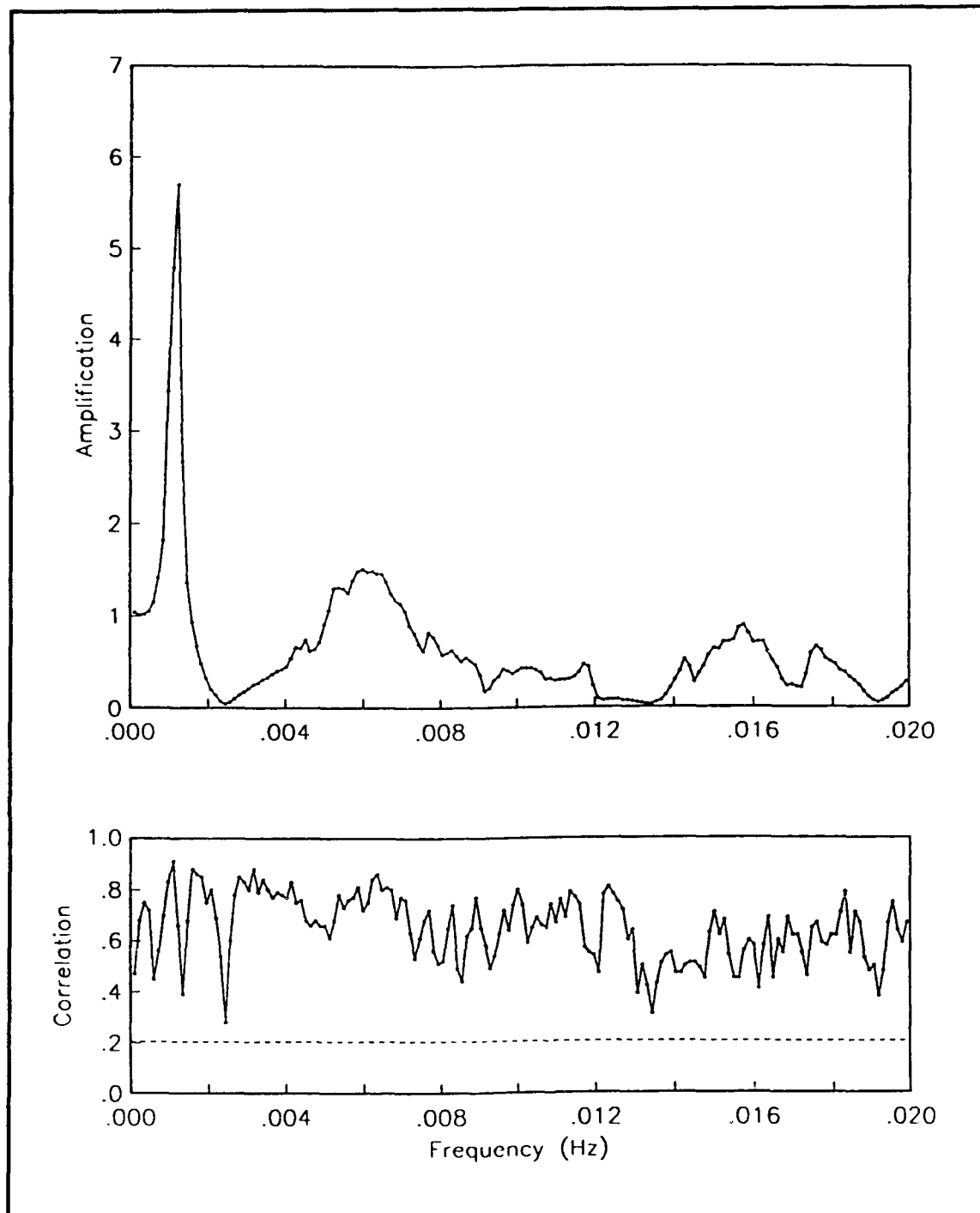
Figure A38. Amplification factors and correlation coefficients, channel midpoint, small boat harbor closed (February 1989 - July 1989), 91 records averaged
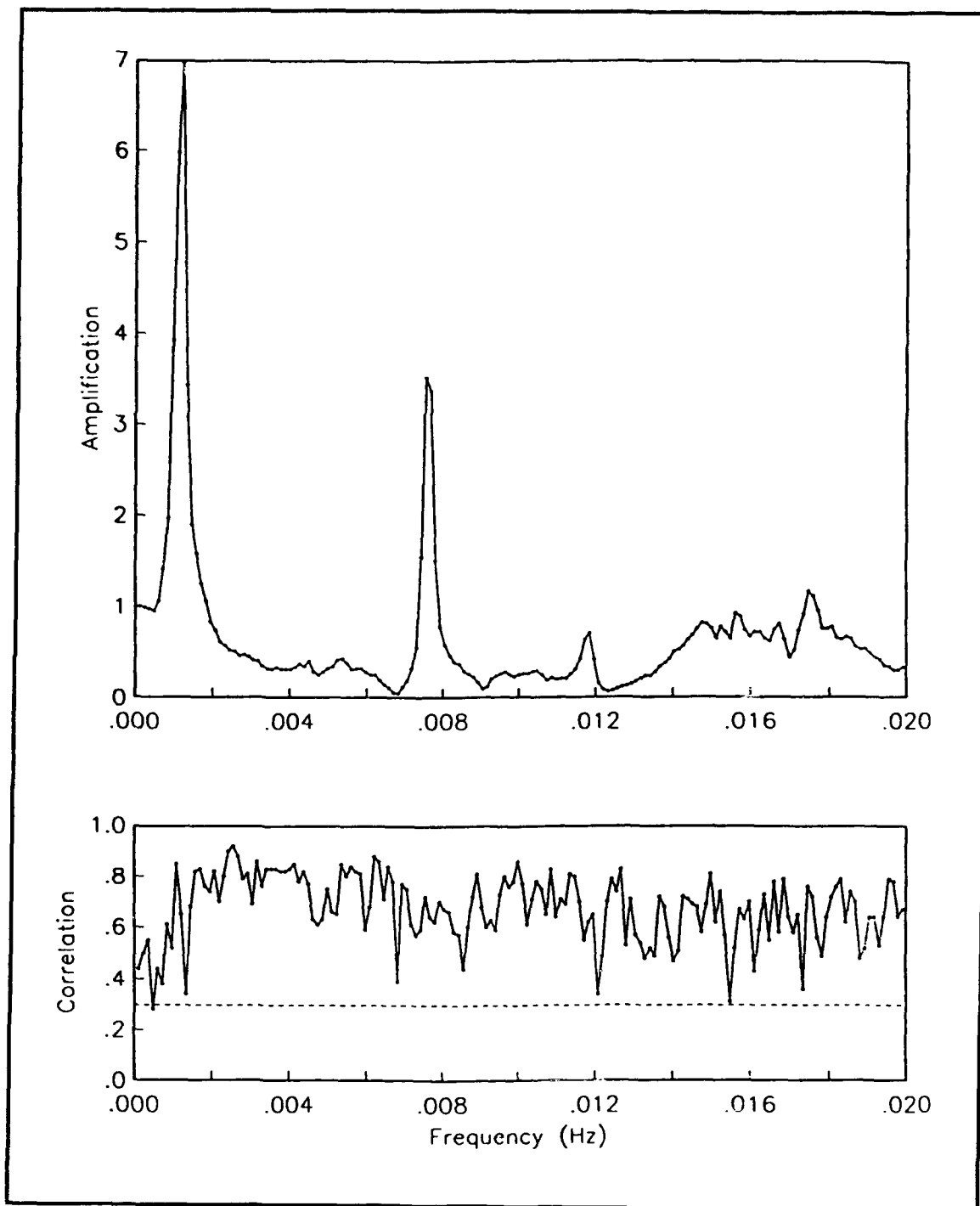
Figure A39. Amplification factors and correlation coefficients, north corner, small boat harbor closed (February 1989 - July 1989), 44 records averaged
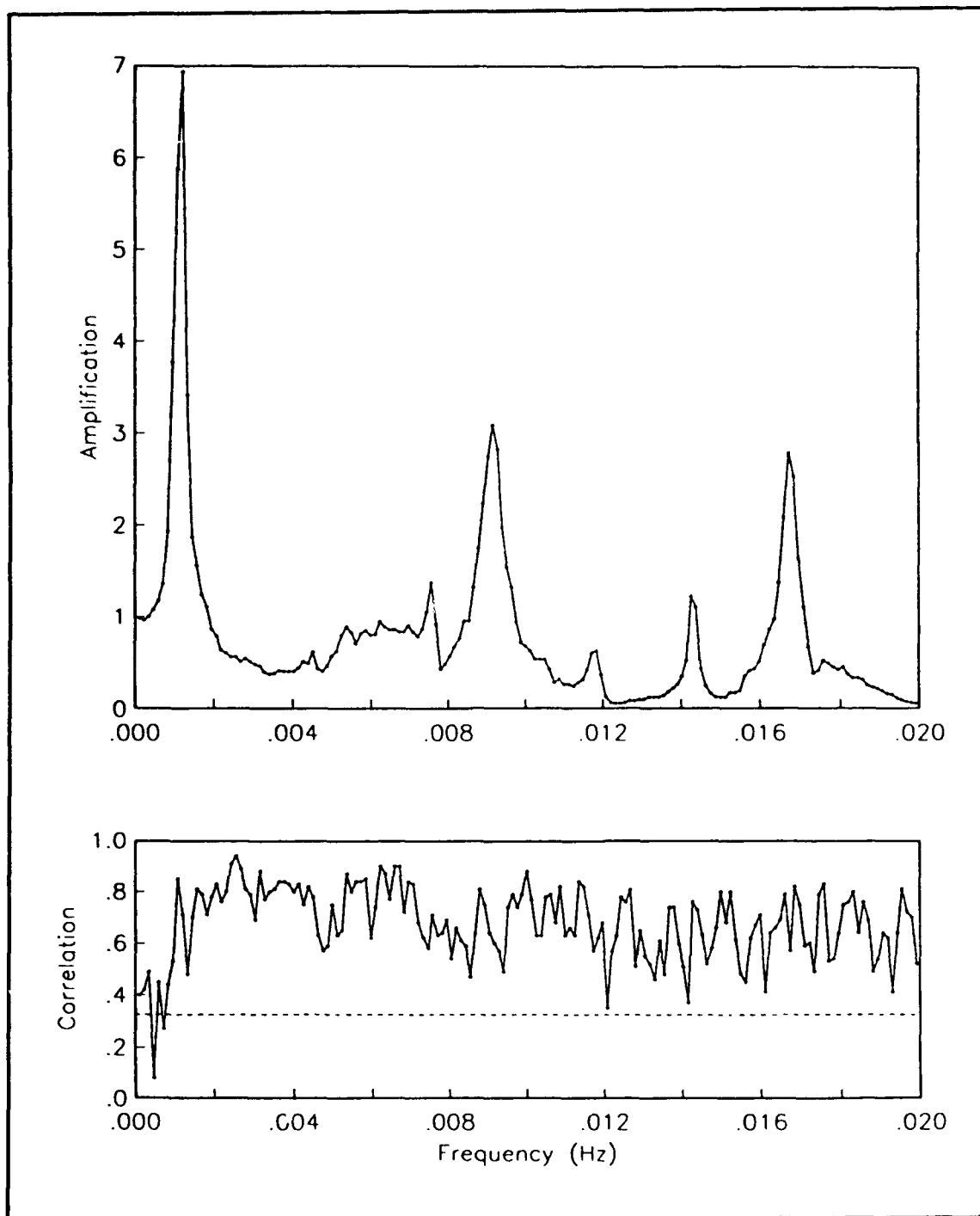
Figure A40. Amplification factors and correlation coefficients, south corner, small boat harbor closed (February 1989 - July 1989), 91 records averaged
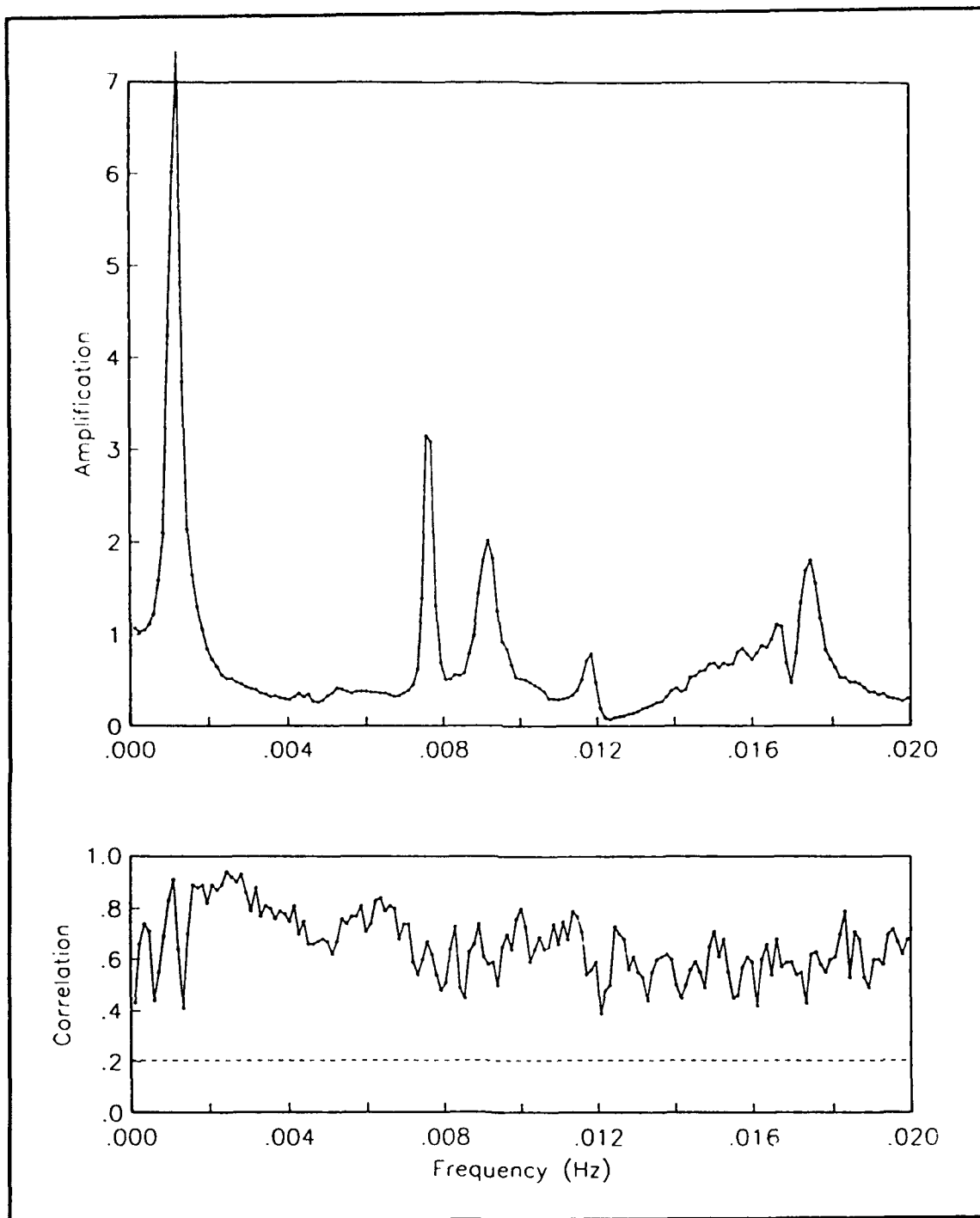
Figure A41. Amplification factors and correlation coefficients, channel midpoint, small boat harbor open (October 1989 - March 1990), 277 records averaged
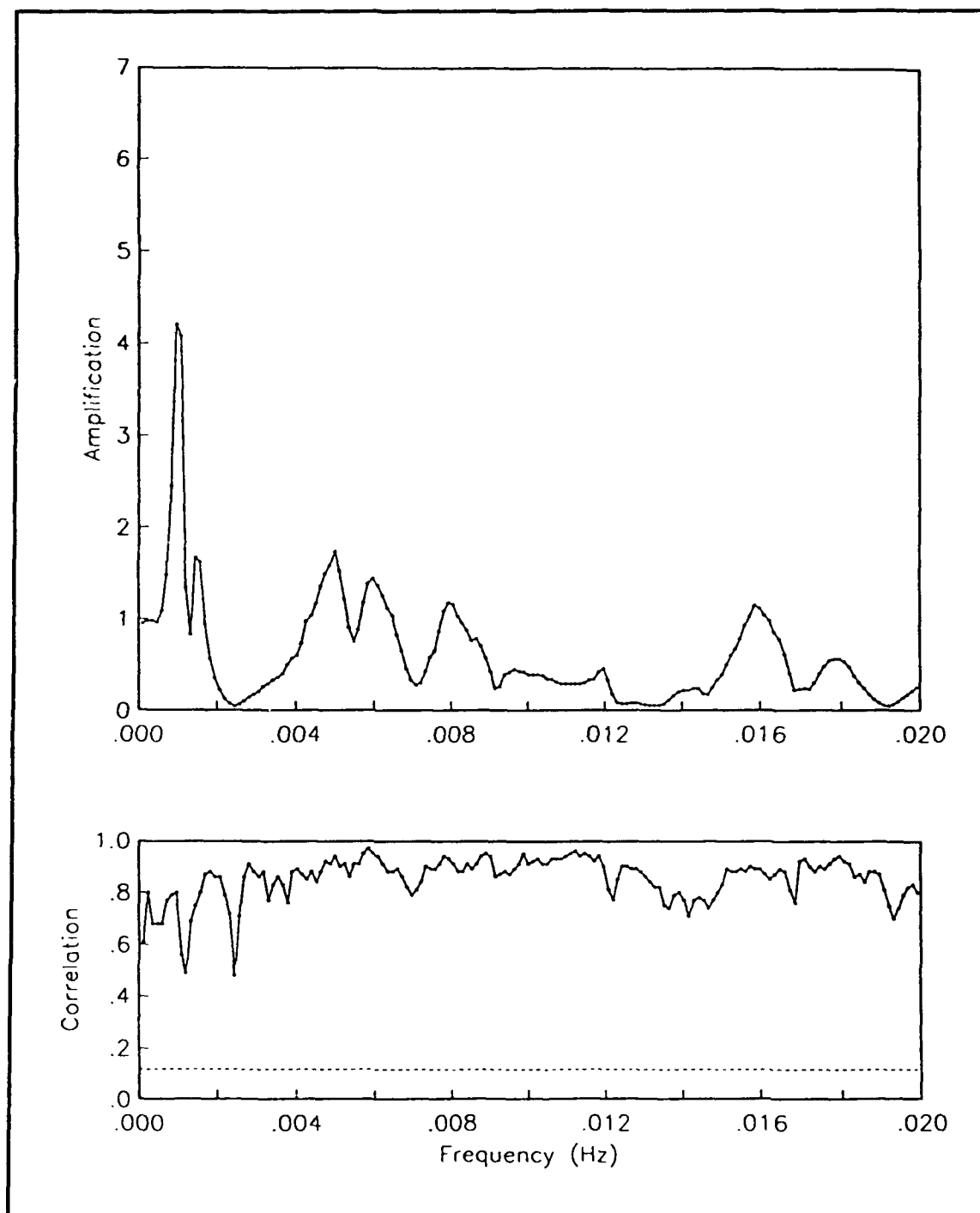
Figure A42. Amplification factors and correlation coefficients, channel midpoint, small boat harbor open (October 1989 - March 1990), 277 records averaged
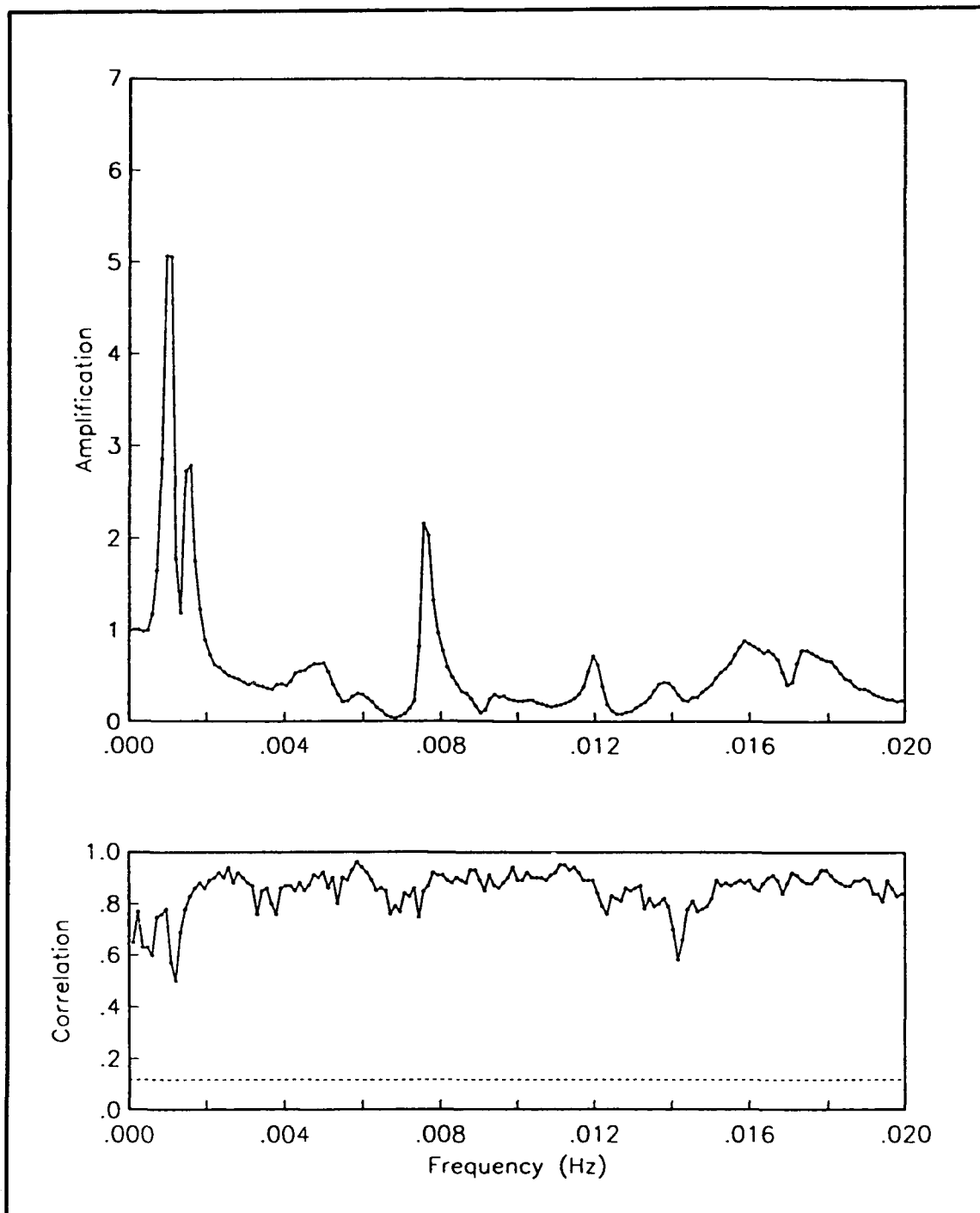
Figure A43. Amplification factors and correlation coefficients, north corner, small boat harbor open (October 1989 - March 1990), 277 records averaged
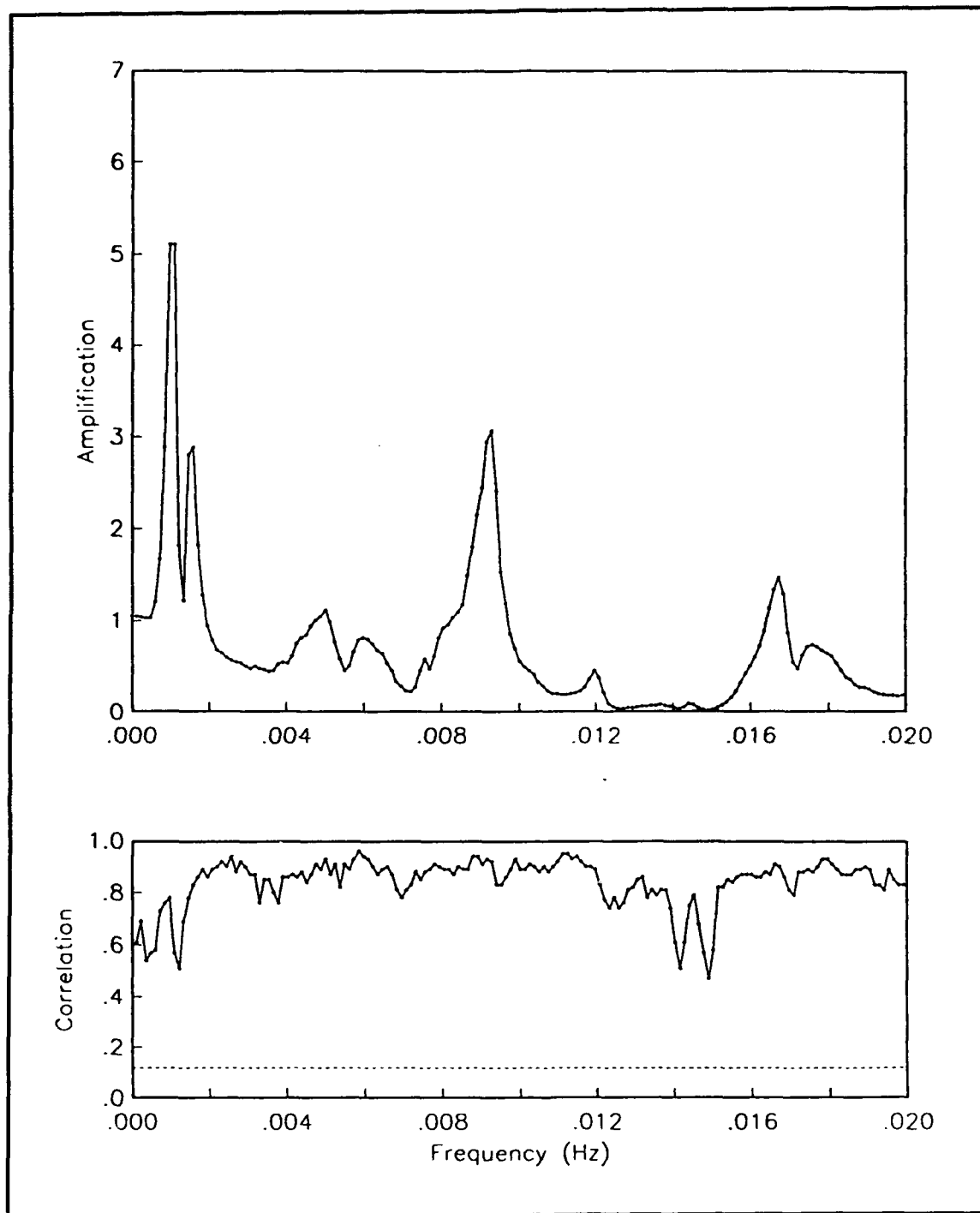
Figure A44. Amplification factors and correlation coefficients, east corner, small boat harbor open (October 1989 - March 1990), 277 records averaged
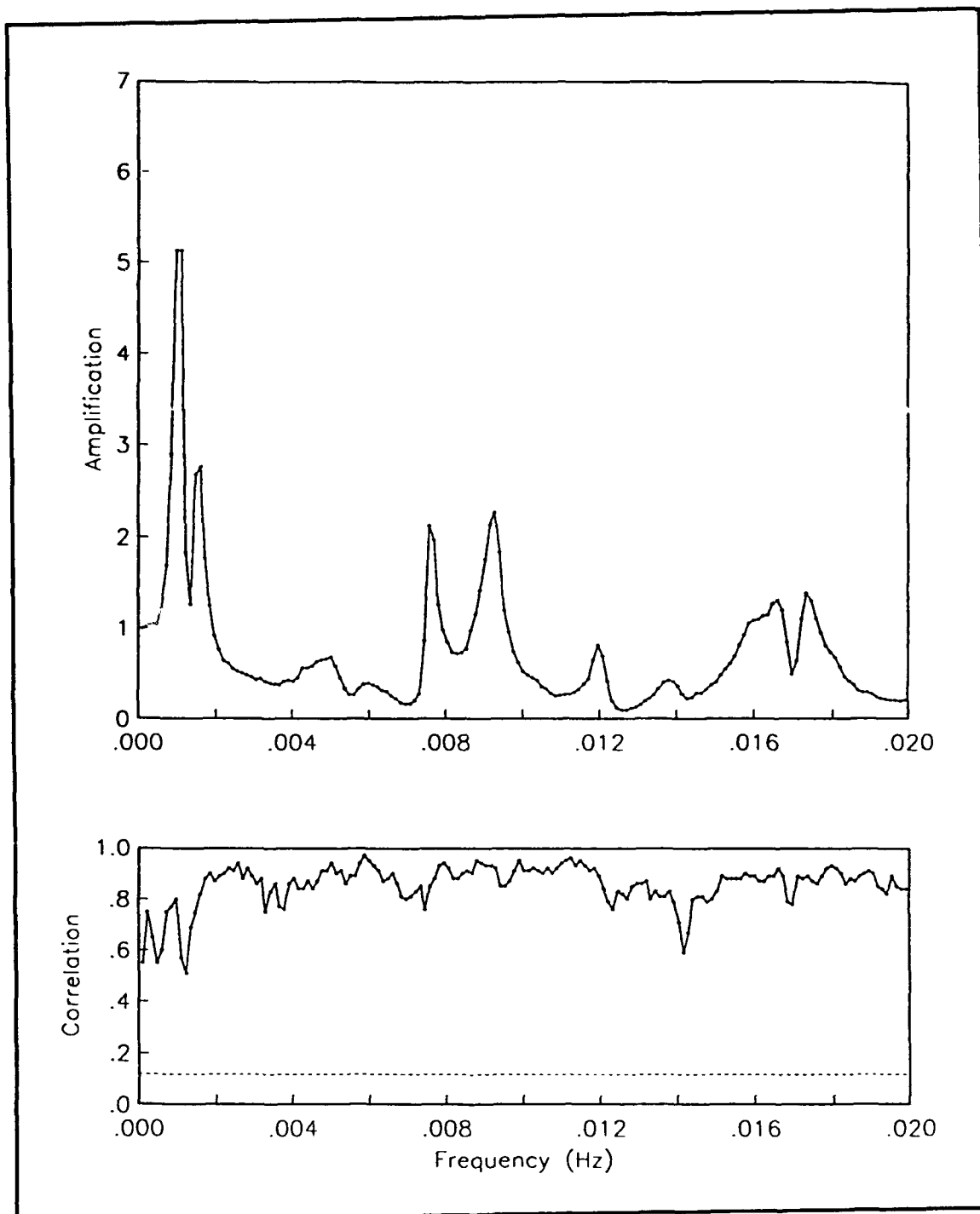
Figure A45. Amplification factors and correlation coefficients, south corner, small boat
harbor open (October 1989 - March 1990), 277 records averaged

Channel Midpoint

North Corner

East Corner

South Corner

Amplification

.000   .004   .008   .012   .016   .020
Frequency (Hz)
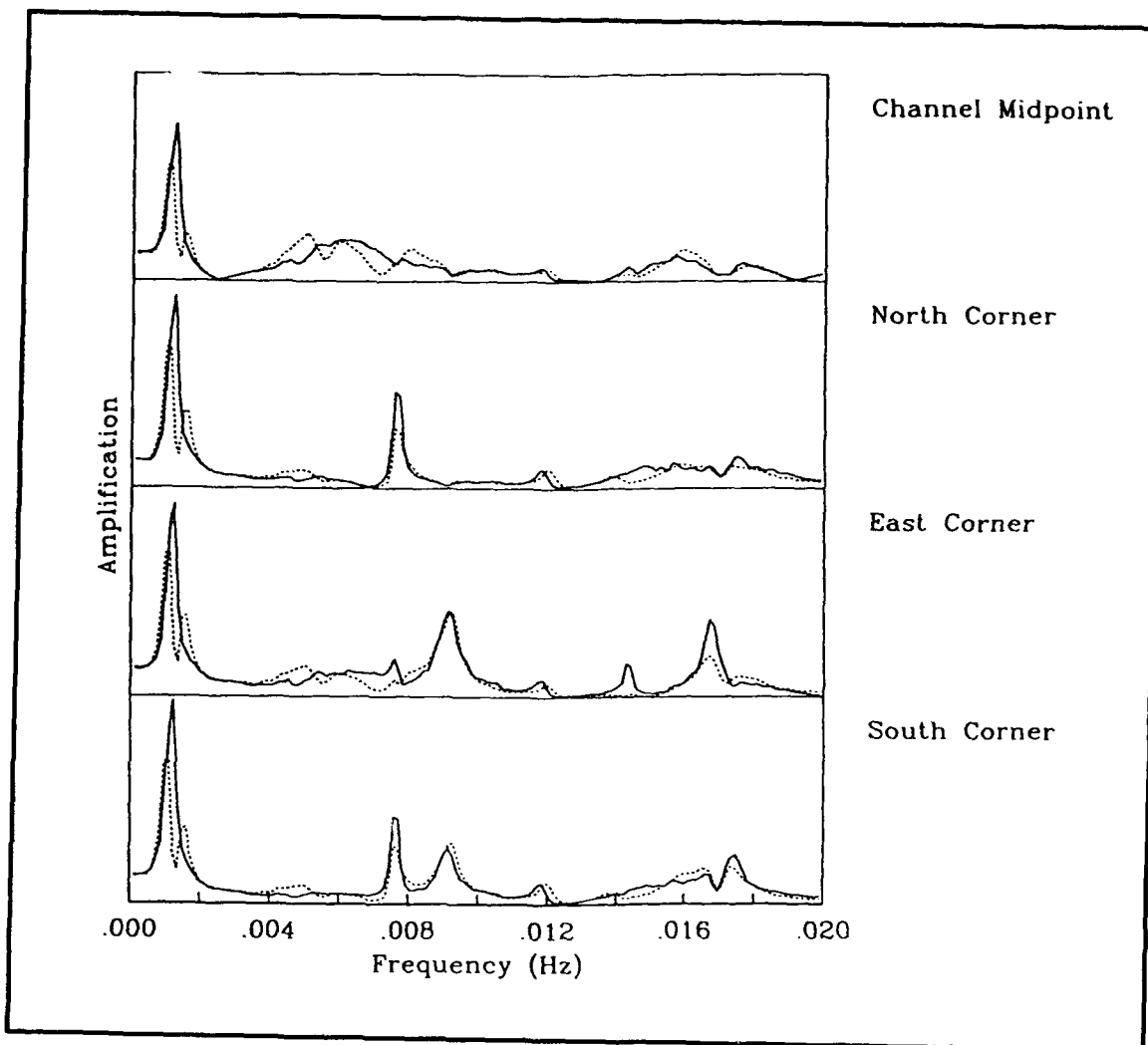
Figure A46. Amplification factors for the period when the small boat harbor was closed
(solid line) and open (dashed line)
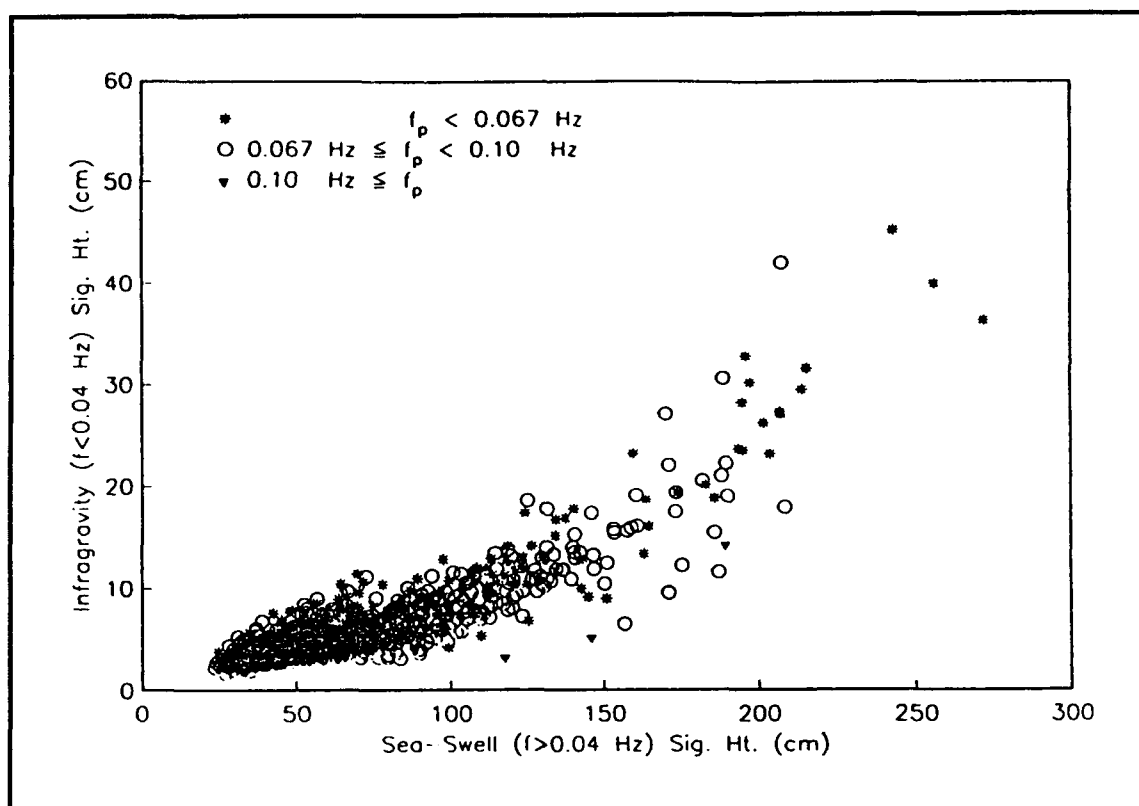
Figure A47. Nearshore coupling between infragravity and sea-swell significant wave
heights measured at Slope 1 (July 1986 - January 1988)
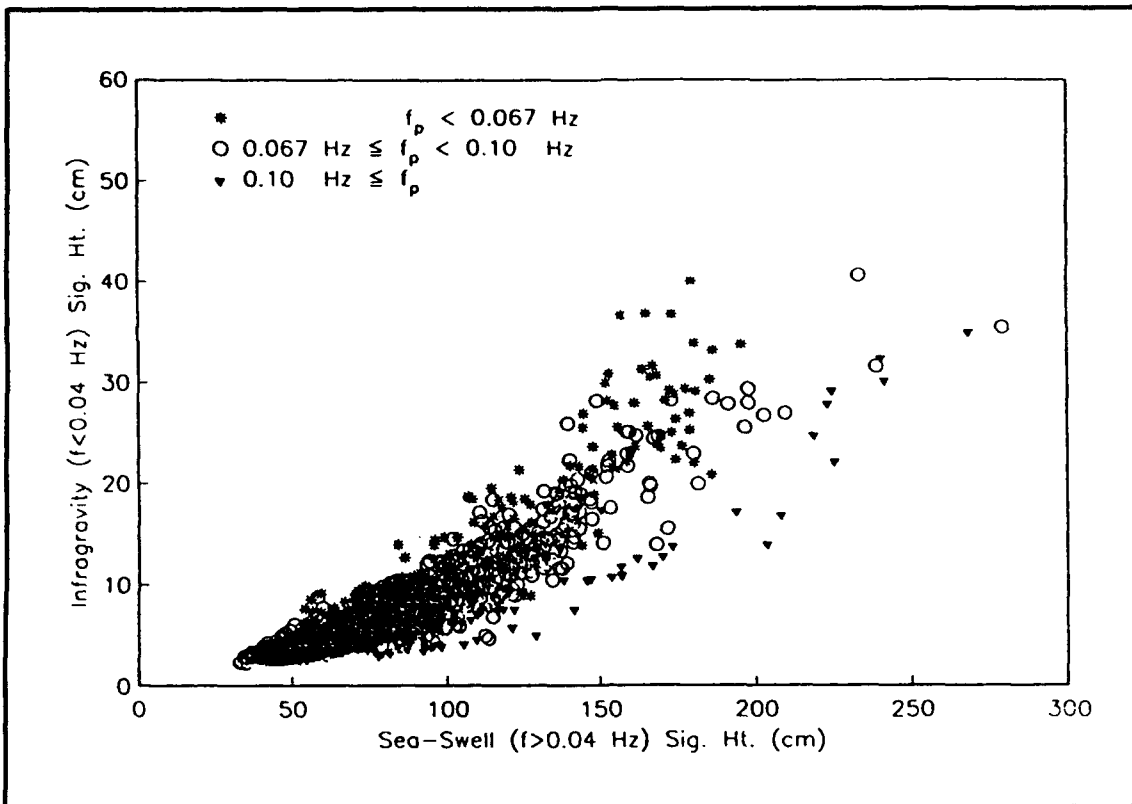
Figure A48. Nearshore coupling between infragravity and sea-swell significant wave heights measured at Slope 2 (June 1988 - March 1990)
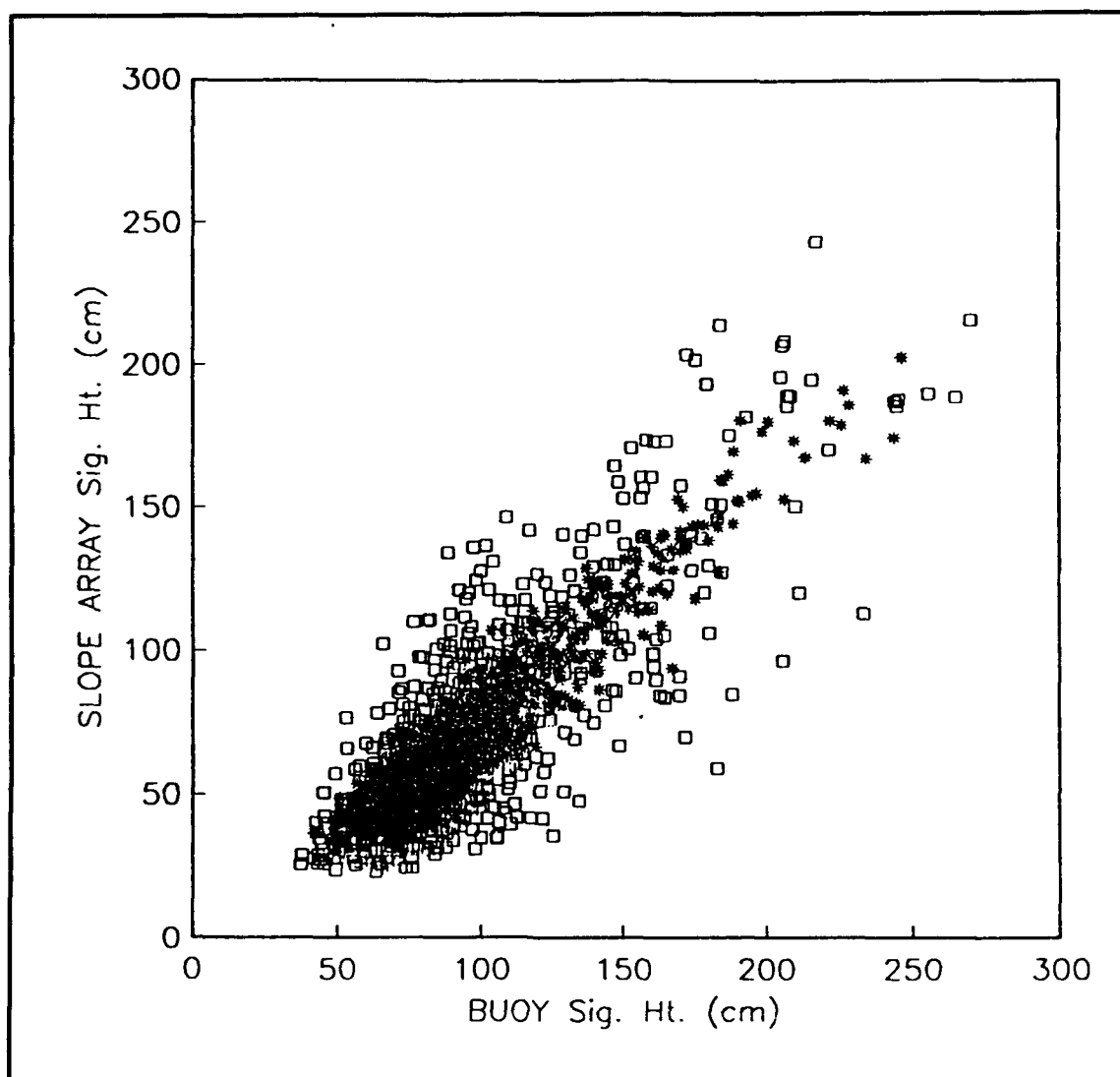
Figure A49. Nearshore (Slope 1 and Slope 2) coupling to deep water (buoy), July 1986 - January 1990
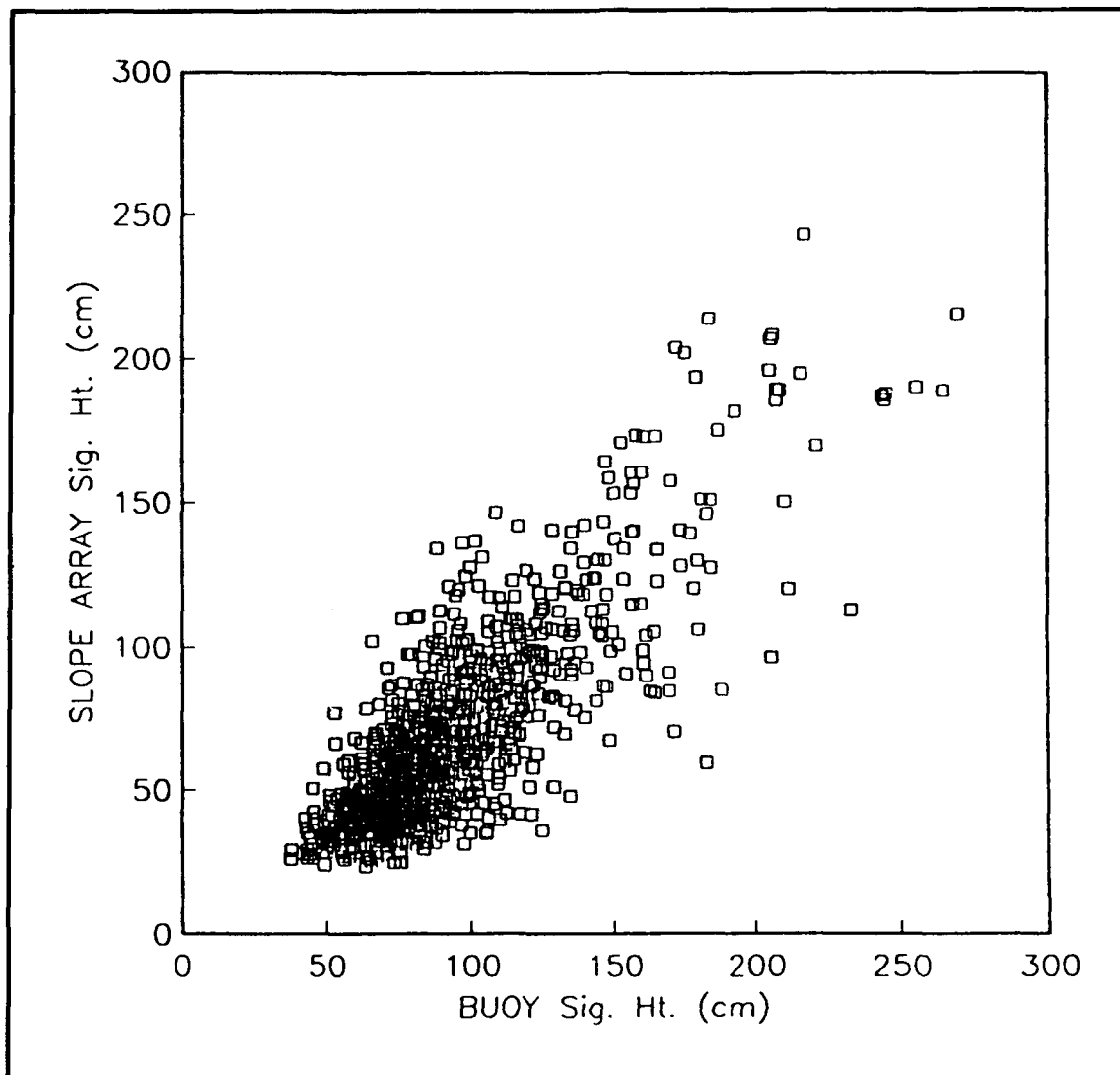
Figure A50. Nearshore (Slope 1) coupling to deep water (buoy), July 1986 - January 1988
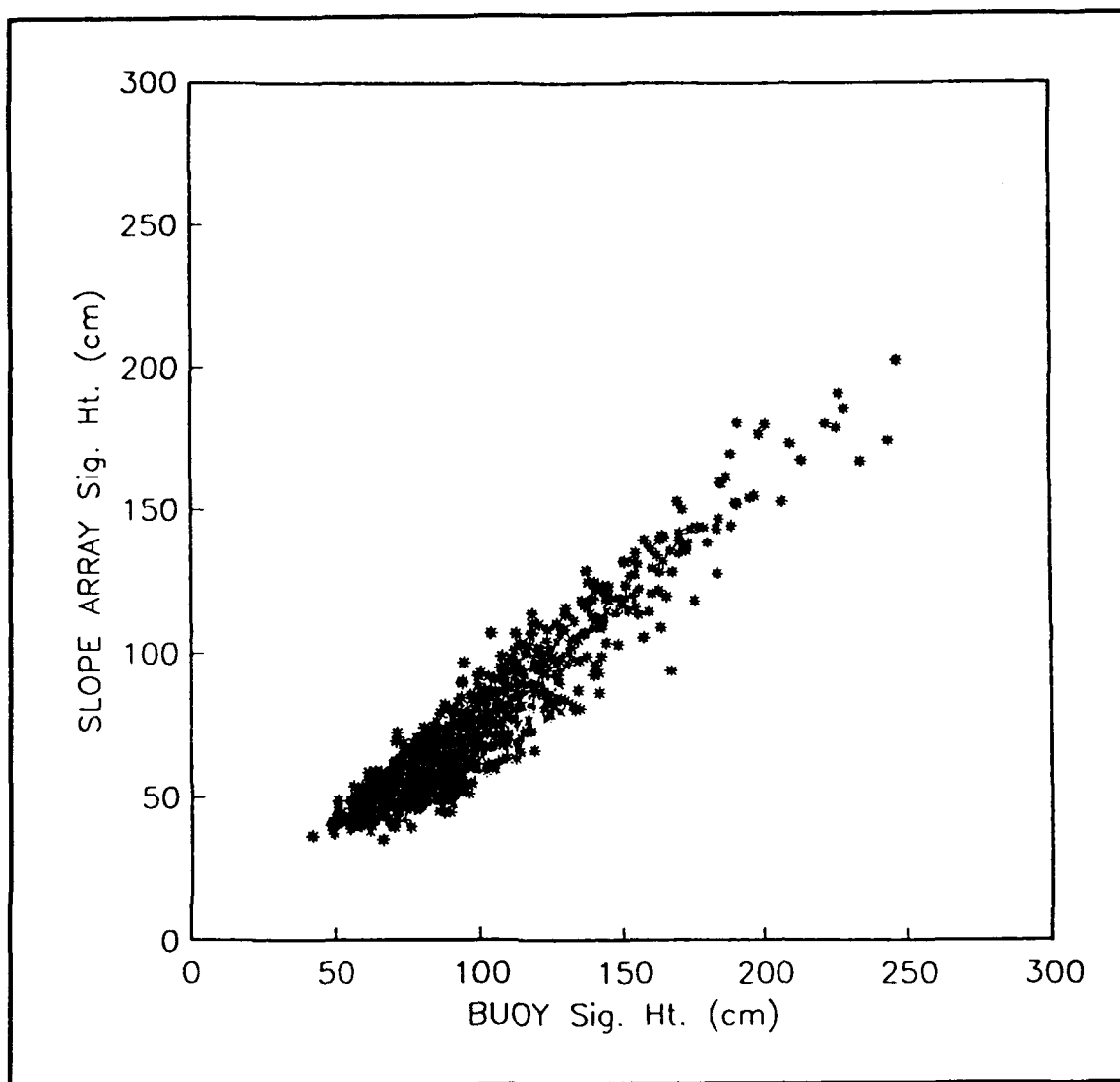
Figure A51. Nearshore (Slope 2) coupling to deep water (buoy), June 1988 - January 1990
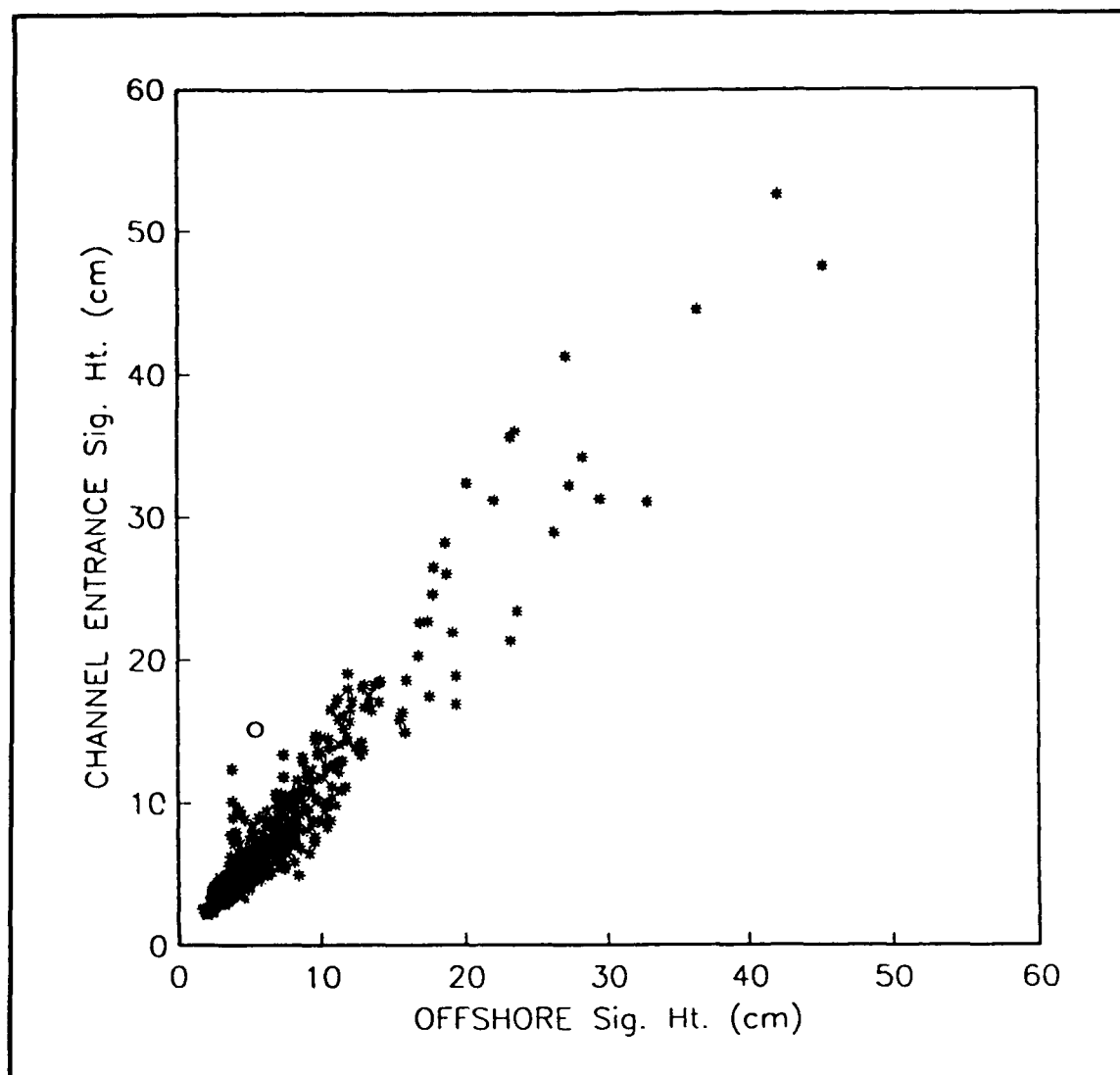
Figure A52. Coupling between infragravity significant wave heights measured at the channel entrance and Slope 1, July 1986 - January 1988, Correlation = 0.96 (857 data records)
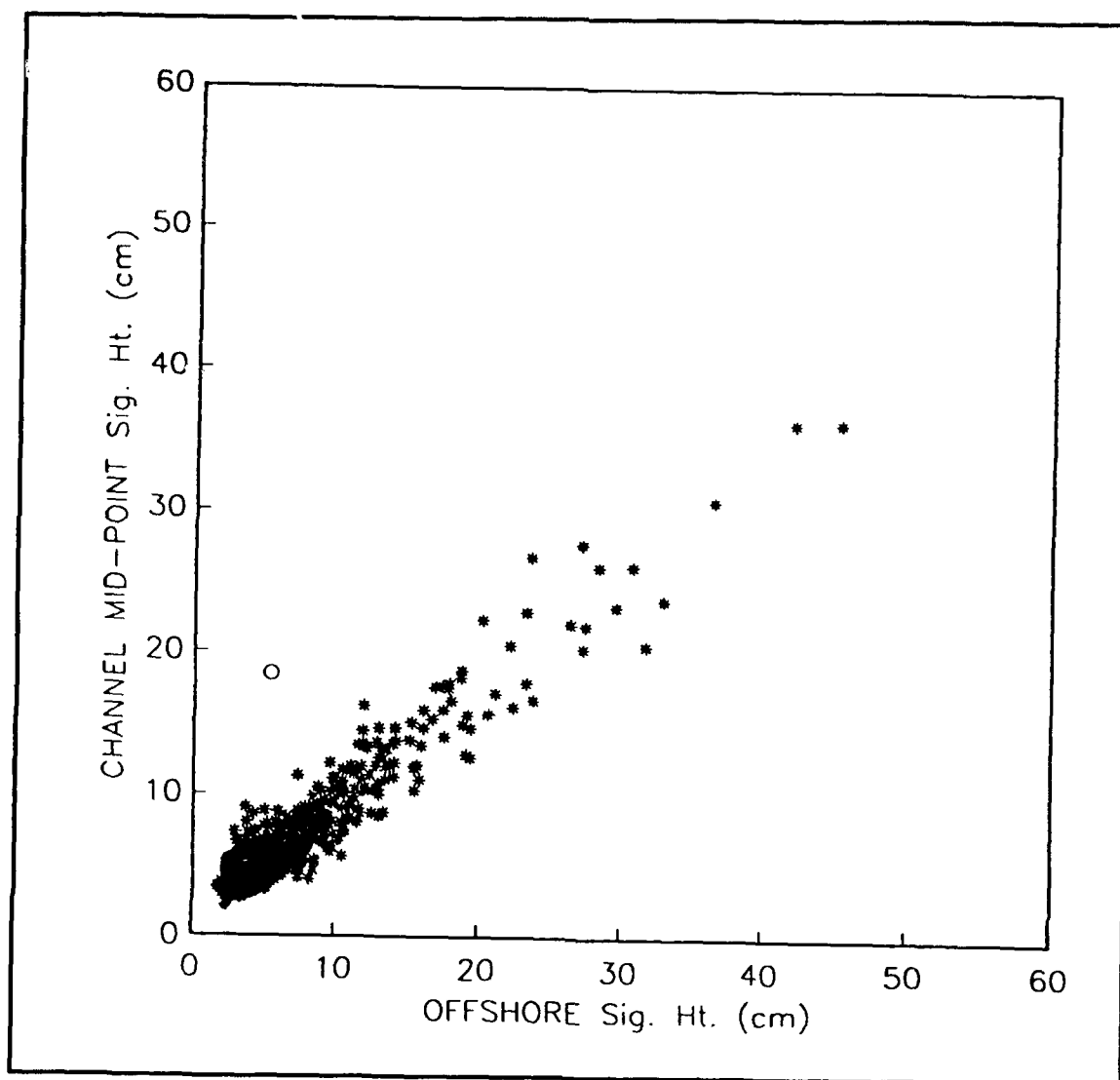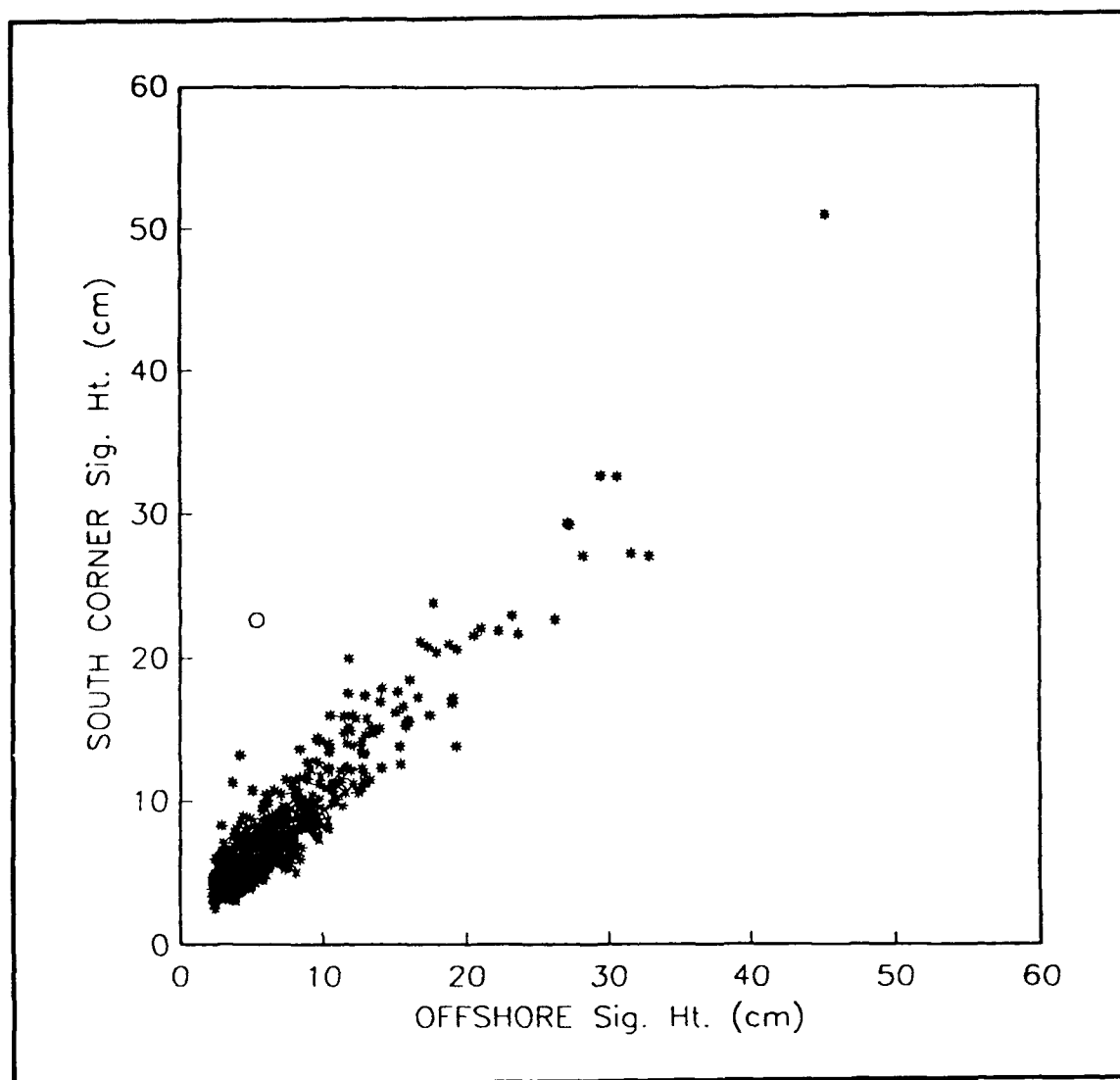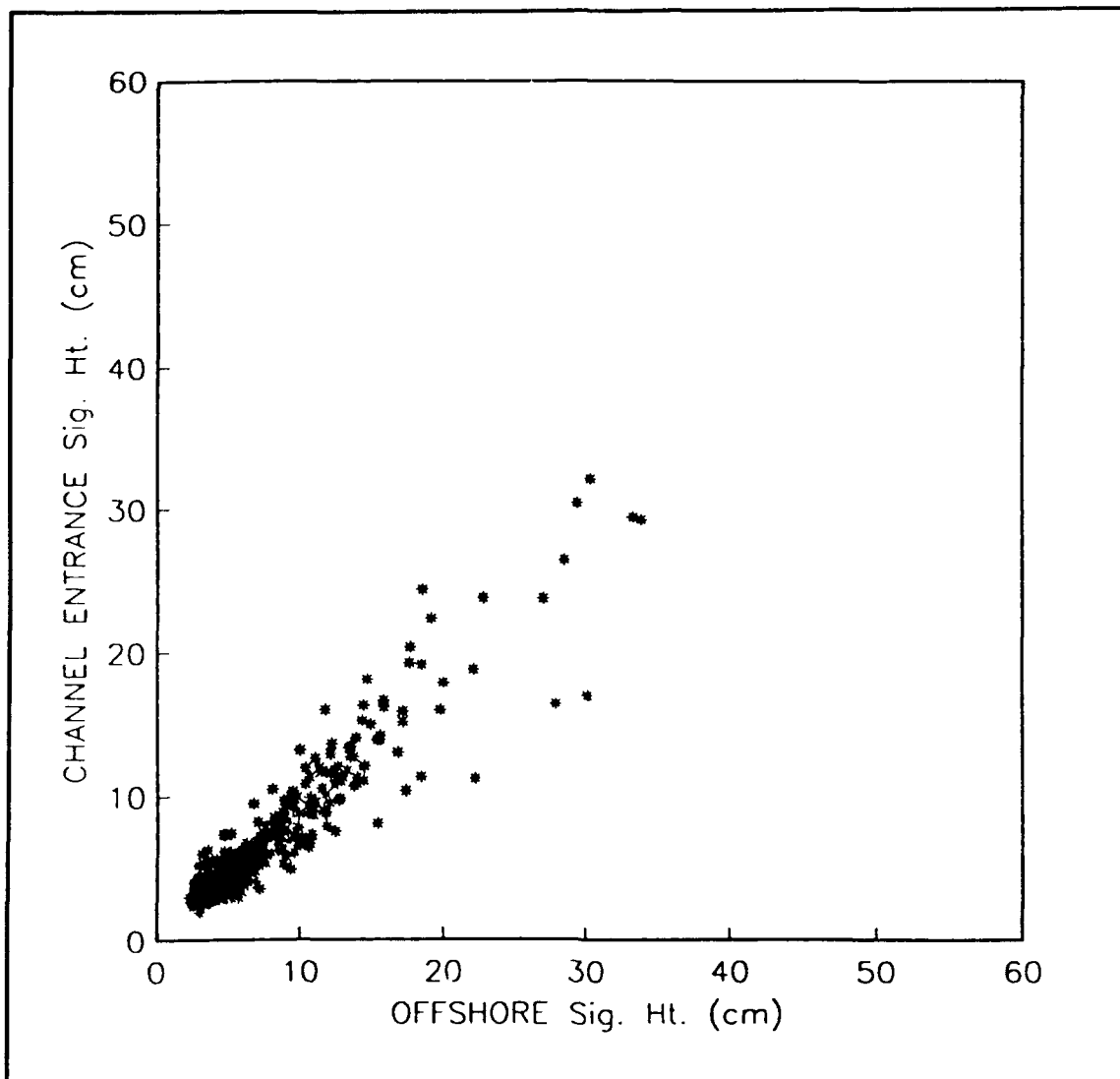
Figure A53. Coupling between infragravity significant wave heights measured at the channel midpoint and Slope 1, July 1986 - January 1988, Correlation = 0.93, 1,247 data records
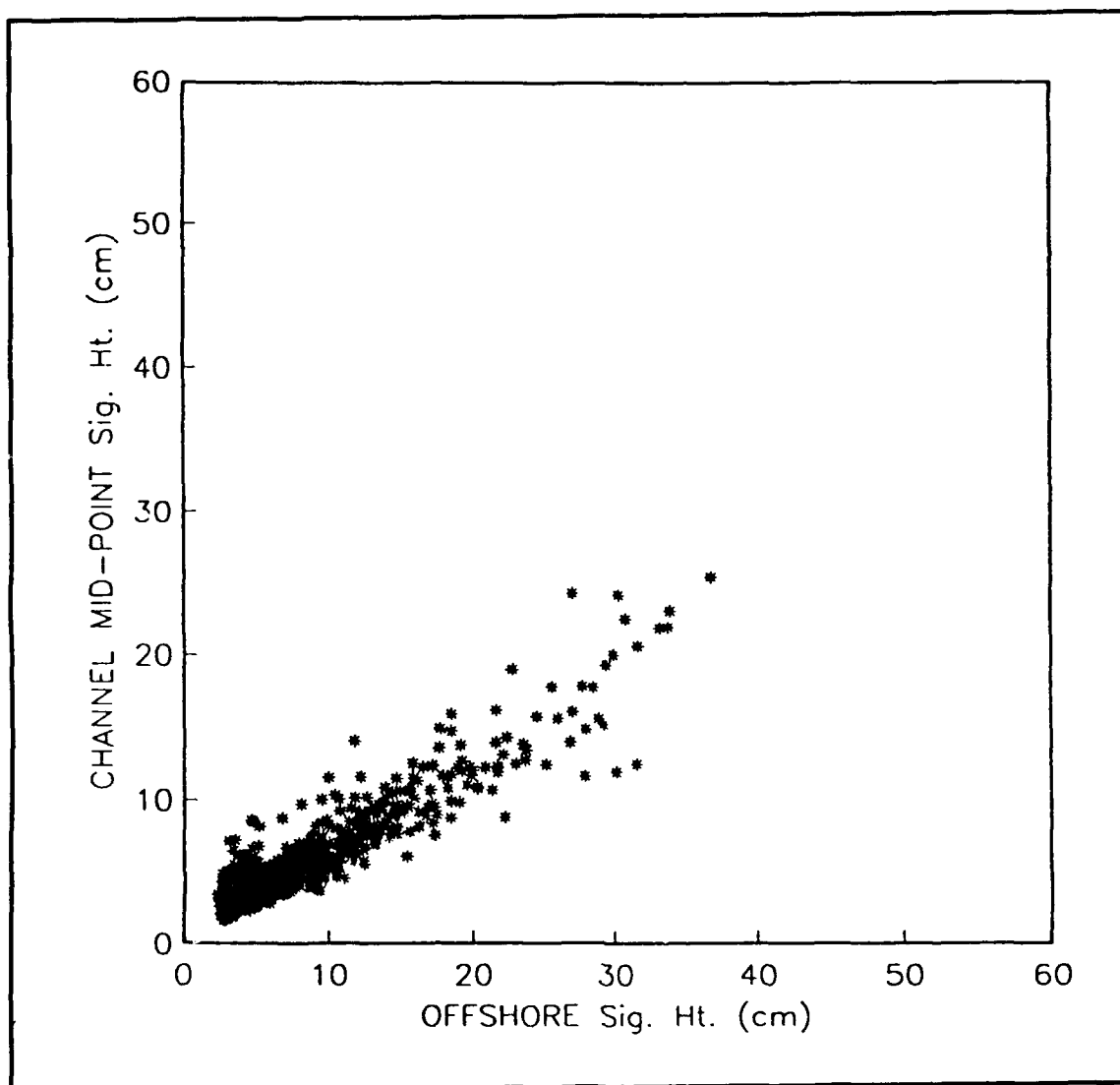
Figure A54. Coupling between infragravity significant wave heights measured at the south corner and Slope 1, July 1986 - January 1988, Correlation = 0.93, 1,004 data records

Figure A55. Coupling between infragravity significant wave heights measured at the channel entrance and Slope 2, June 1988 - March 1990, Correlation = 0.94 (757 data records)

Figure A56. Coupling between infragravity significant wave heights measured at the channel midpoint and Slope 2, June 1988 - March 1990, Correlation = 0.92, 1,790 data records
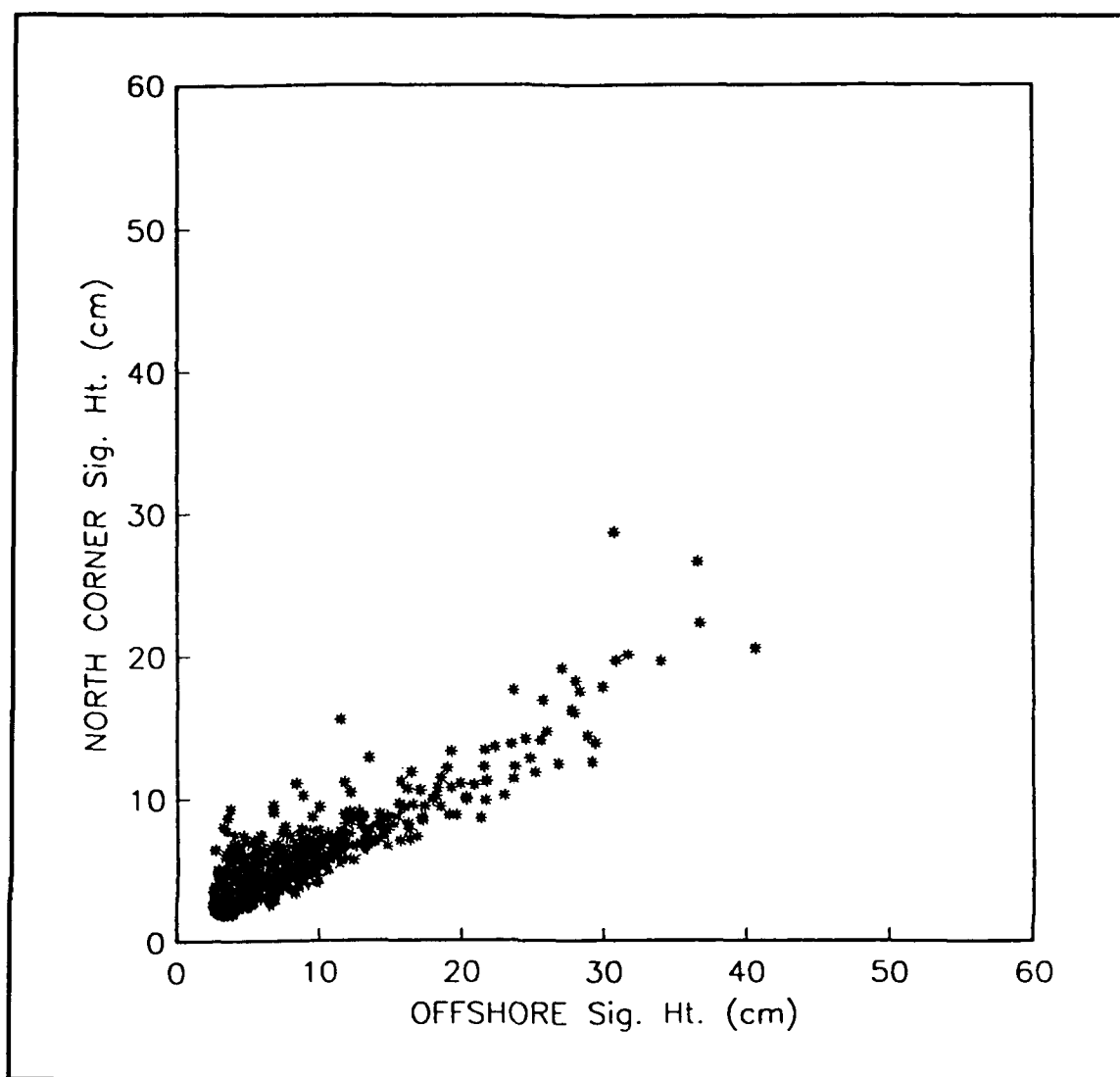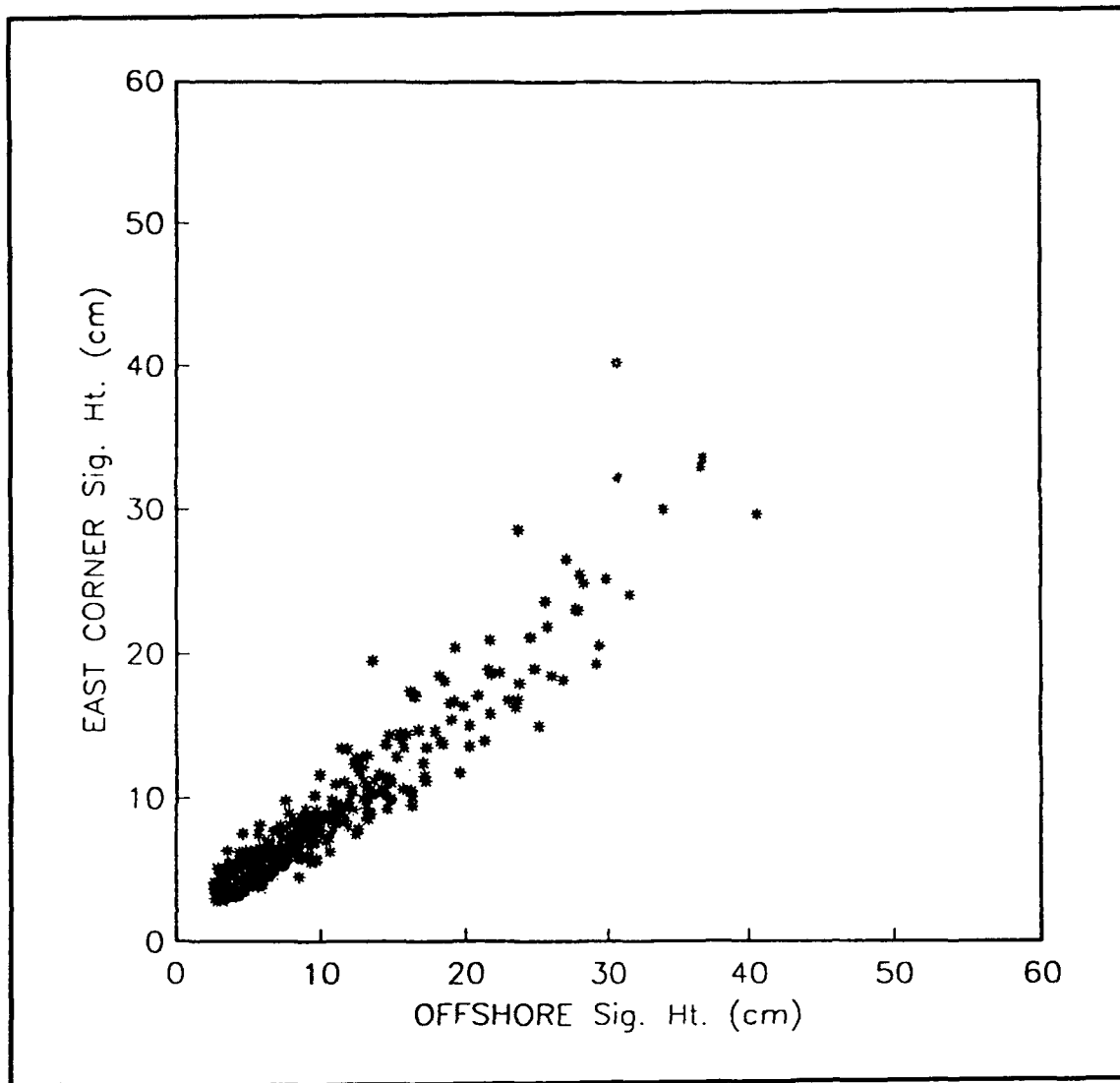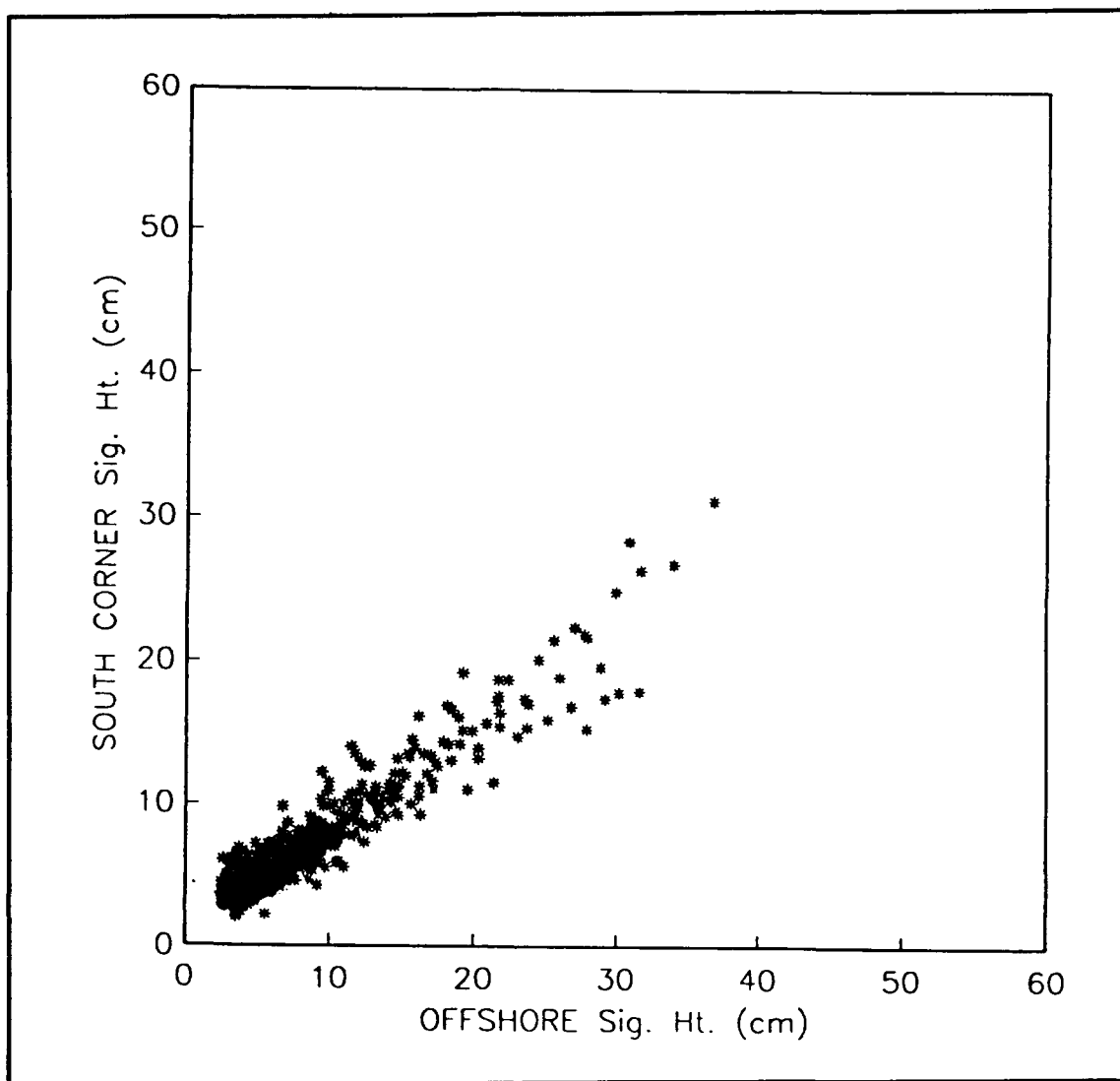
Figure A57. Coupling between infragravity significant wave heights measured at the north corner and Slope 2, June 1988 - March 1990, Correlation = 0.89 (1,252 data records)

Figure A58. Coupling between infragravity significant wave heights measured at the east corner and Slope 2, June 1988 - March 1990, Correlation = 0.95, 627 data records

Figure A59. Coupling between infragravity significant wave heights measured at the south corner and Slope 2, June 1988 - March 1990, Correlation = 0.95, 1,199 data records
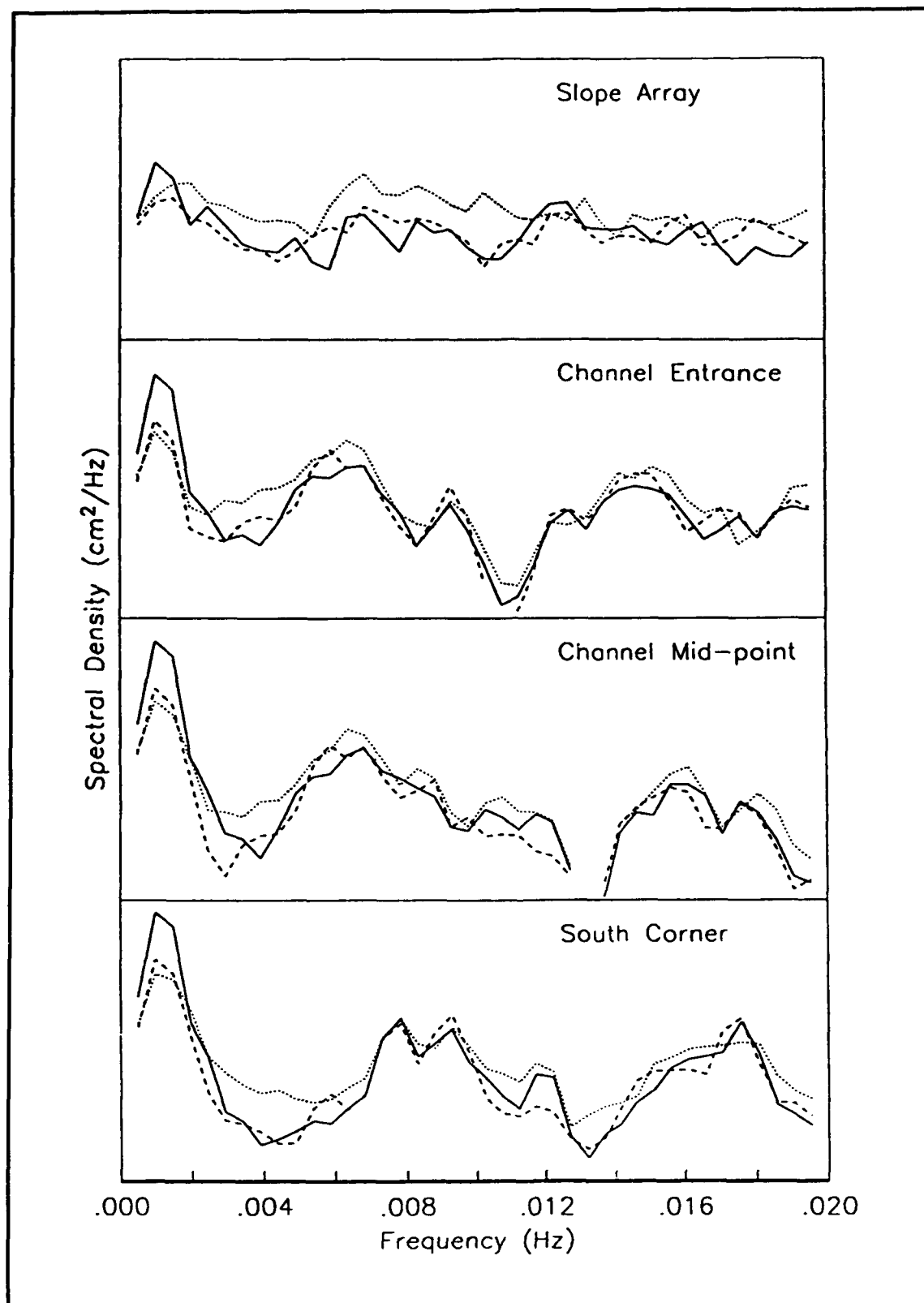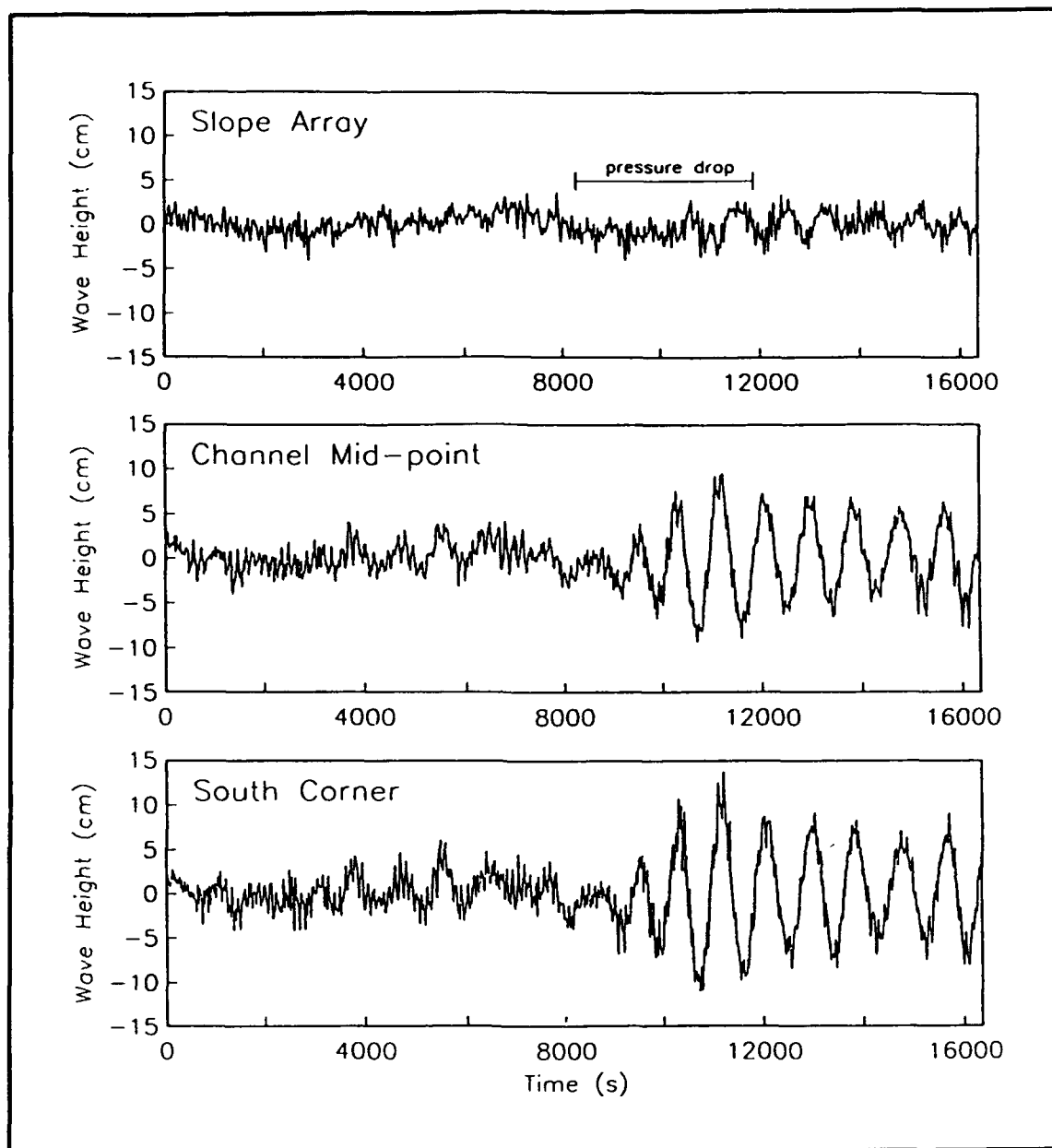
Figure A60. Atmospheric pressure disturbance event. Wave spectra before (dashed line), during (solid line), and after (dotted line) the surge event

Figure A61. Time series before and during atmospheric pressure surge event. Sea level pressure drop is indicated in top panel

REPORT DOCUMENTATION PAGE

Public reporting burden for this collection of information is estimated to average 1 hour per response, including the time for reviewing instructions, searching existing data sources, gathering and maintaining the data needed, and completing and reviewing the collection of information. Send comments regarding this burden estimate or any other aspect of this collection of information, including suggestions for reducing this burden, to Washington Headquarters Services, Directorate for Information Operations and Reports, 1215 Jefferson Davis Highway, Suite 1204, Arlington, VA 22202-4302, and to the Office of Management and Budget, Paperwork Reduction Project (0704-0188), Washington, DC 20503.

1. AGENCY USE ONLY (Leave blank)	2. REPORT DATE September 1993	3. REPORT TYPE AND DATES COVERED Final report

4. TITLE AND SUBTITLE
Barbers Point Harbor, Oahu, Hawaii
Monitoring Study

5. FUNDING NUMBERS
WU 22119

6. AUTHOR(S)
Linda S. Lillycrop, Michael J. Briggs, Gordon S. Harkins, Stanley J. Boc,
Michele S. Okihiro

7. PERFORMING ORGANIZATION NAME(S) AND ADDRESS(ES)
U.S. Army Engineer Waterways Experiment Station, Coastal Engineering Research
Center, 3909 Halls Ferry Road, Vicksburg, MS 39180-6199
U.S. Army Engineer Division, Pacific Ocean, Fort Shafter, HI 96858-5440
Scripps Institution of Oceanography

8. PERFORMING ORGANIZATION REPORT NUMBER
Technical Report CERC-93-18

9. SPONSORING/MONITORING AGENCY NAME(S) AND ADDRESS(ES)
U.S. Army Corps of Engineers
Washington, DC 20314-1000

10. SPONSORING/MONITORING AGENCY REPORT NUMBER

11. SUPPLEMENTARY NOTES
Available from National Technical Information Service, 5285 Port Royal Road, Springfield, VA 22161.

12a. DISTRIBUTION/AVAILABILITY STATEMENT
Approved for public release; distribution is unlimited.

12b. DISTRIBUTION CODE

13. ABSTRACT (Maximum 200 words)

This report summarizes the field monitoring program and physical and numerical model studies that have been conducted to date for Barbers Point Harbor, Oahu, HI. This harbor was selected for study as part of the Monitoring Completed Coastal Projects (MCCP) Program in FY 85. The report describes the following: (a) previous physical and numerical model studies conducted in the planning stages of the harbor, (b) state-of-the-art physical and numerical model studies used to estimate harbor response in the existing harbor complex, (c) a field monitoring program for collecting wind wave and long-period waves outside and inside the harbor, (d) intercomparison among previous and current model studies and field data relative to harbor response and deepwater and nearshore coupling between infragravity and wind waves, and (e) evaluation of the effectiveness of the existing rubble-mound wave absorber in dissipating wave energy inside the harbor. Conclusions and recommendations are presented and an extensive appendix containing monitoring program results is provided.

14. SUBJECT TERMS

Barbers Point Harbor	Numerical models
Harbor modeling	Physical models
Harbor monitoring	Prototype measurement

15. NUMBER OF PAGES
237

16. PRICE CODE

17. SECURITY CLASSIFICATION OF REPORT UNCLASSIFIED	18. SECURITY CLASSIFICATION OF THIS PAGE UNCLASSIFIED	19. SECURITY CLASSIFICATION OF ABSTRACT	20. LIMITATION OF ABSTRACT